

Racing-red *chassis*



Advancing *Rhodobacter sphaeroides* as platform for isoprenoid production

Enrico Orsi

Propositions

1. Development of a microbial cell factory is an interdisciplinary effort.
(this thesis)
2. The high PHB producing capacity of *Rhodobacter sphaeroides* can be exploited for growth-independent isoprenoid synthesis.
(this thesis)
3. Science and politics differ in how mantric repetition of a statement is embraced by the audience.
4. Story telling is key for the impact of a scientific paper.
5. XXI century's biological and technological revolutions modified the supply chain of plant aromas from inter-national to intra-cellular networks.
6. Irrationality and emotional consensus are at the core of political legitimacy.
7. Language reflects the forma mentis of a nation and vice versa.

Propositions belonging to the thesis, entitled
“Racing-red *chassis*: advancing *Rhodobacter sphaeroides* as
platform for isoprenoid production”

Enrico Orsi

Wageningen, 30th October 2020

Racing-red *chassis*

Advancing *Rhodobacter sphaeroides* as
platform for isoprenoid production

Enrico Orsi

Thesis Committee

Promotors

Prof. Dr Ruud A. Weusthuis

Personal chair, Bioprocess Engineering

Wageningen University & Research

Prof. Dr Gerrit Eggink

Special chair, Industrial Biotechnology

Wageningen University & Research

Co-promotor

Dr Servé W. M. Kengen

Assistant professor, Laboratory of Microbiology

Wageningen University & Research

Other members

Prof. Dr Eddy J. Smid, Wageningen University & Research

Prof. Dr Hendrik J. Bosch, Wageningen Plant Research

Dr Anita Loeschcke, Heinrich Heine University Düsseldorf

Prof. Dr Bas Teusink, Vrije Universiteit Amsterdam

This research was conducted under the auspices of Graduate School VLAG (Advanced studies in Food Technology, Agrobiotechnology, Nutrition and Health Sciences).

Racing-red *chassis*

Advancing *Rhodobacter sphaeroides* as platform for isoprenoid production

Enrico Orsi

Thesis

submitted in fulfilment of the requirements for the degree of doctor

at Wageningen University

by the authority of the Rector Magnificus,

Prof. Dr A.P.J. Mol,

in the presence of the

Thesis Committee appointed by the Academic Board

to be defended in public

on Friday 30th October 2020

at 4 p.m. in the Aula.

Enrico Orsi

Racing-red *chassis*: advancing *Rhodobacter sphaeroides* as platform for
isoprenoid production

290 pages.

PhD thesis, Wageningen University, Wageningen, the Netherlands (2020)

With references, with summary in English

ISBN 978-94-6395-313-9

DOI <https://doi.org/10.18174/514533>

Contents

Chapter 1	Introduction and thesis outline	1
Chapter 2	Characterization of heterotrophic growth and sesquiterpene production by <i>Rhodobacter sphaeroides</i> on a defined medium	17
Chapter 3	Efficient Cas9-based genome editing of <i>Rhodobacter sphaeroides</i> for metabolic engineering	45
Chapter 4	Functional replacement of isoprenoid pathways in <i>Rhodobacter sphaeroides</i>	95
Chapter 5	Metabolic flux ratio analysis by parallel ¹³ C labeling of isoprenoid biosynthesis in <i>Rhodobacter sphaeroides</i>	131
Chapter 6	Growth-uncoupled isoprenoid synthesis in <i>Rhodobacter sphaeroides</i>	171
Chapter 7	General discussion	205
Summary		235
References		243
About the author		265
Acknowledgements		273



Chapter 1

Introduction and thesis outline

This chapter has been adapted from the submitted manuscript: Orsi, E., Beekwilder, J., Eggink, G., Kengen, S. W. & Weusthuis, R. A. (2020). The transition of *Rhodobacter sphaeroides* into a microbial cell factory.

Microbial cell factories: workhorses for the bioeconomy

Bioeconomy is an emerging concept which aims to reform economic systems via a sustainable use of renewable biological resources (1). This concept has gained importance over the last decade, and is proposed as possible solution to several contemporary challenges: climate change, food security, health, industrial restructuring and energy supply (2). Implementation of a bioeconomy requires a transition from fossil-based to bio-based products (2, 3). Such a transition is strongly influenced by a technical perspective, led by biotechnological research, which can provide innovative solutions in this regard (1, 2, 4).

Biotechnology for the bioeconomy often involves investigations in applied microbiology (2), where microbial cell factories are optimized for synthesizing bio-based products (5, 6). These products belong to different market sectors and, graphically, they can be organized in a pyramid (**Fig. 1**). At the top of this pyramid lays the market sector of pharmacologically active compounds (7), which includes high-value molecules with a small market volume. Descending the pyramid, the price per kilo of the compounds decreases, while the market volume increases. Therefore, following this order fine chemicals (*e.g.* fragrances and nutraceuticals) (8, 9), commodity chemicals (10) and biofuels (11, 12) are included among the bio-based products.

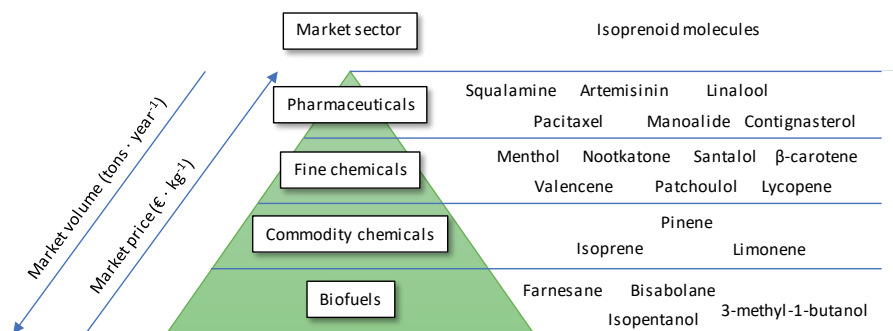


Figure 1. Overview of the bioeconomy pyramid, including some relevant isoprenoid molecules for each market sector.

The most studied microbial *chassis* for bioproduction are the bacterium *Escherichia coli* and the yeast *Saccharomyces cerevisiae* (13–15). Recent improvements in genome editing tools and -omics technologies allowed to investigate novel types of microorganisms as new platform strains for industrial applications (6, 16–18). Usually, these microorganisms show intrinsic traits that make them ideal hosts for an intended industrial bioprocess. Several works describe these characteristics, although they might differ based on the process conditions (5, 16–20). Usually, these features include: i) genetic accessibility & availability of genetic toolboxes, ii) ability to consume inexpensive feedstock, iii) (at least partially) sequenced genome, iv) functional characterization, v) available metabolic model, vi) phenotypic alignment with process conditions and vii) ability to excrete the product of interest for easier downstream processing. Once the ideal *chassis* is identified (16), its improvement into a microbial cell factory occurs via iterative Design-Build-Test-Learn cycles.

The Design-Build-Test-Learn (DBTL) cycle for improving microbial *chassis*

Improvement of microbial *chassis* can occur via metabolic engineering. Such a discipline seeks to optimize the synthesis of a desired compound by modifying microbial metabolism (21–23). Often, metabolic engineering borrows tools from

synthetic biology to genetically engineer target organisms (24–26). Moreover, it can employ analytical power from -omics disciplines (transcriptomics, proteomics, metabolomics, fluxomics) for testing the effects of these modifications (27). Eventually, these are combined for providing useful insights for further improving titers ($\text{g} \cdot \text{L}^{-1}$), rates ($\text{g} \cdot \text{L}^{-1} \cdot \text{h}^{-1}$) and yields ($\text{g} \cdot \text{g substrate}^{-1}$) of a product of interest (28).

Through the years, the aforementioned approaches have been structured within the Design-Build-Test-Learn (DBTL) concept (**Fig. 2**) (29, 30). This iterative pipeline standardizes and streamlines the process for engineering and characterizing microbial *chassis*. For each round, a new ‘design’ phase is corroborated by the ‘learn’ phase of the previous cycle. Moreover, the ‘build’ phase implements the changes proposed by the ‘design’ module, and these modifications are assessed in the ‘test’ phase. Ultimately, results are evaluated in the ‘learn’ phase, whose insights can be used for the start of a new DBTL round. Therefore, each module of the cycle is highly interdependent from the others (28, 30), and relies on discipline-specific expertise.

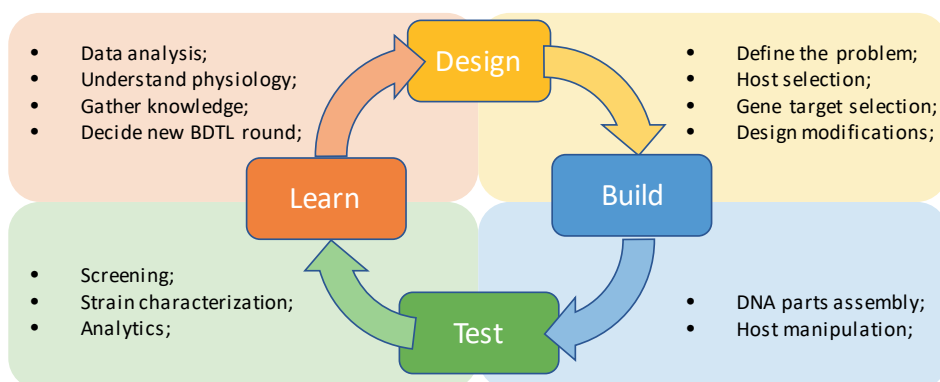


Figure 2. Schematic overview of the iterative Design-Build-Test-Learn (DBTL) model. For each phase, the most important aspects are listed.

Diminishing the turnaround time of DBTL cycles is a crucial aspect for accelerating the development of microbial *chassis* (31, 32). Cutting edge advances in fields like systems biology (33), machine learning (34), metabolomics (35), automation (31), or genome engineering (36–38) can contribute to accelerate one or more parts of the DBTL cycle. Biofoundries have been realized, in which automated and high-throughput DBTL cycles are integrated for rapidly and efficiently reprogramming cell factories (31, 39).

While rapid and standardized DBTL cycles can be performed for model organisms like *E. coli* or *S. cerevisiae*, their use for non-model microorganisms is not trivial (15). For example, potentially interesting *chassis* might lack genetic accessibility, which would render the ‘build’ phase cumbersome. Also, the metabolic pathways supporting product formation could be unknown. Therefore, implementation of DBTL cycles in non-traditional microorganisms is an intriguing challenge for biotechnology. Succeeding in such a task would allow to investigate and assess non-traditional microorganisms as potential cell factories.

Isoprenoid compounds: a successful example for the bioeconomy obtained via DBTL cycles

The case of semi-synthetic artemisinin synthesis in yeast

Probably the most scientifically relevant achievement obtained via DBTL cycles is the microbial synthesis of the antimalarial drug artemisinin (40). Such a compound is natively produced by the plant *Artemisia annua*, but dependence on yearly harvesting makes its production challenging (41). Therefore, alternatives like microbial synthesis were explored for feasible and cost-competitive artemisinin production (40, 41). This endeavour started with the implementation of a heterologous production pathway in *E. coli* (42), and was concluded a decade later by producing up to 25 g/L of artemisinic acid in

recombinant yeast (7). Once extracted from the culture broth, this molecule was converted to artemisinin via straightforward organic chemistry (7). An exhaustive and interesting review summarizes all the achievements of this challenging *Semi-synthetic Artemisinin Project* (40).

Isoprenoids and their relevance for the bioeconomy

Artemisinin belongs to the family of isoprenoids. These class of compounds (also known as terpenoids) is very vast and includes more than 50 thousand molecules. Isoprenoids are ubiquitous in all organisms. In fact, they are involved in several functions necessary for life, like respiration and photosynthesis by ubiquinone, chlorophyll and carotenoids. Moreover, isoprenoid-derived molecules like hopanoids and sterols are crucial for the fluidity of cellular membranes. In nature, synthesis of isoprenoids occurs via two independent and phylogenetically distinguished pathways (**Fig. 3**): the 2-C-methyl-D-erythritol 4-phosphate (MEP) and the mevalonate (MVA) pathway. With few exceptions, the MEP pathway is expressed in prokaryotes, whereas the MVA occurs in eukaryotes and archaea (43). Photosynthetic eukaryotes harbor both pathways naturally, compartmentalizing the MEP pathway within the chloroplast while the MVA pathway operates in the cytosol (44). The MEP pathway starts with the condensation of glyceraldehyde-3-phosphate (GAP) with pyruvate (PYR), while the MVA pathway uses acetoacetyl-CoA (AA-CoA) and acetyl-CoA (Ac-CoA) as substrates. The products of the two pathways, isopentenyl-pyrophosphate (IPP) and its isomer dimethylallyl-pyrophosphate (DMAPP), are the starting compounds for all isoprenoids (45).

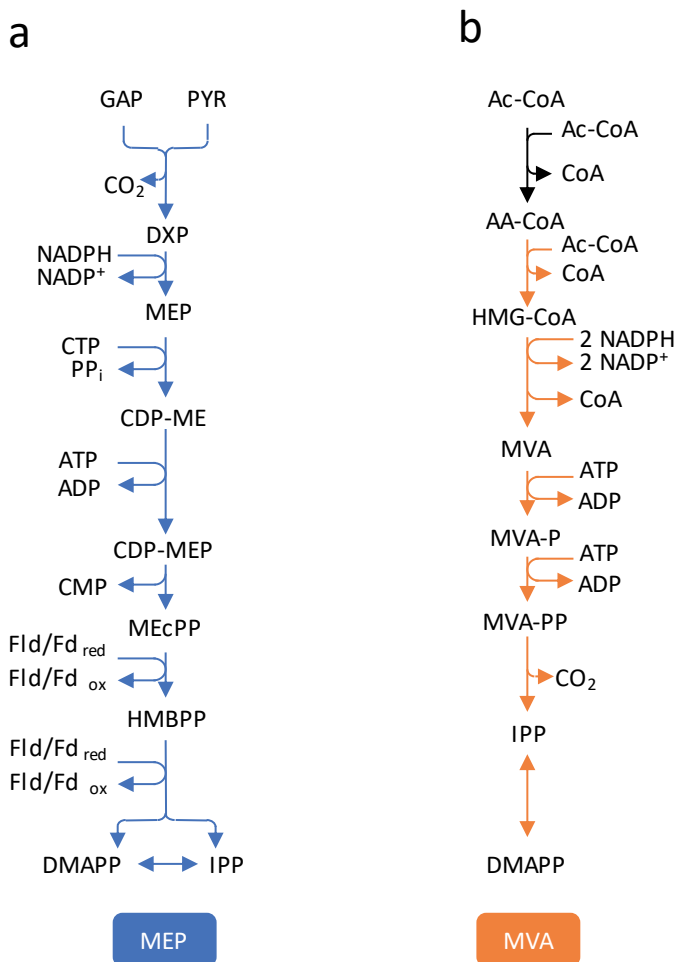


Figure 3. The two isoprenoid biosynthetic routes. a) 2-C-methyl-D-erythritol 4-phosphate (MEP) pathway, blue arrows. b) the mevalonate (MVA) pathway, orange arrows. Abbreviations: GAP, glyceraldehyde-3-phosphate; PYR, pyruvate; DXP, 1-deoxy-D-xylulose 5-phosphate; CDP-ME, 4-(cytidine 5B-diphospho)-2-C-methyl-D-erythritol; CDP-MEP, 2-phospho-4-(cytidine 5'-diphospho)-2-C-methyl-D-erythritol; MEcPP, 2-C-methyl-D-erythritol 2,4-cyclodiphosphate; HMBPP, (E)-4-hydroxy-3-methylbut-2-en-1-yl diphosphate; IPP, isopentenyl diphosphate; DMAPP, dimethylallyl diphosphate; Fld, flavodoxin; Fd, ferredoxin; red, reduced; ox, oxidized; Ac-CoA, acetyl-CoA; AA-CoA, acetoacetyl-CoA; HMG-CoA, 3-hydroxy-3-methylglutaryl-CoA; MVA-P, mevalonate phosphate; MVA-PP, mevalonate diphosphate.

Apart from artemisinin, other isoprenoid molecules are potential candidates as pharmaceuticals (46, 47). Moreover, many terpenoids have raised interest as

aromas and fragrances (8) (**Table 1**), nutraceuticals (9, 48, 49), commodity chemicals (50) and also biofuels (11, 51–53). Therefore, isoprenoids are interesting compounds for the bioeconomy (**Fig. 1**), and several strategies have been already explored for improving isoprenoid synthesis in microbial *chassis* (50, 54–57).

Table 1. Industrial isoprenoid flavours produced by microbial cell factories, adapted from (8).

Company	Commercialized products	Market sector	Microbial platform
Amyris	β -farnesene	Flavours & fragrances; Biofuels;	Yeast
Evolve	valencene nootkatone α - and β -santalol	Flavours & fragrances;	Yeast
Firmenich	patchulol sclareol	Flavours & fragrances;	Yeast or <i>E. coli</i>
Isobionics	valencene nootkatone β -elemene sandalwood α - and β -farnesene trans- α -bergamotene	Flavours & fragrances;	<i>R. sphaeroides</i>

Towards non-traditional microbial platforms for isoprenoid synthesis

It was previously reasoned that an ideal platform organism should support a streamlined flux towards universal precursors for the synthesis of a wide range of products (58, 59). Therefore, an isoprenoid-cell factory should synthesize the isoprenoid building-blocks IPP and DMAPP at a high rate. Subsequently, genes for the synthesis of any isoprenoid of interest can be plugged in for the intended bioprocess. Bulk synthesis of isoprenoid molecules via *E. coli* and *S. cerevisiae* has already been obtained (60, 61). Nevertheless, recent improvements in

genome editing tools for faster metabolic engineering have allowed to explore other microorganisms as potential platforms (16, 20). Usually, these candidates are chosen due to their unique properties of their physiology and metabolism, which in principle could outperform traditional microbial platforms.

***Rhodobacter sphaeroides*: a model bacterium for fundamental studies with potential as cell factory for isoprenoid synthesis**

A microorganism known to have an interesting metabolism and physiology is *Rhodobacter sphaeroides* (62). This purple non-sulfuric (PNS) bacterium is a Gram-negative microorganism belonging to the class of α -proteobacteria, and has been employed as model organism to study photosynthesis (63, 64), quorum sensing (65) and chemotaxis (66). It is also a natural producer of economically relevant compounds like hydrogen (67), poly- β -hydroxybutyrate (68), carotenoids (69) and coenzyme Q₁₀ (CoQ₁₀) (49). The high metabolic versatility of *R. sphaeroides* (62, 70) is reflected by its ability to thrive under multiple growth conditions, using a wide range of substrates. In fact, this species can grow photolithoautotrophically, photoheterotrophically, chemolithoautotrophically and chemoheterotrophically (71). It is also able to fix nitrogen and CO₂, evolve hydrogen and utilize oxygen and other electron acceptors for respiratory purposes (71).

Regulatory networks in *R. sphaeroides*

This bacterium's metabolism is subjected to an intricate regulatory network (72), especially regarding the transition from aerobic to anaerobic growth, and *vice versa* (72). In fact, oxygen availability is known to modulate three regulatory systems in this species (73). In summary, two transcription factors (FnrL and PrrA) directly activate transcription of photosynthetic genes at low oxygen tension (Fig. 4a, b). On the other hand, PpsR represses the expression of those

genes at high oxygen tension (**Fig. 4c**). Molecular oxygen controls the FnrL protein, which contains a [4Fe-4S] cluster. When oxygen is limiting, this protein is in its active conformation and activates transcription of photosynthetic genes (**Fig. 4a**). On the other hand, increasing oxygen tensions determine the oxidation of the metal cluster of FnrL, thereby inactivating its transcriptional function (**Fig. 4a**). The second known regulatory mechanism is monitored by the *cbb₃*-type cytochrome *c* oxidase (**Fig. 4b**), which can sense the electron flow through the cytoplasmic membrane as consequence of respiration. When a proton motive force is established over the membrane, the *cbb₃* oxidase protein inhibits the two-component system formed by the transcriptional activators PrrA and PrrB, which are responsible to regulate expression of photosynthetic and CO₂ fixing genes. The third regulatory system is coordinated by the AppA-PpsR proteins (**Fig. 4c**), which is also responsible of controlling expression of photosynthetic machinery depending on oxygen tensions. More precisely, at high oxygen tension PpsR inhibits synthesis of *bchl* (bacteriochlorophylls) and *crt* (carotenoids) biosynthetic operons, while AppA acts at low oxygen tensions as derepressor on PpsR. Integration of the knowledge from these regulatory studies allowed to get a better comprehension on the physiology of *R. sphaeroides* while transitioning between aerobic and photosynthetic growth (74, 75). These oxygen-dependent regulatory networks revealed to be involved also in morphological changes in *R. sphaeroides*. In fact, upon low oxygen tensions, intracytoplasmic membranes are generated, which get packed with photosynthetic machineries containing isoprenoid-derived molecules like carotenoids (69) or bacteriochlorophylls (76).

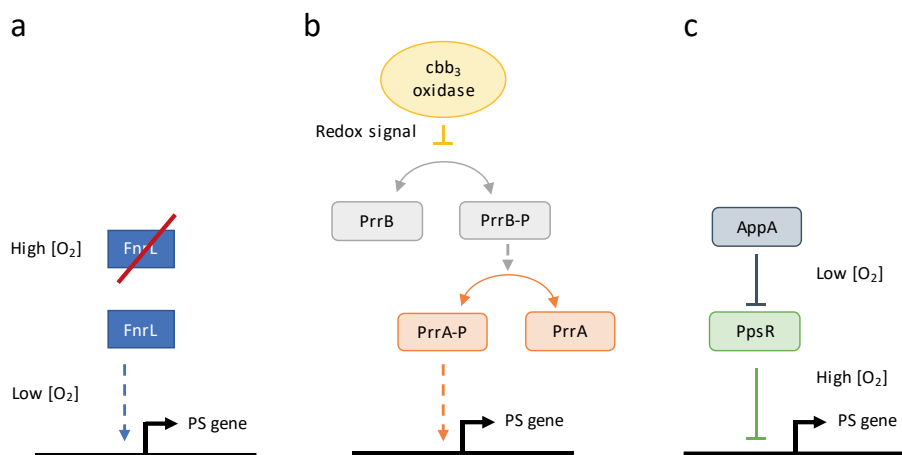


Figure 4. Representation of the three regulatory mechanisms controlling oxygen-based genes expression in *R. sphaeroides*. a) FnrL, b) *cbb₃*-type cytochrome c oxidase and PrrA-PrrB and c) PpsR/AppA. PS gene: photosynthetic gene. The figure is adapted from (75).

Developing *R. sphaeroides* as microbial cell factory for isoprenoid synthesis

R. sphaeroides is a natural producer of the isoprenoid coenzyme Q_{10} (CoQ₁₀) (49, 77), a compound with antioxidant properties and therefore interesting as nutraceutical. Studies on different growth modes were made to assess TRY values for CoQ₁₀ production in this organism, revealing that chemoheterotrophic cultivation under aerobic-dark condition with low oxygen tension is superior to anaerobic-light cultivation (78). Then, different reactor types and cultivation strategies were investigated for the production of CoQ₁₀ in this species (79, 80), eventually leading to pilot scale cultivation in a 150-L-reactor (81). Moreover, employment of phosphate limitation has been reported to increase CoQ₁₀ production in *R. sphaeroides* (82).

Genetic toolboxes are available for this species, which is genetically accessible via biparental conjugation (83), although electroporation has also been reported once (84). These tools consist of a replicative plasmid for heterologous gene expression (85, 86), a suicide plasmid for gene deletions or insertions (87) and a

set of characterized promoters and ribosome-binding-sites (RBSs) (88, 89). These tools have been used for exploring heterologous production of non-native isoprenoids like lycopene (90) and sesquiterpenes (91, 92), thereby expanding the portfolio of isoprenoids produced by this species. Also, application of a heterologous mevalonate pathway has been reported (91). In addition, several works reported metabolic engineering approaches for increasing CoQ₁₀ production. For example, expression of MEP pathway enzymes has been thoroughly tuned by using heterologous promoters and regulators (93). Moreover, debottlenecking of the downstream pathway towards CoQ₁₀ has been implemented (94, 95). Also, reports are available on strategies for engineering oxygen uptake rate (96), as well as the manipulation of the regulatory protein PpsR (97). Eventually, engineering of the redox metabolism for enhanced production has also been reported (96, 98, 99). Although a genome-scale metabolic model exists for this species (100, 101), its use for studying isoprenoid synthesis has not been reported yet.

Challenges for consolidating *R. sphaeroides* as cell factory for isoprenoid synthesis

Standardized and rapid DBTL cycles would allow to strengthen *R. sphaeroides* role as microbial cell factory for isoprenoid synthesis. All the aforementioned studies for understanding and improving isoprenoids production in *R. sphaeroides* have been performed in rich media, containing undefined substrates like yeast extract, molasses or corn steep liquor. Such a medium composition makes determination of substrate contributions to production cumbersome. On the contrary, employment of defined media would allow to thoroughly characterize the effect of different substrates to isoprenoid synthesis. Implementation of such a setup is encouraged for standardizing the ‘test’ phase of DBTL cycles. Also, determination of intracellular fluxes

contributing to product formation would aid the design of new rational engineering approaches for increasing isoprenoid biosynthesis. Moreover, although genetic tools are available for this bacterium, improving their efficiency would accelerate the ‘build’ phase of the cycle. Eventually, these tools could be integrated for better understanding and engineering isoprenoid metabolism in *R. sphaeroides*. These considerations motivated the study presented in this thesis.

Aim and outline of this thesis

The goal of this thesis is to implement tools for accelerating DBTL cycles in *R. sphaeroides*, while studying and improving isoprenoid production in this species.

Chapter 2 describes how we designed a system based on a defined medium for studying the physiology of *R. sphaeroides* during chemoheterotrophic isoprenoid synthesis. Moreover, we cloned the gene for the synthesis of an excretable isoprenoid reporter molecule (amorpha-4,11-diene) for facilitating product determination. We therefore used such a setup for screening different carbon substrates and determining the impact of nutrient limitations (nitrogen and oxygen) to product yields.

To improve the genome editing toolkit in this species, we developed a highly-efficient CRISPR-Cas9 editing tool in **chapter 3**. Moreover, we employed this new tool for characterizing the pathway supporting poly- β -hydroxybutyrate (PHB) synthesis during growth on glucose.

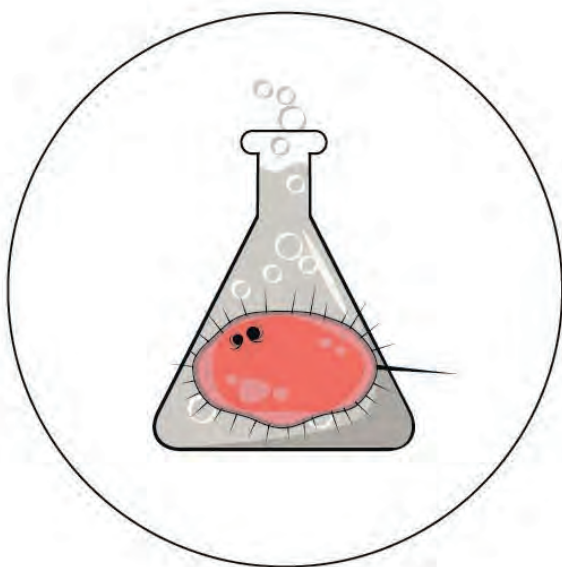
We reasoned that the regulation acting on the endogenous MEP pathway might entangle engineering efforts for improving isoprenoid production. **Chapter 4** shows how we designed and implemented the functional replacement of this pathway with a heterologous MVA pathway. We used ^{13}C cultivation to

determine the functional replacement of the two isoprenoid pathways. Eventually, we assessed the effect of increasing MVA enzymes expression on the novel strain and compared it to the parental one still expressing both isoprenoid pathways.

In **chapter 5**, we developed a ^{13}C -based method for assessing pathway contributions to isoprenoid synthesis. This method employed parallel labeling cultivations with $[1-^{13}\text{C}]$ - and $[4-^{13}\text{C}]$ glucose as tracers. Therefore, it was used to measure the metabolic flux ratio within the glycolysis and in isoprenoid metabolism, and study the effect of co-expressing both isoprenoid pathways.

Eventually, in **chapter 6** we combined the knowledge from all previous chapters for uncoupling isoprenoid synthesis from microbial growth. We assessed the effect of inactivating PHB synthesis and the endogenous MEP pathway for isoprenoid production. We assessed these effects during different growth conditions by determining the titers, rates and yields of the reporter molecule amorphaadiene.

Chapter 7 contains a summary of the work presented in this thesis. Moreover, it further discusses the results within the general scope of the thesis, while including additional experiments not reported in the previous chapters. In conclusion, suggestions for further understanding and improving isoprenoid synthesis in *R. sphaeroides* are reported, as well as a final consideration of this bacterium as platform for isoprenoid production.



Chapter 2

Characterization of heterotrophic growth and sesquiterpene production by *Rhodobacter* *sphaeroides* on a defined medium

This chapter has been published as: Orsi, E., Folch, P. L., Monje-López, V. T., Fernhout, B. M., Turcato, A., Kengen, S. W., Eggink, G. & Weusthuis, R. A. (2019). Characterization of heterotrophic growth and sesquiterpene production by *Rhodobacter sphaeroides* on a defined medium. *Journal of industrial microbiology & biotechnology*, 46(8), 1179-1190.

Abstract

R*hodobacter sphaeroides* is a metabolically versatile bacterium capable of producing terpenes natively. Surprisingly, terpene biosynthesis in this species has always been investigated in complex media, with unknown compounds possibly acting as carbon and nitrogen sources. Here, a defined medium was adapted for *R. sphaeroides* dark heterotrophic growth, and was used to investigate the conversion of different organic substrates into the reporter terpene amorphaadiene. The amorphaadiene synthase was cloned in *R. sphaeroides*, allowing its biosynthesis via the native 2-methyl-D-erythritol-4-phosphate (MEP) pathway and, additionally, via a heterologous mevalonate one. The latter condition increased titers up to 8-fold. Consequently, better yields and productivities to previously reported complex media cultivations were achieved. Productivity was further investigated under different cultivation conditions, including nitrogen and oxygen availability. This novel cultivation setup provided useful insight into the understanding of terpene biosynthesis in *R. sphaeroides*, allowing to better comprehend its dynamics and regulation during chemoheterotrophic cultivation.

Keywords

Rhodobacter sphaeroides, amorphaadiene, PHB, MEP, Mevalonate.

Introduction

The purple non-sulfur bacterium *Rhodobacter sphaeroides* is a metabolically versatile microorganism capable of growing *e.g.* aerobically and anaerobically, photoautotrophically and heterotrophically (70, 102). *R. sphaeroides* is therefore used as a model organism to study transcriptional regulation occurring during the transition from aerobic to photosynthetic metabolism (64, 73, 103). Additionally, its photosystem (104) and its quorum sensing mechanism (65) have been investigated. More recently, industrial application of *R. sphaeroides* has been explored with respect to photoheterotrophic hydrogen biosynthesis (67) and chemoheterotrophic terpene production (91, 93).

Terpenes form the largest class of natural products with regard to their structural diversity and are synthesized by all organisms (105). Interest for their application in the bioeconomy is increasing. Currently they are used in the pharma and nutraceutical sectors (8, 40, 46, 106, 107), and they show potential for application also in the polymer industry (108) and as advanced biofuel (53, 109).

The structure of terpenes consists of a backbone of one or multiple isoprene units, with optional addition of other functional groups. Isoprene is synthesized via the mevalonate (MVA) pathway or the 2-methyl-D-erythritol-4-phosphate (MEP) pathway. The MVA pathway uses acetyl-CoA (Ac-CoA) and acetoacetyl-CoA (AA-CoA) as precursors, while the MEP pathway branches from glyceraldehyde-3-phosphate (GAP) and pyruvate. The MVA pathway is present in eukaryotes, most archaea and some Gram-positive bacteria, whereas all other prokaryotes use the MEP pathway. Only a few bacteria have both pathways (107). Eventually, the two metabolic routes converge in the synthesis of the isoprene unit isopentenyl diphosphate (IPP) and its isomer dimethylallyl

diphosphate (DMAPP). These two compounds are the building blocks for generating the different terpenes.

R. sphaeroides is well known for its production of carotenoids and coenzyme Q₁₀ (CoQ₁₀). Both are synthesized via the MEP pathway, which is the native terpene biosynthetic route of *R. sphaeroides* (93). Regulation of this pathway is known to occur through feedback inhibition by IPP and DMAPP (110) and, at the transcriptional level, by oxygen tension (78, 111). Various genetic engineering approaches have been performed on the MEP pathway of *R. sphaeroides* with the aim to increase the yield of CoQ₁₀ (95, 99, 112). The natural ability of *R. sphaeroides* to form terpenes has also been used for the production of aromatic terpenes for fragrances by expressing non-native terpene synthases, like valencene synthase (91). To increase the terpene production capacity the MVA pathway from *Paracoccus zeaxanthinifaciens* (113) has been introduced (114). This microorganism was chosen because it is a member of the α -proteobacteria class, and therefore phylogenetically more closely related to *R. sphaeroides*.

To further improve terpene production in *R. sphaeroides*, thorough understanding of its physiology and regulation are required. All knowledge obtained so far regard this species is focused on CoQ₁₀ production (80, 95), with the exception of lycopene (90). Nevertheless, the current cultivation system has the following disadvantages: laborious extraction procedure for intracellular product determination (need of biomass collection and solvents-based extraction), and low yields and titers of CoQ₁₀ despite cultivation in rich media. It is therefore preferred to switch to a setup with defined medium and single carbon source. Moreover, the employment of a secreted reporter molecule would make product recovery and quantification easier.

In this work, adaptation of a defined Siström's minimal medium (115) for dark heterotrophic growth and terpene production is presented. Moreover, the sesquiterpene amorphadiene (amorpha-4,11-diene (amorphadiene from now on)) was chosen as reporter molecule, allowing to obtain comparable yields to the literature employing rich medium for CoQ₁₀ biosynthesis. Therefore, amorphadiene production was described in respect of growth and growth-limited conditions induced by nutrients limitation. Two *R. sphaeroides* strains were used for this study. While one strain relies on IPP production exclusively via the native MEP pathway (MEP strain), the other additionally employs a heterologous MVA pathway (MEP+MVA strain). The results obtained contribute to improve the understanding of the versatile metabolism of *R. sphaeroides*. It also offers a new cultivation setup for further investigating the potential of its dark heterotrophic metabolism for biotechnological applications.

Material and methods

Bacterial strains and plasmids

The strains and plasmids used are listed in **Table 1**. The strains and the plasmids not generated in this study were kindly provided by Isobionics BV.

Table 1. Bacterial strains and plasmids used in this study.

	Characteristics	Reference
Strains		
MEP	Derivative of <i>R. sphaeroides</i> ATCC 35053 carrying pMEP. It expresses the gene amorphadiene synthase (<i>ads</i>) and supports terpene production via the native MEP pathway.	This study
MEP+MVA	Derivative of <i>R. sphaeroides</i> ATCC 35053 carrying pMVA. It expresses the gene amorphadiene synthase (<i>ads</i>) and supports terpene production via the native MEP pathway and the heterologous MVA pathway	(91, 114)
<i>E. coli</i> S17-1 (ATCC 47055)	Donor strain for di-parental conjugation	(116)
Plasmids		
pBBR1MCS-2	pBBR1 origin of replication, Km ^R , Mob site for mobilization during conjugation	(117)
pMEP	pBBR1MCS-2 + <i>crtE</i> promoter and <i>ads</i> (amorphadiene synthase)	This study
pMVA	pBBR1MCS-2 + <i>PcrtE-ads</i> + MVA enzymes	(114)

Plasmid construction

The pBBR-*ads* plasmid (pMEP) was generated via restriction digestion. The amorphadiene synthase gene (*ads*) and its promoter *PcrtE* harbored in the pBBR-MVA-*ads* (pMVA) plasmid were PCR amplified with overhangs for BamHI and

SacI using the primers P17 (CAAAGAGCTCGGCGCGGGGCGCG) and P18 (ATTTGGATCCTTATCAGATCGACATGGGGTACACGAGC). The PCR amplicon and an empty pBBR1MCS-2 plasmid were digested with the two restriction enzymes and ligated in competent *Escherichia coli* TOP10 cells. Ligation was confirmed by colony PCR and sequencing. The isolated plasmid was conjugated in *R. sphaeroides* via di-parental conjugation mediated by *E. coli* S17-1 (ATC 47055). Successful conjugants were isolated, and the plasmid was sequenced. The primers used for sequencing were: P47: ATGTGCTGCAAGGCGATT; P48: TGACCGAGGAAAAGCCGAT; P49: AACTATAAGGACAAGAACGG; P50: TCGAGTGCTATTCTGGGG; P51: AGGAGTGCTCCGCTCCT; P52: GTTGAACAGGTCCGTGCG.

Growth conditions

Cultivation of *R. sphaeroides* on defined minimal medium was performed using a modified Sistrom's minimal medium (SMM) containing, if not differently specified: 3 or 10 g/L glucose, 3.48 g/L KH_2PO_4 , 0.5 g/L NH_4Cl , 0.1 g/L glutamic acid, 0.04 g/L L-aspartic acid, 0.5 g/L NaCl, 0.02 g/L nitrilotriacetic acid, 0.3 g/L $\text{MgSO}_4 \cdot 7\text{H}_2\text{O}$, 0.0334 g/L $\text{CaCl}_2 \cdot 2\text{H}_2\text{O}$, 0.002 g/L $\text{FeSO}_4 \cdot 7\text{H}_2\text{O}$, 0.0002 g/L $(\text{NH}_4)_6\text{Mo}_7\text{O}_{24}$. Trace elements were added 0.01 % v/v from a stock solution containing: 17.65 g/L disodium EDTA, 109.5 g/L $\text{ZnSO}_4 \cdot 7\text{H}_2\text{O}$, 50 g/L $\text{FeSO}_4 \cdot 7\text{H}_2\text{O}$, 15.4 g/L $\text{MnSO}_4 \cdot 7\text{H}_2\text{O}$, 3.92 g/L $\text{CuSO}_4 \cdot 5\text{H}_2\text{O}$, 2.48 g/L $\text{Co}(\text{NO}_3)_2 \cdot 6\text{H}_2\text{O}$, 0.0114 g/L H_3BO_3 . Vitamins were added 0.01 % v/v from a stock containing: 10 g/L nicotinic acid, 5 g/L thiamine HCl, 0.1 g/L biotin.

Preculturing of *R. sphaeroides* containing either pMEP or pMVA started by transferring the strains from frozen stock to Luria Bertani (LB) agar plates supplemented with kanamycin 50 $\mu\text{g}/\text{mL}$. Plates were incubated at 30 °C up to 72 h, until colonies were visible. Single colonies were passed from LB plates to 5

mL liquid LB containing 50 µg/mL kanamycin and incubated for 24 h at 30 °C with agitation rates of 250 rpm. Subsequently, the LB culture was conveyed in 250- or 300-mL Erlenmeyer flasks with 20% v/v of liquid Sistrom's minimal medium (SMM) with 10 g/L glucose, 3.5 g/L NH₄Cl and 50 µg/mL kanamycin. The precultures were incubated overnight at 30 °C, 250 rpm. Exponentially growing precultures were then harvested and, if necessary, washed twice with 9 g/L NaCl before being transferred to the cultivation medium.

Screening for alternative carbon substrates

All cultivations were performed in a Kühner shaker incubator at 30 °C and with agitation rates of 250 rpm. *R. sphaeroides* strain MEP+MVA was grown on SMM using glucose as carbon source until mid-log phase. The cells were harvested by centrifugation at 8000g for 10 min at room temperature, washed with 9 g/L NaCl and inoculated in SMM supplemented with the selected carbon source at a concentration (normalized for 10 g/L glucose) of 0.333 Cmol/L. Biological duplicates for each carbon source were grown in square bottom Applikon deep-well microtiter 24 wells polystyrene plates, incubated at 30 °C and agitation rates of 250 rpm. Growth was monitored over time by measuring the absorbance at OD₆₀₀ using a Tecan Infinite M200 plate reader. In parallel, for amorphadiene detection, biological duplicates were inoculated in 100-mL shake flasks filled with 20 mL SMM with the selected carbon source and containing 10% v/v filter sterilized dodecane in the liquid phase.

Shake flasks cultivation

Cultivation in shake flasks was performed in 250-mL Erlenmeyer flasks filled with 50 mL of SMM medium and filter sterilized dodecane (10% v/v of the liquid phase). The cultures were inoculated with a starting OD₆₀₀ of 0.1 from exponentially growing precultures on SMM medium. The flasks were incubated

as biological duplicates at 30 °C under an agitation of 250 rpm. Growth was monitored by measuring the absorbance at 600 nm. For assessment of nitrogen limitation on production, SMM medium with different initial NH_4Cl concentrations (0.25 – 1.0 g/L) was employed. Initial glucose concentration was set at 3 g/L. Amorphadiene was measured once glucose depleted, and the pellet composition was analysed using the Total Organic Carbon analyser (TOC-L, Shimadzu).

Bioreactor cultivation

R. sphaeroides containing either pMEP (MEP strain) or pMVA (MEP+MVA strain) were cultivated at 30 °C in 0.5-L MiniBio 500 reactors from Applikon, with a working volume of 400 mL and 10% v/v of dodecane as organic phase. The bioreactors were sparged with 5 mL/min of compressed technical air and a continuous stirring of 1000 rpm was applied.

The dissolved oxygen tension (DO) was kept at 40% by automatically varying the ratio between technical air and N_2 . The pH was maintained at 7.0 by automatic addition of 2.5 M NaOH. The bioreactors were inoculated with a starting OD_{600} of 0.25 from precultures grown in 250-mL shaker flasks containing 50 mL medium and 3.5 g/L NH_4Cl . Samples of 2-15 mL were regularly taken to determine cell density and composition, substrate consumption and product formation.

Effect of aeration on terpene biosynthesis

The effect of aeration on terpene biosynthesis was assessed by calculating amorphadiene yield on glucose (mg/g) after 48 h cultivation of 250-mL Erlenmeyer flasks containing different medium volumes. The medium used was SMM with 3 g/L of glucose and 1 g/L of NH_4Cl (starting C/N in the medium below

5.5), which allowed an extended exponential growth. Preculturing of the MEP and MEP+MVA strains followed the protocol described in the correspondent section. Exponentially growing precultures were inoculated with a starting OD₆₀₀ of 0.1 in the following volumes of SMM (10 % v/v of dodecane): 10, 25, 100, 200 mL. At the end of the cultivation, the content of the flask was spun at 4255 g for 5 minutes; the dodecane layer and the supernatant were collected for amorphadiene and glucose detection, respectively.

Experimental design and statistical analysis

The cell density was monitored by measuring the optical density (OD₆₀₀). The amorphadiene concentration was determined by dissolving 5% or 10% of the dodecane collected from the cultivations in ethyl acetate containing 0.2 mM tetradecane as internal standard. Samples were analysed on GC-FID 7890A from Agilent using a RESTEK Rxi-5ms column 0.25 µm (5% diphenyl, 95% dimethylpolysiloxane). Since amorphadiene is not commercially available, its isomer valencene (80% pure, kindly provided by Isobionics BV) was used as standard for calibration. The glucose and organic acids concentrations were determined by using an Agilent 1290 Infinity (U)HPLC equipped with a guard column (Security Guard Cartridge System, Phenomenex). The compounds were separated on an organic acid column (Rezex ROA-Organic acid H⁺ 8% column, Phenomenex) at 55 °C with a flow of 0.5 mL/min 0.005 M H₂SO₄ as eluent. Alternatively, glucose was also measured with YSI 2950 from Shimadzu.

PHB was determined by centrifuging 10 mL culture at 4255 g for 20 min at room temperature. The supernatant was discarded and the cells were washed and centrifuged twice with MilliQ water. Finally, the pellet was dried at 100 °C. The dried pellet was treated as described previously (118) and the PHB concentration was determined as crotonic acid using an Agilent 1290 Infinity (U)HPLC, using the

same guard and elution column as for the glucose and organic acids determination.

The organic carbon and nitrogen content in pellet and supernatant was measured as non-purgeable organic carbon (NPOC) and as total nitrogen (TN) using a Total Organic Carbon analyser (TOC-L) from Shimadzu. The nitrogen content measured in the pellet was used to calculate the amount of active biomass using the elemental composition of *R. sphaeroides* $\text{CH}_{1.99}\text{O}_{0.5}\text{N}_{0.19}$, previously described in literature for photoheterotrophic growth (119). The C/N of the cells was calculated by dividing the NPOC and the TN values measured for the pellets.

Results

Amorphadiene as reporter molecule

Previous studies demonstrated that the best cultivation condition for terpene production in *R. sphaeroides* is heterotrophic dark cultivation (78) and this operational mode has been used ever since (79–81). An attempt to summarize the yields and productivities already reported in literature for this species is shown in **Table 2**. As can be observed, all the data focused on production of coenzyme Q₁₀ (CoQ₁₀, C₅₉H₉₀O₄). Studying terpene biosynthesis using this molecule has several disadvantages, including the need of extraction for product quantification. Moreover, its complex structure and high molecular weight (863 g/mol) do not make it an ideal candidate for that purpose. Therefore, it was decided to engineer *R. sphaeroides* for producing the sesquiterpene amorphadiene as reporter molecule. Such approach was already established in model organisms like *Escherichia coli* or *Saccharomyces cerevisiae* (42, 61). This molecule (204 g/mol) is easily secreted by the microorganism and can be collected in an organic layer using a two-phase cultivation. *R. sphaeroides* was

conjugated with a pBBR1MCS2 plasmid containing a heterologous MVA pathway derived from *Paracoccus zeaxanthinifaciens* (113, 114) expressing the gene for amorphaadiene synthase (*ads*). From this plasmid, the *ads* gene under the control of the *PcrtE* promoter was amplified and inserted via restriction-ligation in an empty pBBR1MCS2 plasmid. Therefore, two *R. sphaeroides* strains were used, one synthesizing amorphaadiene based only on the contribution of the native MEP pathway (MEP strain) and the other via co-expression of the MEP and constitutive MVA pathways (MEP+MVA strain). Product formation was confirmed for both strains via GC-FID determination.

Table 2. Comparative results of terpene yields and productions from various cultivation types using complex and defined media.

Strain	Cultivation type	Yield (mol/mol glucose)	Production (mg/g CDW)	Medium	Reference
2.4.1 wt	Fed Batch	0.00030	3.53	Complex	(99)
2.4.1 Δ <i>sdhB</i>		0.00039	4.59	Complex	
2.4.1 wt	Batch	0.00026	3.66	Complex	(96)
2.4.1 <i>RspPpsR</i>		0.00037	4.91	Complex	
2.4.1 <i>RspPE</i>		0.00038	5.67	Complex	
2.4.1 <i>RspMSC</i>		0.00024	3.48	Complex	
2.4.1 <i>RspMegx</i>	Batch	0.0004	8.92	Complex	(95)
2.4.1 <i>RspMQd</i>		0.00072	12.94	Complex	
KACC 91339P	Batch	*	6.34	Complex	(81)
	Fed Batch	*	8.12	Complex	
BCRC 13100	Batch	*	4.6	Complex	(79)
	Fed Batch	*	4.4	Complex	
BCRC 13100	Batch	0.0003	8.0	Complex	(78)
ATCC35053 derived MEP	Reactor - Batch	0.0006 \pm 0.0001	1.41 \pm 0.11	Defined	This study
ATCC35053 derived			10.99 \pm 3.35	Defined	
MEP+MVA		0.0051 \pm 0.0014			

All results presented with complex medium are associated to previous literature focused on CoQ₁₀; instead, the data referred to defined medium was obtained using amorphaadiene as reporter terpene.

*cannot be obtained since molasses was used as carbon source.

Selection of carbon source for heterotrophic terpene biosynthesis

Another relevant feature shown in **Table 2** is the utilization of complex media for the biosynthesis of CoQ₁₀. Such an approach encumbers interpretation of substrates contribution to terpene biosynthesis. Nevertheless, Sistrof's minimal medium (SMM) is a defined medium already employed for growing *R. sphaeroides*, although under photoheterotrophic conditions (115).

We chose the same medium to assess its suitability for chemoheterotrophic growth using several carbon sources (at a concentration of 0.333 Cmol/L) as single substrates. The candidates chosen already proved to support growth under photoheterotrophic conditions (101), and can be relevant feedstocks for a biobased economy. As criteria for comparison, 'final amorphadiene titer' and 'biomass concentration' were used. The latter was expressed as maximal optical density (OD) measured at 600 nm. The outcome shows that sugars overall performed better than organic acids for supporting growth and terpene production (**Fig. 1**). While biomass concentrations and amorphadiene titers gave a similar outcome when sugars were used as substrates, a more pronounced variation was observed when organic acids were employed. The final ODs differed significantly, and not all acids supported amorphadiene synthesis. For instance, acetate resulted in a comparable biomass concentration as the sugars, but did not lead to any amorphadiene production. Succinate and malate resulted in similar microbial biomass concentrations, but the latter did not result in amorphadiene production. Glucose resulted in the highest biomass and terpene production, and was therefore chosen for further research.

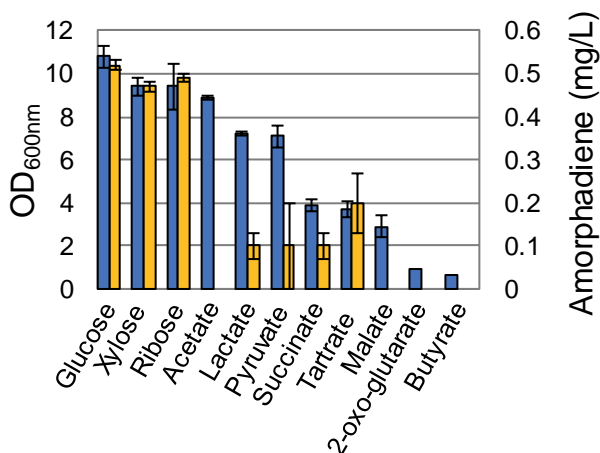


Figure 1. Screening of substrates for chemoheterotrophic amorphadiene biosynthesis in *Rhodobacter sphaeroides*. (MEP+MVA strain) was cultivated in modified Sistrom's minimal medium using microtiter plates. OD at 600nm (blue bars) and final amorphadiene titers (yellow bars) were used as parameters for the comparison. The initial concentration of the different substrates was normalized to 0.333 Cmol/L.

Growth and amorphadiene production in shake flasks

Further characterization of *R. sphaeroides* continued in shake flasks, where the behavior of MEP and MEP+MVA strains was compared. Growth was monitored over time (**Fig. 2**), and amorphadiene production was determined at the end of the cultivation. Two different initial glucose concentrations were tested: 3 g/L and 10 g/L. The two strains revealed a similar growth rate of $0.12 \pm 0.01 \text{ h}^{-1}$ at both sugar concentrations. After a short exponential phase, increase in absorbance continued in a rather linear mode until glucose depletion. This was observed best at the higher glucose concentration (**Fig. 2c, d**).

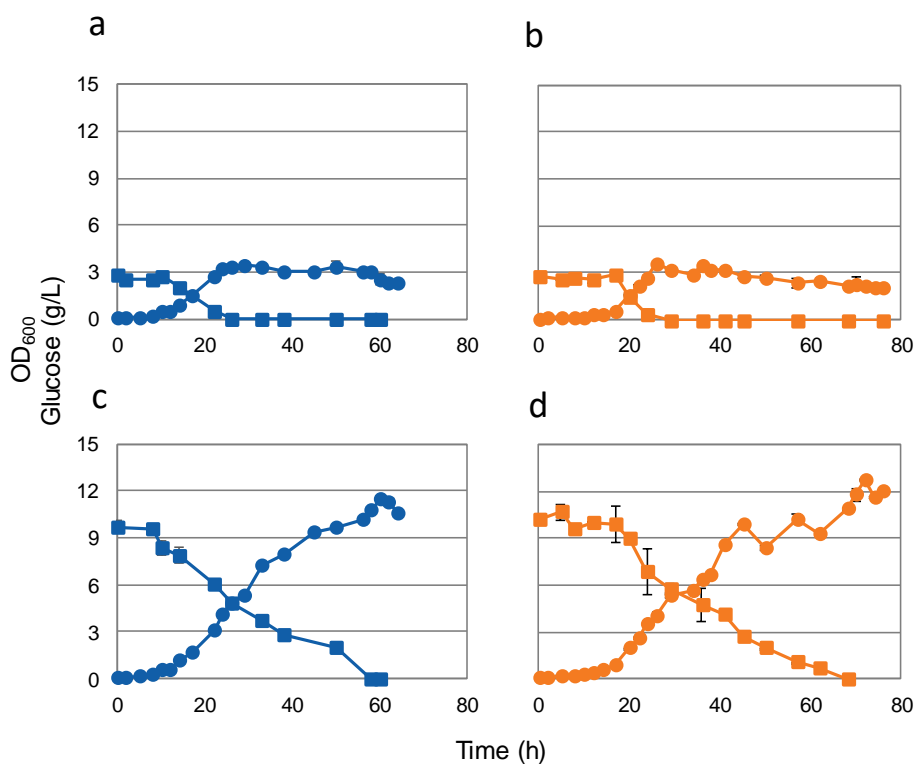


Figure 2. Growth profile in shake flasks. OD₆₀₀ and glucose profiles of 250-mL shake flasks cultivations of *Rhodobacter sphaeroides* MEP (a, c) and MEP+MVA strains (b, d) grown at the initial concentration of 3 g/L (a, b) or 10 g/L glucose (c, d). Circles: OD at 600nm; squares: glucose (g/L).

Amorphadiene titers amounted to similar levels for both glucose concentrations in the MEP strain. Their values were 1.8 ± 0.1 and 2.2 ± 0.2 mg/L for the 3 g/L and 10 g/L concentrations, respectively. For the MEP+MVA strain the difference between the two conditions was bigger. A 35% higher titer was measured in the culture with 10 g/L initial glucose concentration (30 ± 2 mg/L), compared to the 3 g/L initial glucose cultivation (22 ± 4 mg/L). The yield (mg amorphadiene/g glucose) was 12-fold higher and 13.5-fold higher for the MEP+MVA strain at 3 g/L and 10 g/L of glucose, respectively.

Aerobic growth and production of amorphadiene and PHB in a reactor

The linear growth observed (**Fig. 2c, d**) could be consequence of nutrient deficiency. In shake flasks oxygen is known to be a limiting nutrient (120). Moreover, low oxygen tension is known to be a major effector of important metabolic switches in *R. sphaeroides* (73). In order to allow enough oxygen transfer to the cultures, the batch cultivation was repeated in a 500-mL bioreactor, where the dissolved oxygen tension (DO) was kept constant at 40% air saturation (**Fig. 3**). Both the MEP and MEP+MVA strains were cultivated in SMM with 10 g/L of glucose, with 10% v/v dodecane as organic phase.

Amorphadiene production increased over time, with a 10-fold difference measured between the two strains at the end of the cultivation (**Fig. 3a**). The yield on glucose calculated at the end of the fermentation was included in **Table 2** for both strains. Analysis of the fermentation broth by HPLC showed that, except for glucose, no other organic compounds were present. Also in this case, a linear increase in OD was observed after a short exponential phase (μ_{\max} MEP+MVA: $0.123 \pm 0.002 \text{ h}^{-1}$ and μ_{\max} MEP: $0.136 \pm 0.006 \text{ h}^{-1}$). As the DO was maintained at 40% air saturation, linear growth could not have been caused by oxygen limitation. Evaluation of the medium composition indicated that nitrogen limitation could have occurred during the fermentation. N-limitation can be circumvented by fixing molecular N_2 , and *R. sphaeroides* is known to fix N_2 via a nitrogenase complex (119). Activity of the nitrogenase complex is extremely sensitive to oxygen (121). Therefore, no N_2 fixation was expected by *R. sphaeroides* under this experimental condition. To confirm a possible nitrogen limitation, the culture supernatant was analysed for total nitrogen (TN, via TOC-L). Moreover, the cell pellet was analysed for non-purgeable organic carbon (NPOC) and TN (both via TOC-L).

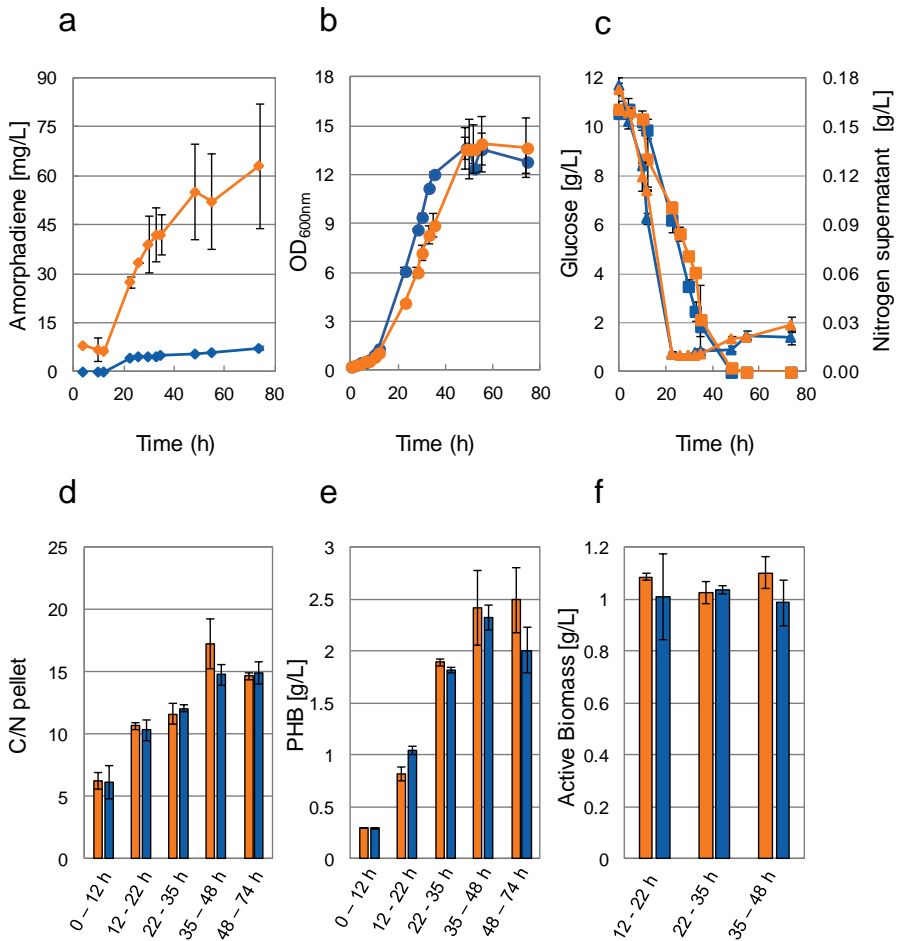


Figure 3. Heterotrophic cultivation of *Rhodobacter sphaeroides* MEP and MEP+MVA strains in 500-mL bioreactor. (a) Amorphadiene profile (diamonds) over time [mg/L]. (b) OD₆₀₀ profile (spheres). (c) Concentrations profiles [g/L] in the supernatant of glucose (squares) and nitrogen (triangles). (d) Pellet C/N and (e) intracellular PHB [g/L] during different time intervals within the batch cultivation. (f) Active biomass concentrations [g/L] during three different time intervals within the linear increase of OD₆₀₀. Blue: MEP strain; orange: MEP+MVA strain.

The switch from exponential to linear growth observed at 22 h (**Fig. 3b**) coincided with a depletion of nitrogen in the medium (**Fig. 3c**). This switch triggered the increase of the C/N ratio of the pellet over time, suggesting accumulation of a

storage compound (**Fig. 3d**). The increase of the C/N ratio of the pellet was constant through the whole linear phase and levelled off at the stationary phase. Phototrophically grown *R. sphaeroides* is known to accumulate poly- β -hydroxybutyrate (PHB) when cultivated under nitrogen-limiting conditions (119, 122). Accumulation of PHB under the applied heterotrophic growth conditions could explain the change in C/N ratio of the pellet. PHB accumulation could indeed be detected (**Fig. 3e**). Its accumulation stopped when the glucose in the medium was depleted, and the stationary phase was reached. From the TN measured in the pellet, it was possible to calculate the amount of active biomass (**Fig. 3f**) assuming the elemental composition of *R. sphaeroides* without PHB as $\text{CH}_{1.99}\text{O}_{0.5}\text{N}_{0.19}$, which corresponds to a C/N of 5.3 (119). The amount of active biomass did not increase during the linear growth phase and remained stable at about 1 g/L for both strains. Knowledge of the active biomass concentration allowed to calculate the specific productivity at the end of the fermentation, which resulted in about 8-fold increase comparing MEP to MEP+MVA strain (**Table 2**).

Growth phase dependent changes in PHB and amorphaadiene

To better comprehend the observed changes in PHB and amorphaadiene levels, we studied their production rates for each growth phase (**Fig. 4**): exponential (up to 22 h), linear (22-48 h), and stationary (48-74 h). Both strains showed a similar rate of PHB accumulation, which was highest during the linear growth phase (**Fig. 4a**). During the stationary phase, PHB was hardly produced, or even consumed. The rates of amorphaadiene biosynthesis differed significantly between the two strains (**Fig. 4b**). For both, the value was highest during the exponential phase, and – as observed before – was significantly higher for the MEP+MVA strain. Once PHB accumulation started, amorphaadiene biosynthesis stopped in the MEP strain. On the contrary, the MEP+MVA strain continued to produce

amorphadiene, albeit lower when compared to the exponential phase. During the stationary phase the MEP+MVA strain still produced amorphadiene, whereas production was negligible in the MEP strain. Interestingly, the fold difference in rates between the two strains was consistent during the exponential and stationary phases (5-fold higher for MEP+MVA strain). Nevertheless, during the PHB accumulation phase the MEP+MVA strain's rate was 20-fold higher compared to the one of the MEP strain. This suggest that the biggest difference in production between the two strains occurs during the accumulation of the storage compound.

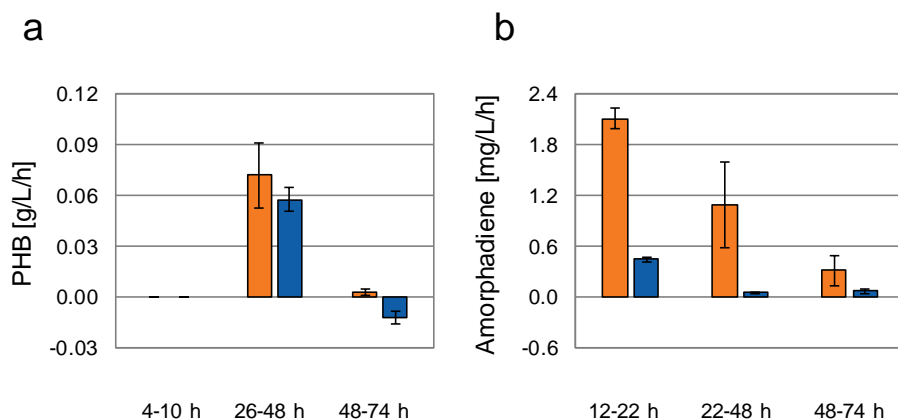


Figure 4. Volumetric rates. Values calculated for a) PHB and b) amorphadiene production calculated for the exponential, linear and stationary phase during chemoheterotrophic batch cultivation of *Rhodobacter sphaeroides* in a 500-mL bioreactor using defined medium. Orange: MEP+MVA strain, blue: MEP strain.

Effect of nitrogen limitation on cells' productivity

Volumetrically, amorphadiene biosynthesis seemed growth-associated. Nevertheless, growth-independent production of biotechnological compounds is an interesting approach, since less substrate would be consumed for biomass formation, allowing higher productivity per cell (123). To assess the potential as

growth-independent production platforms, the MEP and MEP+MVA strains were cultivated with different initial medium C/N. Amorphadiene productivity per grams of biomass was calculated at glucose depletion (**Fig. 5a**). Cells C/N was measured from the pellets at the end of the cultivation to confirm the different gradient of nutrient limitation (**Fig. 5b**). For both strains, the lowest NH_4Cl concentration (highest cells C/N) corresponded to the highest specific production (MEP: 15.6 ± 0.1 mg/g biomass; MEP+MVA: 109.6 ± 18.9 mg/g biomass). These values correspond respectively to a 5.6-fold and 4.4-fold increase compared to the condition with the highest NH_4Cl concentration (1 g/L, no nutrient limitation). Co-expression of MEP and MVA pathways in the MEP+MVA strain increased production during nutrient limitation, resulting in about 7-fold higher yield on biomass compared to the MEP strain at 0.25 g/L NH_4Cl .

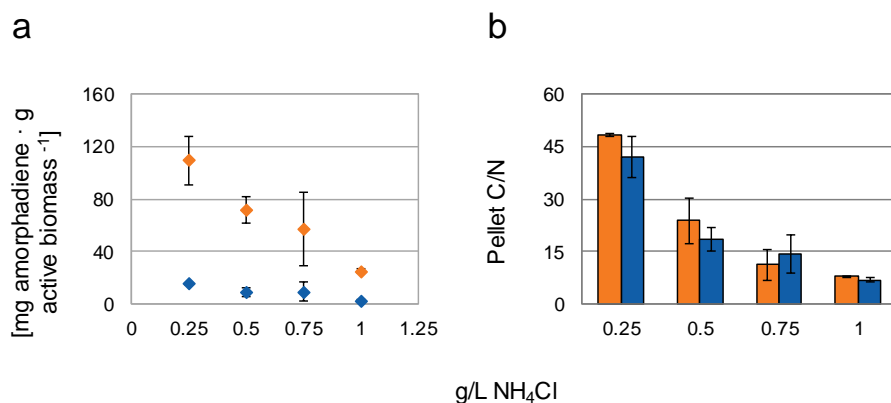


Figure 5. Effect of initial nitrogen concentration on a) amorphadiene/biomass ratio and b) on pellet C/N ratio in *R. sphaeroides*. Cultivation was performed in 250-mL shake flasks containing SMM with 3 g/L of glucose as substrate and different initial NH_4Cl concentrations. Amorphadiene was measured from the organic layer once glucose depleted in the spent medium. Orange diamonds: MEP+MVA strain, blue diamonds: MEP strain.

Effect of aeration on terpene yield

Experimental evidence excluded a role of oxygen in determining the aforementioned transition from exponential to linear growth (**Fig. 2, 3b**). Nevertheless, oxygen tension is known to trigger important metabolic and morphologic changes in *R. sphaeroides* (72, 73). In fact, a drop in the aeration determines biosynthesis of photosynthetic machineries, bacteriochlorophyll and carotenoids (76). Using a defined medium could allow to determine the effect of aeration on terpene yields and assess its regulatory effect when expressing an additional heterologous MVA pathway. Cultivations of MEP and MEP+MVA strains have been performed with different volumes of SMM medium. The volume of medium in the flask affects the size of surface available for oxygen exchange between liquid and gas phases. Therefore, a relatively high and low oxygen level was obtained by applying respectively a high and low headspace/liquid ratio in the flasks (124).

The SMM employed contained 3 g/L of glucose and 1 g/L of NH_4Cl . This initial C/N ratio in the medium of 4.6 would allow exponential growth until glucose depletion. Therefore, no PHB accumulation is expected to occur. Each strain yielded the highest amount of amorphadiene when the ratio between medium and the working volume of the flask was the highest (0.8 v/v). Both strains showed a pronounced yield improvement with the increase of media volume over total flask volume (**Fig. 6a**). Comparison of the yields between the two strains showed that the biggest difference occurred at the highest headspace/liquid ratio (**Fig. 6b**). In fact, the MEP+MVA strain gave an almost 50-fold higher yield than the MEP strain. This difference in yield gradually decreased with the increase of medium volume in the flask. Interestingly, also the fold changes in yields within the same strain were different. For the MEP strain

changing from maximal to minimal headspace/liquid ratio resulted in almost 40-fold yield increase, while for the MEP+MVA the change was barely 2-fold.

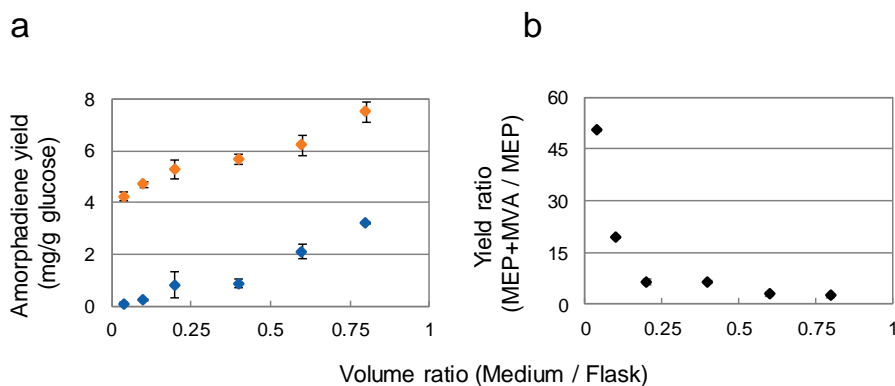


Figure 6. Effect of aeration on amorphadiene yield. *Rhodobacter sphaeroides* was cultivated with increasing volumes of liquid Sistrom's minimal medium in 250-mL shake flasks containing 1 g/L NH_4Cl and 3 g/L glucose. (a) Correlation between liquid volume ratio in the flasks and yield of amorphadiene on glucose for the MEP (blue diamonds) and MEP+MVA (orange diamonds) strains. (b) Relationship between the liquid volume ratio in the flasks and the yield ratio between the two strains.

Discussion

The bio-based economy can benefit from the exploitation of industrial microorganisms for the production of economically relevant molecules (6). Terpenes are among this type of compounds. Because of its versatile metabolism, the natural terpenoid producer *R. sphaeroides* offers an interesting platform for studying chemoheterotrophic production of these compounds and their regulation. Surprisingly, no information was available yet about chemoheterotrophic terpenoid biosynthesis in this bacterium employing defined medium. Here, a defined cultivation method was developed for identifying substrate-to-product conversions during terpene biosynthesis. Moreover, by expressing the amorphadiene synthase (*ads*) gene, it was possible to select an easily detectable reporter terpene via a two-phase cultivation

system. Eventually, biosynthesis of amorphadiene on SMM allowed to reach comparable or even higher yields (mol/mol) to the ones reported for CoQ₁₀ synthesized via complex medium (**Table 2**). Therefore, the proposed setup allowed to further characterize the physiological behaviour associated to terpene biosynthesis in *R. sphaeroides* while using a single substrate.

An initial screening was performed to determine the optimal substrate supporting chemoheterotrophic growth and amorphadiene production in *R. sphaeroides*. The outcome revealed that consumption of sugars resulted in higher amorphadiene titers compared to organic acids. In particular, glucose resulted in the highest amorphadiene titer. Because measurement of the biomass concentration as OD₆₀₀ was affected by nitrogen limitation, interpretation of effect of the substrate on growth can be biased. Since glucose catabolism revealed to be associated with the accumulation of a storage compound, a similar interpretation can in principle be extended to consumption of other substrates.

Amorphadiene biosynthesis in the MEP strain was clearly growth-associated since production occurred only during biomass formation. This result was coherent with what was previously shown for *R. sphaeroides* producing CoQ₁₀ (78). Exponential growth resulted in the highest rate of amorphadiene biosynthesis also for the MEP+MVA pathway. Nevertheless, growth inhibition caused by nutrient limitation resulted in no amorphadiene production in the MEP strain. On the contrary, it allowed terpene biosynthesis in the MEP+MVA strain while PHB was stored, reaching a 8-fold increase in titer and productivity. PHB accumulation has already been described as major by-product also during photoheterotrophic H₂ fermentation as consequence of nitrogen limitation (125, 126). Both PHB and MVA pathways share acetoacetyl-CoA as committed

precursor. Such proximity between the two metabolic routes and constitutive expression of the MVA enzymes could explain the persistence of amorphadiene production also during growth limitation.

Incremented intracellular PHB resulted in increase of pellet C/N, and resulted in a linear increase in OD₆₀₀. The absence of other organic compounds detected via HPLC implies that PHB was the major by-product of the process. Accumulation of this storage compound is known to function as carbon sink and as NADPH oxidation option during nutrient limitation (127). NADP⁺ regeneration via PHB formation could help in providing a sink for reducing equivalent to support glucose catabolism when biomass accumulation is prevented. Two pathways can reduce NADP⁺ during glucose catabolism. These are the pentose phosphate pathway and the Entner-Doudoroff (ED) pathway. The latter is known to be the main glycolytic pathway employed by *R. sphaeroides* (128). Therefore, it is suggested that PHB formation could be exploited as carbon sink and cofactor regeneration pathway for supporting glucose catabolism via the ED pathway during nutrient limitation. Such hypothesis could benefit from cultivation with ¹³C substrates for quantifying glycolytic pathways contribution under these conditions. Nevertheless, connection between the reducing equivalents of ED and PHB pathways was already proven in *E. coli* (127). Additional supporting evidence of their association was that overexpression of the NADP(H)-dependent enzymes of the two pathways resulted in increased PHB accumulation in the same species (129).

Although the highest volumetric rate of amorphadiene production occurred during exponential growth (**Fig. 4b**), its molecular formula (C₁₅H₂₄) suggests that its biosynthesis could in principle increase during nitrogen-limited conditions (123). In such scenario no carbon would be directed towards amino acid and

protein biosynthesis, allowing a higher carbon flux towards amorphaadiene, as previously suggested for its production in *E. coli* (60). Consistently, cultivation of *R. sphaeroides* under nutrient limitation increased cells productivity (**Fig. 5**). Expression of a heterologous MVA pathway proved to support amorphaadiene biosynthesis even further under these circumstances. Further research to increase terpene biosynthesis under growth-independent conditions (*e.g.* via rational re-design of *R. sphaeroides* metabolism) is therefore desirable.

Oxygen is known to be a major environmental factor regulating *R. sphaeroides* metabolism. Variations in oxygen tension affect the transcriptional regulation coordinated by three main systems: FnrL, PrrA/PrrB and PpsR (73, 130). Among these candidates, PpsR is known to inhibit transcription of carotenoids and MEP associated genes (97, 131). By varying the volume of headspace transfer in the cultures, it was possible to qualitatively assess the effect of aeration on amorphaadiene biosynthesis. The first piece of evidence was that both strains produced the highest amount of amorphaadiene when the headspace volume was lowest. Nevertheless, presence of the MVA pathway allowed higher yields also when the headspace volume was maximal, suggesting a bypass of the native oxygen-based regulation affecting the native MEP pathway. By reducing the volume of air in the flask, and accordingly the oxygen supply, the yield difference between the two strains decreased progressively. Accordingly, the MEP strain showed a higher yield-fold increase switching from maximal to minimal headspace volume, while for the MEP+MVA strain this increase was moderate. MEP pathway expression is triggered by low oxygen tension (131), when it supports biosynthesis of photosystem-associated molecules like carotenoids. Therefore, its activation can be expected under micro-aerobic conditions in both strains. Interestingly, the two strains showed a similar trend of variation in yield moving from maximal to minimal headspace volume. This suggests that an

improved yield in the MEP+MVA strain could be orchestrated by an increased contribution of the native MEP pathway. This speculation would benefit from analysis of the split ratio of the two terpene biosynthetic routes *e.g.* by ^{13}C -labeled cultivation. Furthermore, genetic engineering approaches could be used for deregulating the native MEP pathway, as already attempted for reducing competitive expression of carotenoids during coenzyme Q₁₀ biosynthesis (97).

This work describes the implementation of a novel cultivation system for studying the heterotrophic metabolism of *R. sphaeroides* under defined culture conditions. Moreover, it was employed for investigating the dynamics of terpene biosynthesis in this species using different organic substrates and nutrients (nitrogen and oxygen) availabilities. When introducing a heterologous mevalonate pathway and amorphaadiene synthase, the highest yields reported for this species were achieved. All in all, this study serves as basis for further improving the metabolism of *R. sphaeroides* for enhanced terpene biosynthesis.

Acknowledgements

We thank P. Uhl for technical assistance and A. Kruis for critical revision of the manuscript. Furthermore, we thank Applikon, The Netherlands, for providing the Mini Bioreactors used in this study.

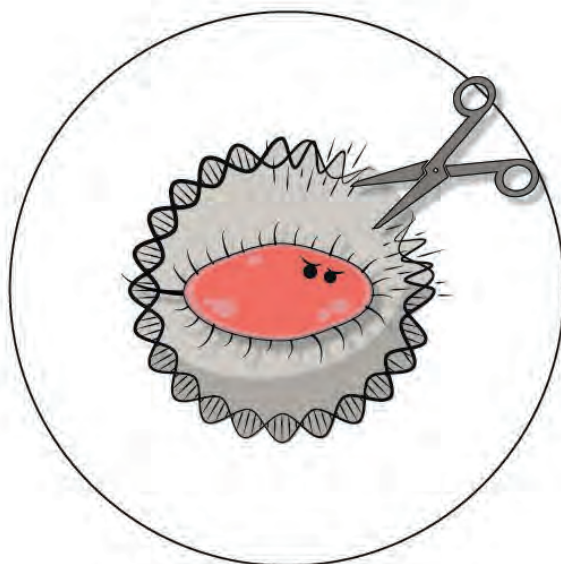
Compliance with Ethical Standards

Funding

This project was financially supported by The Netherlands Ministry of Economic Affairs and by NWO Green (870.15.130, 2015/05279/ALW).

Conflict of Interest

All authors declare that they have no conflict of interest.



Chapter 3

Efficient Cas9-based genome editing of *Rhodobacter sphaeroides* for metabolic engineering

This chapter has been published as: Mougiakos, I.* , Orsi, E.* , Ghiffary, M. R., Post, W., de Maria, A., Kengen, S. W., Eggink, G., Weusthuis, R. A. & van der Oost, J. (2019). Efficient Cas9-based genome editing of *Rhodobacter sphaeroides* for metabolic engineering. *Microbial cell factories*, 18(1), 204.

*contributed equally

Abstract

Background: *Rhodobacter sphaeroides* is a metabolically versatile bacterium that serves as a model for analysis of photosynthesis, hydrogen production and terpene biosynthesis. The elimination of by-products formation, such as poly- β -hydroxybutyrate (PHB), has been an important metabolic engineering target for *R. sphaeroides*. However, the lack of efficient markerless genome editing tools for *R. sphaeroides* is a bottleneck for fundamental studies and biotechnological exploitation. The Cas9 RNA-guided DNA-endonuclease from the type II CRISPR-Cas system of *Streptococcus pyogenes* (SpCas9) has been extensively employed for the development of genome engineering tools for prokaryotes and eukaryotes, but not for *R. sphaeroides*.

Results: Here we describe the development of a highly efficient SpCas9-based genomic DNA targeting system for *R. sphaeroides*, which we combine with plasmid-borne homologous recombination (HR) templates developing a Cas9-based markerless and time-effective genome editing tool. We further employ the tool for knocking-out the uracil phosphoribosyltransferase (*upp*) gene from the genome of *R. sphaeroides*, as well as knocking it back in while altering its start codon. These proof-of-principle processes resulted in editing efficiencies of up to 100% for the knock-out yet less than 15% for the knock-in. We subsequently employed the developed genome editing tool for the consecutive deletion of the two predicted acetoacetyl-CoA reductase genes *phaB* and *phbB* in the genome of *R. sphaeroides*. The culturing of the constructed knock-out strains under PHB producing conditions showed that PHB biosynthesis is supported only by PhaB, while the growth of the *R. sphaeroides* Δ *phbB* strains under the same conditions is only slightly affected.

Conclusions: In this study, we combine the SpCas9 targeting activity with the native homologous recombination (HR) mechanism of *R. sphaeroides* for the development of a genome editing tool. We further employ the developed tool for the elucidation of the PHB production pathway of *R. sphaeroides*. We anticipate that the presented work will accelerate molecular research with *R. sphaeroides*.

Keywords

Rhodobacter sphaeroides, Cas9, genome editing, PHB.

List of abbreviations

PHB: poly- β -hydroxybutyrate

HR: homologous recombination

SCO: single crossover

sacB: levansucrase gene

CRISPR-Cas: Clustered Regularly Interspaced Short Palindromic Repeats-CRISPR associated proteins

DSB: double stranded DNA breaks

sgRNA: single guide RNA

PAM: protospacer adjacent motif

upp: uracyl-phosphoribosyltransferase gene

5-FU: 5-fluorouracil

AA-CoA: acetoacetyl-CoA

phaB: AA-CoA reductase

phbB: AA-CoA reductase

Introduction

The purple non-sulphur bacterium *Rhodobacter sphaeroides* is a microorganism with an extremely adaptable metabolism (101). It is a facultative phototroph that can grow on many different carbon substrates and can respire aerobically and anaerobically with different electron acceptors (102, 132). The metabolic versatility of *Rhodobacter sphaeroides* has raised curiosity for white biotechnological applications. In particular, this microorganism has been largely studied for photoheterotrophic hydrogen production and chemoheterotrophic terpene biosynthesis. In both processes, approaches for improving the metabolic performances of the microorganism were investigated (83, 95, 126, 133, 134). Reducing formation of by-products like the polymer poly- β -hydroxybutyrate (PHB) holds potential for eliminating competition for carbon and reducing power, as already proven to work for H_2 biosynthesis (122, 133). Nonetheless, a lot of work is still required to further increase our knowledge on *R. sphaeroides* metabolism and exploit its biotechnological potential.

The high-throughput exploration of *R. sphaeroides* metabolism requires the development of highly effective and time-efficient genome engineering tools (83). Currently, the introduction of genomic modifications in *R. sphaeroides* is based on suicide-plasmid driven homologous recombination (HR) systems (87, 135). These systems depend on the incorporation of the non-replicating vector into the *R. sphaeroides* genome via an initial single crossover (SCO) event and consequent excision of the vector via a second SCO event upon induction of counter-selection pressure *i.e.* employing a levansucrase gene (*sacB*) carrying vector (68, 87, 90, 97, 136–138). The second SCO can either lead to the reconstitution of a wild type genomic background or to the desired genetic modification (87). The lack of a strict counter-selection method targeting specifically the genomic region of interest usually leads to high rates of wild-type

revertants, especially for essential genes. Therefore, screening of mutants can be time consuming and is frequently unsuccessful.

A wide range of CRISPR-Cas (Clustered Regularly Interspaced Short Palindromic Repeats-CRISPR associated proteins) bacterial and archaeal adaptive immune systems have been repurposed as tools for eukaryotic, prokaryotic and archaeal genome engineering (36, 139–146). Most of these tools exploit the RNA-guided DNA endonuclease from the type II CRISPR-Cas system of *Streptococcus pyogenes*, denoted as SpCas9. As any Cas9 orthologue, SpCas9 can be easily programmed to precisely introduce double stranded DNA breaks (DSB) to a selected DNA sequence, denoted as protospacer. A single, customizable guide RNA (sgRNA) molecule directs Cas9 to the protospacer via complementarity between its exchangeable 5'-end sequence, denoted as spacer, and the protospacer sequence. The only additional requirement for Cas9-based targeting is the presence of a specific, 2-8nt long motif right after the 3'-end of the selected protospacer, denoted as protospacer adjacent motif (PAM)(147). All in all, the simplicity in the design and construction of a Cas9-based DNA targeting system has made it popular as the basis for numerous genome manipulation applications.

A plethora of Cas9-based tools have been developed the last 5 years for prokaryotes (36, 148–153). Cas9 has been extensively used as an efficient HR induction and counter selection tool, when combined with plasmid-based homologous recombination (HR) or recombineering; alternative DSB repairing mechanisms (like the template independent non-homologous end joining, NHEJ) are lacking in most prokaryotes (154). Therefore, Cas9-based DSBs after HR are lethal if introduced to the wild type genomes: unmodified cells will be eliminated

from the treated population, allowing survival only for the recombined ones (154).

In this study, we develop a highly efficient Cas9-based targeting system for *R. sphaeroides*. We further combine it with HR templates, developing an HR-Cas9 counter selection tool. We then employ the tool for the proof-of-principle efficient generation of uracyl-phosphoribosyltransferase (*upp*) gene knock-out and knock-in strains, the latter combined with single nucleotide substitution. The developed process simplifies and accelerates *R. sphaeroides* genome editing, as it requires only 3 days from conjugation to screening of clean mutants. Additionally, we use the developed tool for the construction of acetoacetyl-CoA reductase deletion mutant strains, elucidating the dominant metabolic pathway of *R. sphaeroides* towards PHB production.

Material and methods

Bacterial strains, media and growth conditions

The strains used in this study are listed in **Table 1**. *E. coli* DH5a was used for cloning and routine amplification. *E. coli* S17-1 was used as vector donor for *R. sphaeroides* in diparental conjugation.

Table 1. List of strains used in this study.

Strain	Description	Source of reference
<i>E. coli</i>		
DH5α	<i>fhuA2 Δ(argF-lacZ)U169 phoA glnV44 Φ80 Δ(lacZ)M15 gyrA96 recA1 relA1 endA1 thi-1 hsdR17</i>	Laboratory stock
	Strain for assembly and plasmid amplification	
S17-1	Host strain for transconjugation, <i>thi pro recA hsdR</i> [RP4-2Tc::Mu-Km::Tn7] <i>Tpr Smr</i>	Laboratory stock
<i>R. sphaeroides</i>		
265-9c	Wild type	Derivative of ATCC 35053
<i>Δupp</i>	265-9c <i>Δupp</i>	This study
<i>uppKI</i>	265-9c KI(ATG->GTG) <i>upp</i>	This study
<i>ΔphaB</i>	265-9c <i>ΔphaB</i>	This study
<i>ΔphbB</i>	265-9c <i>ΔphbB</i>	This study
<i>ΔphaB_ΔphbB</i>	265-9c <i>ΔphaB_ΔphbB</i>	This study

Culturing of *R. sphaeroides* was performed in RÄ minimal or LB (Luria-Bertani) medium at 250 rpm, 30 °C. Growth on solid medium was performed on RÄ supplemented with 15% w/v agar. Culturing of *E. coli* strains was performed in LB medium at 250 rpm, 37 °C. Growth on solid medium was performed on LB supplemented with 15% w/v agar. When required, kanamycin (50 µg/mL) was added for all the mentioned growing conditions.

Plasmids construction

The plasmids constructed and the primers used for cloning and sequencing are listed in Supplementary **Tables S1** and **S2**, respectively. All primers for PCR were prepared by Integrated DNA Technologies (IDT) and all the PCR amplifications were performed using Q5 High-Fidelity DNA polymerase Master Mix 2x from New England Biolabs (NEB) according to the manufacturer's protocol. Due to the high GC content of *R. sphaeroides* genome, all PCR reactions using its genomic DNA as template were supplemented with DMSO 3% v/v. PCR fragment assemblies were performed employing the HiFi Assembly kit (NEB). Prior to plasmids assemblies, all PCR products were purified via gel extraction using the Zymoclean Gel DNA Recovery Kit (Zymo Research). Plasmid extractions were performed using the GeneJET Plasmid Miniprep kit (Thermo Fisher Scientific) and *R. sphaeroides* genome extractions were performed using the GeneJET Genomic DNA Purification Kit (Thermo Fisher Scientific).

Generation of the non-targeting Cas9-plasmid

A synthetic construct containing the sgRNA construct (promoter BBa_J95023, sgRNA scaffold and BBa_J95029 terminator) (**Table S3**) was ordered as gBlock from Integrated DNA Technologies (Leuven, Belgium). After restriction digestion with SmaI and SalI (Thermo Fisher Scientific), the sgRNA construct was ligated into the pUC19 vector and transformed into *E. coli* TOP10 cells for storage and amplification. Subsequently, the pUC19 containing the sgRNA construct and the pBBR1MCS2 *E. coli*-*R. sphaeroides* shuttle vector were digested with the same restriction enzymes. After digestion, the sgRNA construct and the pBBR1MCS2 backbone were ligated with T4 ligase (Thermo Fisher Scientific) yielding the pBBR1MCS2-sgRNA. The *cas9* gene was codon-harmonized according to *R. sphaeroides* codon-usage using the Galaxy / Codon harmonizer on-line tool (155). The codon-harmonized *cas9* was synthetically constructed by Baseclear

(the Netherlands) (**Table S4**) with a 6xHis-tag fused at its C-terminus, and delivered inserted in a pUC57 vector backbone. The *cas9* gene was PCR amplified using the pUC57hSpCas9 vector as template and primers BG10937/BG10938. The pBBR-sgRNA vector was linearized using primers BG10939/BG10941. The construction of the non-targeting plasmid pBBR_Cas9_NT vector (**Figure S1**) was done via HiFi assembly of the two aforementioned PCR amplicons and the *cas9* amplicon was inserted downstream of the *lac* promoter site of the pBBR-sgRNA. The lack of *lacI* repressor gene or its homolog in *R. sphaeroides* genome allowed constitutive transcription of the harmonized *cas9* gene.

Generation of the *upp* targeting plasmids

The spacers introduced in the sgRNA construct of the pBBR_Cas9 vectors are listed in the Supplementary **Table S5**. The spacers were selected employing the chopchop web tool (<https://chopchop.cbu.uib.no/>). The spacer selection parameters were set to avoid self-complementarity of the sgRNA, have efficiency more than 50 and no predicted off-targets. Using the plasmid pBBR_Cas9_NT as template, it was possible to substitute the non-targeting spacer contained in the sgRNA construct with three different targeting spacers for the gene uracyl-phosphoribosyltransferase *upp* (sp1-sp3). The pBBR_Cas9_NT was used as template for PCR amplification of the backbone, the start codon and part of the *cas9* gene, employing primers BG11415/BG11416. The remaining *cas9* sequence and the promoter of the sgRNA construct were PCR amplified employing primer BG11412 in combination with primers BG11486, BG11487 and BG11411, which also contained the spacer 1, 2 and 3 sequences respectively as overhangs. The remaining part of the backbone and the constant part of the sgRNA construct were PCR amplified employing primer BG11413 in combination with primers BG11488, BG11489 and BG11414 which also contained the spacer 1, 2 and 3 sequences respectively as overhangs. 3 fragments assemblies were

performed and the reaction mixtures were transformed in DH5 α *E. coli* competent cells (NEB) via heat shock, for storage and plasmid amplification. Upon sequence verification, the pBBR_Cas9_NT plasmid was transformed to *E. coli* S17-1 cells.

Generation of vectors for gene knock-out (KO) and gene knock-in (KI)

Homologous recombination (HR) followed by Cas9-based counter selection was used for the KO of the *upp* gene, as well as the KI of the *upp* gene back to its original place in the *R. sphaeroides* genome combined with single nucleotide substitution.

Plasmids for *upp* KO

We started by constructing the HR control, non-targeting plasmids pBBR_Cas9_ Δ upp500HR_NT and pBBR_Cas9_ Δ upp1000HR_NT. The pBBR_Cas9_NT backbone was PCR linearized into two fragments using the primers sets BG11886/BG11182 and BG11887/BG11888. The 500bp or 1kb long upstream and downstream flanking sites of the *upp* gene were PCR amplified from the *R. sphaeroides* genome employing the primer sets BG11866/BG11867 and BG11869/BG11871 for the 500 bp sizes and the primer sets BG11866/BG11868 and BG11870/BG11871 for the 1kb sizes. Hifi assembly and transformation to *E. coli* DH5 α cells was followed by sequence verification of the obtained pBBR_Cas9_ Δ upp500HR_NT and pBBR_Cas9_ Δ upp1000HR_NT plasmids. The sequence verified plasmids were transferred to *E. coli* S17-1 cells by transformation.

We proceeded with the construction of the HR-editing, *upp* targeting plasmids pBBR_Cas9_ Δ upp500HR_sp2 and pBBR_Cas9_ Δ upp1000HR_sp2. The previously mentioned couples of primer sets were used for the generation of the 500 bp

and 1 kb HR flanking sites. The pBBR_Cas9_NT vector was employed as template for the PCR amplification of the conserved backbone region with the BG11887/BG11888 primer set. In addition, the spacer sp2 was included in the corresponding position employing the primer sets BG11182/BG11487 and BG11489/BG11886 for the amplification of the *cas9* gene and the sgRNA module respectively. Hifi assembly and transformation to *E. coli* DH5a cells was followed by sequence verification of the obtained pBBR_Cas9_Δupp500HR_sp2 and pBBR_Cas9_Δupp1000HR_sp2 plasmids. *E. coli* S17-1 cells were transformed with sequence verified plasmids.

Plasmids for *upp* KI

We proceeded with the construction of the *upp* knock-in (KI) control pBBR_Cas9_Klupp1000HR_NT plasmid and the *upp* KI plasmids pBBR_Cas9_Klupp1000HR_sp4 and pBBR_Cas9_Klupp1000HR_sp5. The pBBR_Cas9_NT plasmid was used as template for the amplification of the fragments containing the backbone (primer set BG11887/BG11888), the *cas9* gene and the targeting sgRNAs. The *cas9*- and the sgRNA-containing fragments were generated via PCR amplification with primer sets BG11182/BG12907 and BG11186/BG12908 for spacer sp4 and primer sets BG11182/BG12909 and BG11186/BG12910 for spacer 5. Additionally, the HR template for KI of the *upp* gene back to its native position were comprised of the *upp* gene sequence flanked by the 1000 bp genomic regions upstream and downstream of the *upp* gene. The genomic amplification for the 1000 bp long flanking sites was performed using the primer pairs BG12347/BG11868 and BG11870/BG12348. The primers BG12347 and BG12348 introduce a single point mutation in the *upp* start codon (ATG to GTG). The construction of the two editing plasmids, namely pBBR_Cas9_Klupp1000HR_sp4 and pBBR_Cas9_Klupp1000HR_sp5, was performed via 5-fragment assemblies. The assembly mixtures were then

transformed to *E. coli* DH5 α cells. Upon sequence verification, the plasmids were transformed to *E. coli* S17.

Plasmids for *phaB* and *phbB* KO

We employed the previously described cloning strategy for generating three *phaB* KO plasmids (pBBR_Cas9_ Δ phaBHR_sp1, pBBR_Cas9_ Δ phaBHR_sp2 and pBBR_Cas9_ Δ phaBHR_sp3). The pBBR_Cas9_NT plasmid was used as template for the amplification of the fragments containing the backbone (primer set P302/P303), the *cas9* and the targeting sgRNAs. Each plasmid carried a different spacer designed to target a protospacer within the *phaB* sequence. For spacer sp1, the *cas9*- and the sgRNA-containing fragments were generated via PCR amplification with primer sets P301/P383 and P304/P384, respectively. For spacer sp2 the *cas9*- and the sgRNA-containing fragments were generated via PCR amplification with primer sets P301/P385 and P304/P386, respectively. For spacer sp3 the *cas9*- and the sgRNA-containing fragments were generated via PCR amplification with primer sets P301/P387 and P304/P388, respectively. Each of the three *phaB* editing plasmids contained the same HR template, consisted of the genomic regions 1 kb upstream of the *phaB* start codon and 1 kb downstream of the *phaB* stop codon. The regions were generated via PCR amplification with primer sets P379/P380 and P381/P382, respectively. The construction of the three editing plasmids was performed via 5 fragments assemblies. The assembly mixtures were then transformed to *E. coli* S17 cells and the constructed plasmids were sequence verified.

We employed the previously described cloning strategy for generating three *phbB* KO plasmids (pBBR_Cas9_ Δ phbBHR_sp1 and pBBR_Cas9_ Δ phbBHR_sp2). The pBBR_Cas9_NT plasmid was used as template for the amplification of the fragments containing the backbone (primer set P302/P303), the *cas9* and the

targeting sgRNAs. Each plasmid carried a different spacer designed to target a protospacer within the removed *phbB* sequence. For spacer sp1, the *cas9*- and the sgRNA-containing fragments were generated via PCR amplification with primer sets P301/P418 and P304/P417, respectively. For spacer sp2 the *SpCas9*- and the sgRNA-containing fragments were generated via PCR amplification with primer sets P301/P420 and P304/P419, respectively. Each of the two *phbB* editing plasmids contained the same HR template, consisted of a sequence of four stop codons (TAG) and an *EcoRI* restriction site, flanked on the one side by the genomic region 500 bp upstream and 546 bp downstream the *phbB* start codon and on the other side by the genomic region 145 bp upstream and 850 bp downstream the *phbB* stop codon. The regions were generated via PCR amplification with primer sets P415/P416 and P413/P414, respectively, using the *R. sphaeroides* genome as template. Moreover, each plasmid carried a different spacer designed to target a protospacer within the 59 nt long substituted *phbB* region. The construction of the two editing plasmids was performed via 5 fragments assemblies. The assembly mixtures were then transformed to *E. coli* S17 cells and the constructed plasmids were sequence verified.

Diparental conjugation and plasmid curation

R. sphaeroides was inoculated from glycerol stock in 10 mL RÄ medium and incubated for 2 days at 30°C and 200 rpm prior to conjugation. After 48 hours, 50 µL of culture were transferred to fresh 10 mL RÄ medium, incubated for 24 h under the same conditions, and harvested when the OD₆₀₀ was approximately 3. *E. coli* S17-1 harboring the desired plasmid was grown overnight in LB supplemented with kanamycin at 37°C and 200 RPM. Then, the overnight culture was transferred to fresh 2xYT media with antibiotic and grown for 2 h until the OD at 600nm was approximately 1. The cell suspension was harvested and washed twice with 1 mL of RÄ medium, mixed with *R.*

sphaeroides culture at a 1:1 ratio (1 mL each) and centrifuged for 1 minute (maximum speed). The pellet was concentrated by suspension in 100 µL of RÄ medium, which was transferred to a sterile 0.22 µm 47 mm diameter nitrocellulose filter disc (Sigma-Aldrich) on a PY agar plate and incubated for 6 hours at 28°C. The conjugation mixture was harvested and re-suspended in 2 mL of RÄ medium. 100 µL of diluted culture was spread on RÄ agar plates containing kanamycin and incubated at 30°C for 3 days until colonies appeared. Purification of *R. sphaeroides* conjugants from *E. coli* S17-1 donors was performed by subsequent transfer of *R. sphaeroides* colonies to LB agar medium supplemented with kanamycin until no *E. coli* colonies appeared. Finally, a colony PCR was performed using primer set P3/P4 to verify that *E. coli* was not present in the culture.

Plasmid curing from positive *R. sphaeroides* mutants was carried out by cultivating the mutants in 5 mL of RÄ medium without antibiotic for 24 h, twice. The cells from the second cultivation were then diluted and spread on RÄ agar plates. The individual colonies were streaked onto LB agar with and without kanamycin. Those cells that grew on LB without antibiotic but were unable to grow in the presence of antibiotic were considered to have lost the plasmid. Final verification of plasmid curing was conducted by performing PCR with primers BG10937/BG10938, which are specific for the Cas9 gene.

RNA extraction and reverse transcriptase PCR (RT-PCR)

To check expression of the *cas9* gene under the *lac* promoter, total RNA of *R. sphaeroides* conjugated with the pBBR_Cas9_NT plasmid was extracted employing the RNeasy mini kit (Qiagen, Germany) according to the manufacturer's protocol and treated with DNase I (NEB) to remove genomic DNA contamination in the sample. The SuperScript III Reverse Transcriptase kit

(Invitrogen) was used for RT-PCR. When the first strand of cDNA was synthesized, the primers BG11112 and BG11115 were used to verify transcription activity of Cas9 gene using standard PCR.

5-FU screening

For the 5-fluorouracil (5-FU) screening process we prepared RÄ agar plates supplemented with 5-FU up to 100 µg/ml final concentration, using a 50 mg/mL stock solution prepared in dimethyl sulfoxide (DMSO). Colonies obtained from conjugation were picked and streaked on RÄ_5-FU plates with kanamycin. Survival colonies were isolated and their *upp* locus was then PCR amplified and sequenced.

Analytics

Carbon and nitrogen concentrations

To determine active biomass levels and C/N ratios of the biomass, analysis was done using a TOC-L analyzer (Shimadzu). Biomass samples were diluted 3-5 times in a total volume of 15 mL using MilliQ and a stirring bar was added. The TOC-L analysed both non-purgeable organic carbon (NPOC) as well as total nitrogen (TN) content. The TN content was used to calculate the active biomass concentration using the elemental composition of $\text{CH}_{1.99}\text{O}_{0.5}\text{N}_{0.19}$ of *R. sphaeroides* described previously (Waligórska et al. 2009). The C/N ratio was calculated by dividing molar concentrations resulting from NPOC and TN measurements.

Poly-β-hydroxybutyrate (PHB) concentrations

Volumes ranging from 2-5 mL of biomass were spun down and resuspended in MilliQ water. Pellets were dried in an oven at 100 °C. The dried biomass was resuspended in 1 mL of concentrated H_2SO_4 and heated

to 90 °C for 40 minutes. The samples were diluted by addition of 9 mL of 0.09 mM H₂SO₄. Samples were mixed 1:1 with propionic acid. Separation of compounds was done using the same flow and temperature as described elsewhere (134). For quantification, standards with known concentrations of commercially available PHB (Sigma-Aldrich) were treated the same as the samples.

Results and discussion

SpCas9 targeting in *R. sphaeroides*

The first aim of this study was to assess potential toxic effects of SpCas9 expression in *R. sphaeroides* cells, as previously reported for other microbial species (156–158). For this purpose, we constructed the pBBR_Cas9_NT control vector by cloning the *cas9* gene, codon optimized for *R. sphaeroides*, and a sgRNA expressing module with a non-targeting (NT) spacer in the *E. coli*-*Rhodobacter* shuttle vector pBBR1MCS2. The expression of the *cas9* gene was under control of the *P_{lac}* promoter that due to the absence of the *lacI* repressor gene in the *R. sphaeroides* genome, has constitutive transcription activity. Moreover the sgRNA expressing module was under the control of the synthetic constitutive *P_{BBa_J95023}* promoter (89) and the NT spacer sequence was designed in such way that any candidate protospacer within the genome of *R. sphaeroides* would contain at least 6 mismatches in the non-seed region (the 12 PAM-distal nucleotides) and at least 2 extra mismatches in its seed region (the 8 PAM-proximal nucleotides). The pBBR_Cas9_NT vector in parallel with the pBBR1MCS2 control vector were conjugated in *R. sphaeroides* cells (**Fig. S2**). Even though the conjugation efficiency for the pBBR_Cas9_NT vector was reduced compared to the control pBBR1MC2 vector (**Fig. 1a**), it remained high and the size of the pBBR_Cas9_NT containing colonies was comparable to the size of the pBBR1MC2 containing colonies. We then randomly selected 5 of the

colonies conjugated with the pBBR_Cas9_NT vector for culturing and plasmid isolation. The sequence integrity of the *cas9* gene, the sgRNA expressing locus and the corresponding promoters was verified for all the 5 isolated plasmids, leading us to the conclusion that the drop in the conjugation efficiency of the pBBR_Cas9_NT can most likely be attributed to the almost double size of the vector (9566 bp) compared to the control vector (5144 bp) and, at least under the tested conditions, not to toxicity of SpCas9. Moreover, we confirmed the transcription of the *cas9* gene in *R. sphaeroides* by RT-PCR (**Fig. 1b**).

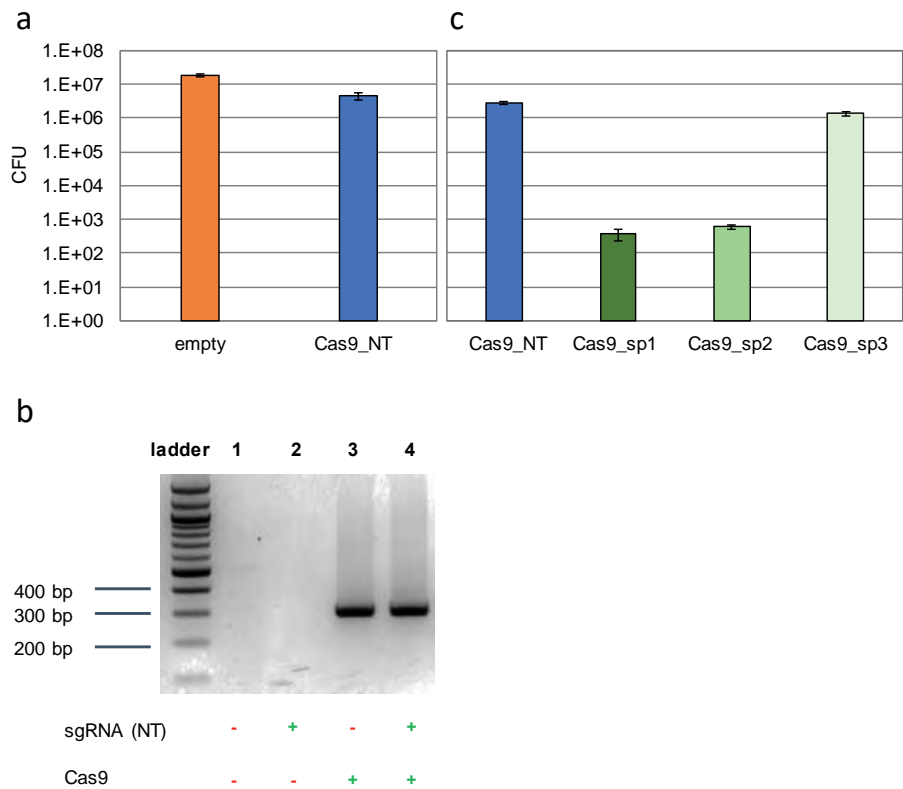


Figure 1. Conjugation of *upp* targeting Cas9 plasmids and Cas9 transcription. (a) Colony forming units (CFUs) obtained after conjugation of pBBR_Cas9_NT plasmid in *R. sphaeroides*. The efficiency was compared to an empty pBBR1MCS2 plasmid. (b) Reverse Transcriptase PCR (RT-PCR) assessing the transcription of the *spcas9* gene under the constitutive P_{loc} promoter in *R. sphaeroides*. *R. sphaeroides* cells were conjugated with pBBR1MCS2 harboring: no additional features (well 1), non-targeting sgRNA (pBBR_NT, well 2), harmonized Cas9 (pBBR_Cas9, well 3) and harmonized Cas9 plus NT-sgRNA (pBBR_Cas9_NT, well 4). The expected size of the *spcas9* cDNA amplicon is 307bp. The primers set used was BG11112/BG11115. (c) CFU obtained after conjugation of the pBBR_Cas9 plasmids harboring different *upp* targeting spacers (pBBR_Cas9_sp1-sp3); the plasmid with the non-targeting spacer (pBBR_Cas9_NT) was used as control. The average values of 3 replicates are shown and the error bars represent SD.

We further developed a SpCas9-based system for efficient introduction of lethal double stranded DNA breaks (DSBs) in *R. sphaeroides*, genome, selecting the *upp* (uracil phosphoribosyl transferase) gene as target. Knock-out mutations of the

upp gene in other bacteria resulted in mutant strains resistant to 5-FU (159, 160). For *R. sphaeroides* we determined that 5-FU is toxic at concentrations as low as 1 µg/mL in RÄ medium and its use could facilitate future screening steps. The pBBR_Cas9_NT vector was employed for the construction of three targeting plasmids (pBBR_Cas9_sp1-3) each containing a unique spacer that corresponds to a different target sequence (protospacer) within the *upp* gene. If the constructed SpCas9 system is efficiently expressed in *R. sphaeroides*, the number of obtained colonies upon conjugation with the targeting plasmids is going to be substantially lower compared to the number of obtained colonies upon conjugation with the control plasmid.

The pBBR_Cas9 series of plasmids was conjugated in *R. sphaeroides* (**Fig. 1c**). The conjugation efficiency for the pBBR_Cas9_sp1 and pBBR_Cas9_sp2 constructs dropped more than 3 orders of magnitude compared to the pBBR_Cas9_NT control, while for the pBBR_Cas9_sp3 the conjugation efficiency dropped only by 50% (**Fig. 1c**). This result shows that the constructed SpCas9 targeting system is highly active in *R. sphaeroides*. To further study the observed fluctuation of targeting efficiency of different spacers, we randomly selected 5 surviving colonies conjugated with the pBBR_Cas9_sp3 plasmid and isolated the plasmids. The plasmid sequencing results did not reveal any indel mutations or single nucleotide substitutions in the *cas9* gene and the sgRNA module that could lead to the deactivation of the SpCas9 targeting system. Previous studies have shown that CRISPR-Cas based chromosomal targeting can induce genomic island excision events, resulting in the removal of the chromosomal target in the surviving population (161, 162). We PCR amplified the *upp* genomic regions from the previously selected 5 surviving colonies conjugated with the pBBR_Cas9_sp3 plasmid; all the amplicons showed the expected wild-type size (**Fig. S3**) and were also sequence verified. This result excluded a genomic island excision event. It

was previously reported that the targeting efficiency of a SpCas9 system relies heavily on the selected spacer and can substantially differentiate amongst different targets, even within the same gene (163). Hence, the most possible explanation for the low targeting efficiency of the SpCas9-based system employing spacer 3 is the comparatively higher efficiency of the native RecA-based repair mechanism that employs untargeted chromosomal copies as repairing templates (163).

Homologous recombination- SpCas9 counter selection for gene deletions

There are multiple studies on bacterial genome editing employing i) homologous recombination (HR) via plasmid-borne templates that carry the desired modifications, and ii) Cas9-induced DSBs for the induction of the cellular HR machinery and as a counter-selection system for the unedited cells (36, 154). Previous studies reported HR activity in *R. sphaeroides* (87) and here we developed a SpCas9 targeting system. Hence, we set out to develop a HR-SpCas9 counter selection system for efficient genome editing in *R. sphaeroides*.

As a proof of principle, we programmed the designed HR-SpCas9 system to knock out the *upp* gene of *R. sphaeroides*, excluding the start codon and the last 12 nucleotides of the gene in order to avoid potential polar effects for neighboring genes of the operon. Two editing plasmids were constructed and tested, both containing the previously described spacer 2 for efficient *upp* targeting and HR templates consisted of either 500 bp (pBBR_Cas9_Δupp500HR_sp2) or 1 kb (pBBR_Cas9_Δupp1000HR_sp2) upstream and downstream genomic regions flanking the selected for deletion *upp* fragment. Two control plasmids (pBBR_Cas9_Δupp500HR_NT and pBBR_Cas9_Δupp1000HR_NT), containing the same HR templates as the editing plasmids but a non-targeting spacer, were also taken along for assessing the contribution of SpCas9 to the efficiency of the tool.

Upon conjugation of the above described constructs in *R. sphaeroides*, a drop was observed 1 order of magnitude in the number of surviving colonies upon conjugation with the editing constructs compared to the non-targeting control construct (**Fig. 2a**). 14 colonies were randomly picked from each plate (the experiment was performed in triplicates, so 42 colonies were selected per conjugated construct) and streaked on RÄ agar plates supplemented with 5-FU. All selected colonies from the conjugation plates with editing constructs - regardless the size of the employed HR template- grew on the 5-FU selection plates (**Fig. 2b**). We genotyped all the selected colonies through colony PCR and sequencing, and we confirmed the desired clean deletions (**Fig. 2c, d**). Meanwhile none of the selected colonies from the conjugation plates with non-targeting control constructs grew on 5-FU selection plates (**Fig. 2b**), underlining the significant contribution of SpCas9 targeting to the high efficiency of the developed HR-SpCas9 counter selection tool in *R. sphaeroides*.

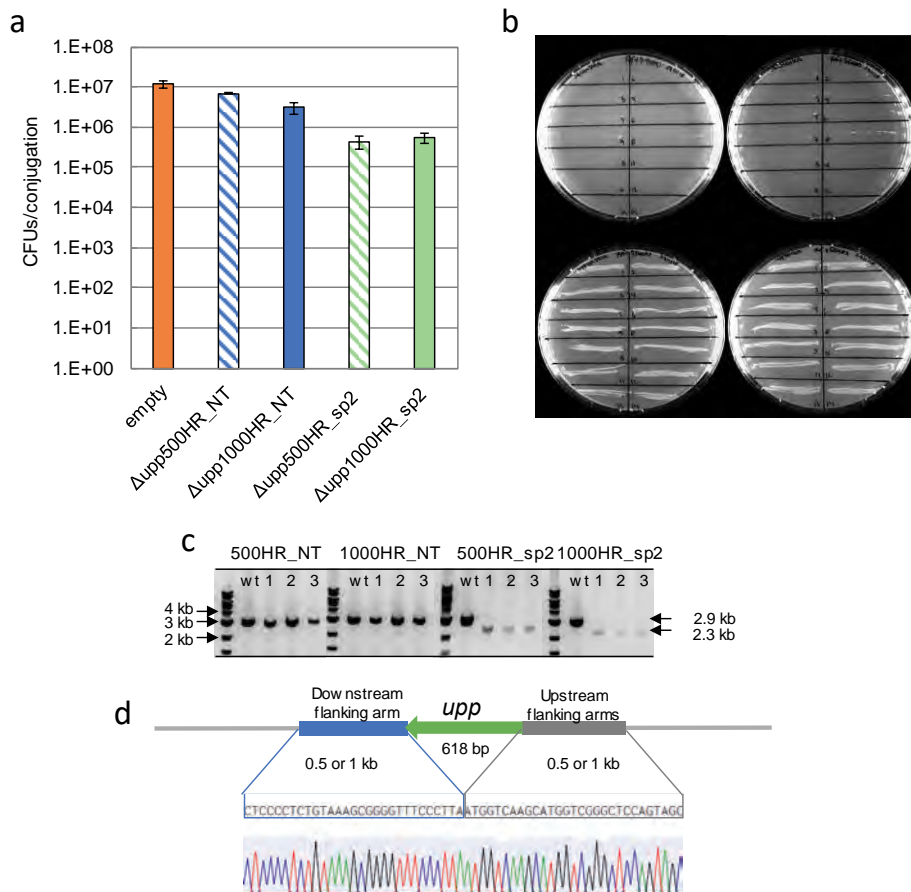


Figure 2. Deletion of *upp* gene from *Rhodobacter sphaeroides* genome. a) Number of colonies obtained on RÄ agar plates plated with 10–3 dilutions of *R. sphaeroides* conjugation mixtures with the homologous recombination (HR) control vectors pBBR_Cas9_Δupp500HR_NT and pBBR_Cas9_Δupp1000HR_NT, and HR editing vectors pBBR_Cas9_Δupp500HR_sp2 and pBBR_Cas9_Δupp1000HR_sp2. The error bars represent standard deviations from three replicate experiments. b) Restreaks of randomly selected colonies from the above mentioned conjugations on RÄ agar plates supplemented with 5-FU. Only Δ*upp* mutants can grow on 5-FU plates. c) Genome specific colony PCR amplification of the *upp* locus in cells conjugated with the pBBR_Cas9_Δupp500HR_NT, pBBR_Cas9_Δupp1000HR_NT, pBBR_Cas9_Δupp500HR_sp2 and pBBR_Cas9_Δupp1000HR_sp2 vectors. Amplification yields a 2992 bp product for the wild type *upp* gene and a 2374 bp product for the deleted *upp* gene. d) Sequence verification of the desired *upp* deletion by Sanger sequencing.

Prerequisite for extensive metabolic engineering studies with the HR-SpCas9 tool in *R. sphaeroides* is the performance of rapid iterative genome editing cycles. This demands the curing of constructed mutants from the SpCas9-harboring editing plasmids via an easy and time-effective way. For this purpose, one of the previously constructed Δupp mutants was grown in LB broth medium without antibiotic for two iterative inoculation cycles of 24 hours each. After plating and incubating the final culture on LB agar plates without antibiotic for two days, 5 colonies were selected and re-streaked on LB agar plates with and without antibiotic (kanamycin). Colonies that grew only on the agar plate without antibiotic were subjected to colony PCR with plasmid specific primers and the plasmid loss was verified (**Fig. S4**). The cured *R. sphaeroides* Δupp strain was further employed for the expansion of the SpCas9-based toolbox.

Homologous recombination-SpCas9 counter selection for gene insertions and single nucleotide substitutions

To further expand the genome editing toolbox of *R. sphaeroides*, we proceeded with the development of a plasmid-based HR-SpCas9 counter selection knock-in (KI) system. As a proof of principle, we designed a system for reinsertion of the *upp* gene in the genome of the previously constructed Δupp mutant strain. We selected two spacers (sp4 and sp5, **Table S5**) for the editing plasmids, aiming to target the remaining fraction of the *upp* gene in the genome of the Δupp mutant (**Fig. 3a**). Moreover, we constructed HR templates containing the *upp* gene - with the “ATG” start codon substituted by the “GTG” as sequence verification marker - flanked by 1 kb upstream and downstream genomic regions (pBBR_Cas9_Klupp1000HR_sp4 and pBBR_Cas9_Klupp1000HR_sp5). Upon reinsertion of the *upp* gene into the Δupp genome the corresponding protospacers would be disrupted, providing resistance from the SpCas9 targeting.

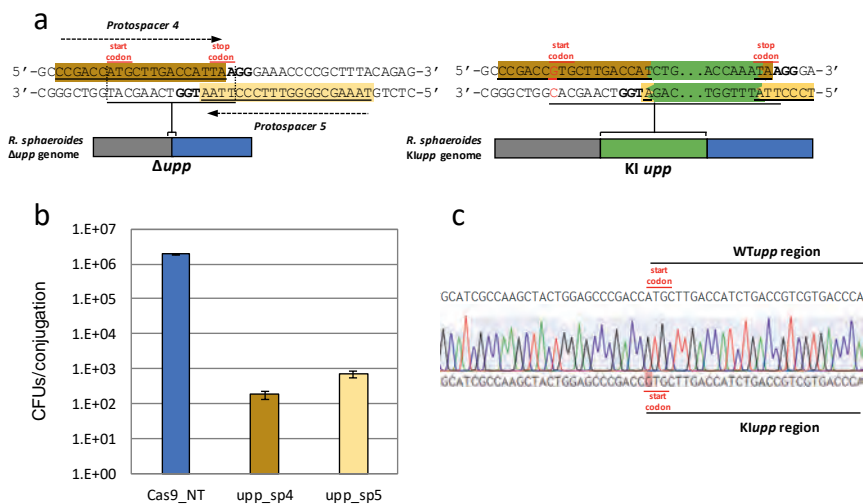


Figure 3. Insertion of the gene *upp* in a Δupp locus with single point mutation. a) Representation of the Δupp locus before (left) and after (right) knock-in of the *upp* gene. The protospacers recognized by spacers sp4 and sp5 are underlined and highlighted with dark and light brown, respectively, and their PAM is in bold. The 1 kb flanking sites surrounding Δupp are in grey and blue, while the inserted *upp* sequence is in green; after introduction of the *upp* sequence, the protospacers sequences are disrupted, and the starting codon ATG is replaced by GTG via a 1 bp substitution (red). b) Colony forming units (CFU) obtained after conjugation with pBBR_Cas9 plasmids (pBBR_Cas9_Klupp1000HR_sp4 and pBBR_Cas9_Klupp1000HR) harboring different Δupp targeting spacers (sp4 and sp5) and 1 kb HR templates for the knock-in of the *upp* gene accompanied by single nucleotide substitution; the plasmid with the non-targeting spacer (pBBR_Cas9_NT) was used as conjugation control. c) Sequence verification of the desired *upp* insertion and single nucleotide substitution, by Sanger sequencing.

The two editing plasmids and the pBBR_Cas9_NT control plasmid were conjugated in the plasmid-cured *R. sphaeroides* Δupp mutant and the experiment was performed in 3 biological replicates. As expected, a decrease in the number of surviving conjugants was observed for both editing plasmids compared to the non-targeting control plasmid (**Fig. 3b**). The *upp* genomic region from 38 to 40 colonies per construct and per conjugation was amplified by colony PCR with genome specific primers. The editing constructs resulted in low editing efficiencies; 16/118 screened colonies for spacer 4 and only 2/120

screened colonies for spacer 5 were KI mutants (**Fig. S5a, S5b**). All the mutants were subsequently sequence verified for the existence of the “GTG” start codon (**Fig. 3c**). This result shows that, unlike the *upp* deletion process, the efficiency of the *upp* knock-in process is much lower, at least for the selected target.

Eliminating PHB accumulation in *R. sphaeroides*

The intracellular accumulation of PHB in *R. sphaeroides* under nitrogen-limited culturing conditions acts as a carbon drain and a NADP⁺ regeneration mechanism, using acetoacetyl-CoA (AA-CoA) as precursor (126, 127, 134) (**Fig. 4a**). Hence, engineering a *R. sphaeroides* strain with reduced PHB production capacity could facilitate the increment of the intracellular NADPH and AA-CoA pools, and the channelling of the *R. sphaeroides* metabolism towards the production of alternative biotechnologically interesting molecules, such as hydrogen and terpenes.

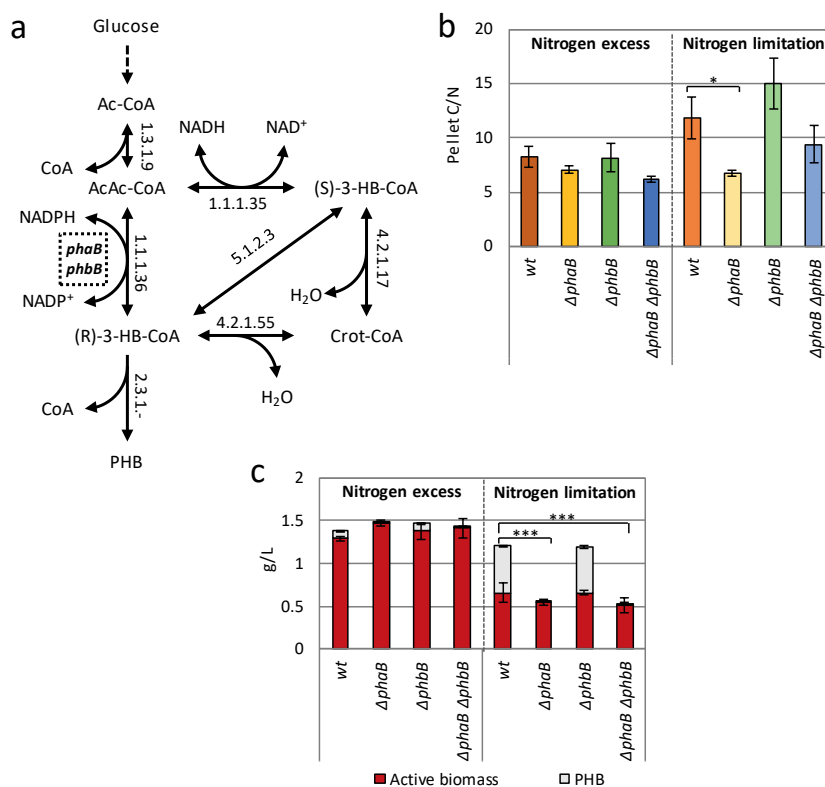


Figure 4. a) The PHB biosynthetic pathway of *Rhodobacter sphaeroides*. The annotation is based on KEGG. Enzymatic conversions are indicated by their EC numbers. Double arrowed reactions describe reversible reactions ($\Delta rG^\circ > -30$ kJ/mol [48]). Ac-CoA acetyl-CoA; AcAc-CoA acetoacetyl-CoA; (R)-3-HB (R)-3-hydroxybutanoate, (R)-3-HB-CoA (R)-3-hydroxybutanoyl-CoA, (S)-3-HB-CoA (S)-3-hydroxybutanoyl-CoA, CroT-CoA crotonyl-CoA; PHB: poly- β -hydroxybutyrate. The interrupted square indicates the metabolic step that is hypothesized to be catalysed by PhaB and/or PhbB. b) Effect of the *phaB* (RSP_0747) and the *phbB* (RSP_3963) knockout, as well as of the combined knockout, on the C/N ratios of the generated mutants in nitrogen excess and limiting conditions on a defined medium. Lower C/N ratio's indicate less PHB accumulation (Student's t-test, *P < 0.05). c) Effect of the *phaB* (RSP_0747) and the *phbB* (RSP_3963) knockout, as well as of the combined knockout, on the active biomass and the PHB accumulation in *R. sphaeroides* (Student's t-test, ***P < 0.001). Concentrations of active biomass and PHB were measured after 24 h cultivation in Sistrom's minimal medium supplied with 1.0 g/L or 0.25 g/L of NH₄Cl (Nitrogen excess and nitrogen limited conditions, respectively). Error bars indicate standard deviations from at least two replicates.

AA-CoA reductases catalyse the NADPH-dependent conversion of AA-CoA into (R)3-hydrobutyrate-CoA ((R) 3HB-CoA) which is the precursor of PHB. There are two predicted AA-CoA reductase genes in the genome of *R. sphaeroides*, namely *phaB* (RSP_0747) and *phbB* (RSP_3963), and the contribution of each corresponding enzyme to the AA-CoA reduction into (R) 3HB-CoA was the focus of this study. For this purpose, the *phaB* and *phbB* genes were separately and jointly knocked-out of the *R. sphaeroides* genome employing the previously described tool. More specifically, three editing plasmids were constructed and employed for the deletion of the *phaB* gene (namely pBBR_Cas9_Δ*phaB*HRR_sp1, pBBR_Cas9_Δ*phaB*HRR_sp2 and pBBR_Cas9_Δ*phaB*HRR_sp3) and two for the knockout of the *phbB* gene (namely pBBR_Cas9_Δ*phbB*HRR_sp1 and pBBR_Cas9_Δ*phbB*HRR_sp2) via the introduction of premature stop codons in the sequence of the gene. We reasoned to not completely delete the *phbB* gene as it is located within an operon in the *R. sphaeroides* genome, unlike *phaB* which is located at the end of an operon (**Fig. S6**). The efficiency of the *phaB* deletion processes was 100% for constructs harboring spacer sp1 (20/20 PCR screened colonies were clean *phaB* deletion mutants) and spacer sp2 (10/10 PCR screen colonies were clean *phaB* deletion mutants), but 0% efficiency for constructs harboring spacer sp3 (0/13 PCR screened colonies were clean *phaB* deletion mutants) (**Fig. S7**). The efficiency of the *phbB* knockout processes was 100% when the pBBR_Cas9_Δ*phbB*HRR_sp1 construct was employed (7/7 PCR screened colonies were clean *phbB* deletion mutants) and 0% when the pBBR_Cas9_Δ*phbB*HRR_sp2 construct was employed (0/8 PCR screened colonies were clean *phbB* deletion mutants) (**Fig. S8**), confirming that the efficiency of the developed Cas9-based is spacer-dependent.

The C/N ratio of microbial biomass increases when PHB is produced. The C/N ratio of the wild type *R. sphaeroides* strain and the generated Δ*phaB*, Δ*phbB* and

ΔphaB_ΔphbB strains was tested for PHB production after 48 hours of cultivation under nitrogen excess and nitrogen-limited conditions. Analysis by TOC-L revealed no statistically relevant difference between the C/N ratios of the strains under nitrogen excess conditions (**Fig. 4b**, left panel). Under nitrogen limitation conditions, a substantial decrease was noticed in the C/N ratio of the *ΔphaB* strain as compared to the wild-type strain (**Fig. 4b**, **Table S6**). This decrease indicated reduced carbon accumulation in the *ΔphaB* and *ΔphaB_ΔphbB* strains in comparison to the wild-type strain, which could be attributed to reduced PHB production.

In order to confirm the reduction in the PHB production, HPLC analysis was performed to quantify the intracellular PHB content of the wild-type, *ΔphaB*, *ΔphbB* and *ΔphaB_ΔphbB* strains. The analysis showed that the PHB content of the wild-type and *ΔphbB* strains can fluctuate between 40-70% (w/w) of the dry cellular weight (DCW), which is consistent with previously reported results (134, 164). The PHB concentrations in the *ΔphaB* and *ΔphaB_ΔphbB* strains were comparable and more than 99% lower compared to the PHB concentrations of the wild type and *ΔphbB* strains. The active biomass of wild-type and mutant strains was calculated based on the TOC-L data (**Fig. 4c**, **Table S6**). Only a minor reduction in the active biomass of the *ΔphaB* and *ΔphaB_ΔphbB* strains, as compared to the active biomass of the wild-type strain, was observed.

Conclusions

In our work we developed a highly active SpCas9-based DNA targeting system for the biotechnologically interesting bacterium *R. sphaeroides*. We further combined the SpCas9 DNA targeting activity with the native homologous recombination (HR) mechanism of *R. sphaeroides* for the development of an efficient HR-SpCas9 counter selection-based genome editing toolbox for gene

knock-outs, knock-ins and single nucleotide substitutions. Hence, the developed toolbox can substantially accelerate fundamental and metabolic engineering studies on *R. sphaeroides*, e.g. on membrane and photosynthetic reaction centre proteins, as well as metabolic engineering studies for improved hydrogen production and terpene synthesis, as already have been achieved for other microorganisms with developed SpCas9 toolboxes. Finally, we employed the developed toolbox to elucidate the genetic background of PHB production in *R. sphaeroides* and we constructed mutant strains with dramatically reduced PHB production capacity and almost unaffected growth. Hence, the constructed *R. sphaeroides* mutant strains can be the basis for further engineering towards the enhanced production of alternative biotechnologically interesting molecules, such as hydrogen and terpenes.

Ethics approval and consent to participate

Not applicable.

Consent for publication

Not applicable.

Availability of data and material

The datasets supporting the conclusions of this article are included within the article (and its additional files).

Competing interests

The authors declare no competing financial interests.

Funding

This project was financially supported by The Netherlands Ministry of Economic Affairs and a public-private NWO-Green Foundation for sustainable production

and supply chains in agriculture and horticulture (870.15.130, 2015/05279/ALW).

Authors' contributions

IM, EO, SWMK, RAW and JvO designed the work. IM, EO, MRG, AM, WP and BAP conducted, analyzed, and interpreted the experiments. IM and EO drafted and wrote the manuscript. All authors read and approved the final manuscript.

Acknowledgements

We acknowledge Isobionics BV for providing the *Rhodobacter sphaeroides* strain used in the study. Any request for the strain and its derivatives should be directed to Isobionics BV.

Supplementary information

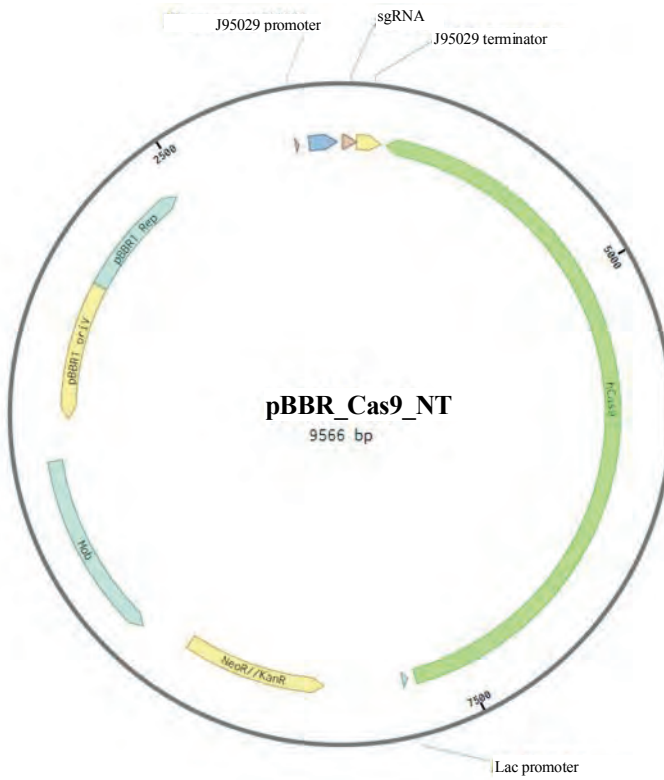


Figure S1. Graphical representation of the pBBR_Cas9_NT plasmid map.

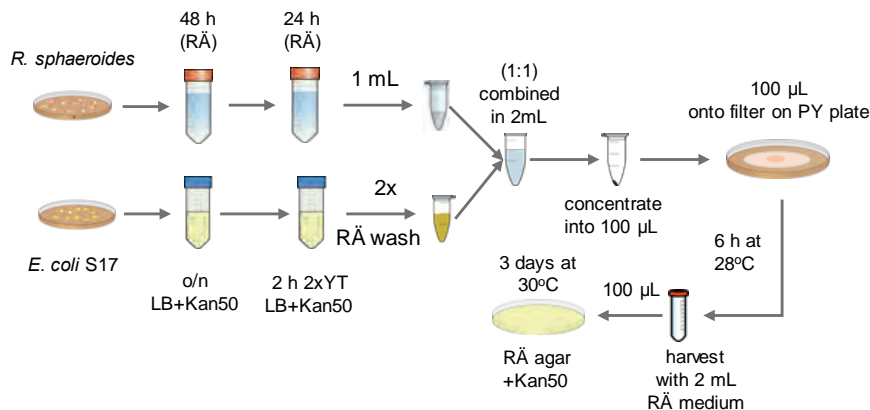


Figure S2. Schematic overview of the di-parental conjugation protocol used: detailed description of the protocol can be found in the Material and Methods section.

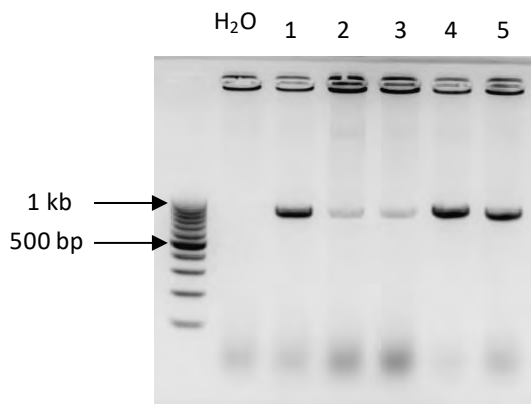


Figure S3. 1% agarose electrophoresis showing the PCR amplified *upp* genomic regions from 5 surviving colonies conjugated with the pBBR_Cas9_sp3 plasmid; all the amplicons showed the wild-type size.

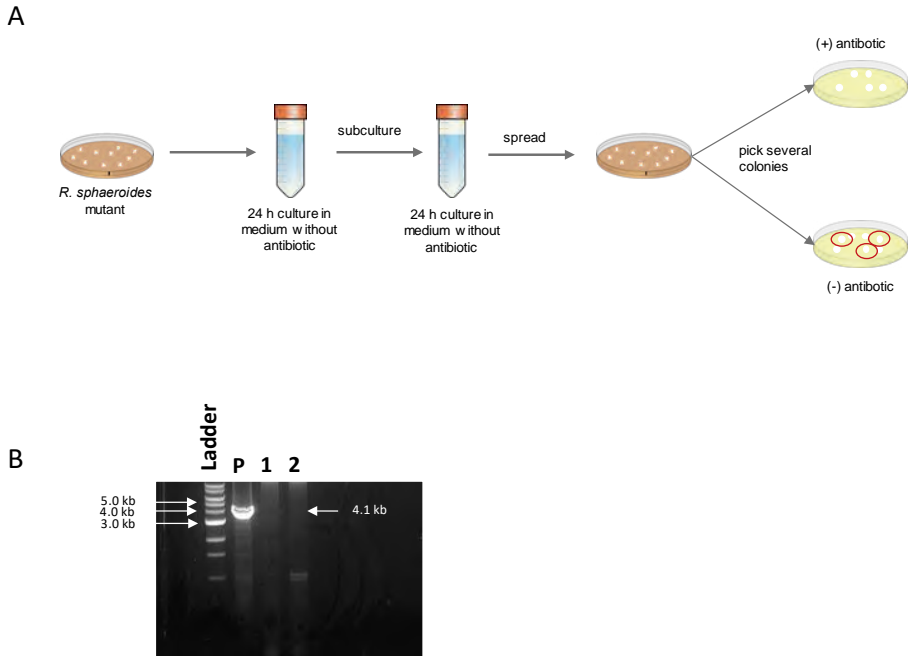


Figure S4. Curing from the plasmid after successful conjugation. A) Schematic overview of the workflow: mutants from *R. sphaeroides* were transferred twice to liquid medium without antibiotic and incubated over-night. Subsequently, the liquid culture was spread on LB plates. Once colonies formed, they were transferred to LB plates with and without antibiotic. B) The colonies that grew only on the plate without antibiotic were PCR amplified with primers annealing to the Cas9 gene in the vector backbone using primers set BG10937/BG10938 (P: plasmid control, 1 and 2: curated *R. sphaeroides* mutants).

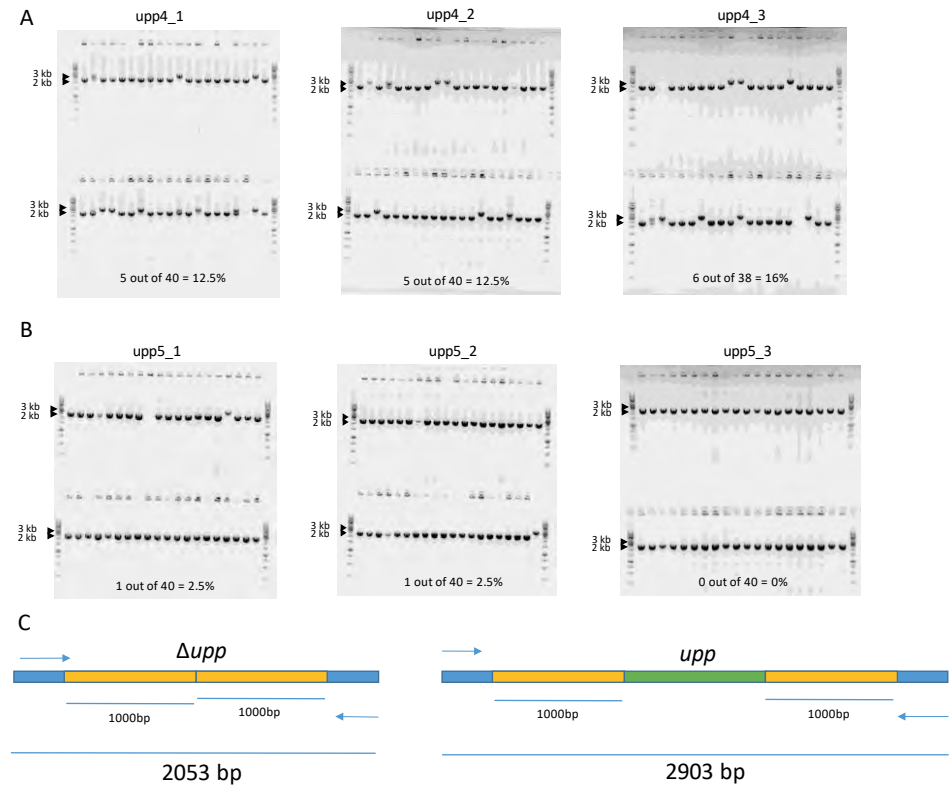


Figure S5. 1% agarose electrophoresis showing the 3 rounds of colony PCRs after the conjugations of the *R. sphaeroides* Δupp strain with the plasmids for *upp* insertion. A) pBBR_Cas9_Klupp1000HR_sp4. B) pBBR_Cas9_Klupp1000HR_sp5. C) Schematic representation of the amplicons generated via colony PCR: the Δupp gene leads to an amplicon of 2053 bp (left), while a restored *upp* gene (green) generates an amplicon of 2903 bp. The homology regions are highlighted in yellow.

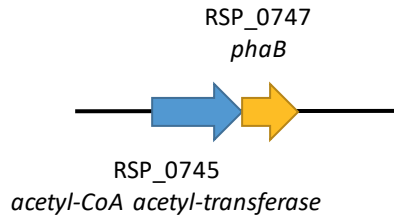
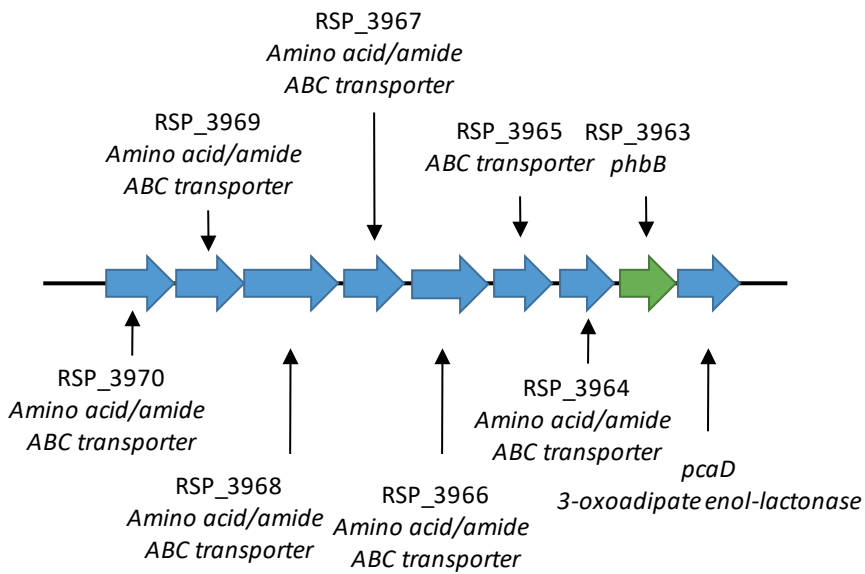
phaB operon:*phbB* operon:

Figure S6. Genomic landscape of the *phaB* and *phbB* genes within the *R. sphaeroides* genome.

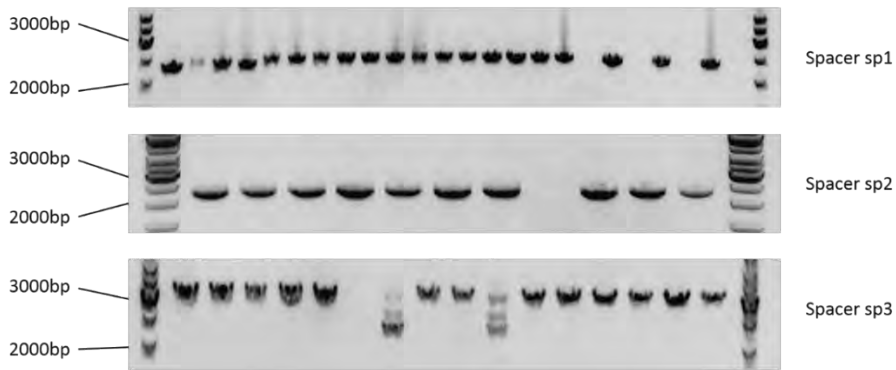


Figure S7. 1.2% agarose electrophoresis showing the colony PCRs after the conjugation of the WT strain of *R. sphaeroides* with the plasmids for knockout of *phaB*. Upper panel: pBBR_Cas9_ΔphaBHR_sp1, middle panel: pBBR_Cas9_ΔphaBHR_sp2, lower panel: pBBR_Cas9_ΔphaBHR_sp3. Wildtype *phaB* amplification yields an amplicon of 2947 bp whereas Δ*phaB* would result in a 2224 bp fragment.



Figure S8. 1.2% agarose electrophoresis showing restriction digestion by *EcoRI* of colony PCRs after the conjugation of the WT strain of *R. sphaeroides* with the plasmids for knockout of *phbB*. Left panel: pBBR_Cas9_ΔphbBHR_sp1, right panel: pBBR_Cas9_ΔphbBHR_sp2. Wild-type *phbB* digestion would yield fragments of 786 and 1383 bp whereas Δ*phbB* would lead to fragments of 261, 786 and 1099 bp.

Table S1. List of plasmids used in this study.

Plasmid	Description	Source
pUC57hCas9	pUC57 vector containing DNA encoding the <i>cas9</i> gene harmonized for expression in <i>Rhodobacter sphaeroides</i> (<i>cas9_h</i>)	Baseclear
pBBR1MCS2-sgRNA	pBBR1MCS2-sgRNA derivative. Contains the BBa_J95023 promoter followed by two BsaI restriction sites, the sgRNA scaffold sequence and the BBa_J95029 terminator	Baseclear, Huo et. al, 2011, this study
pBBR1MCS2_Cas9_NT	Broad host range plasmid (KanR) containing the <i>cas9_h</i> under the control of the constitutive P _{lac} promoter and the non-targeting sgRNA under the control of the BBa_J95023 promoter and the BBa_J95029 terminator	This study
pBBR1MCS2_Cas9_sp1	pBBR1MCS2_Cas9_NT derivative, containing sgRNA with spacer 1 for targeting the <i>upp</i> gene	This study
pBBR1MCS2_Cas9_sp2	pBBR1MCS2_Cas9_NT derivative, containing sgRNA with spacer 2 for targeting the <i>upp</i> gene	This study
pBBR1MCS2_Cas9_sp3	pBBR1MCS2_Cas9_NT derivative, containing sgRNA with spacer 3 for targeting the <i>upp</i> gene	This study
pBBR_Cas9_Δupp500HR_NT	pBBR1MCS2_Cas9_NT derivative containing a non-targeting sgRNA and the genetic sequences 500 bp upstream and downstream of the <i>upp</i> gene -fused in one fragment- serving as homologous recombination template	This study
pBBR_Cas9_Δupp1000HR_NT	pBBR1MCS2_Cas9_NT derivative containing a non-targeting sgRNA and the genetic sequences 1 kb upstream and downstream of the <i>upp</i> gene -fused in one fragment- serving as homologous recombination template	This study

Plasmid	Description	Source
pBBR_Cas9_Δupp500HR_sp2	pBBR1MCS2_Cas9_NT derivative containing a sgRNA with spacer 2 and the genetic sequences 500 bp upstream and downstream of the <i>upp</i> gene -fused in one fragment- serving as homologous recombination template	This study
pBBR_Cas9_Δupp1000HR_sp2	pBBR1MCS2_Cas9_NT derivative containing a sgRNA with spacer 2 and the genetic sequences 1 kb upstream and downstream of the <i>upp</i> gene -fused in one fragment- serving as homologous recombination template	This study
pBBR_Cas9_Klupp500HR_sp4	pBBR1MCS2_Cas9_NT derivative containing a sgRNA with spacer 4 for targeting the <i>Δupp</i> genomic locus previously and 500 bp-long flanking sites for knock-in of the <i>upp</i> gene back in the <i>Δupp</i> strain via homologous recombination	This study
pBBR_Cas9_Klupp500HR_sp5	pBBR1MCS2_Cas9_NT derivative containing a sgRNA with spacer 5 for targeting the <i>Δupp</i> genomic locus previously and 500 bp-long flanking sites for knock-in of the <i>upp</i> gene back in the <i>Δupp</i> strain via homologous recombination	This study
pBBR_Cas9_Klupp1000HR_sp4	pBBR1MCS2_Cas9_NT derivative containing a sgRNA with spacer 4 for targeting the <i>Δupp</i> genomic locus previously and 1 kb-long flanking sites for knock-in of the <i>upp</i> gene back in the <i>Δupp</i> strain via homologous recombination	This study
pBBR_Cas9_Klupp1000HR_sp5	pBBR1MCS2_Cas9_NT derivative containing a sgRNA with spacer 5 for targeting the <i>Δupp</i> genomic locus previously and 1 kb-long flanking sites for knock-in of the <i>upp</i> gene back in the <i>Δupp</i> strain via homologous recombination	This study

Plasmid	Description	Source
pBBR_Cas9_ΔphaBHR_sp1	pBBR1MCS2_Cas9_NT derivative containing a sgRNA with spacer 1 targeting the <i>phaB</i> gene the genetic sequences 1 kb upstream and downstream of the <i>phaB</i> gene -fused in one fragment- serving as homologous recombination template	This study
pBBR_Cas9_ΔphaBHR_sp2	pBBR1MCS2_Cas9_NT derivative containing a sgRNA with spacer 2 targeting the <i>phaB</i> gene the genetic sequences 1 kb upstream and downstream of the <i>phaB</i> gene -fused in one fragment- serving as homologous recombination template	This study
pBBR_Cas9_ΔphaBHR_sp3	pBBR1MCS2_Cas9_NT derivative containing a sgRNA with spacer 3 targeting the <i>phaB</i> gene the genetic sequences 1 kb upstream and downstream of the <i>phaB</i> gene -fused in one fragment- serving as homologous recombination template	This study
pBBR_Cas9_ΔphbBHR_sp1	pBBR1MCS2_Cas9_NT derivative containing a sgRNA with spacer 1 targeting the <i>phbB</i> gene the genetic sequences 1 kb upstream and downstream of the <i>phbB</i> gene -fused in one fragment- serving as homologous recombination template	This study
pBBR_Cas9_ΔphbBHR_sp2	pBBR1MCS2_Cas9_NT derivative containing a sgRNA with spacer 2 targeting the <i>phbB</i> gene the genetic sequences 1 kb upstream and downstream of the <i>phbB</i> gene -fused in one fragment- serving as homologous recombination template	This study

Table S2. List of primers used in this study.

	Oligo	Sequence	Description
Ubiquitin PCR	P3- Ec_ubi1	GATAGCGTCCTAACGGCGTT	FW for ubiquitin PCR to check post-conjugational <i>E. coli</i> contamination. Anneals to <i>E. coli</i> genome
	P4- Ec_ubi2	GGGTTTGTGAGCAGAATGA	RV for ubiquitin PCR to check post-conjugational <i>E. coli</i> contamination. Anneals to <i>E. coli</i> genome
	P5- Rs_ubi105 F	GAACCCCTGCCGGCTGGATTACA	FW for ubiquitin PCR to check post-conjugational <i>E. coli</i> contamination. Anneals to <i>R. sphaeroides</i> genome
	P6- Rs_ubi501 R	CATGGCGAAGCTCTGGGATTG	RV for ubiquitin PCR to check post-conjugational <i>E. coli</i> contamination. Anneals to <i>R. sphaeroides</i> genome
RT-PCR Cas9	BG11112	GCCCGTTCTCGAGTTCG	FW to check Cas9 transcription in pBBR_Cas9_NT
	BG11115	GAATCGATCCTCCCAAGAG	RV to check Cas9 transcription in pBBR_Cas9_NT
Non-targeting: pBBR_Cas9_NT	BG10937	GACAAAAAGTACTCGATTGGGC	FW for amplifying <i>cas9_h</i> from pUC57
	BG10938	CTAATGGTGATGGTGATGGTGATC	RV for amplifying <i>cas9_h</i> from pUC57
	BG10939	GCCCAATCGAGTACTTTTGTGTC CATAGCTGTTTCCTGTGTGAAATT G	FW for linearizing pBBR1MCS2-sgRNA with homologous overhang for Gibson assembly with <i>cas9_h</i>
	BG10941	TCACCATCACCATCACCATT GGAGGTCGACGGTGATTGATTG AG	RV for linearizing pBBR1MCS2-sgRNA with homologous overhang for Gibson assembly with <i>cas9_h</i>
upp targeting	BG11415	ACCTTAACAAGCTCGTCGACGAC	FW for linearizing the conserved parts of <i>cas9_h</i> and backbone of pBBR_Cas9_NT
	BG11416	GCTATCTGGACAAGGGAAAAACG C	RV for linearizing the conserved parts of <i>cas9_h</i> and backbone of pBBR_Cas9_NT

Oligo	Sequence	Description
BG11412	GTCGTCGACGAGCTTGTTAAGGT	RV conserved for amplifying part of the <i>hCas9</i> gene and include the spacer of interest for <i>upp</i> in the sgRNA (provided by FW)
BG11411	CGGCGTCTGGATCGTCGTCGGT TTTAGAGCTAGAAATAGCAAGTT AAA ATAAGGCTAGTC	FW to combine with BG11412 for amplifying the sgRNA including the spacer 3 for <i>upp</i> and part of <i>hCas9</i> gene
BG11486	CACCTTCGCATAATATTGCAGTT TTAGAGCTAGAAATAGCAAGTTA A AATAAGGCTAGTC	FW to combine with BG11412 for amplifying the sgRNA including the spacer 1 for <i>upp</i> and part of <i>cas9_h</i> gene
BG11487	ATCGATCTCCTGAAGGAGAAGTT T TAGAGCTAGAAATAGCAAGTTAA AA TAAGGCTAGTC	FW to combine with BG11412 for amplifying the sgRNA including the spacer 2 for <i>upp</i> and part of <i>cas9_h</i> gene
BG11413	GCGTTTTCCCTTGTCAGATAGC	FW conserved for amplifying the conserved part of the backbone and include the spacer of interest for <i>upp</i> in the sgRNA (provided by RV)
BG11414	CGACGACGATCCAGACGCCGAA C CAGCGATCCCGTCCG	RV to combine with BG11413 for amplifying the sgRNA including the spacer 3 for <i>upp</i> and part of <i>pBBR1MCS2-sgRNA</i> backbone
BG11488	TGCAATATTATGCGAAGGTGAA CCAGCGATCCCGTCCG	RV to combine with BG11413 for amplifying the sgRNA including the spacer 1 for <i>upp</i> and part of <i>pBBR1MCS2-sgRNA</i> backbone
BG11489	TTCTCCTCAGGAGATCGATAAC C AGCGATCCCGTCCG	RV to combine with BG11413 for amplifying the sgRNA including the spacer 2 for <i>upp</i> and part of <i>pBBR1MCS2-sgRNA</i> backbone

	Oligo	Sequence	Description
upp knock-out	BG11886	gtgcgggcctcttcgtatta	FW to amplify pBBR_Cas9NT including the sgRNA with non-targeting spacer and the <i>cas9_h</i> gene
	BG11182	CCATGTCGGCAGAATGCTTAATG	RV to amplify pBBR_Cas9NT including the sgRNA with non-targeting spacer and the <i>cas9_h</i> gene
	BG11887	CATTAAGCATTCTGCCGACATGG	FW to amplify pBBR_Cas9NT including the backbone
	BG11888	gcctgaatggcgaatggaaattgtaa	RV to amplify pBBR_Cas9NT including the backbone
	BG11866	CTCTGTAAAGCGGGTTTCC CTTAATGGTCAAGCATGGTCGGG C	FW for 500/1000 bp amplification of the first homology region of <i>upp</i> . It contains overhangs with BG11871
	BG11867	taatagcgaagaggcccgacCGACGA GACGGTGGGCAA	RV for 500 bp amplification of the homology region of <i>upp</i> .
	BG11869	ttacaatttcattcgccattcaggcTTT CCACGTCTTCGCCGG	FW for 500 bp amplification of the second homology region of <i>upp</i> .
	BG11871	TAAGGGAAACCCGCTTTACA GAG	RV for 500/1000 bp amplification of the second homology region of <i>upp</i> . It contains overhangs with BG11866
	BG11868	taatagcgaagaggcccgacCGC ATCTGGGCCTCTCCAA	RV for 1000 bp amplification of the first homology region of <i>upp</i> .
	BG11870	ttacaatttcattcgccattcaggcTG TCTCTAGCGGAGGAATGCGT	FW for 1000 bp amplification of the second homology region of <i>upp</i> .
upp knock-in	BG12347	GATGGTCAAGCACGGTCGGG	FW for <i>upp</i> flanking site 1 amplification, including overhang for BG12348 and point mutation for the start ATG codon
	BG12348	CCCGACCGTGCTTGACCATC	RV for <i>upp</i> flanking site 1 amplification, including overhang for BG12347 and

Oligo	Sequence	Description	
BG12908		point mutation for the start ATG codon	
	TAATGGTCAAGCATGGTCGGA ACCAGCGATCCCGTCCG	RV to combine with BG11886 for amplifying the sgRNA including the spacer 4 for <i>Δupp</i> and part of <i>pBBR1MCS2-sgRNA backbone</i>	
	CCGACCATGCTTGACCATTAGT TTTAGAGCTAGAAATAGCAAGT TAAATAAAGGCTAGTC	FW to combine with BG11182 for amplifying the sgRNA including the spacer 4 for <i>Δupp</i> and part of <i>hCas9</i> gene	
	TTAAGGGAAACCCCGCTTTAA CCAGCGATCCCGTCCG	RV to combine with BG11886 for amplifying the sgRNA including the spacer 5 for <i>Δupp</i> and part of <i>pBBR1MCS2-sgRNA backbone</i>	
BG12909	TAAAGCGGGGTTTCCCTTAAGTT TTAGAGCTAGAAATAGCAAGTT AAAATAAGGCTAGTC	FW to combine with BG11182 for amplifying the sgRNA including the spacer 5 for <i>Δupp</i> and part of <i>hCas9</i> gene	
<i>phaB</i> and <i>phbB</i> knock-out	P301	CCATGTCGGCAGAATGCTTAATG	RV to amplify pBBR_Cas9NT including the sgRNA with non-targeting spacer and the <i>hCas9</i> gene
	P302	CATTAAGCATTCTGCCGACATGG	FW to amplify pBBR_Cas9NT including the backbone
	P303	gcctgaatggcgaatggaaattgtaa	RV to amplify pBBR_Cas9NT including the backbone
	P304	gtgcgggcctcttcgctatta	FW to amplify pBBR_Cas9NT including the sgRNA with non-targeting spacer and the <i>hCas9</i> gene
	P379	taatagcgaagaggccgcac ATGTCC AGCTGGGCGAC	RV for <i>phaB</i> flanking site 1, amplification, with overhang for the backbone
	P380	TTTTCAGGATGAGAAGATCC GAT C CCTCCTTCAAATATCCGC	FW for <i>phaB</i> flanking site 1, amplification, with overhang for flanking site 2

Oligo	Sequence	Description
P381	GGATATTTGAAGGAGGGATCGG A TCTTCTCATCCTGAAAACCA	RV for <i>phaB</i> flanking site 1, amplification, with overhang for flanking site 1
P382	ttacaatttcattcgccattcaggcGAGC C TCTGTCTCGC	FW for <i>phaB</i> flanking site 1, amplification, with overhang for the backbone
P383	GACCTACAAATGGTCCGTCGGTT TT AGAGCTAGAAATAGCAAGTTAA A ATAAGGCTAGTC	FW for sgRNA sp1 , spCas9 and backbone
P384	CGACGGACCATTGTAGGTCAAC CA GCGATCCCGTCCG	RV for sgRNA sp1 , backbone, overhang for flanking site 1
P385	CGGGCAGGCGAACTATTCGGGT TTT AGAGCTAGAAATAGCAAGTTAA AA TAAGGCTAGTC	FW for sgRNA sp2 , spCas9 and backbone
P386	CCGAATAGTTCGCCTGCCCCAAC CA GCGATCCCGTCCG	RV for sgRNA sp2 , backbone, overhang for flanking site 1
P387	CAATCTCTCCGGTTCGCCGTTT TA GAGCTAGAAATAGCAAGTTAAA ATA AGGCTAGTC	FW for sgRNA sp3 , spCas9 and backbone
P388	CGGCGAACCGGAGGAGATTGAA CC AGCGATCCCGTCCG	RV for sgRNA sp3 , backbone, overhang for flanking site 1
P413	taatagcgaagaggcccgacAGGAGA AT ATCGAGCTCGGC	RV for <i>phbB</i> flanking site 1, amplification, with overhang for the backbone
P414	TAGGAATTCCTACTACTACTACAC GG TGATGCCGAAGG	FW for <i>phbB</i> flanking site 1, amplification, with overhang for flanking site 2
P415	GTGTAGTAGTAGTAGGAATTCCT ACGATGCGGCGCTGGCC	RV for <i>phbB</i> flanking site 1, amplification, with overhang for flanking site 1
P416	ttacaatttcattcgccattcaggcTTGC G CGCCCGGTCTCA	FW for <i>phbB</i> flanking site 1, amplification, with overhang for the backbone

Oligo	Sequence	Description
P417	TCGGCAGCTGCTTCGGACCGAAC CAGCGATCCCGTCCG	FW for sgRNA sp1 , spCas9 and backbone
P418	CGGTCCGAAGCAGCTGCCGAGTT T TAGAGCTAGAAATAGCAAGTTAA AATAAGGCTAGTC	RV for sgRNA sp1 , backbone, overhang for flanking site 1
P419	CGGTCCGAAGCAGCTGCCGAAA CCAGCGATCCCGTCCG	FW for sgRNA sp2 , spCas9 and backbone
P420	TCGGCAGCTGCTTCGGACCGGTT T TAGAGCTAGAAATAGCAAGTTAA AATAAGGCTAGTC	RV for sgRNA sp2 , backbone, overhang for flanking site 1
sequencing	BG12037	GGCCGAAGGGCTGCATC for Δupp sequencing
	BG12038	CATGGCAACGATCCACCTT for Δupp sequencing
	P409	AGCATCAACCAGGTCTGCGG For sequencing <i>phaB</i> knockout
	P410	ACAACGGCATCCCGACGA For sequencing <i>phaB</i> knockout
	P423	CGAGGACCGGCGCATCTT For ΔphbB sequencing
	P424	CGGGCATCCTGTTCTGATGT For ΔphbB sequencing

Table S3. The sequence of the sgRNA expressing module (promoter BBa_J95023, sgRNA scaffold and BBa_J95029 terminator) in FASTA format.

>sgRNA-module

```
TCGTCTCTTCGTCATTTTTCTCTTGCGGGTTTTTTTGCAGTTCCCTAGATAGCGCCTACCGAA
GCGGAACGGCGACGGTGACGGGGTTGAGAGGCGGCGGTGCTGCCTTGAGGCTTTTCGGAAAT
CTGGAAGATGAGGCGGACGGGATCGCTGGTTNNNNNNNNNNNNNNNNNNNGTTTTAGA
GCTAGAAATAGCAAGTTAAATAAGGCTAGTCCGTTATCAACTGAAAAAGTGGCACCGAGTC
GGTGCTTTGATCCGGTGGATGACCTTTTGAATGACCTTTAATAGATTATATTACTAATTAATTG
GGGACCCTAGAGTCCCCTTTTTATTTTAAAAATTTTTTACAAAACGGTTTACAAGCATAAA
GCTTGCTCAATCAATCACC
```

Table S4. The sequence of the codon harmonised *cas9* gene (hcas9) for *R. sphaeroides* in FASTA format.

>hcas9

```
ATGGACAAAAAGTACTCGATTGGGCTCGACATCGGGACCAACTCCGTTGGGTGGGCTGTTATC
ACCGACGAGTACAAAGTCCCTTGAAGAAATTTAAAGTCTTGGGGAACACCGATCGTCATAGC
ATCAAGAAGAACCTTATTGGAGCGCTTCTCTCGATAGCGGGGAAACCGCTGAGGCTACCCGG
```

TTGAAGCGAACCGCGCGGAGGAGGTACACCCGGCGAAAAAACCGGATCTGCTACCTTCAGGA
AATCTTCTCGAACGAAATGGCTAAGGTTGACGACAGCTTTTCCACCGTCTTGAGGAATCGTTC
CTTGTTGAGGAGGATAAAAAACACGAGCGGCACCCCATCTTCGGGAACATTGTTGACGAGGT
CGCGTACCACGAAAAGTACCCACCATCTACCACTTGCGTAAGAAGCTTGTTGACTCGACCGA
CAAGGCTGACCTTCGTCTCATCTACCTTGACTCGCTCACATGATCAAATCCGGGGGCACTTC
CTTATCGAAGGGGACCTCAACCCGACAACAGCGACGTTGATAAGCTTTTCATCCAGCTTGTTT
AGACGTACAACAGCTCTTCGAGGAGAACCCCATCAACGCTAGCGGGGTTGACGCGAAGGCT
ATCCTTTCGGCTCGTCTTAGCAAGTCGAGGCGTCTCGAGAACTTGATCGCGCAGTTGCCTGGG
GAAAAAAGAACGGGCTCTTCGAAACTTGATCGCGCTTTCGCTTGGGCTTACGCCAACTTC
AAGTCGAACCTTCGACCTTGCTGAGGACGCGAAGCTCCAGCTTTCGAAGGACACCTACGACGAC
GACCTCGACAACCTCCTTGCTCAGATCGGGGACCAGTACGCGGACCTTTCTTGCTGCGAAA
AACCTCTCGGACGCGATCCTCCTTTCGGACATCCTTAGGGTTAACACCGAGATTACCAAAGCGC
CTCTTTCGGCGTCGATGATCAAGCGTTACGACGAGCACCACCAGGATCTTACCCTTCTCAAGGC
GCTCGTCCGTCAGCAGCTTCCCGAGAAATACAAGGAGATCTTCTCGACCAGTCGAAGAACGG
GTACGCTGGGTACATCGACGGAGGGGCGTCCAGGAGGAGTTCTACAAGTTTCATCAAGCCCA
TCCTCGAGAAGATGGACGGGACCGAAGAGCTCCTTGTTAAGCTTAACCGGGAGGACCTTTTGC
GTAACAGCGAACGTTTCGATAACGGGTCGATCCCTCACCAGATCCATCTTGGGGAATTGCACG
CGATCCTTAGGAGGCAGGAGGATTTCTACCCCTTCTCAAGGATAACCGGGAAAAAATCGAG
AAGATCCTTACCTTCCGTATCCCCTACTACGTGGGCCCTTGCTCGGGGGAACAGCCGGTTG
CTTGGATGACCCGAAAATCGGAGGAGACCATCACGCCCTGGAACCTTCGAGGAGGTCTGTTGAC
AAGGGGGCGTCGGCGCAGTCGTTATCGAGCGTATGACCAACTTCGACAAGAACCTTCCCAAC
GAGAAGGTTCTCCCAAGCACAGCCTTCTTACGAATACTTCACGGTCTACAACGAGCTTACCA
AAGTTAAGTACGTACCCGAGGGGATGCGTAAGCCCGCTTCTTTCGGGGGAGCAGAAAAAG
GCAATCGTCGACCTCTTGTTTAAGACCAACCGTAAGGTTACGGTCAAACAGCTCAAGGAGGAC
TACTTTAAGAAGATTGAGTGCTTCGACAGCGTCGAGATCTCGGGGTCGAGGACAGGTTCAA
CGCGTCGCTCGGGACGTACCACGACCTTCTAAGATCATCAAGGACAAGGACTTCTTGACAA
CGAGGAGAACGAGGACATCCTCGAAGACATCGTCTCACCCCTTACGCTCTTCGAGGACAGGG
AAATGATCGAAGAGAGGCTTAAGACCTACGCGCATTTGTTTCGACGACAAAGTTATGAAGCAG
CTTAAGCGGCGTCGGTACACCGGTGGGGGCGGCTTTCGCGTAAGCTTATCAACGGGATCAG
GGACAAACAGTCGGGGAAGACCATTCTCGACTTCTTAAGTCGGACGGGTTTCGAAACCGTA
ACTTCATGCAGTTGATCCACGACGACAGCCTTACCTTCAAGGAGGATATCCAGAAGGCTCAGG
TTTCGGGGCAGGGGGACAGCCTCCACGAGCACATCGCTAACCTCGCGGGGTCCCCCGGATC
AAGAAGGGGATCCTCCAGACCGTTAAGGTCGTCGACGAGCTTGTTAAGGTTATGGGACGACA
CAAACCCGAGAACATCGTCATCGAGATGGCTCGGGAGAACCAGACCACCCAGAAAGGGCAGA
AGAACTCCCCTGAACGGATGAAGCGTATCGAGGAGGGGATCAAGGAGCTCGGGAGCCAGAT
CCTTAAGGAACACCCCGTCGAGAACACCCAGCTTCAGAACGAGAAATTGTACTTGTAACCTT
GCAGAACGGGAGGGATATGTACGTTGATCAGGAGCTCGACATCAACCGGCTCAGCGACTACG
ACGTTGACCATATCGTCCCCAGAGCTTCTTAAGGATGACTCGATTGATAACAAAGTTCTCAC
GCGGTCGGACAAGAACCGGGGGAAAGTCCGACAACGTCCCAGCGAGGAGGTTGTTAAGAAA
ATGAAGAACTACTGGAGGCAGCTTCTTAACGCAAACTCATCACCCAGCGGAAATTCGACAAC
CTCACGAAGGCGGAGCGGGGGGGGCTTAGCGAGCTTGACAAGGCGGGGTTTCATCAAGCGTC
AGCTTGTCGAGACCCGTCAGATACCAAACACGTTGCTCAGATCCTTGACAGCCGTATGAACA
CCAAGTACGACGAGAACGACAAGCTTATCCGTGAAGTCAAGGTTATCACGCTCAAGTCGAAG
CTCGTCTCGGATTTTCGTAAGGACTTTCAGTTTTACAAGGTTTCGGGAAATCAACAACTACCACC
ACGCACACGACGCTTACCTTAACGCAGTTGTCGGGACCGCGCTTATCAAAAAGTACCCCAAGC

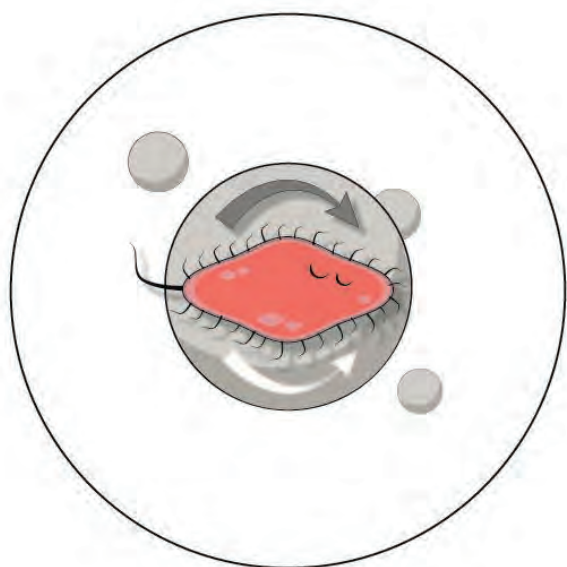
TTGAGTCCGAATTCGTTTACGGGGACTACAAGGTCTACGACGTCCGGAAGATGATCGCGAAAT
 CGGAACAGGAGATTGGGAAGGCTACGGCTAAGTACTTTTTCTACTCGAACATCATGAACTTTT
 TTAAGACCGAGATCACCTTGCTAACGGGGAAATCCGTAAGCGTCCCCTTATCGAGACCAACG
 GAGAGACCGGGGAGATCGTTTGGGACAAGGGACGTGACTTCGCAACCGTTCGTAAGGTTCTT
 TCCATGCCTCAGGTAAACATCGTTAAAAAGACCGAGGTTAGACCGGGGGGTTTCCAAAGAA
 TCGATCCTCCCAAGAGGAACCTCGATAAACTATCGCGCGGAAGAAGGATTGGGACCCCAA
 GAAGTACGGGGGGTTCGACAGCCCCACGGTTGCGTACTCGGTTCTTGTGTCGCGAAAGTTG
 AGAAGGGAAAGTCCAAAAAAGTCAAGTCCGTCAAGGAACCTCTTGAATCACCATCATGGAG
 AGGAGCTCCTTCGAGAAGAACCCTATCGATTTCTCGAGGCGAAGGGGTACAAAGAGGTCAA
 GAAGGATCTCATCATCAAGCTTCCCAAGTACAGCCTTTTCGAACTCGAGAACGGGCGGAAGCG
 AATGTTGGCGAGCGCAGGGGAGCTCCAGAAGGGGAACGAATTGGCGTTGCCCTCCAAGTAC
 GTTAACTTCTCTACCTCGCGAGCCACTACGAGAACTTAAAGGGAGCCCCGAGGACAACGAG
 CAGAAGCAGCTTTTCGTTGAACAGCACAAACACTACCTCGACGAAATCATCGAACAGATCAGC
 GAGTTCTCGAAACGGGTATCCTCGCTGACGCAAACCTCGACAAGGTCCTTAGCGCTTACAAC
 AAGCACAGGGATAAGCCCATTGCGGAGCAGGCTGAGAACATCATCCACCTCTTCACGCTTACG
 AACCTTGGGGCGCCTGCGGCGTTCAAGTACTTCGACACCACCATCGACCGGAAGCGTTACAG
 TCGACCAAGGAGGTCCTCGACGCAACCCTATCCACCAGTCCATCACCGGGCTTACGAGACC
 CGTATCGACCTTAGCCAGCTTGGGGGGGATTAA

Table S5. List of spacers used for targeting *Rhodobacter sphaeroides*' genomic DNA.

Spacer name	Sequence (5' -3')	PAM	Targeted gene
NT	AGGAGGGACGTTGCGACAAG	---	
sp1	CACCTTCGCATAATATTGCA	CGG	<i>upp</i>
sp2	ATCGATCTCCTGAAGGAGAA	GGG	<i>upp</i>
sp3	CGGCGTCTGGATCGTCGTCG	TGG	<i>upp</i>
sp4	CCGACCATGCTTGACCATTA	AGG	Δupp
sp5	TAAAGCGGGGTTTCCCTTAA	TGG	Δupp
sp1	GACCTACAAATGGTCCGTCG	CGG	<i>phaB</i>
sp2	CGGGCAGGCGAACTATTCGG	CGG	<i>phaB</i>
sp3	CAATCTCCTCCGGTTCGCCG	AGG	<i>phaB</i>
sp1	CGGTCCGAAGCAGCTGCCGA	AGG	<i>phbB</i>
sp2	TCGGCAGCTGCTTCGGACCG	CGG	<i>phbB</i>

Table S6. Effect of the *phaB* (RSP_0747) and the *phbB* (RSP_3963) knockout, as well as of the combined knockout, on the C/N ratios the acids production and the PHB accumulation in *Rhodobacter sphaeroides* under nitrogen excess and limiting conditions on a defined medium.

	Active biomass (g/L)	PHB (g/L)
WT	0.81 ± 0.12	0.34 ± 0.018
<i>ΔphaB</i>	0.69 ± 0.11	0.002 ± 0.002
<i>ΔphbB</i>	0.79 ± 0.09	0.35 ± 0.0035
<i>ΔphaB ΔphbB</i>	0.78 ± 0.11	0.0001 ± 0.00



Chapter 4

Functional replacement of isoprenoid pathways in *Rhodobacter sphaeroides*

This chapter has been published as: Orsi, E.*, Beekwilder, J.*, van Gelder, D., van Houwelingen, A., Eggink, G., Kengen, S. W. M. & Weusthuis, R. A. (2020). Functional replacement of isoprenoid pathways in *Rhodobacter sphaeroides*. *Microbial Biotechnology*, 13(4), 1082-1093.

*contributed equally

Abstract

Advances in synthetic biology and metabolic engineering have proven the potential of introducing metabolic by-passes within cell factories. These pathways can provide a more efficient alternative to endogenous counterparts due to their insensitivity to host's regulatory mechanisms. In this work, we replaced the endogenous essential 2-C-methyl-D-erythritol 4-phosphate (MEP) pathway for isoprenoid biosynthesis in the industrially relevant bacterium *Rhodobacter sphaeroides* by an orthogonal metabolic route. The native 2-C-methyl-D-erythritol 4-phosphate (MEP) pathway was successfully replaced by a heterologous mevalonate (MVA) pathway from a related bacterium. The functional replacement was confirmed by analysis of the reporter molecule amorpha-4,11-diene after cultivation with [4-¹³C]glucose. The engineered *R. sphaeroides* strain relying exclusively on the MVA pathway was completely functional in conditions for sesquiterpene production and, upon increased expression of the MVA enzymes, it reached even higher sesquiterpene yields than the control strain co-expressing both MEP and MVA modules. This work represents an example where substitution of an essential biochemical pathway by an alternative, heterologous pathway leads to enhanced biosynthetic performance.

Keywords

Rhodobacter sphaeroides, Isoprenoid pathways, MEP, MVA, pathway replacement, ¹³C glucose

Introduction

Synthetic biology conceptualizes biological functions as independent parts which can be manipulated, and whose effects can be analyzed (165). Applying this view to cellular metabolism, the metabolic network of a microorganism can be divided into metabolic pathways (modules resembling operation units) which can be modelled and optimized (26). Engineering *modules* as parts of *wholes* (26, 166) is an expression that suggests the interchangeability of parts within biological systems, which can still result in functional organisms. Application of this concept allowed to achieve remarkable results in terms of metabolic optimization for a wide range of biotechnological applications (167–171).

Isoprenoid biosynthesis provides an example of “natural” independence between essential modules. Two essentially different biosynthetic routes exist that branch from the central metabolism and converge to the isoprene units isopentenyl-diphosphate (IPP) and dimethylallyl-diphosphate (DMAPP). These are the 2-C-methyl-D-erythritol 4-phosphate (MEP) and the mevalonate (MVA) pathway. With few exceptions, they are generally phylogenetically distinct, with MEP being present in prokaryotes, and MVA in eukaryotes and archaea. Photosynthetic eukaryotes harbor both pathways naturally, compartmentalizing the MEP pathway within the chloroplast while the MVA pathway operates in the cytosol (44). The MEP pathway starts with the condensation of glyceraldehyde-3-phosphate (GAP) with pyruvate (PYR), while the MVA pathway uses acetoacetyl-CoA (AA-CoA) and acetyl-CoA (Ac-CoA) as substrates. The products of the two pathways, IPP and its isomer DMAPP, are the starting compounds for all terpenoids (45). These compounds are essential for the organism, as they are involved in several functions necessary for life, like respiration and photosynthesis by ubiquinone, chlorophyll and carotenoids. Moreover, many

terpenoids have raised attention in biotechnology as interesting compounds for pharmaceutical, flavors, chemicals and also biofuels (8, 11, 46, 51, 53, 172).

Biotechnological production of terpenoids by engineered microbial cell factories (or *chassis*) has been extensively described, co-expressing both MEP and MVA pathways together, mainly for bypassing the regulation on the host's native biosynthetic route (106, 173). An example of organism that has undergone this type of engineering is *Rhodobacter sphaeroides* (91). In fact, this bacterium is raising interest as potential platform for biotechnological isoprenoid production. In this species, low oxygen conditions lead to formation of intracellular membranes rich of isoprenoid-derived compounds like carotenoids and bacteriochlorophylls. Moreover, several studies have been performed to exploit this microorganism for the production of coenzyme Q₁₀ and sesquiterpenes (91, 95, 134).

Here, the effect of fully replacing the native MEP pathway by a heterologous MVA pathway is described for *R. sphaeroides*. The resulting microorganism relies exclusively on the MVA pathway, and produces sesquiterpenes at an even higher yield than the parental strain harboring both MEP and MVA pathways. This work represents an example of replacement of an essential pathway by an independent module, resulting in an improvement of the metabolic capacities of a *chassis*.

Materials and methods

Strains, preculturing and culturing

The strains and plasmids used are listed in **Table S1**. The strain Rs265 was kindly provided by Isobionics BV. Unless specified, all *R. sphaeroides* cultivations were performed using Sistrof's minimal medium (SMM), containing: 3 g/L glucose, 3.48 g/L KH_2PO_4 , 1.0 g/L NH_4Cl , 0.1 g/L glutamic acid, 0.04 g/L L-aspartic acid, 0.5 g/L NaCl, 0.02 g/L nitrilotriacetic acid, 0.3 g/L $\text{MgSO}_4 \cdot 7\text{H}_2\text{O}$, 0.00334 g/L $\text{CaCl}_2 \cdot 2\text{H}_2\text{O}$, 0.002 g/L $\text{FeSO}_4 \cdot 7\text{H}_2\text{O}$, 0.0002 g/L $(\text{NH}_4)_6\text{Mo}_7\text{O}_{24}$. Trace elements were added 0.01 % v/v from a stock solution containing: 17.65 g/L disodium EDTA, 109.5 g/L $\text{ZnSO}_4 \cdot 7\text{H}_2\text{O}$, 50 g/L $\text{FeSO}_4 \cdot 7\text{H}_2\text{O}$, 15.4 g/L $\text{MnSO}_4 \cdot 7\text{H}_2\text{O}$, 3.92 g/L $\text{CuSO}_4 \cdot 5\text{H}_2\text{O}$, 2.48 g/L $\text{Co}(\text{NO}_3)_2 \cdot 6\text{H}_2\text{O}$, 0.114 g/L H_3BO_3 . Vitamins were added 0.01 % v/v from a stock containing: 10 g/L nicotinic acid, 5 g/L thiamine HCl, 0.1 g/L biotin.

Preculturing of the strains started by their passage from glycerol stocks to LB plates supplemented with kanamycin 50 $\mu\text{g}/\text{mL}$ and incubated at 30°C. After 48-72 h, once colonies were visible on the plates, they were transferred to Greiner tubes containing 5 mL liquid LB medium and kanamycin (50 $\mu\text{g}/\text{mL}$). The tubes were incubated for 24 h at 30°C and 250 rpm. Subsequently, an aliquot of 500 μL was transferred to a 250-mL Erlenmeyer flask containing 25 mL of SMM. Accordingly, incubation of the flasks at 30°C and 250 rpm followed. After 16-20 h, the strains were diluted to an initial OD_{600} of 0.1 in 50 mL fresh SMM. When necessary, 10% v/v of dodecane was added to the aqueous phase.

Genomic integration of the mevalonate pathway

Genome editing of *R. sphaeroides* was performing using RÄ medium, which contained: 3 g/L malic acid (as only carbon source), 0.2 g/L $\text{MgSO}_4 \cdot 7\text{H}_2\text{O}$, 1.2 g/L $(\text{NH}_4)_2\text{SO}_4$, 0.07 g/L $\text{CaCl}_2 \cdot 2\text{H}_2\text{O}$, 1.5 mL of microelements stock solution, 2 mL of

vitamin stock solution and 5 mL of phosphate buffer. In case of RÄ agar medium, 15 g/L agar was added. The microelements solution contained: 0.5 g/L Fe(II)-Citrate, 0.02 g/L $\text{MnCl}_2 \cdot 4\text{H}_2\text{O}$, 0.005 g/L ZnCl_2 , 0.0025 g/L KBr, 0.0025 g/L KI, 0.0023 g/L $\text{CuSO}_4 \cdot 5\text{H}_2\text{O}$, 0.041 g/L Na_2MoO_4 , 0.005 g/L $\text{CoCl}_2 \cdot 6\text{H}_2\text{O}$, 0.0005 g/L $\text{SnCl}_2 \cdot 2\text{H}_2\text{O}$, 0.0006 g/L $\text{BaCl}_2 \cdot 2\text{H}_2\text{O}$, 0.031 g/L AlCl, 0.41 g/L H_3BO_3 , 0.02 g/L EDTA. The vitamin solution contained: 0.2 g/L nicotinic acid, 0.4 g/L thiamine HCl, 0.008 g/L biotin, 0.2 g/L nicotinamide. The phosphate buffer contained 0.6 g/L KH_2PO_4 and 0.9 g/L K_2HPO_4 .

The mevalonate operon from *P. zeaxanthinifaciens* was cloned from pBBR-MVA plasmid (113, 114) into pUC18Not plasmid (Biomedal, Sevilla, Spain) using restriction enzymes EcoRI and SphI. From the resulting plasmid pUC18Not-MVA, the operon was taken out and cloned into pUT-Mini-Tn5-Sp/Sm (Biomedal, Sevilla, Spain) using restriction enzyme NotI, according to the manufacturer's instructions. Orientation of the MVA operon in pUT-Mini-Tn5-Sp/Sm was confirmed by SphI digestion, and by sequencing using primers Tn5-fw and Tn5-Re (**Table S2**). Two clones called pUT-Tn5-MVA#1 and #2, each of them with a different orientation of the insert, were selected.

pUT-Tn5-MVA#1 and #2 were introduced into *Escherichia coli* S17-1 λ pir (Biomedal, Sevilla, Spain), and were selected on ampicillin (100 $\mu\text{g}/\text{ml}$) and spectinomycin (50 $\mu\text{g}/\text{ml}$). For conjugation, Rs265 harboring pBBR-CnVS plasmid (91) was grown at 30°C in liquid RÄ medium supplemented with kanamycin (50 $\mu\text{g}/\text{ml}$). *E. coli* S17-1 λ pir with pUT-Tn5-MVA#1 and #2 were grown overnight at 37°C in LB medium with ampicillin (100 $\mu\text{g}/\text{ml}$) and spectinomycin (50 $\mu\text{g}/\text{ml}$). *R. sphaeroides* and *E. coli* cells were washed and mixed for conjugation according to standard procedures, co-incubated on filters and finally plated on RÄ agar with kanamycin (50 $\mu\text{g}/\text{ml}$) and spectinomycin (50 $\mu\text{g}/\text{ml}$). Resulting colonies were

purified on selective RS102 medium by re-streaking, and were further selected by colony PCR, for the presence of mevalonate pathway (primers *mvaA* fw/re; *mvd* fw/re), *CnVS* (*cnvs*-fw/re) and *R. sphaeroides* DNA (*Rs-rps1* fw/re), and the absence of transposase (*tnp*-fw/re), to confirm integration of the MVA in the genome and absence of the plasmid. Thus, three independent lines of Rs265-MVA + pBBR-*CnVS* (#5, #6 and #7) were selected.

Plasmid assembly for deletion of *dxr*

All the primers used in this work are listed in the **Table S2**. For designing *dxr* deletion, the recently developed CRISPR-Cas9 toolbox for *R. sphaeroides* (174) was used. The plasmids used harbored the information for genomic *dxr* removal by homologous recombination (HR) and subsequent counter-selection via Cas9 targeting on the *wild-type* genomic copy of *dxr*. Assembly of the plasmid was performed by five-fragments HiFi Assembly (New England Biolabs, USA) as previously described (174). The non-targeting pBBR_Cas9_NT plasmid was used for amplification of the backbone with the primers P302/P303. Moreover, it was also used for amplifying the harmonized *spCas9* amplicon including the *lac* promoter upstream to the coding sequence, while downstream contained the sgRNA module with the targeting spacer as overhang. Two spacers were used for targeting *dxr*, therefore two variants of this amplicon were generated with the primers sets P301/P403 and P301/P407 for *sp1* and *sp2*, respectively. The third amplicon generated using pBBR_Cas9_NT as template was obtained by using the complementary sequence of the spacers as overhang, and amplified a short fragment until the insertion point of the flanking sites for HR. Hence, since two spacers were used, the two amplicons were generated with the primers sets P304/P404 and P304/P408. The remaining two fragments included the flanking sites for HR. These two 1 kb fragments were designed for completely removing the *dxr* coding sequence (1185 bp). They were amplified from *R. sphaeroides*

genomic DNA using the primers P399/P400 and P401/P402, and contained overhangs in their primers for assembly of the plasmids pBBR_Cas9_Δ*dxr*_sp1 and pBBR_Cas9_Δ*dxr*_sp2.

Deletion of *dxr* for endogenous MEP inactivation

The two *dxr* targeting plasmids pBBR_Cas9_Δ*dxr*_sp1 and pBBR_Cas9_Δ*dxr*_sp2 were transferred to *R. sphaeroides* containing the integrated MVA pathway by conjugation as previously described (174). Conjugants were transferred to RÄ plates supplemented with kanamycin 50 µg/mL. Genomic DNA screening for presence of mutants was done by using the primers P437/P438. Additional colony PCRs for determining latent *dxr* copies were done with the primers P469/P471 and P468/P470. Validation of Δ*dxr* by colony PCR screening was followed by sequencing using the primers P455 and P456 for confirming *dxr* deletion from the genomic locus. Mutants were cured from the targeting plasmid by several passages in RÄ plates (kanamycin free). As control, each colony was additionally transferred in parallel to RÄ plates supplemented with kanamycin 50 µg/mL. Once the loss of antibiotic resistance was observed on plates supplemented with kanamycin, the plasmid removal was confirmed by PCR using the primers P368/P369, which amplify part of the coding sequence of the *spCas9* sequence. Δ*dxr* colonies were therefore conjugated with *E. coli* S17-1 λpir harboring the pBBR-*ads* or pBBR-MVA-*ads* plasmids.

Growth and production assays

Quantitative physiological data on the strains were obtained by incubating the cultures with an initial OD₆₀₀ of 0.1 in 250-mL Erlenmeyer flasks containing 45 mL of SMM and 5 mL of dodecane. The medium was supplemented with kanamycin (50 µg/mL) for maintaining the pBBR-*ads* or pBBR-MVA-*ads* plasmid. The flasks were incubated at 30°C and 250 rpm. Growth was followed for the first 12 h for

determining the growth (following OD) and glucose consumption rates (using YSI 2950 from Shimadzu). After 24 h, the cultivations were stopped, and the cultures were collected by centrifugation of the whole cultivation broth at 4255 x g for 15 min. From the dodecane layer, amorphadiene concentrations were determined using a GC-FID 7890A from Agilent as previously described (134). From the aqueous phase, the residual glucose concentrations were measured using YSI 2950 from Shimadzu. The pellet was resuspended in MilliQ water to its original volume, and the biomass concentration at the end of the cultivation was calculated by measuring the total nitrogen in the suspension using a Total Organic Carbon analyzer (TOC-L) from Shimadzu.

¹³C glucose cultivation

Cultivation was performed in 10-mL Erlenmeyer flasks containing 1.8 mL of SMM with 100% labelled [4-¹³C]glucose (Sigma Aldrich) at a concentration of 3 g/L. 200 µL of dodecane were added, and the initial OD₆₀₀ was 0.1. Incubations lasted for 24 h at 30°C and 250 rpm. At the end of the cultivation, the content of the flask was transferred to a 2-mL Eppendorf tube, and centrifugation at 14000 g for 1 minute followed. Then, the dodecane layer was collected and analyzed by GC-MS. Chemical analysis was performed on an Agilent 7890A gas chromatograph connected to a 5975C mass selective Triple-Axis Detector (Agilent Technologies). For quantification of amorphadiene, each sample was injected at 250°C in split-less mode on a ZB-5MS column (Zebron, Phenomenex, 30 m x 250 mm x 0.25 mm film thickness) with 5 m guard column, with a constant flow of helium at 1 mL/min. The oven was programmed for 1 min at 45°C, then ramped at 10°C/min to 300°C and kept as such for 5 min with a solvent delay of 12.5 min, for a final run time of 31.5 min. ¹³C atoms incorporation was determined analyzing the increase in m/z values in the pool of secreted amorphadiene. As reference, the original m/z of 204 for amorphadiene was used.

Determination of endogenous terpenoids

For determination of the endogenous *R. sphaeroides* terpenoids, cultivation of the microorganisms was performed in 50 mL of SMM in a 250-mL Erlenmeyer flask. The cultivation started with an initial OD₆₀₀ of 0.1, and lasted for 24 hours at 30°C with 250 rpm. At the end of the cultivation, two aliquots of 10 mL of culture were centrifuged for 15 minutes at 4255 g. The first pellet was resuspended in MilliQ, and its nitrogen content was analyzed by TOC-L from Shimadzu for active biomass determination. The second pellet was freeze dried and further analyzed for endogenous terpenoids determination. 10 mg of freeze-dried material was extracted by adding 2.5 ml of methanol with 0.1% butylhydroxytoluene (BHT), followed by addition of 2.5 ml of 50 mM Tris (pH=7.5) + 1 M NaCl and 2 ml of chloroform + 0.1% BHT. After centrifugation, the chloroform phase was collected, and chloroform was aspired under a nitrogen flow. The pellet was dissolved in 100 µl ethylacetate + 0.1% BHT, and analyzed on HPLC as described previously (175). Compounds were identified based on absorption spectra, as already described (176), and by comparison to original standards.

Results and discussion

Strategy for isoprenoid pathway replacement

Substitution of an endogenous pathway by an independent and heterologous alternative requires inactivation of the former, while including all the information needed for the functioning of the latter. In *R. sphaeroides*, the MEP pathway connects GAP and PYR to IPP and DMAPP via 7 enzymatic steps. Additionally, it requires at least two types of cofactors for its activity, which are NADPH and flavodoxin or ferredoxin (**Fig. 1a**). On the other hand, the MVA pathway consists of 6 enzymatic reactions that link AA-CoA to IPP and DMAPP. Different from the MEP pathway, the only cofactor required by the MVA pathway is NADPH (**Fig. 1a**). Therefore, replacement of the isoprenoid pathway in this species should be feasible by just combining MEP inactivation to MVA introduction. Other authors suggested the possibility of substituting the native MEP pathway by autonomous bypasses towards IPP and DMAPP (177–180). Nevertheless, in all these cases the non-native routes implemented required additional carbon sources for their functioning (*e.g.* mevalonate or isoprenol), leading to auxotrophic organisms, whose growth was dependent on a two-substrates cultivation system. Only under this condition the engineered microorganisms were able to grow and synthesize isoprenoids, often with important growth deficits (178). Conversely, the goal of our design is to replace the isoprenoid pathway without interfering with the rest of the host's metabolism.

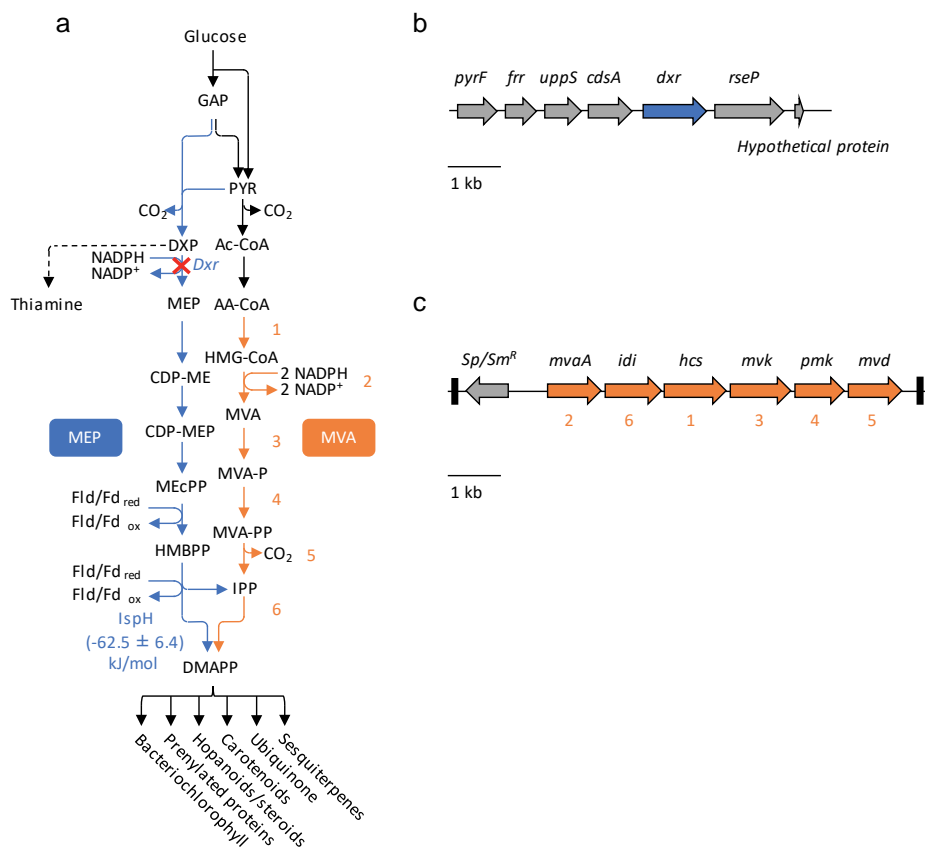


Figure 1. Overview of the strategy for isoprenoid pathway replacement in *Rhodobacter sphaeroides*. a) representation of the two isoprenoid modules 2-C-methyl-D-erythritol 4-phosphate (MEP, blue arrows) and mevalonate (MVA, orange arrows). Both modules branch from the central metabolism (black arrows) and converge to isopentenyl-diphosphate (IPP) and dimethylallyl-diphosphate (DMAPP), which are the precursors of all terpenoids (some listed below DMAPP). MVA pathway requires NADPH as cofactor, while the endogenous MEP additionally requires reduced flavodoxin (Fld) or ferredoxin (Fd) for its functioning (red: reduced, ox: oxidized). The proposed position for inactivation of the native MEP pathway is also shown and corresponds to the enzyme 1-deoxy-D-xylulose 5-phosphate reductoisomerase (Dxr, red cross). Its substrate 1-deoxy-D-xylulose 5-phosphate (DXP) is also involved in thiamine biosynthesis (black dashed line). The last step of the MEP pathway is catalyzed by 4-hydroxy-3-methylbut-2-enyl diphosphate (HMBPP) reductase (IspH). For this enzyme, the Gibbs free energy under standard conditions was calculated (in blue). The highly negative $\Delta_r G^{\circ}$ of the reaction (-62.5 ± 6.4 kJ/mol) indicates irreversibility of its enzymatic activity. On the other hand, introduction of the MVA module requires the correct functioning of 6 enzymes (numbered in orange).

b) overview of the operon including the target gene *dxr*. All the other genes included are involved in growth-related functions (see **Table S3** for more information). c) overview of the MVA operon from the α -proteobacterium *Paracoccus zeaxanthinifaciens* used for integration via mini transposon system pUT-Mini-Tn5-Sp/Sm. The numbers below the genes represent their position in the pathway depicted in panel a), while Sp/Sm^R refers to spectinomycin/streptomycin resistance. The image is adapted from (113). Other abbreviations: GAP (glyceraldehyde-3-phosphate), PYR (pyruvate), CDP-ME (4-(cytidine 5'-diphospho)-2-C-methyl-D-erythritol), CDP-MEP (2-phospho-4-(cytidine 5'-diphospho)-2-C-methyl-D-erythritol), MEcPP (2-C-methyl-D-erythritol 2,4-cyclodiphosphate), *pyrF* (uridylate kinase, gene), *frt* (ribosome recycling factor, gene), *uppS* (undecaprenyl-diphosphate synthase, gene), *cdsA* (phosphatidate cytidyltransferase, gene), *rseP* (Regulator of sigma E protease, gene) Ac-CoA (acetyl-CoA), AA-CoA (acetoacetyl-CoA), HMG-CoA (S)-3-hydroxy-3-methylglutaryl-CoA, MVA-P ((R)-5-phosphomevalonate), MVA-PP ((R)-5-diphosphomevalonate), *mvaA* (HMG-CoA reductase, gene), *idi* (IPP isomerase, gene), *hcs* (HMG-CoA synthase, gene), *mvk* (mevalonate kinase, gene), *pmk* (phosphomevalonate kinase, gene), *mvd* (MVA-PP decarboxylase, gene).

The most obvious approach for MEP pathway deletion would be targeting the first enzyme branching from the central metabolism, 1-deoxy-D-xylulose 5-phosphate synthase (Dxs). However, this strategy has two disadvantages. Firstly, the product of Dxs, 1-deoxy-D-xylulose 5-phosphate (DXP), is required for thiamine biosynthesis (**Fig. 1a**). Secondly, recently discovered metabolic pathways could in principle still generate DXP in case of *dxs* deletion. These are the 5'-methylthioadenosine-isoprenoid shunt (181) and the putative route from pentose phosphates to DXP (177). Therefore we considered to inactivate the second enzyme of the MEP pathway, 1-deoxy-D-xylulose 5-phosphate reductoisomerase, Dxr. This enzyme is not known to be involved in other biosynthetic processes. The operon including *dxr* contains genes required for cellular growth and proliferation (**Fig. 1b**, **Table S3**). Aiming not to affect the expression of the genes downstream of *dxr*, a clean knock out with the removal of 1188 bp on the *dxr* locus was proposed. For this purpose, two pBBR_Cas9_Δ*dxr* plasmids were constructed, each one containing a different targeting spacer (sp1, sp2, **Table S4**, **Fig. S1**).

To assess the likeliness of a reverse flux from IPP via the MEP pathway as result of *dxr* inactivation, we calculated (182) the Gibbs free energies of the two pathways (**Table S5**). The last step of the native isoprenoid pathway catalyzed by 4-hydroxy-3-methylbut-2-enyl diphosphate (HMBPP) reductase (IspH) has a highly negative $\Delta_r G'^0$ (-62.5 ± 6.4 kJ/mol) (**Fig. 1a**). Therefore, reverse flux via the MEP pathway is not expected to occur at any situation.

Introduction of a functional MVA pathway requires the harmonious expression of 6 different genes. Previous work demonstrated the possibility of integrating an MVA pathway in the genome of a photosynthetic microorganism (183). Phylogenetically, the traditional distinction that couples MEP pathway to the prokaryotic domain and MVA to eukaryotes and archaea has been revised (43). The α -proteobacterium *Paracoccus zeaxanthinifaciens* (113) harbors a complete MVA pathway, with all required genes organized in an operon. This operon already proved to be functional when expressed on a replicative plasmid in *R. sphaeroides* (91). Therefore, the MVA operon from *P. zeaxanthinifaciens* was chosen for genomic integration and cloned into a mini Tn5 transposon system harboring spectinomycin resistance (**Fig. 1c**). Two reporter genes were used to determine the effect of the heterologous pathway on sesquiterpene production: valencene synthase and amorpha-4, 11-diene synthase (91, 134).

Replacement of isoprenoid pathways

A first attempt to delete *dxr* was performed on a wild-type strain of *R. sphaeroides* (Rs265). The number of colonies obtained after conjugation was very low (< 10 in a plate with 10^{-2} dilution). They revealed to be all *wt* genotypes, indicating that isoprene synthesis is essential for cell survival. Therefore, an alternative strategy was adopted, which consisted in first integrating the MVA module by transposon insertion, followed by MEP inactivation. For this purpose,

a strain harboring the valencene synthase gene (Rs265 + pBBR-CnVS) (91) was chosen. The MVA pathway was successfully introduced into the *R. sphaeroides* genome by transposition. 15 independent transposition events were tested for valencene production. For all the Rs265-MVA strains, an increase of ± 1.5 times compared to the Rs265 control strain was observed (**Fig. 2a**). This indicates that multiple integration sites within the *R. sphaeroides* genome could equally support expression and functionality of the heterologous MVA pathway (**Fig. 2a**).

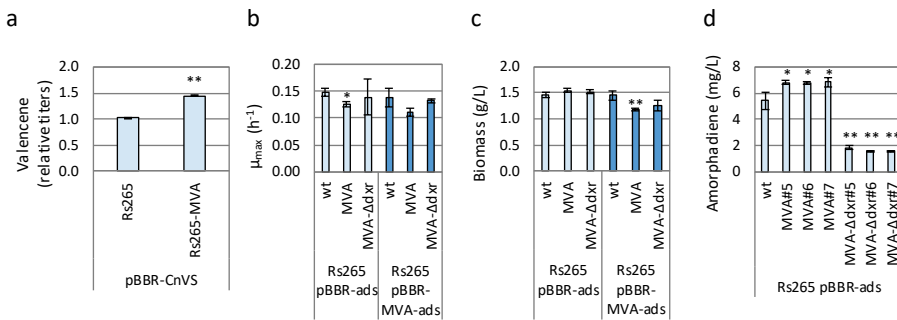


Figure 2. Effect of isoprenoid pathways replacement on physiological parameters in *Rhodobacter sphaeroides*. Comparison of a) relative valencene titers between Rs265 + pBBR-CnVS and the average of 15 biological replicates Rs265-MVA + pBBR-CnVS obtained after transposon insertion of the MVA operon. Bars show the average between the replicates \pm SD of the replicates. Comparison of b) growth rates and c) biomass concentration after 24 hours cultivation on defined medium. The Rs265 strains tested are wild-type (wt), integrated mevalonate (MVA), and Δdxr on MVA integrated background (MVA- Δdxr). Strains were tested before and after the addition of extra copies of the MVA module on a plasmid (pBBR-*ads*, light blue and pBBR-MVA-*ads*, dark blue). d) Effect of MVA pathway integration and 2-C-methyl-D-erythritol 4-phosphate (MEP) pathway inactivation on amorphadiene titers. The strains tested were incubated for 24 hours and amorphadiene was measured at the end of the cultivation. The measurement includes the biological replicates 5, 6 and 7 obtained after transposon insertion of the MVA pathway (panel a). As for b) and c), also here the wt strain was compared to strains co-expressing isoprenoid modules (MVA) or the MVA module exclusively (MVA- Δdxr). Unless expressed differently, the error bars are obtained from averages between at least biological triplicates. Significant differences are marked by either one or two asterisks (*: $p < 0.05$, **: $p < 0.01$). They were evaluated by comparing the set of replicates for the mutants Rs265- MVA (MVA) and Rs265- MVA- Δdxr (MVA- Δdxr) to the replicates obtained by the Rs265 (wt) strain by means of Student's *t* test.

After confirmation of the MVA integration, *dxr* inactivation followed. Indeed, *dxr* knock-out colonies were obtained. This result indicated that, at least under plate conditions, it is possible to successfully replace the native MEP pathway by the MVA pathway (**Fig. S2**). Here, the number of conjugants obtained was two orders of magnitude higher than for the Rs265, and resulted in a high efficiency of *dxr* deletion (Δdxr), independently from the spacer used. In fact, Cas9 counter-selection with both spacers showed a high success rate, with 98% and 77% of deletions obtained for sp1 and sp2, respectively (**Table S6**). Therefore, due to the essentiality of isoprenoids for cellular anabolism and homeostasis (107), inactivation of the native MEP module was possible only after integration of the heterologous MVA pathway

Quantitative physiological characterization after functional pathway replacement

The resulting Rs265-MVA- Δdxr strain with integrated MVA and inactivated MEP pathway was cured from the pBBR-*CnVS* plasmid, and subsequently conjugated with the pBBR-*ads* plasmid harboring the amorpha-4,11-diene synthase gene. Cultivation of this strain showed similar growth rates to the parental strains relying on the native MEP pathway (Rs265) or on the co-expression between MEP and MVA (Rs265-MVA) (**Fig. 2b, Fig. S3, 4**). Moreover, the biomass concentration obtained after 24 h incubation was comparable to the one of the two parental strains (**Fig. 2c**). Thus, the Rs265-MVA- Δdxr strain can efficiently and exclusively rely on the integrated MVA module for its functioning. In addition to growth measurements, final amorphadiene titers were measured for three different biological replicates of Rs265-MVA- Δdxr (#5, 6 and 7), and compared to Rs265-MVA and Rs265 strains (**Fig. 2d**). The resulting values indicate that, while the co-expression of MEP and MVA increased amorphadiene titers of about 1.2 fold, inactivation of the MEP pathway resulted in a decrease of about

3-fold. A similar assessment was performed on endogenous terpenoids, including carotenoids, coenzyme Q₁₀ and bacteriochlorophyll (Fig. 3). Also for these compounds, replacement of MEP with the MVA module leads to a decrease in relative abundances for Rs265-MVA- Δdxr between 2- to 5-folds compared to Rs265. This suggests that, although efficiently supporting growth, the integrated MVA pathway carries a lower flux towards IPP and DMAPP compared to the endogenous MEP pathway (Fig. 2d).

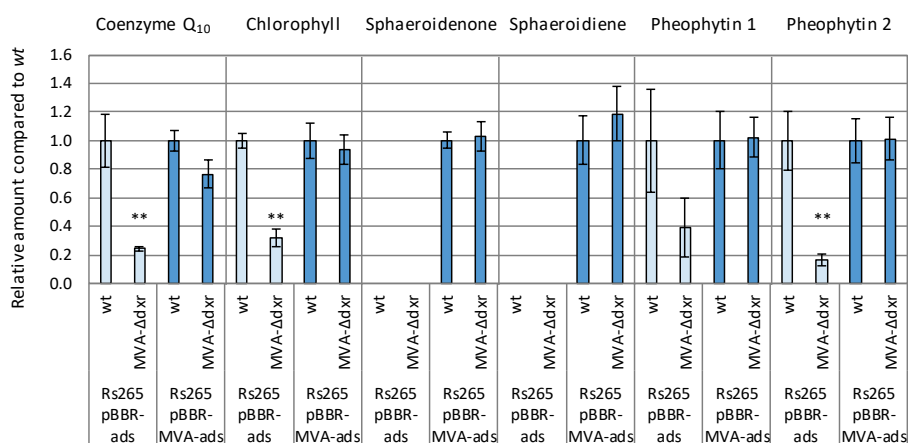


Figure 3. Effect of isoprenoid pathways replacement on biosynthesis of endogenous terpenoids. Accumulation of endogenous terpenoids in *Rhodospirillum rubrum* Rs265 relying exclusively on the native MEP pathway (wt), or on the heterologous mevalonate pathway (MVA- Δdxr). The values represent the relative comparisons of MVA- Δdxr to the wt control for several endogenous terpenoids (mentioned above each chart). Both MVA- Δdxr and wt genotypes were tested before and after the addition of extra copies of the MVA module on a multi-copy plasmid (pBBR-ads, light blue, and pBBR-MVA-ads, dark blue). Titers were measured after 24 hours incubation on defined medium supplied with glucose. Errors represent the standard deviations between biological triplicates. Significant differences are marked by two asterisks (**: $p < 0.01$). They were evaluated by comparing the set of replicates for the mutants Rs265- MVA- Δdxr to the replicates obtained by the Rs265 (wt) strain by means of Student's *t* test.

Previous works tried to achieve the same functional replacement of isoprenoid pathways by expressing a bacterial MEP pathway in *Saccharomyces cerevisiae* while inactivating the native MVA metabolic route (184–186). In all cases, the

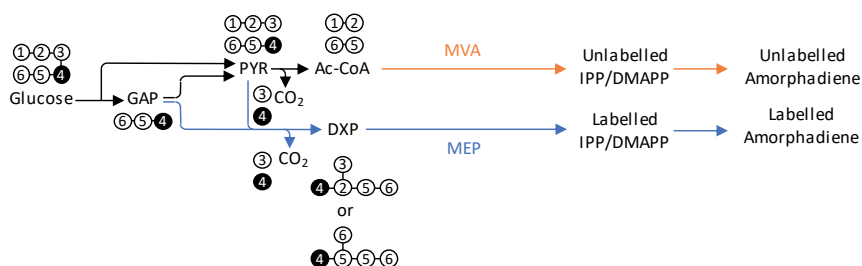
pathway replacement was inefficient or suboptimal, suggesting insufficient complementation of the detrimental effect associated to endogenous MVA inactivation. As reported by the authors, the last two steps of the MEP pathway catalyzed by IspG and IspH rely on [4Fe-4S] clusters and on cytosolic ferredoxin and/or flavodoxin (the latter non-native in *S. cerevisiae*). Moreover, assembly of these clusters requires a specific iron-sulfur cluster (ISC) machinery, which is not native in *S. cerevisiae*. A more recent approach (186) involved a screening of natural IspG and IspH homologs. Combined with selection and engineering of heterologous redox partners and of ISC machinery, this approach led to a functionally integrated MEP pathway, as shown by ^{13}C cultivation. Nevertheless, inactivation of the MVA pathway resulted in suboptimal growth of the mutant, which could moderately grow exclusively under a low aeration range and only by previous supply of mevalonate in the preculture stage on plate (186). In this work, possibly, the lack of non-native metal-clusters and cofactors required for the MVA pathway enabled its complete functional expression in *R. sphaeroides*.

Confirmation of pathway replacement by ^{13}C analysis

To the genetic evidence of *dxr* inactivation (**Fig. S2**), phenotypic demonstration of isoprenoid biosynthesis exclusively via the MVA module followed. To further confirm the lack of a catalytically active MEP pathway, we performed ^{13}C -cultivations with strain Rs265-MVA- Δdxr + pBBR-*ads* and compared them to strains Rs265 + pBBR-*ads* and Rs265-MVA + pBBR-*ads*. The strains were cultivated with defined medium supplied with [4- ^{13}C]glucose as only carbon source. By using this substrate (**Fig. 4a**), isopentenyl-diphosphate (IPP) originating from the MEP pathway will maintain the ^{13}C atom in its backbone, which eventually will be incorporated into the reporter sesquiterpene amorphadiene (187). In contrast, the ^{13}C atom will be lost in the MVA pathway, as CO_2 is released in the conversion of pyruvate to acetyl-CoA, which precedes

the entry point of the orthogonal pathway (**Fig. 4a**). After 24 h of cultivation, the mass distribution of amorphaadiene was analysed by GC-MS. The three strains (**Fig. 4b**) showed clearly different mass distribution patterns. In the Rs265 + pBBR-*ads* strain, amorphaadiene was generated exclusively from a pool of IPPs synthesized by the MEP pathway, as evidenced by the major peak of mass m/z $M+3$. In the strain Rs265-MVA + pBBR-*ads* with the integrated MVA pathway, IPP can be synthesized by both MEP and MVA pathways, and consequently both labelled and unlabeled IPPs will be incorporated into amorphaadiene. As a result, amorphaadiene molecules of mass M and $M+1$ are detected in equal amounts. Accordingly, in the strain Rs265-MVA- Δdxr + pBBR-*ads* yielded mostly unlabeled amorphaadiene, as was also observed in the control cultivation with unlabeled [^{12}C]glucose using Rs265 + pBBR-*ads*. In both cases, the peak of unlabeled amorphaadiene was higher than 80% (**Fig. 4b**). The frequency of $\sim 15\text{-}18\%$ of the $M + 1$ fraction originates from the natural occurrence of ^{13}C atoms ($\sim 1\%$), which randomly incorporated in one of the 15 atoms of amorphaadiene ($\text{C}_{15}\text{H}_{24}$). Therefore, the isotope profile of the secreted reporter molecule amorphaadiene confirmed that the isoprenoid flux via the MEP pathway was completely replaced by the MVA pathway in the Rs265-MVA- Δdxr + pBBR-*ads* strain.

a



b

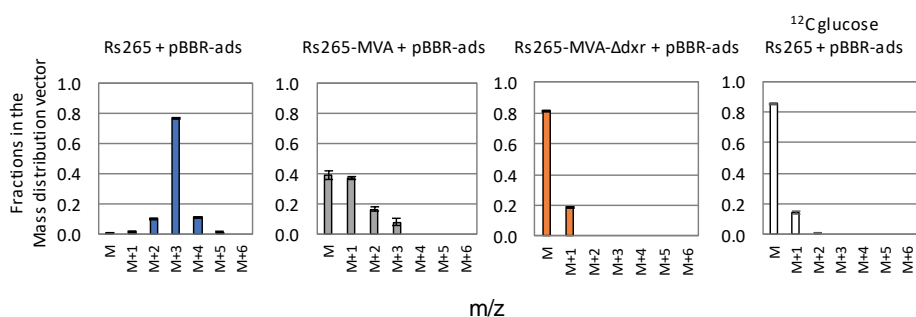


Figure 4. Comparison of amorphaadiene mass distribution vectors (MDVs) after [⁴⁻¹³C]glucose cultivation. a) Schematic representation of ¹³C atoms incorporation in amorphaadiene after [⁴⁻¹³C]glucose cultivation. Glycolysis in *Rhodobacter sphaeroides* will generate 1 molecule of glyceraldehyde-3-phosphate (GAP) and 1 molecule of pyruvate (PYR) per glucose consumed. Additionally, GAP can be converted to PYR by the lower glycolysis. In case of isopentenyl-pyrophosphate (IPP) biosynthesis via the MEP pathway, the ¹³C atom from GAP will be maintained within the carbon backbone. Differently, when PYR is converted to acetyl-CoA (Ac-CoA), the decarboxylation step results in ¹³C atom removal from the carbon skeleton. Therefore, the IPP and dimethylallyl-diphosphate (DMAPP) molecules generated via the MVA pathway will be unlabeled, whereas they will maintain the ¹³C atom if generated from MEP. Eventually, three molecules of IPP and DMAPP are condensed in one molecule of amorphaadiene, whose isotopes spectra will be analyzed by GC-MS. b) Qualitative comparison between the MDVs of the secreted amorphaadiene after [⁴⁻¹³C]glucose cultivation. Due to the presence of three labelled IPP/DMAPP units, the strain exclusively expressing the MEP pathway (Rs265 + pBBR-*ads*) shows the highest density of ¹³C incorporation within its backbone as a shift of M+3 in m/z. The relative amount of ¹³C within amorphaadiene decreases when the two modules are co-expressed due to the presence of unlabeled IPP/DMAPP units in amorphaadiene (Rs265-MVA + pBBR-*ads*). Eventually, the amount of ¹³C incorporated when only MVA is active (Rs265-MVA-Δ*dxr* + pBBR-*ads*) equals the natural distribution of ¹³C that is incorporated by a strain relying on MEP exclusively grown on [¹²C]glucose (white bars). Error bars represent the standard deviation of biological triplicates.

Overexpression of the MVA module allows maximal isoprenoid biosynthesis in the Rs265-MVA- Δdxr strain

The Rs265-MVA- Δdxr strain synthesizes isoprenoid exclusively via the non-native MVA module (**Fig. 4b**). Clearly, the single MVA copy integrated in the genome showed limited capacity for supporting biosynthesis of both endogenous and heterologous isoprenoids (**Fig. 2d**). To enhance the flux through the MVA pathway, the Rs265-MVA- Δdxr strain was conjugated with the multi-copy pBBR-MVA-*ads* plasmid, which expresses an extra copy of the MVA module. The growth parameters of this strain did not differ from the parental Rs265 + pBBR-MVA-*ads* (**Fig. 2 b, c, Table S7, Fig. S4**). Moreover, enhanced expression of the MVA pathway restored biosynthesis of the endogenous terpenoids in Rs265-MVA- Δdxr to levels that are not significantly different from the Rs265 + pBBR-MVA-*ads* strain (**Fig. 3**). Surprisingly, the Rs265-MVA + pBBR-MVA-*ads* strain (with the integrated MVA operon, the plasmid-borne MVA enzymes copies and a still catalytically active MEP pathway) showed a slightly lower growth rate compared to the other two strains (**Fig. 2b**), and resulted in a lower final biomass concentration (**Fig. 2c**). This could indicate a possible burden in this strain due to the augmented expression levels of the MVA pathway.

The main advantage of harnessing non-endogenous and autonomous pathways for metabolic engineering purposes is the bypass of host's native regulation mechanisms (188). We assessed this principle by determining the effect of extra copies of the MVA module in the presence and absence of the endogenous MEP pathway. Therefore, we determined the effect of increased MVA expression in terms of amorphaadiene yield on glucose. This value was compared between the two strains harboring the integrated MVA operon. These are the Rs265-MVA- Δdxr and the Rs265-MVA strains, with the latter still maintaining a functional MEP pathway. For both strains, augmentation in expression of the MVA pathway

due to the pBBR-MVA-*ads* plasmid resulted in an increase in amorphaadiene yield (**Fig. 5**). Remarkably, the effect on the Rs265-MVA- Δdxr strains was much more pronounced than for the Rs265-MVA strain, reaching a final yield of about 8 mg/g glucose (Rs265-MVA- Δdxr), while for the parental strain (Rs265-MVA) the yield approached a value of only 4 mg/g glucose. In terms of relative yield increase, this means up to 18-fold increase for the Rs265-MVA- Δdxr strain, while it limits to a value of 2.5-fold for the parental Rs-MVA strain (**Fig. 5**). This important increase for the Rs265-MVA- Δdxr strain persisted independently in all three biological replicates tested (**Fig. 5**), confirming to be independent from the genomic location of the MVA operon integration.

These results suggested that the augmented MVA capacity could be exploited at full potential when the MEP pathway was inactivated, resulting in a higher flux towards IPP compared to the strain co-expressing both MEP and MVA modules. Apparently, the MVA pathway can be affected by the endogenous MEP pathway when still active, as already shown for Rs265-MVA + pBBR-MVA-*ads* (**Fig. 2b, c**). Hence, exclusive use of the heterologous MVA module holds promising potential for biotechnological production of relevant isoprenoid compounds in *R. sphaeroides*.

In addition, our data indicate the existence of an interaction between MEP and MVA pathways, which limited the increase in amorphaadiene yield in the Rs265-MVA + pBBR-MVA-*ads* strain. Further research by metabolomics or ^{13}C metabolic flux analysis could help in unravelling the nature of the interaction between these two metabolic pathways.

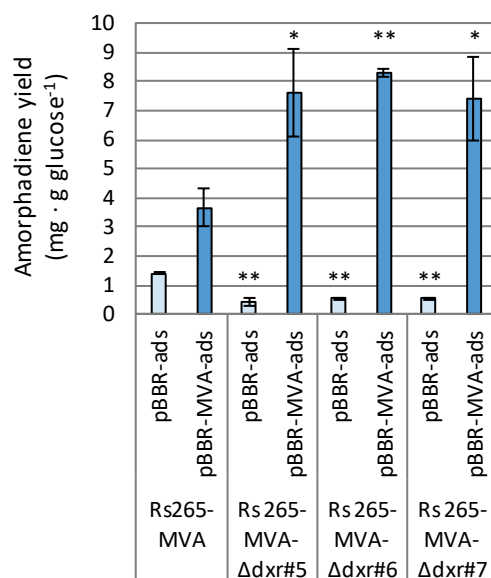


Figure 5. Effect of increasing enzyme copies of the MVA module on amorphadiene yield. Comparison of amorphadiene yields on glucose after 24 hours incubation on defined medium. The parental strain co-expressing the native endogenous MEP pathway and the integrated mevalonate module (Rs265-MVA) is compared to the three biological replicates of the knock-out strains exclusively relying on the orthogonal MVA module (Rs265-MVA-Δdxr #5, 6 and 7). For all the strains, the yields were compared between strains relying exclusively on the integrated MVA module (pBB-ads, light blue) and others expressing additional MVA copies on a multi-copy plasmid (pBBR-MVA-ads, dark blue). The error bars represent the standard deviations of biological triplicates. Significant differences are marked by either one or two asterisks (*: $p < 0.05$, **: $p < 0.01$). They were evaluated by comparing the set of replicates for the mutants Rs265- MVA-Δdxr to the replicates obtained by the Rs265- MVA strain by means of Student's t test.

Conclusions

In this work we showed that, in *R. sphaeroides*, the essential pathway for isoprenoid biosynthesis can be functionally replaced by an alternative, heterologous pathway, without penalty on growth or isoprenoid production capacity. Overexpression of the non-native MVA pathway enzymes allowed to achieve similar endogenous membrane-bound terpenoids titers compared to the control strain. Moreover, overexpression of the MVA module had much

larger effects on heterologous sesquiterpene titers when the endogenous MEP pathway was inactivated, resulting in a 2-fold higher yield on glucose compared to the strain where the MEP pathway was still active. Therefore, this work is an example of the power of independent pathway substitutions for biotechnological optimization strategies, which holds potential for the generation of novel types of deregulated cell factories.

Acknowledgements

We acknowledge Isobionics BV for providing the *Rhodobacter sphaeroides* strain and the pBBR-MVA-*ads* plasmid used in the study. Any request for the strain and its derivatives should be directed to Isobionics BV.

Authors' contributions

EO, JB and RW designed the work. EO, JB, DvG and AvH conducted, analyzed, and interpreted the experiments. EO and JB drafted and wrote the manuscript. All authors read and approved the final manuscript.

Competing interests

The authors declare no competing financial interests.

Funding

This project was financially supported by The Netherlands Ministry of Economic Affairs and a public-private NWO-Green Foundation for sustainable production and supply chains in agriculture and horticulture (870.15.130, 2015/05279/ALW).

Supplementary information

Table S1. List of strains and plasmids used in this study.

Strain	Description	Reference
Rs265	wild-type <i>R. sphaeroides</i>	(134)
Rs265-MVA	Rs265 with native mevalonate pathway from <i>P. zeaxanthinifaciens</i> under the control of the native promoter integrated via mini transposon system pUT-Mini-Tn5-Sp/Sm	This study
Rs265-MVA- Δdxr	Rs265 -MVA strain with deletion of <i>dxr</i>	This study
<i>Escherichia coli</i> S17-1	Host strain for transconjugation, <i>thi pro recA hsdR [RP4-2Tc::Mu-Km::Tn7] Tp^r Sm^r</i>	Laboratory stock
Plasmids	Description	Reference
pUT-Mini-Tn5-Sp/Sm	Plasmid for the transposonal integration of the MVA pathway	This study
pBBR_Cas9_ Δdxr (sp1 and sp2)	Plasmids for <i>dxr</i> removal by homologous recombination and Cas9 counter-selection using spacers sp1 and sp2	This study
pBBR- <i>CnVS</i>	Plasmid containing the <i>CnVS</i> gene for valencene synthase	(91)
pBBR- <i>ads</i>	Plasmid containing the <i>ads</i> gene for amorphadiene synthase	(134)
pBBR-MVA- <i>ads</i>	Plasmid containing the <i>ads</i> gene for amorphadiene synthase together with an extra copy of the MVA pathway	(134)

Table S2. Primers used in this work. See methods section in the manuscript for details about the primers combinations used.

Name	Sequence (5' to 3')	Description
302	CATTAAGCATTCTGCCGACATGG	For assembly of the pBBR_Cas9_Δdxr plasmids
303	gcctgaatggcgaatggaaattgtaa	For assembly of the pBBR_Cas9_Δdxr plasmids
301	CCATGTCGGCAGAATGCTTAATG	For assembly of the pBBR_Cas9_Δdxr plasmids
403	GATGGATTGCGGATGGACGAGTTT AGAGCTAGAAATAGCAAGTTAAAA TAAGGCTAGTC	For assembly of the pBBR_Cas9_Δdxr plasmids
407	GCTTGCGCGAGACGTCATGGGTTT TAGAGCTAGAAATAGCAAGTTAA AATAAGGCTAGTC	For assembly of the pBBR_Cas9_Δdxr plasmids
304	gtgcgggcctcttcgctatta	For assembly of the pBBR_Cas9_Δdxr plasmids
404	TCGTCCATCCGCAATCCATCAACCA GCGATCCCCTCCG	For assembly of the pBBR_Cas9_Δdxr plasmids
408	CCATGACGTCTCGCGCAAGCAACC AGCGATCCCCTCCG	For assembly of the pBBR_Cas9_Δdxr plasmids
399	CCAAGGGCTGGATGCTTTTCAGTCCCC	For assembly of the pBBR_Cas9_Δdxr plasmids. Anneals to the genomic DNA for flanking sites amplification
400	taatagcgaagaggcccgacGACCCGGATC TGGT	For assembly of the pBBR_Cas9_Δdxr plasmids. Anneals to the genomic DNA for flanking sites amplification
401	tttcattcgccattcaggcTGGTGATGGTCTG	For assembly of the pBBR_Cas9_Δdxr plasmids. Anneals to the genomic DNA for flanking sites amplification
402	GAAAAGCATCCAGCCCTTGGACATT	For assembly of the pBBR_Cas9_Δdxr plasmids. Anneals to the genomic DNA for flanking sites amplification
437	AGGTTGCAGGAGGAGAT	For colony PCR for determining deletion of <i>dxr</i>
438	CGGCCGCGACGAGTT	For colony PCR for determining deletion of <i>dxr</i>

Name	Sequence (5' to 3')	Description
469	CCAGCGGATCTCCATCGACA	For colony PCR for confirming absence of latent <i>dxr</i> copies at 5' and 3' end of the gene
471	GCATGGCGATGAACCAGATG	For colony PCR for confirming absence of latent <i>dxr</i> copies at 5' and 3' end of the gene
468	CCAGTACAATCAGCGCCT	For colony PCR for confirming absence of latent <i>dxr</i> copies at 5' and 3' end of the gene
470	GCTTCCTCTGCCGCTCT	For colony PCR for confirming absence of latent <i>dxr</i> copies at 5' and 3' end of the gene
455	CGTTGGCCACGCGCAC	For genotyping of the <i>dxr</i> locus
456	CTCGGCGGCCCAAG	For genotyping of the <i>dxr</i> locus
mvaA-fw	ATCCAGGTCTCGCTGGTCGAC	Primer for colony PCR for the presence of the integrated MVA pathway
mvaA-re	ATAGTTCTTCTCGTAGTTCAG	Primer for colony PCR for the presence of the integrated MVA pathway
mvd-fw	TGACTGATGCCGTCCGCGACATG	Primer for colony PCR for the presence of the integrated MVA pathway
mvd-Re	GTCGCGCGAACTGAAAGGCTTG	Primer for colony PCR for the presence of the integrated MVA pathway
tnp-fw	GAGCTTGAGCCTGCGCAGTGG	Primer for colony PCR for the absence of transposase
tnp-re	CAGTCTAGCTATCGCCATGTAAG	Primer for colony PCR for the absence of transposase
cnvs-fw	CAATGATGGCAGCTCCTGCATG	Primer for colony PCR for the presence of valencene synthase on replicative plasmid
cnvs-re	CATCATCTCCAGCTTGCGTC	Primer for colony PCR for the presence of valencene synthase on replicative plasmid
Tn5-fw	ACCGTGAAGGTCCAGGTCATC	For sequencing the orientation of the MVA operon in the pUT-Mini-Tn5-Sp/Sm plasmid
Tn5-re	CACGCCTTCGATGGCTTCCGA	For sequencing the orientation of the MVA operon in the pUT-Mini-Tn5-Sp/Sm plasmid

Table S3. Biological functions of the genes belonging to the *dxr* operon.

ORF	Gene	Protein	EC number	Pathway/function
1	<i>pyrH</i>	Uridylate kinase	2.7.4.22	pyrimidines biosynthesis
2	<i>frr</i>	Ribosome recycling factor	-	proteins translation
3	<i>uppS</i>	Undecaprenyl-diphosphate synthase	2.5.1.31	terpenoids biosynthesis
4	<i>cdsA</i>	Phosphatidate cytidyltransferase	2.7.7.41	phospholipid metabolism
5	<i>dxr</i>	1-deoxy-D-xylulose 5-phosphate reductoisomerase	1.1.1.267	terpenoids biosynthesis
6	<i>rseP</i>	Regulator of sigma E protease	3.4.24.-	cell cycle
7	Hypothetical protein	-	-	-

Table S4. Spacers used for targeting *dxr*

Spacers	Sequence (5' - 3')	PAM
sp1	GATGGATTGCGGATGGACGA	CGG
sp2	ACATGGTCCAGTCGGCCGGC	CGG

Table S5. Overview of the standard Gibbs free energies of the different enzymatic reactions for the two isoprenoid biosynthetic routes. Values are calculated using Equilibrator (182).

MEP			Calculated from Equilibrator	
enzyme	EC	Substrate	Products	ΔG°
DOXP synthase (Dxs; DXR)	2.2.1.7	Pyruvate + D-glyceraldehyde 3-phosphate	1-deoxy-D-xylulose 5-phosphate + CO ₂	-29.0 ± 6.7
DXP reductoisomerase (Dxr, IspC; DXR)	1.1.1.1267	1-deoxy-D-xylulose 5-phosphate + NADPH	2-C-methyl-D-erythritol 4-phosphate + NADP ⁺	-23.2 ± 2.4
2-C-methyl-D-erythritol 4-phosphate cytidyltransferase (YgbP, IspD; CMS)	2.7.7.60	CTP + 2-C-methyl-D-erythritol 4-phosphate	diphosphate + 4-(cytidine 5'-diphospho)-2-C-methyl-D-erythritol	-4.7 ± 9.4
4-diphosphocytidyl-2-C-methyl-D-erythritol kinase (YchB, IspE; CMK)	2.7.1.148	ATP + 4-(cytidine 5'-diphospho)-2-C-methyl-D-erythritol	ADP + 2-phospho-4-(cytidine 5'-diphospho)-2-C-methyl-D-erythritol	-5.3 ± 8.1
2-C-methyl-D-erythritol 2,4-cyclodiphosphate synthase (YgbB, IspF; MCS)	4.6.1.12	2-phospho-4-(cytidine 5'-diphospho)-2-C-methyl-D-erythritol	2-C-methyl-D-erythritol 2,4-cyclodiphosphate + CMP	N.D.
HMB-PP synthase (GspE, IspG; HDS)	1.17.7.1	2-C-methyl-D-erythritol 2,4-cyclodiphosphate + 2 reduced ferredoxin	(E)-4-hydroxy-3-methylbut-2-en-1-yl diphosphate + H ₂ O + 2 oxidized ferredoxin	N.D.
HMB-PP reductase (LytB, IspH; HDR)	1.17.1.4	(E)-4-hydroxy-3-methylbut-2-en-1-yl diphosphate + 2 reduced ferredoxin [iron-sulfur] cluster + 2 H(+)	Isopentenyl diphosphate + 2 oxidized ferredoxin [iron-sulfur] cluster + H ₂ O or Dimethylallyl diphosphate + 2 oxidized ferredoxin [iron-sulfur] cluster + H ₂ O	-62.5 ± 6.4

Table S5. Overview of the standard Gibbs free energies of the different enzymatic reactions for the two isoprenoid biosynthetic routes. Values are calculated using EQuilibrator (182). (continued)

MVA	EC	Substrate	Products	Calculated from EQuilibrator
enzyme				ΔrG°
Acetoacetyl-CoA thiolase	2.3.1.9	2 Acetyl-CoA	CoA + acetoacetyl-CoA	26.1 ± 1.7
HMG-CoA synthase	2.3.3.10	Acetyl-CoA + H ₂ O + acetoacetyl-CoA	(S)-3-hydroxy-3-methylglutaryl-CoA + CoA	-16.9 ± 15.8
HMG-CoA reductase	1.1.1.34	(S)-3-hydroxy-3-methylglutaryl-CoA + 2 NADPH	(R)-mevalonate + CoA + 2 NADP ⁺	-8.2 ± 15.4
mevalonate-5-kinase	2.7.1.36	ATP + (R)-mevalonate	ADP + (R)-5-phosphomevalonate	-13.5 ± 4.6
phosphomevalonate kinase	2.7.4.2	ATP + (R)-5-phosphomevalonate	ADP + (R)-5-diphosphomevalonate	-2.7 ± 4.1
mevalonate-5-pyrophosphate decarboxylase	4.1.1.33	ATP + (R)-5-diphosphomevalonate	ADP + phosphate + isopentenyl diphosphate + CO ₂	-33.2 ± 7.9
isopentenyl pyrophosphate isomerase	5.3.3.2	Isopentenyl diphosphate	dimethylallyl diphosphate	-4.9 ± 5.8

Table S6. Efficiencies of *dxr* deletion via spacers sp1 and sp2.

spacer sp1				
Replicate	Dilution factor	Colonies screened	Mutants	Efficiency
#144	1000	9	9	100%
#145	1000	10	10	100%
#146	1000	9	8	88.88%
#147	1000	9	9	100%
#148	1000	7	7	100%
overall		43 out 44		97.73%
spacer sp2				
Replicate	Dilution factor	Colonies screened	Mutants	Efficiency
#144	1000	9	9	100%
#145	1000	8	6	75%
#146	1000	7	4	57.14%
#147	1000	10	8	80%
#148	1000	8	7	88%
overall		34 out 42		77.27%

Table S7. Glucose consumption rates in strains Rs265-MVA and Rs265-MVA- Δdxr .

Strain	g glucose · g biomass ⁻¹ · hour ⁻¹	
	pBBR- <i>ads</i>	pBBR-MVA- <i>ads</i>
Rs265-MVA	0.072 ± 0.010	0.052 ± 0.021
Rs265-MVA- Δdxr	0.068 ± 0.008	0.070 ± 0.013

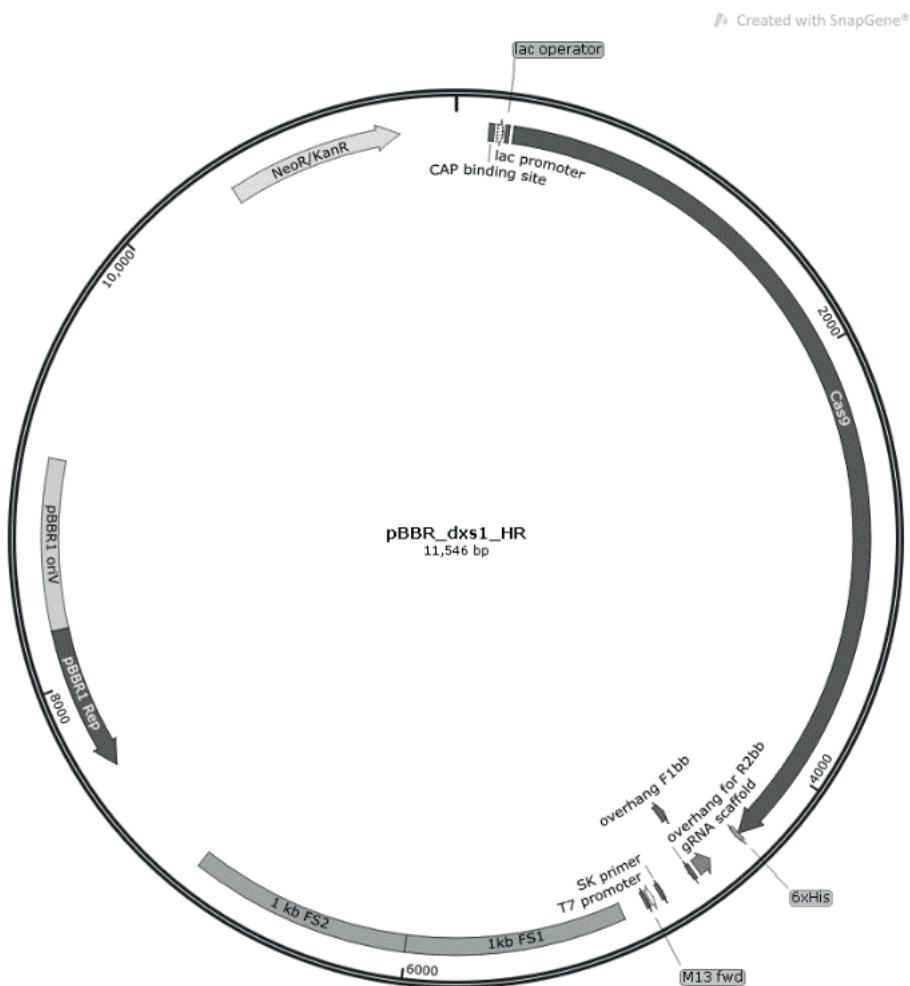


Figure S1. Plasmids map of pBBR-Cas9-*dxr*-HR plasmid. In this map, the spacer sp1 is included.

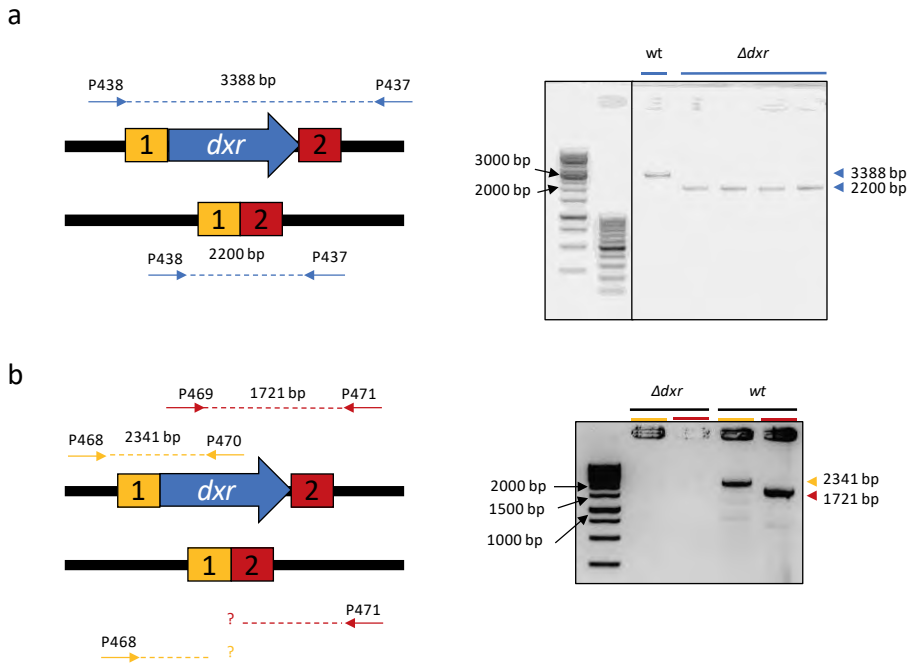


Figure S2. Genetic evidence of endogenous MEP pathway inactivation by deletion of *dxr*. a) Colony PCR using the primer set P437/P438, annealing outside the flanking sites employed for homologous recombination. The expected fragment size is 3388 bp for the wild-type, while it is 2200 bp for Δdxr . b) Colony PCR for detecting latent wild-type *dxr* copies within the genome. This amplification aims to identify possible copies of *dxr* which might have escaped the Cas9 counter-selection and might have not been detected by the primer set P437/P438. The two primer sets P468/P470 and P469/P471 amplify fragments of *dxr* at the 5' and 3'ends, respectively. Only in case of *dxr* presence, the PCR product would result in the creation of two bands of the length of 2341 and 1721 bp.

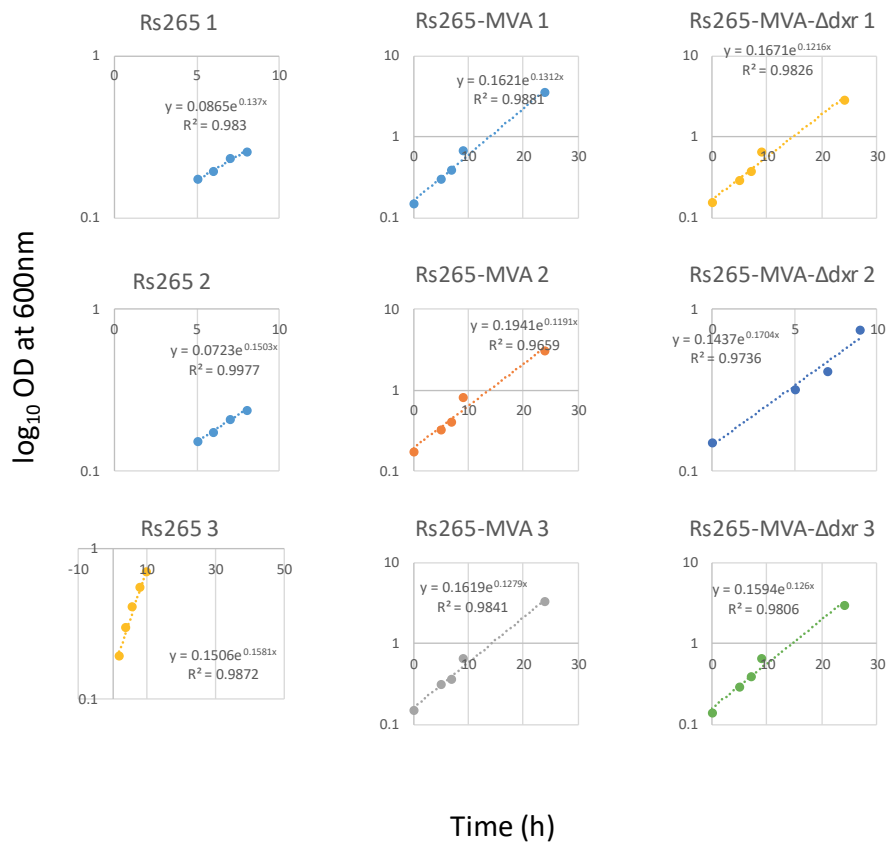


Figure S3. Growth rate profiles for the strains containing the pBBR-*ads* plasmid.

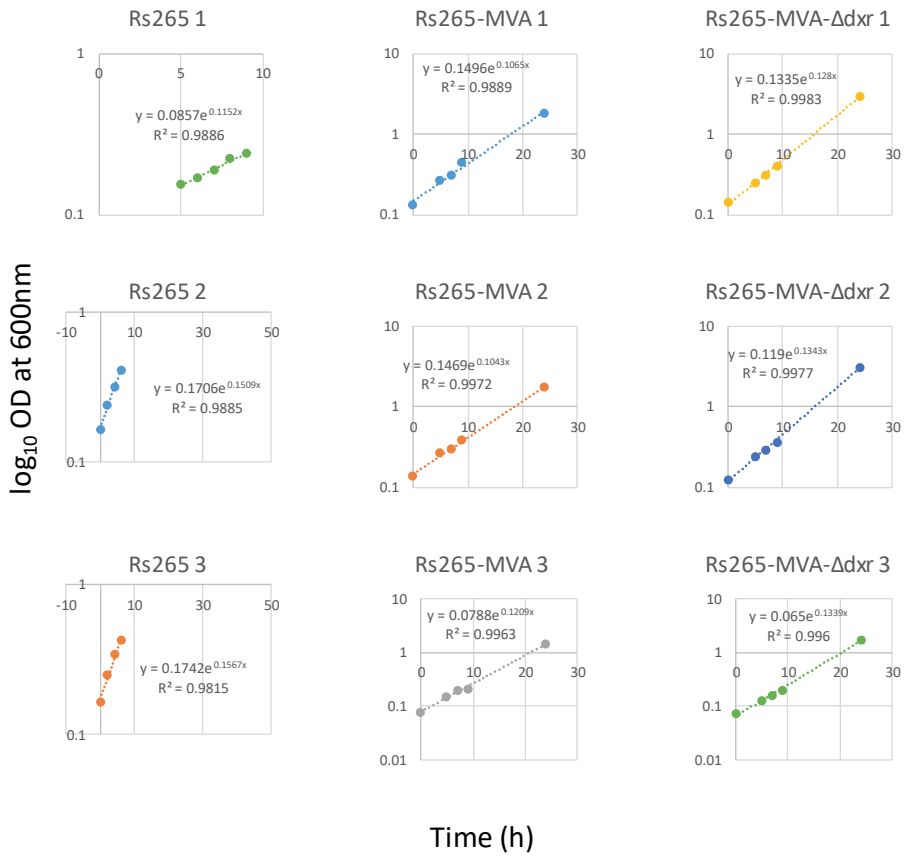
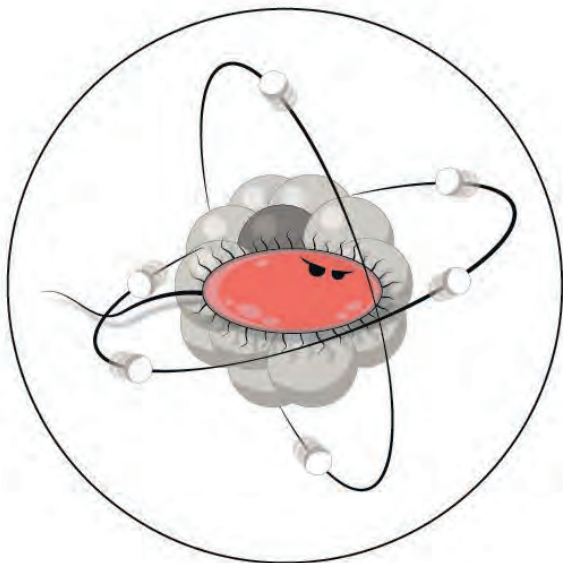


Figure S4. Growth rate profiles for the strains containing the pBBR-MVA-ads plasmid.



Chapter 5

Metabolic flux ratio analysis by parallel ^{13}C
labeling of isoprenoid biosynthesis in
Rhodobacter sphaeroides

This chapter has been published as: Orsi, E., Beekwilder, J., Peek, S., Eggink, G., Kengen, S. W., & Weusthuis, R. A. (2020). Metabolic flux ratio analysis by parallel ^{13}C labeling of isoprenoid biosynthesis in *Rhodobacter sphaeroides*. *Metabolic Engineering*, 57, 228-238.

Abstract

Metabolic engineering for increased isoprenoid production often benefits from the simultaneous expression of the two naturally available isoprenoid metabolic routes, namely the 2-methyl-D-erythritol 4-phosphate (MEP) pathway and the mevalonate (MVA) pathway. Quantification of the contribution of these pathways to the overall isoprenoid production can help to obtain a better understanding of the metabolism within a microbial cell factory. Such type of investigation can benefit from ^{13}C metabolic flux ratio studies. Here, we designed a method based on parallel labeling experiments (PLEs), using [1- ^{13}C]- and [4- ^{13}C]glucose as tracers to quantify the metabolic flux ratios in the glycolytic and isoprenoid pathways. By just analyzing a reporter isoprenoid molecule and employing only four equations, we could describe the metabolism involved from substrate catabolism to product formation. These equations infer ^{13}C atom incorporation into the universal isoprenoid building blocks, isopentenyl-pyrophosphate (IPP) and dimethylallyl-pyrophosphate (DMAPP). Therefore, this renders the method applicable to the study of any of isoprenoid of interest. As proof of principle, we applied it to study amorpha-4,11-diene biosynthesis in the bacterium *Rhodobacter sphaeroides*. We confirmed that in this species the Entner-Doudoroff pathway is the major pathway for glucose catabolism, while the Embden-Meyerhof-Parnas pathway contributes to a lesser extent. Additionally, we demonstrated that co-expression of the MEP and MVA pathways caused a mutual enhancement of their metabolic flux capacity. Surprisingly, we also observed that the isoprenoid flux ratio remains constant under exponential growth conditions, independently from the expression level of the MVA pathway. Apart from proposing and applying a tool for studying isoprenoid biosynthesis within a microbial cell factory, our work reveals

important insights from the co-expression of MEP and MVA pathways, including the existence of a yet unclear interaction between them.

Keywords

Parallel labeling experiments, ¹³C metabolic flux ratios analysis, isoprenoid biosynthesis, MEP, MVA, *Rhodobacter sphaeroides*.

Introduction

Isoprenoids (also referred to as terpenoids) form a large and diverse class of natural products (44, 105), that have raised a lot of interest due to the many potential applications for bio-based industries (8, 46, 51, 106). Short chain isoprenoids (hemiterpenoids) are generated from a single isoprene precursor, either isopentenyl-pyrophosphate (IPP) or dimethylallyl-pyrophosphate (DMAPP). All other isoprenoids are obtained via condensation of both precursors. IPP and DMAPP can be synthesized by two distinct isoprenoid pathways, viz. the 2-methyl-D-erythritol 4-phosphate (MEP) pathway, typical of prokaryotes, and the mevalonate (MVA) pathway, which is typical of eukaryotes and archaea. Higher isoprenoid titers have been obtained in different microorganisms by co-expression of both isoprenoid pathways (42, 91, 183, 186, 189). However, because they share identical building blocks and isoprenoid products, a detailed understanding of how these two metabolic routes are contributing to the total isoprenoid titer is still lacking. Moreover, both isoprenoid pathways are supplied with metabolites that may originate from different glycolytic pathways like the Embden-Meyerhof-Parnas (EMP), the Entner-Doudoroff (ED) and pentose-phosphate pathway (PPP).

An industrially relevant organism which harbors all these pathways is the bacterium *Rhodobacter sphaeroides*. This organism is known as native producer of ubiquinone (coenzyme Q10). Moreover, when growing under low oxygen tensions, it develops intracytoplasmic membrane structures rich of isoprenoid-derived molecules like bacteriochlorophyll and carotenoids. In this species, higher isoprenoid titers have been obtained by co-expression of the MEP and MVA pathway (8, 91, 134). Moreover, its acknowledged metabolic versatility (62) is reflected in the presence of all the aforementioned glycolytic pathways, although the PPP is virtually inactive (128). To be able to efficiently engineer

isoprenoid synthesis in this species it is essential that the contribution of each metabolic route to the product titer can be determined, i.e. by ^{13}C flux analysis (190).

About two decades ago, ^{13}C -metabolic flux analysis (^{13}C -MFA) has been introduced for *in vivo* metabolic studies (191, 192). By using such an approach, intracellular fluxes that would otherwise remain undetermined can be identified and quantified. Since its introduction, ^{13}C -MFA has predominantly been used for investigating the central metabolism during steady state conditions by analysis of ^{13}C -enriched proteins (23, 191, 193, 194). Because interpretation of the data generated by NMR-spectroscopy or mass spectrometry (MS) can be complex, several computational tools have been developed (195). Over the years various ^{13}C labeling approaches were developed (190). A major development in this field was the use of 'parallel labeling experiments' (PLEs) (196), where two or more ^{13}C -tracers are used in parallel. The data obtained from PLEs can be combined, improving the quality of the flux estimations (197–199).

To study isoprenoid biosynthesis by means of ^{13}C flux analysis, we designed a PLE involving independent cultivations with labeled [1- ^{13}C]- and [4- ^{13}C]glucose as substrates. By just measuring a reporter isoprenoid molecule, the method enables the quantification of the contribution of the glycolytic and isoprenoid pathways to the formation of the building blocks IPP and DMAPP. Therefore, in principle this approach can be used to study the biosynthesis of any isoprenoid of interest. We employed it to study the isoprenoid metabolism in *R. sphaeroides*, assessing the effect of genetic variations to the metabolic flux ratios. The method confirmed the existence of an interaction between the MEP and MVA pathway, which enhances the capacity of both metabolic routes.

Material and methods

Labeled material

[1-¹³C]glucose (99 atom% ¹³C), [4-¹³C]glucose (99 atom% ¹³C), [U-¹³C]glucose (99 atom% ¹³C) tracers were purchased from Sigma-Aldrich (USA).

Strains and cultivation conditions

The strains and plasmids used in this study are listed in the Supplementary **Table S1**. Cultivation of *R. sphaeroides* for metabolic studies was performed on Siström's minimal medium (SMM) supplemented with 50 µg/mL kanamycin as previously described (134). As carbon source, 3.0 g/L of labeled or unlabeled glucose was used. As nitrogen source, NH₄Cl was used at an initial concentration of 1.0 g/L.

Preculturing of *R. sphaeroides* was performed by transferring the strains from frozen glycerol stocks to Luria-Bertani (LB) agar plates supplied with 50 µg/mL kanamycin and incubated at 30 °C. When colonies were visible, single colonies were passed to 5 mL of liquid LB supplied with the same antibiotic, and incubated at 30 °C with an agitation rate of 250 rpm. After 24 h, 500 µL of LB culture was transferred into 250-mL Erlenmeyer flasks with 10% v/v of liquid SMM with 3.0 g/L of glucose, 1.0 g/L of NH₄Cl. Then, the flask was incubated overnight at 30 °C with an agitation rate of 250 rpm.

Generation of plasmid vectors for genes deletion

For genome editing of *R. sphaeroides*, homologous recombination (HR) combined with Cas9 counter-selection was used (174). The targeting spacers used in this work are listed in the Supplementary **Table S2**. The primer sets used for plasmid cloning, conjugant checking and genotyping are listed in the Supplementary **Table S3**. All the plasmids harboring the *cas9* construct were

generated as follows. First, a set of three PCR amplifications was performed on the pSGC template plasmid (for the *cas9* and the guide RNA array). The three PCR amplicons included a conserved region of the backbone (primers set P302/P303), a fragment containing the *cas9* gene and the gRNA including the targeting spacer, and a short fragment to connect the gRNA to the homology arms for gene deletion. Secondly, a set of two PCRs was performed using the *R. sphaeroides* genomic DNA as template for the amplification of the two homology arms surrounding the target gene. If necessary, the design for gene deletions included stop codons and a sequence for a restriction enzyme in the overhangs between the homology arms. Subsequently, the PCR amplicons (five in total) were assembled using the HiFi Assembly kit from New England Biolabs (NEB, USA). If necessary, to increase the chances of successful cleavage, more variants of Cas9 targeting plasmid were assembled containing a different variant of a targeting gRNA. Assembled plasmids were then transformed into *Escherichia coli* S-17 strains, purified and sequenced using primers P368-P378.

Diparental conjugation of *R. sphaeroides*

Diparental conjugation was performed as previously described (174) for plasmid transfer using *E. coli* S-17 as donor strain. Selection of the conjugants was obtained on defined medium agar (RÄ) plates containing malic acid as substrate. RÄ medium contained: 3 g/L malic acid, 0.2 g/L MgSO₄·7H₂O, 1.2 g/L (NH₄)₂SO₄, 0.07 g/L CaCl₂·2H₂O, 1.5 mL of microelements stock solution, 2 mL of vitamin stock solution and 5 mL of phosphate buffer. In case of RÄ agar medium, 15 g/L agar was added. The microelements solution contained: 0.5 g/L Fe(II)-Citrate, 0.02 g/L MnCl₂·4H₂O, 0.005 g/L ZnCl₂, 0.0025 g/L KBr, 0.0025 g/L KI, 0.0023 g/L CuSO₄·5H₂O, 0.041 g/L Na₂MoO₄, 0.005 g/L CoCl₂·6H₂O, 0.0005 g/L SnCl₂·2H₂O, 0.0006 g/L BaCl₂·2H₂O, 0.031 g/L AlCl₃, 0.41 g/L H₃BO₃, 0.02 g/L EDTA. The vitamin solution contained: 0.2 g/L nicotinic acid, 0.4 g/L thiamine HCl, 0.008 g/L biotin,

0.2 g/L nicotinamide. The phosphate buffer contained 0.6 g/L KH_2PO_4 and 0.9 g/L K_2HPO_4 .

The donor *E. coli* harbored either a Cas9 targeting plasmid for genome editing, or a plasmid for amorphadiene production. RÄ plates containing 3 g/L of malic acid as carbon source were used for conjugation. These plates contained a trace element solution adapted for *R. sphaeroides* (128). The stock solution (10,000x concentrated) contained (per liter) 1.5 g of nitrilotriacetic acid, 3.0 g of $\text{MgSO}_4 \cdot 7\text{H}_2\text{O}$, 0.5 g of $\text{MnSO}_4 \cdot \text{H}_2\text{O}$, 1.0 g of NaCl, 0.1 g of $\text{FeSO}_4 \cdot 7\text{H}_2\text{O}$, 0.1 g of $\text{CoCl}_2 \cdot 6\text{H}_2\text{O}$, 0.135 g of $\text{CaCl}_2 \cdot 2\text{H}_2\text{O}$, 0.1 g of $\text{ZnSO}_4 \cdot 7\text{H}_2\text{O}$, 0.01 g of $\text{CuSO}_4 \cdot 5\text{H}_2\text{O}$, 0.01 g of H_3BO_3 , 0.01g of $\text{Na}_2\text{MoO}_4 \cdot 2\text{H}_2\text{O}$, 0.015 g of NiCl_2 , and 0.02 g of Na_2SeO_3 ; the pH was adjusted to 6.5 with KOH.

For assessing gene deletions after conjugation with Cas9 targeting plasmid, conjugants were checked by colony PCR with the following primers sets: P411/P412 (*zwf*), P281/P284 (*pgi*), P435/P436 (*gdh*) and P472/P475 (*eda*). All primer sets annealed on the genomic DNA outside the flanking sites cloned within the Cas9 targeting plasmid. Upon confirmation of gene deletions, the PCR fragments were genotyped with the following primers sets: P451/P452 (*zwf*), P282/P283 (*pgi*), P435/P436 (*gdh*) and P472/P475 (*eda*).

Growth and amorphadiene production in 250-mL and 10-mL Erlenmeyer flasks

After overnight preculturing on SMM, the *R. sphaeroides* cultures were transferred to fresh SMM with a starting OD at 600nm of 0.1. Depending on the experiment, at this stage the SMM was containing either 100 % unlabeled or 100 % labeled glucose.

Cultivations for measuring amorphadiene titers were performed in 250- or 10-mL Erlenmeyer flasks. Each flask was filled with 50 mL or 2 mL of SMM medium

and filter-sterilized dodecane (10 % v/v of the liquid phase). Amorphadiene titers were measured after glucose depletion. At the end of the cultivation, the content of the flasks was harvested by centrifugation and further processed for analytical measurements.

For monitoring growth, samples of 400 μL were taken at regular time intervals, and the OD was measured at 600nm. In case of growth in 10-mL Erlenmeyer flasks, multiple flasks were inoculated at the same time, and the content of a single flask was sacrificed for each time point measurement.

Analytics via GC-MS

Determination of amorphadiene titers and mass spectra were performed as previously described (134). For mass spectra determination, an Agilent 7890A gas chromatograph connected to a 5975C mass selective Triple-Axis Detector (Agilent Technologies) was used. For quantification of amorphadiene isotopologs, each sample was injected at 250°C in splitless mode on a ZB-5MS column (Zebron, Phenomenex, 30 m x 250 mm x 0.25 mm film thickness) with 5 m guard column, with a constant flow of helium at 1 mL/min. The oven was programmed for 1 min at 45°C, then ramped at 10°C/min to 300°C and kept as such for 5 min with a solvent delay of 12.5 min, for a final run time of 31.5 min. Metabolic flux ratios were determined by exclusive analysis of secreted amorphadiene. Correction of amorphadiene mass distribution vectors (MDVs) for natural ^{13}C and ^2H isotopes incorporation was performed as previously described (200). The resulting MDV* was used for calculation of the metabolic flux ratios. Moreover, the effect of unlabeled preculture on amorphadiene MDV was assessed by measuring the amount of ^{12}C atoms incorporated within amorphadiene after cultivation with 99% pure $[\text{U-}^{13}\text{C}]\text{glucose}$. This effect was negligible.

Theoretical design of the PLE for glycolytic and isoprenoid flux ratio analysis

We designed the PLE to determine the contribution of the different pathways to product formation by analysis of one specific reporter isoprenoid. For such purpose, we chose the molecule amorphaadiene, already known as precursor of the antimalarial drug artemisinin. Amorphaadiene biosynthesis in *R. sphaeroides* may involve two glycolytic pathways (EMP and ED; the latter also covering its semi-phosphorylated variant, semi-P ED) and two isoprenoid biosynthetic pathways (MEP and MVA). Such a system composed of two modules, each including two pathways, can be analyzed by the parallel use of two different glucose tracers. By parallel cultivation on a defined medium supplied with 100% [1-¹³C]- and [4-¹³C]glucose, ¹³C atoms will be incorporated into IPP (or its isomer DMAPP) when the glucose degradation occurs via EMP pathway (for [1-¹³C]glucose), and when the metabolism towards isoprenoids occurs via the MEP pathway (for [4-¹³C]glucose) (Fig. 1). Hence, the information of the two PLE can be complemented to understand the flux contribution to IPP/DMAPP formation. Three IPP/DMAPP units (C₅) are condensed to generate amorphaadiene (C₁₅). By analyzing via GC-MS the mass spectra of amorphaadiene (*m/z*) it is possible to quantify the fractions of the molecules that have led to the incorporation of the ¹³C atoms, and create a mass distribution vector (MDV) of these molecules. Thus, each *m/z* fraction in the MDV corresponds to a different number of ¹³C-labeled IPPs incorporated into amorphaadiene.

By using [1-¹³C]glucose as positional label, flux via the EMP pathway can lead to 0, 1, 2 or 3 ¹³C-atoms into IPP and DMAPP fractions (**Fig. 1**).

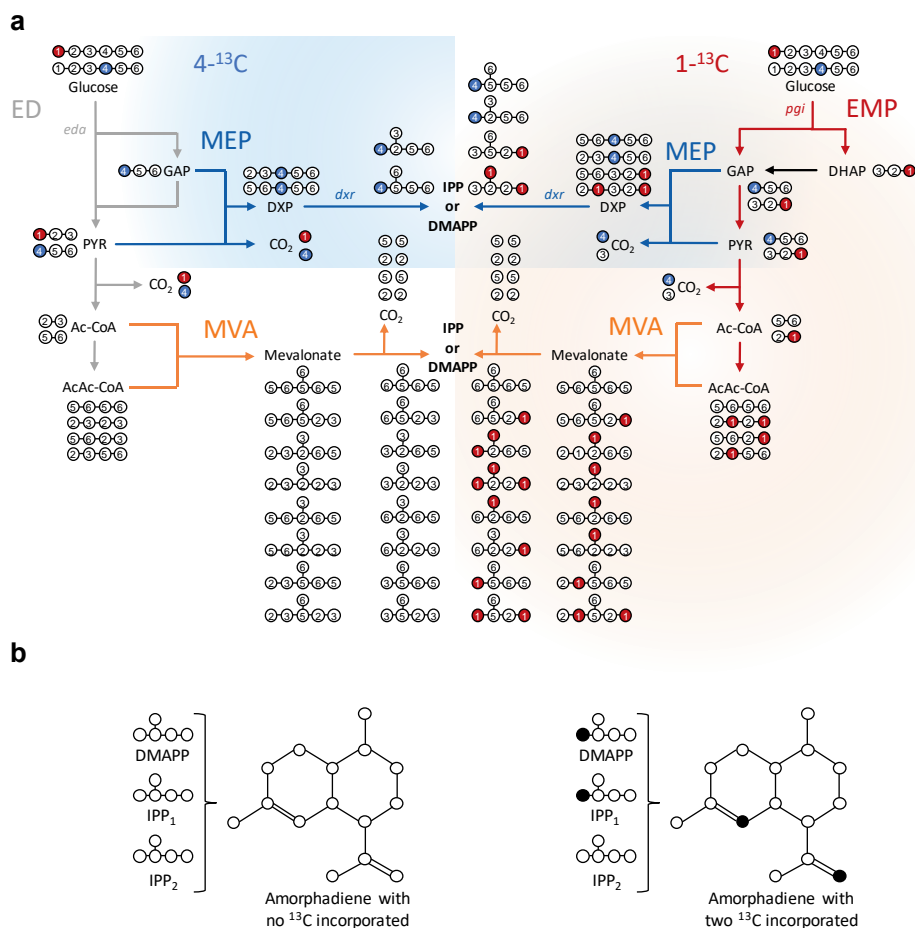


Figure. 1. Schematic overview of ¹³C incorporation into IPP by parallel labeling cultivation. a) [1-¹³C]glucose (red spheres); [4-¹³C]glucose (blue spheres). The scheme shows all possible isotopomers in glucose catabolism (numbers within circles) upon glycolysis via either the ED pathway (grey) or the EMP pathway (red). Isoprenoid biosynthesis towards IPP or DMAPP via MEP (blue) or MVA (orange) pathways is also shown. Target genes for pathway inactivation are also included: *eda* (2- dehydro-3-deoxy-phosphogluconate aldolase), *pgi* (phosphoglucoisomerase) and *dxr* (DXP reductase). Other abbreviations: GAP, glyceraldehyde-3-phosphate (GAP); pyruvate (PYR); dihydroxyacetone phosphate (DHAP); acetyl-CoA (Ac-CoA); acetoacetyl-CoA (AcAc-CoA); 1-deoxy-D-xylulose 5-phosphate (DXP). b) Eventually, the equivalent of 2 IPP and 1 DMAPP units are condensed to generate amorphaadiene. As example, the top scheme represent amorphaadiene generated after the condensation of 3 unlabeled IPP/DMAPP units, while the bottom scheme shows the incorporation of two ¹³C atoms within amorphaadiene as consequence of the condensation of 2 labeled and 1 unlabeled IPP/DMAPP units.

Interpretation of the MDV of amorphadiene must take these different labeling scenarios into account for the accurate interpretation of M+1, M+2 and M+3 fractions. These have been predicted (**Fig. 2**).

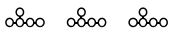
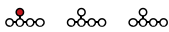




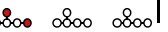
[1- ¹³ C]glucose					¹³ C IPP/DMAPPs No ¹³ C IPP/DMAPPs		¹³ C / No ¹³ C
<i>m/z</i>		Option 1	Option 2	Option 3			
204	M				0	3	0
205	M+1				1	2	0.333
206	M+2				3	3	0.5
207	M+3				6	3	0.667

Figure. 2. Overview of the predicted ¹³C atoms incorporation into isopentenyl-pyrophosphate/dimethylallyl-pyrophosphate (IPP/DMAPP) as effect of [1-¹³C]glucose cultivation. When the increase in amorphadiene *m/z* is of M+2 or more, more than one option for ¹³C incorporation into IPP/DMAPP is possible, and this should be amended. For example, the M+2 fraction can be composed by a set of three IPP/DMAPP units, with two IPP/DMAPPs containing one ¹³C atom each; alternatively, the same fraction can contain a single IPP/DMAPP unit with two ¹³C atoms and two unlabeled IPP/DMAPPs. As consequence, the factors for the conversion of the mass distribution vector (MDV) into labeled IPP/DMAPP fractions were corrected accordingly (bold numbers). These correction factors are the ones presented in **Table 1** and **eq. 1** in the manuscript.

As consequence, correction fractions 1/3, 1/2 and 2/3 are included as multipliers for the M+1, M+2 and M+3 fractions, respectively (**Table 1**).

Table 1. Conversion factors for the transformation of mass distribution vectors (MDV) fractions into amount of labeled IPP units.

MDV fraction	Glucose tracer	
	1- ¹³ C*	4- ¹³ C
M+1	0.333	0.333
M+2	0.500	0.667
M+3 (or more)	0.667	1.000

*further details on how conversion values for [1-¹³C]glucose label were obtained can be found in **Fig. 2**.

Once these products are summed, the exact fraction of labeled IPP/DMAPPs isotopologs derived from [1-¹³C]glucose can be quantified. As shown in **Fig. 1**, this fraction corresponds to 9 units of IPP/DMAPPs out of 12 total units that can be generated by using this positional label. Therefore, this fraction must be amended for including the 3/12 fraction of unlabeled IPP/DMAPPs isotopologs still contributing to the EMP split ratio. Such correction is obtained by multiplying the determined labeled IPP/DMAPP fraction by 12/9. In **eq. 1**, all these considerations are summarized:

$$J_{EMP\%} = \left(\frac{1}{3} MDV^*_{1[1-^{13}C]} + \frac{1}{2} MDV^*_{2[1-^{13}C]} + \frac{2}{3} MDV^*_{3[1-^{13}C]} \right) * \frac{12}{9}; \text{ (eq. 1)}$$

Since the contribution of EMP is complementary to ED, ED flux ratio is determined as follows:

$$J_{ED\%} = 1 - J_{EMP\%}; \text{ (eq. 2)}$$

For [4-¹³C]glucose cultivation, no more than one ¹³C-atom is expected to be incorporated per IPP/DMAPP unit (**Fig. 1**). Therefore, for this positional label, correction factors for the amorphadiene MDV* will match with the increase of *m/z* (**Table 1**). Yet, a fraction of IPP/DMAPP isotopologs derived from the EMP

pathway and MEP pathway will remain unlabeled (**Fig. 1**). It can be observed that, in a strain relying exclusively on the MEP pathway for isoprenoid biosynthesis, the fraction of unlabeled IPP/DMAPPs isotopologs derived from [4-¹³C]glucose corresponds to half of the isoprenoid pool generated via the EMP pathway. Hence, this $J_{EMP\%}/2$ quantity is added to **eq. 3** for obtaining the whole MEP flux ratio:

$$J_{MEP\%} = \sum_{i=1}^3 A_i + \frac{J_{EMP\%}}{2}, \text{ where } A_i = \frac{i}{3} * MDV^*_{i[4-^{13}C]}; \quad (\text{eq. 3})$$

Because the MVA pathway contributes to the whole isoprenoid flux, it can be determined as follows:

$$J_{MVA\%} = 1 - J_{MEP\%}; \quad (\text{eq. 4})$$

Nevertheless, it must be noted that addition of $J_{EMP\%}/2$ in equation 3 becomes an approximation when also the MVA pathway is present. Still, as shown later, correctness of this formula was proven empirically, and resulted in no degree of freedom (and therefore 100% flux) via either the MEP or MVA pathway, when one of these two pathways was exclusively active.

Since IPP/DMAPP are the building blocks of any isoprenoid, this approach and formulas can in principle be adjusted and applied for flux determination of any isoprenoid of interest.

Results

Validation of the ¹³C labeling method

Scale down of the ¹³C cultivation system

A graphical overview of the PLE setup is shown in **Fig. 3a**. Since the use of labeled substrates can be costly, the cultivation volume was reduced from 50 mL to 2 mL using 10-mL Erlenmeyer flasks. Using unlabeled [¹²C]glucose, growth was followed in both cultivation volumes to observe possible limitation effects. In both cases, growth occurred exponentially and stopped within 24 h, with no significant difference in growth rates (μ_{\max} of $0.17 \pm 0.01 \text{ h}^{-1}$ and $0.16 \pm 0.01 \text{ h}^{-1}$ for 2 mL and 50 mL volumes, respectively) (**Fig. 3b**). Moreover, final amorphaadiene titers were similar (**Fig. 3c**), indicating that scaling down the cultivation volume to 2 mL did not affect terpene synthesis.

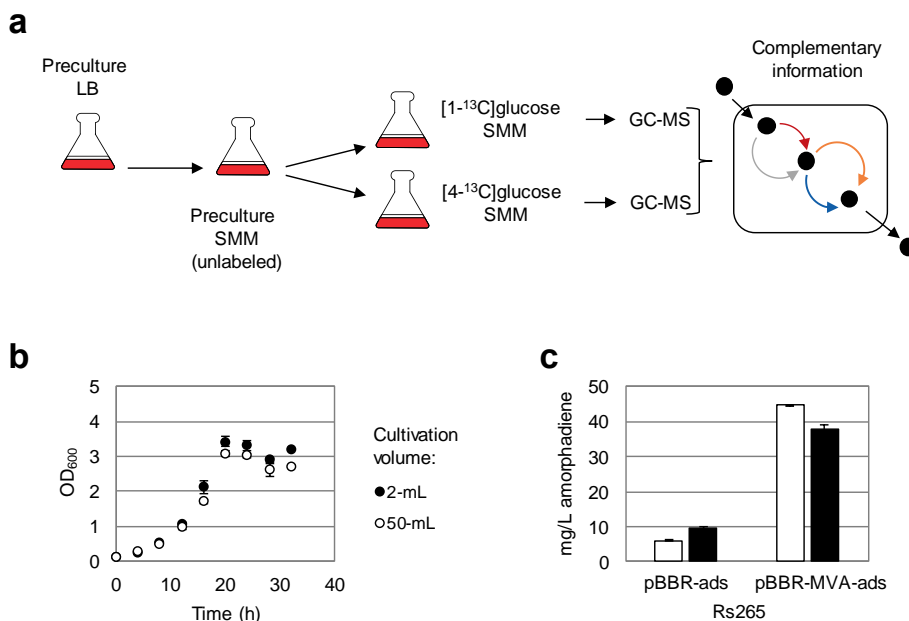


Figure 3. Scale down and validation of the ¹³C cultivation. a) Setup for parallel labeling experiment (PLE). Preculturing occurs in rich medium (LB), followed by another preculturing for adaptation to unlabeled Sistrom’s minimal medium (SMM). Then, PLE proceeds with parallel incubation on two labeled tracers [1-¹³C]- and [4-¹³C]glucose. At the end of the cultivation, the amorphaadiene collected from PLE is analysed by GC-MS, and then the data obtained is combined for solving the network. b) Growth profile of *R. sphaeroides* using different cultivation volumes. c) Comparison of final amorphaadiene titers after cultivation in 50 mL (white) or 2 mL (black) of SMM.

Generation of knock-out strains for method validation

Since discrimination between pathway contributions relies on the presence or absence of labeled carbon(s) in the IPP/DMAPP units, this system will generate a “yes or no” type of outcome. To validate this method, strains with selectively inactivated glycolytic and isoprenoid pathways were generated using homologous-recombination (HR) and CRISPR-Cas9 counter-selection (174). Eventually, the strains implemented for the validation had a deletion in one of

the pathways of interest. Deletions concerned the genes encoding for *glucose-6-phosphate isomerase* (*pgi*, EMP pathway), *2-keto-3-deoxy-6-phosphogluconate aldolase* (*eda*, ED pathway) and *1-deoxy-D-xylulose 5-phosphate reductoisomerase* (*dxr*, MEP pathway). The latter was obtained after previous integration of the MVA pathway in the chromosome(201). Once the knockouts were confirmed by sequencing, the pBBR-*ads* plasmid expressing amorphadiene synthase was introduced by conjugation. Prior to ¹³C cultivation, a growth assessment on the strains was performed using unlabeled glucose. The mutant Rs265 Δ *eda* was able to grow on LB medium, but not on glucose. Therefore, it could not be used for further testing. The ED pathway is known to be the major contributor to glucose catabolism in this species (125, 128). Prior attempts to eliminate this pathway showed a dramatic decrease in cell growth (202). Therefore, it is probable that also this strain of *R. sphaeroides* largely relies on ED for glucose catabolism. All other mutants were able to grow on glucose, with a μ_{\max} similar to the *wt* (Table 2).

Table 2. Growth rates of the mutant strains used for ¹³C method validation.

Genome	μ_{\max} (h ⁻¹)
Rs265	0.134 ± 0.002
Rs265 Δ <i>pgi</i>	0.124 ± 0.011
Rs265 Δ <i>eda</i>	N.G.*
Rs265_MVA- Δ <i>dxr</i>	0.139 ± 0.032

*N.G. = no growth. Growth rates were calculated from cultures containing dodecane (10% v/v of the liquid phase).

In vivo ¹³C parallel labeling experiment method validation

The generated knock-outs were used for validating the ¹³C method. Correct design of the PLE should result in no degree of freedom (and consequently 100% of flux ratio) for either the glycolytic or the isoprenoid metabolism. Since

amorphadiene is a volatile molecule (203), once secreted it accumulates in the organic layer. In principle, by sampling at the end of the exponential phase it is possible to quantify each pathway contribution to the overall batch. Therefore, at glucose depletion the MDVs of amorphadiene, obtained by PLE cultivations of the mutant strains, were determined from the dodecane layer using GC-MS (Supplementary **Tables S4, S5**).

To assess the robustness of the method, we tested it on the knock-out strains. Deletion of the *pgi* gene in central metabolism was expected to block the flux via the EMP pathway (**Fig. 4a**). As expected, this flux ratio was the lowest determined in this study (0.01 ± 0.00). Consequently, almost all glucose conversion occurred via the ED pathway (0.99 ± 0.00). Since Rs265 Δpgi contained the pBBR-*ads* plasmid, amorphadiene biosynthesis occurred only via the endogenous MEP pathway. Application of the method confirmed amorphadiene biosynthesis completely via the native pathway (0.99 ± 0.01) and no flux was detected through the MVA pathway (0.01 ± 0.00) (**Fig. 4a**). Sensitivity of the method for the isoprenoid pathways was further tested by measuring the split ratio on the Rs265-MVA- Δdxr mutant (inactivated MEP pathway), in a strain with the MVA pathway integrated in the chromosome (**Fig. 4b**). Here, the split ratio was reversed, showing a complete flux via the MVA pathway (0.97 ± 0.03), while virtually no flux occurred via the MEP pathway (0.03 ± 0.00). In the same strain, the glycolytic module indicated an active flux via the EMP pathway, which was significantly higher (0.04 ± 0.01 , $p < 0.01$ after Student's t-test) compared to Rs265 Δpgi strain. Nevertheless, most of the glucose oxidation was still performed via the ED pathway (0.96 ± 0.01). In summary, the specific pathway knock-outs confirmed the reliability of the proposed ^{13}C parallel labeling method.

Sensitivity of the ¹³C method was further tested by adding the specific MEP pathway inhibitor fosmidomycin (204, 205). The metabolic flux ratio in Rs265 + pBBR-MVA-*ads* was determined in the presence of different concentrations of fosmidomycin. The glycolytic split ratio was not affected by the MEP inhibitor (**Fig. 5a**). On the other hand, increasing fosmidomycin concentrations resulted in a decrease of MEP pathway flux (from 0.31 ± 0.01 to 0.20 ± 0.01), while flux via the MVA pathway increased (from 0.69 ± 0.01 to 0.80 ± 0.01) (**Fig. 5b**, Supplementary **Table S9**). The fosmidomycin concentrations used were not high enough to completely inactivate the pathway. Nevertheless, with 2 mM of the inhibitor, the titers obtained via the MEP pathway were reduced to more than 70% compared to conditions with no fosmidomycin (**Fig. 5c**). This outcome agreed with what was expected from MEP inhibition by fosmidomycin, and further confirmed the reliability of the method.

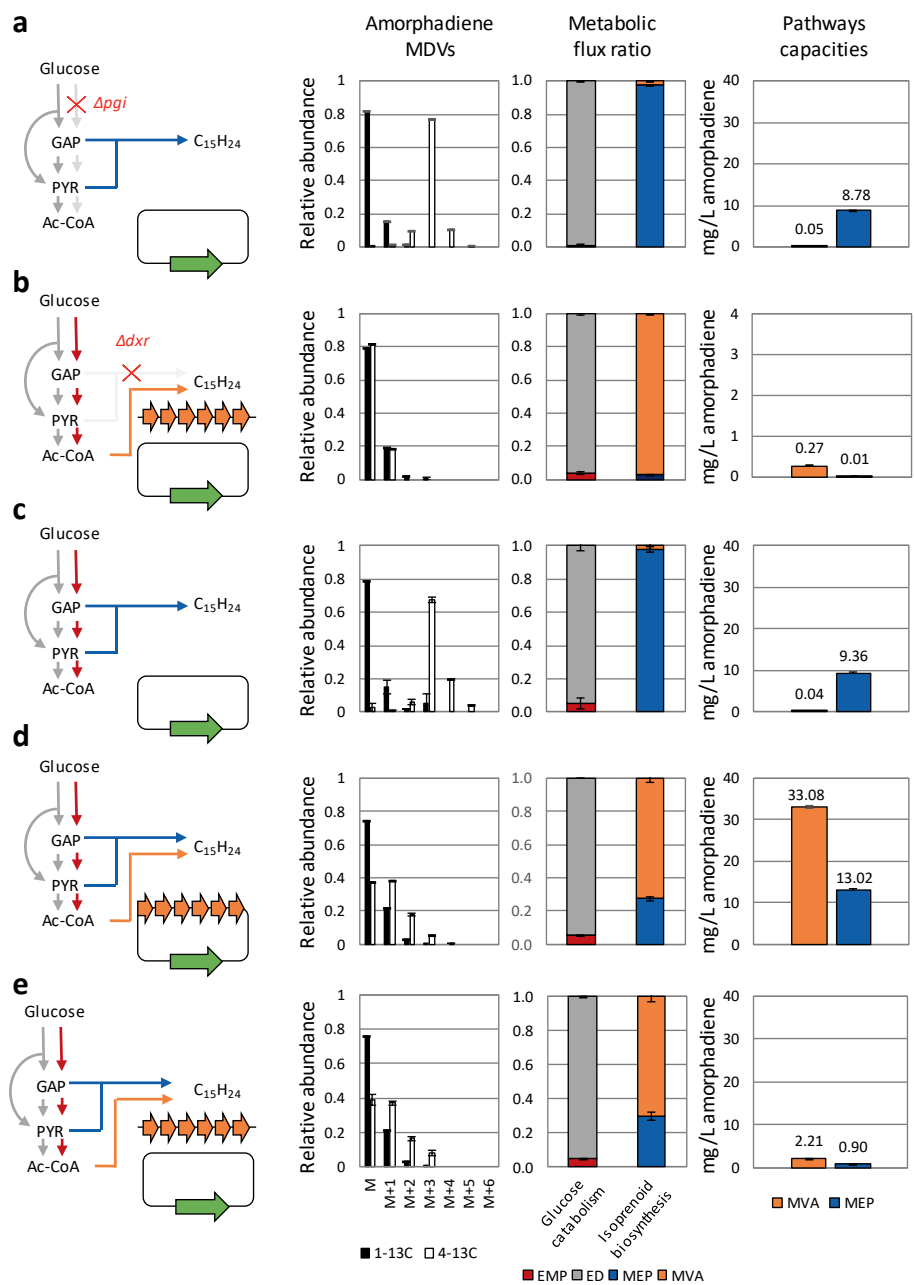


Figure. 4. ¹³C metabolic flux ratios for several *R. sphaeroides* strains. Schemes on the left show the genetic composition of strain used. Colors refer to investigated pathways: ED (grey), EMP (red), MEP (blue) and MVA (orange). Red cross indicates gene deletion.

Orange arrows represent the MVA operon. This is either integrated in the chromosome (black line) or inserted on a plasmid (black circle). The plasmid also contains the amorphaadiene synthase gene (*ads*, green arrow). $\text{C}_{15}\text{H}_{24}$ represent amorphaadiene. Left bar chart represent amorphaadiene mass distribution vectors (MDVs). It consists of abundances of fractions determined via analysis of amorphaadiene m/z (for more detailed information, see **Tables S4-9**). Fractions refer to cultivation with $[1-^{13}\text{C}]\text{glucose}$ (black bar) and $[4-^{13}\text{C}]\text{glucose}$ (white bar). Central stack bar charts represent metabolic split ratios calculated for glycolysis and isoprenoid modules. Right bar charts quantify pathways contribution to amorphaadiene titers measured at the end of batch cultivation. a) Rs265 Δpgi + pBBR-*ads*; b) Rs265-MVA- Δdxr + pBBR-*ads*; c) Rs265 + pBBR-*ads*; d) Rs265 + pBBR-MVA-*ads*; e) Rs265-MVA + pBBR-*ads*.

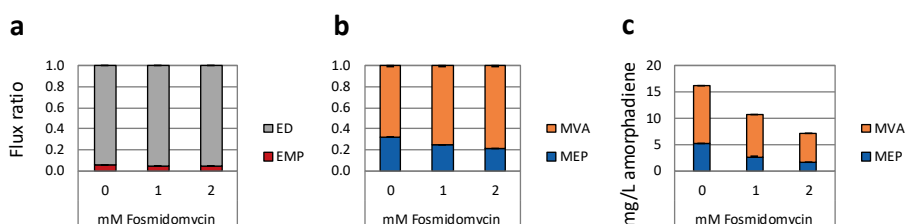


Figure 5. Effect of fosmidomycin on metabolic flux ratios. Overview of a) central metabolism and b) isoprenoid pathways flux ratios. c) Effect of fosmidomycin on the isoprenoid pathways capacities, expressed in mg/L amorphaadiene obtained at the end of the cultivation. The concentrations of fosmidomycin used are listed below each bar chart.

Application of the method for the *in vivo* study of isoprenoid metabolism

Metabolic flux ratio in the glycolytic module: measuring the capacities of ED, semi-P ED and EMP pathways

First, we used the validated ^{13}C method to assess the metabolic flux ratios around the glucose 6-phosphate node in the glycolytic module (**Fig. 6a**). The Rs265 + pBBR-*ads* strain was cultivated using the ^{13}C tracers and the metabolic flux ratios were determined (Supplementary **Table S6**, **Fig. 4c**). Although most of the flux was carried via the ED pathway (0.94 ± 0.02), the ^{13}C method disclosed a residual, but significant, EMP pathway contribution (0.06 ± 0.02). This result proves that

the EMP pathway is also involved in glucose catabolism during dark heterotrophic growth.

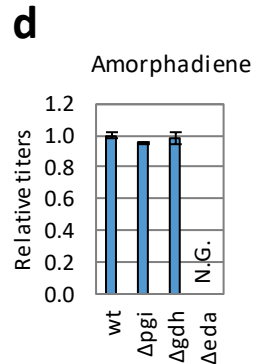
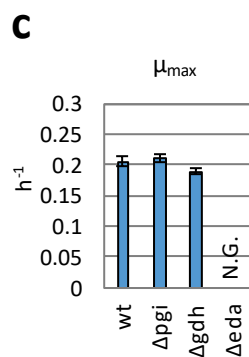
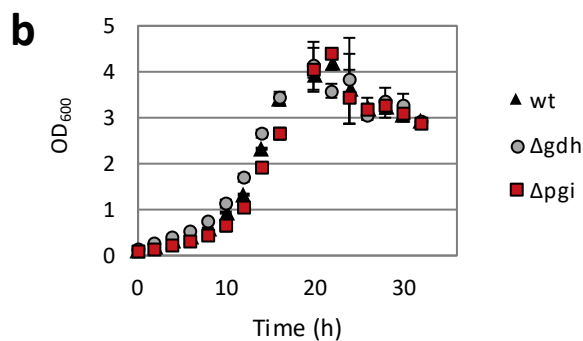
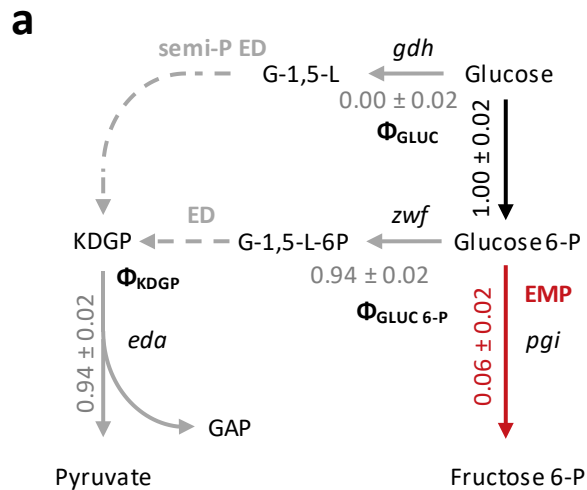


Figure 6. Elucidation of the metabolic flux ratio in the central metabolism in *R. sphaeroides*. a) Schematic representation of glycolytic pathways with key enzymes indicated: *gdh* (*quino protein glucose dehydrogenase*), *zwf* (*glucose-6-phosphate 1-dehydrogenase*) and *pgi* (*phosphoglucoisomerase*). Grey arrows represent the ED/semi-P ED module which converge flux via the gene *eda* (2-dehydro-3-deoxy-phosphogluconate aldolase). Red arrow represent the flux via EMP pathway. Colored numbers represent metabolic split ratio determined for each of pathway of the module. Continuous lines represent reactions catalyzed by enzymes encoded by correspondent gene. Dashed lines are lumped reactions. Abbreviations: G-1,5-L, glucono-1,5-lactone; G-1,5-L-6P, 6-phospho-glucono-1,5-lactone; KDPG, 2-keto-3-deoxy-6-phosphogluconate. The symbols Φ_{GLUC} , $\Phi_{\text{GLUC 6-P}}$, Φ_{KDPG} represent the split ratios for the nodes of the glycolytic pathways within the investigated network. b) Growth profiles of the different *R. sphaeroides* mutants. c, d) Growth rates (μ_{max}) determined in medium without dodecane, and relative amorphadiene titers determined in SMM (without dodecane). Rs265 Δeda could not grow on glucose (N.G., no growth).

As explained before, since the method determines the flux via Eda activity (**Fig. 1**), both the ED and the semi-P ED pathways could in principle contribute to the flux via this enzyme (**Fig. 6a**). To assess the role of the two ED pathways, we targeted both *quino protein glucose dehydrogenase* (*gdh*) and *glucose-6-phosphate 1-dehydrogenase* (*zwf*) for deletion (**Fig. 6a**). While a Δgdh strain was obtained, no mutant was found for the *zwf*, despite several attempts with different targeting spacers (sp1-6). The Rs265 Δgdh strain obtained was further cultivated (**Fig. 6b**), and its μ_{max} and amorphadiene titers were compared to those of the other glycolytic mutants (**Fig. 6c, d**). The results show that blocking Eda does not allow growth on glucose, and blocking Gdh does not dramatically affect growth or the amorphadiene titer ($p > 0.05$ after Student's t-test for both parameters). This result, combined with the inability to create a *zwf* deletion, indicates that the ED pathway carries all the flux in the ED/semi-P ED pathway when grown on glucose.

Effect of the presence of a functional MVA pathway on the capacity of the MEP pathway

Previous research demonstrated that the amorphadiene titer increased about 8-fold when the heterologous MVA pathway was expressed on a plasmid in *R. sphaeroides* (134). This increase has been explained as a result of a 7-fold higher flux of the MVA pathway compared to the MEP pathway. Here, we used the ^{13}C -labeling method to quantify the flux through the native MEP pathway and the heterologous MVA pathway. Therefore, we analyzed the metabolic flux ratio in the strain containing the plasmid-encoded MVA pathway (Rs265 pBBR-MVA-*ads*) in addition to the native MEP pathway and compared it to the MEP-only strain (Rs265 pBBR-*ads*) (**Fig. 4c, d**). The strain with the dual isoprenoid pathways showed a 0.28 ± 0.01 contribution via the native MEP and a 0.72 ± 0.01 contribution via the heterologous MVA pathway (**Fig. 4d**). In the control strain (Rs265 + pBBR-*ads* strain; **Fig. 4c**) all amorphadiene was synthesized via the native MEP pathway (0.98 ± 0.02). This indicates that the ratio between the MVA and MEP contribution is of about 2.6, and not 5 as the increase in total amorphadiene titer would suggest (**Table 3, Fig. 4c, d**). By quantifying the effect of the split ratios on amorphadiene titers measured via GC-FID (**Fig. 4c, d**), it can be concluded that in the dual pathway strain the volumetric capacity of the native MEP pathway increased by 39% compared to the MEP-only strain (**Table 3, $p < 0.01$ after Student's t-test**). Thus, constitutive expression of the heterologous MVA pathway not only resulted in an overall enhancement of amorphadiene biosynthesis, but also caused a higher flux through the endogenous MEP pathway.

Effect of the presence of a functional MEP pathway on the capacity of the MVA pathway

We also tested the effect of the presence of an active native MEP pathway on the MVA pathway. Amorphadiene production and flux ratios in the Rs265-MVA- Δdxr (relying exclusively on an integrated MVA pathway) were compared to strain Rs265-MVA, which co-expressed MEP and MVA (integrated) pathways and synthesized amorphadiene via plasmid-borne amorphadiene synthase pBBR-*ads* (134). Amorphadiene titers in Rs265-MVA- Δdxr resulted in 0.27 ± 0.01 mg/L of product (**Fig. 4b**), which was exclusively produced via the MVA pathway, as was shown by ¹³C labeling (**Fig. 3b**). Total isoprenoid titer in the Rs265-MVA strain co-expressing both pathways was ~10-fold higher (**Table 3**, 3.11 ± 0.03 mg/L) (**Fig. 4e**). Interestingly, metabolic flux ratios for both isoprenoid pathways were similar to those found earlier using the plasmid-encoded MVA pathway (**Fig. 4d**), with a flux ratio of 0.29 ± 0.02 for the MEP pathway, and 0.71 ± 0.06 for the MVA pathway, respectively (**Fig. 4e**). Hence, the capacity of the integrated MVA pathway greatly improved when the native MEP pathway was active, with an ~8-fold increase from 0.27 ± 0.01 mg/L to 2.21 ± 0.03 mg/L of amorphadiene (**Table 3, Fig. 4e**).

As already mentioned, incubation of the Rs265 + pBBR-MVA-*ads* strain with increasing concentrations of fosmidomycin resulted in a decrease in the relative contribution of the MEP pathway (**Fig. 5b**). Consequently, the isoprenoid flux ratio indicated an increased relative contribution of the MVA pathway (**Fig. 5b**). Nevertheless, as effect of MEP pathway inhibition the overall flux towards amorphadiene decreased (**Fig. 5c**). Interestingly, also the flux via the MVA pathway was susceptible to the inhibition, reducing its contribution by approximately 50% (**Fig. 5c**). Altogether, these results indicate that both isoprenoid pathways influence each other by some unknown mechanism.

Moreover, both pathways can mutually benefit from each other when an active flux is present in both.

Isoprenoid flux ratio is insensitive to MVA enzymes copy number

When the MVA pathway was expressed on a plasmid, it showed a ~15-fold higher capacity compared to when integrated in the genome (33.08 ± 1.12 mg/L for plasmid-MVA, 2.21 ± 0.03 mg/L for integrated-MVA) (**Fig. 4d, e**). This increase in capacity follows the increase in copy number conferred by the pBBR1MCS2 plasmid, which ranges from 9 to 14 copies in *R. sphaeroides* (85). However, the split ratio between both isoprenoid pathways was the same, irrespective of the plasmid- or chromosome-based expression (Rs265 + pBBR-MVA-*ads* and Rs265-MVA + pBBR-*ads* (**Fig. 4d, e**). To our surprise, the lower flux via the integrated MVA pathway limited the capacity of the native MEP pathway, which decreased ~14-fold in the Rs265-MVA + pBBR-*ads* strain compared to the Rs265 + pBBR-MVA-*ads* (MEP-derived titers of 0.90 ± 0.01 mg/L and 12.66 ± 0.43 mg/L, respectively).

Table 3. Overview of changes in pathways capacities determined via PLE.

Strain	Description	Total amorphaadiene titers (mg/L) ^a	Fold- change (titers) ^b	Pathway-derived titers (mg/L) ^c			MVA/MEP ratio	Focus (pathway)	Fold-change due to co- expression of orthogonal pathway
				MEP	MVA	MEP			
Rs265 + pBBR-<i>ads</i>	MEP only	9.40 ± 0.05	4.9 ± 0.1	9.36 ± 0.04	0.04 ± 0.04	-	-	MEP	1.39 ± 0.03 ^d
Rs265 + pBBR-MVA-<i>ads</i>	MEP + MVA (plasmid)	46.10 ± 0.50		13.02 ± 0.24	33.08 ± 1.12		2.5 ± 0.1	MEP pathway	
Rs265_MVA Δ<i>dxr</i> + pBBR-<i>ads</i>	MVA integrated, MEP inactivated	0.28 ± 0.01	11.1 ± 0.4	0.01 ± 0.01	0.27 ± 0.01		-	MVA pathway	8.19 ± 0.32 ^e
Rs265_MVA + pBBR-<i>ads</i>	MVA integrated	3.11 ± 0.03		0.90 ± 0.03	2.21 ± 0.03		2.5 ± 0.1		

^a determined via GC-FID.^b obtained as ratio between the titers of the strain co-expressing both isoprenoid pathways and the control strain relying exclusively on the MEP or MVA pathway.^c Data obtained by multiplying titers measured via GC-FID for the metabolic flux ratios obtained via PLE. The values reported are shown also in Figure 4.^d expresses the ratio between titers obtained via the MEP pathway in the Rs265 + pBBR-MVA-*ads* (13.02 ± 0.24 mg/L) and the Rs265 + pBBR-*ads* (9.36 ± 0.04 mg/L) strains.^e expresses the ratio between titers obtained via the MVA pathway in the Rs265_MVA + pBBR-*ads* (2.21 ± 0.03 mg/L) and the Rs265_MVA Δ *dxr* + pBBR-*ads* (0.27 ± 0.01 mg/L) strains.

Discussion

To study the isoprenoid metabolism of *R. sphaeroides*, we developed a technique for ^{13}C metabolic flux ratio analysis based on parallel labeling experimentation using $[1-^{13}\text{C}]$ and $[4-^{13}\text{C}]\text{glucose}$ as tracer (**Fig. 3a**). By the exclusive analysis of one reporter isoprenoid, this method can qualitatively and quantitatively infer the metabolic flux ratios in the glycolytic pathways and in the isoprenoid pathways leading to IPP and DMAPP. More precisely, by analysis via GC-MS of amorphaadiene, it was possible to assess whether glucose was catabolized via the EMP or the ED/semi-P pathway and whether amorphaadiene was synthesized via the MEP or the MVA pathway (**Fig. 1**). The key molecules of the analysis, IPP and DMAPP, are the universal precursors of all isoprenoids; hence, we believe that this method can in principle be extended to study the biosynthesis of any isoprenoid of interest.

Traditionally, ^{13}C -MFA approaches recommend the use of steady state conditions for determining flux partitioning (206). This is suggested to prevent reversible reactions that would otherwise affect ^{13}C incorporation into protein-bound amino acids. Here, due to the high volatility of amorphaadiene (203), we did not expect reverse reactions to occur between the secreted amorphaadiene and the intracellular metabolism. Hence, by accumulating the isoprenoid within a dodecane layer, it was possible to determine the contribution of the different pathways to the overall product formation. Since the experiments required 100% labeled substrates, we needed to decrease the cultivation volume to reduce experimental costs. Scaling down the cultivation volume from 50 mL to 2 mL resulted in comparable growth profiles and amorphaadiene titers (**Fig. 3b, c**). Thus, smaller cultivation volumes could be used.

The network conceived in this work could be solved by applying a set of four equations (**eq. 1-4**). Therefore, this setup demonstrates that it is possible to extend the use of labeling experiments to the investigation of secondary metabolism, without the need of any computation step. The ^{13}C metabolic flux ratio method was then validated *in vivo* by using mutants in which one of the 4 involved pathways was blocked (**Fig. 4a, b**). Therefore, it was used to study the isoprenoid metabolism of *R. sphaeroides*.

First, we applied the method to elucidate the metabolic flux ratio in the glycolytic module. By combining PLE with specific knock-outs of genes of both glycolytic pathways, we could demonstrate that the ED pathway is the main pathway responsible for glucose catabolism, and that the semi-P ED (Rs265 Δgdh) does not carry significant flux towards amorphaadiene (**Fig. 6**), as has also been shown for photoheterotrophic growth on glucose (202). The failure to generate a Rs265 Δzwf strain indicates that Zwf is essential during growth on malic acid as only carbon source (substrate of the RÄ medium, used for conjugation). In fact, this enzyme is shared between ED and the PPP, and is required for NADPH generation. Moreover, it can be required for the biosynthesis of erythrose 4-phosphate and ribulose 5-phosphate, which are both essential for microbial growth. Previously published research never reported an EMP contribution during dark heterotrophic growth (128, 207). Conversely, by using PLE we could prove that, although to a small extent (~5%), the EMP pathway contributes to glucose catabolism and amorphaadiene biosynthesis (**Fig. 4, 6**). Ultimately, direct measurement of the glycolytic split ratio can increase our understanding of the effects of metabolic engineering approaches for increased isoprenoid biosynthesis on the central metabolism. Examples of such approaches can be direct manipulation of glycolytic enzymes (*e.g.* overexpression), or more indirect, *e.g.* targeting of regulatory mechanisms or engineering of the redox metabolism.

Second, the *in vivo* study of isoprenoid biosynthesis by PLE led to important insights about MEP and MVA co-expression. The most important one is that when the two pathways are co-expressed, a mutual enhancement of their fluxes occurs. In fact, both the MEP pathway and the MVA pathway increased their capacity when the other pathway was also active. This synergy between the two isoprenoid pathways has been described before in *E. coli* when both were expressed at high levels (205). There, it was also reported that the increased flux via the overexpressed MEP enzymes required an active flux via the MVA pathway. Here, we demonstrated that this principle applies also for the orthogonal MVA pathway in *R. sphaeroides*, whose capacity was increased upon an active flux via the endogenous MEP pathway (**Fig. 4b, e, 5c**).

Although the endogenous MEP pathway was not altered from its native expression level, it was still stimulated by the plasmid-borne MVA pathway (**Fig. 4c, d**). Yet, the explanation of this stimulation is not clear. pBBR-MVA-*ads* plasmid contained also the *idi* gene, encoding isopentenyl diphosphate isomerase, which was proven to be crucial for enhancing the flux via the MEP pathway in *E. coli* (208). It could be that, upon presence of more *Idi* copies, IPP isomerization to DMAPP occurs more efficiently. As a consequence, more DMAPP is available for the condensation with IPP to further generate amorphadiene.

Another interesting observation obtained via PLE is that the metabolic flux ratio between MEP and MVA remains constant, despite different expression levels of the MVA pathway, which led to different final titers (**Fig. 4d, e**). In fact, the copy number of the pBBR1MCS2 plasmid (from which pBBR-MVA-*ads* is derived) is known to be about 9 to 14 copies in *R. sphaeroides* (85), whereas a Tn5 integrated MVA operon in principle is a single copy. Still, it remains unclear why

the expression levels of the MVA pathway do not influence the isoprenoid flux ratio. As a consequence, this interaction between MEP and MVA pathways resulted in a limitation of the endogenous MEP pathway in the Rs265-MVA strain (Fig. 4e). Most probably, this low flux via the endogenous MEP pathway was dictated by the low capacity of the integrated MVA pathway.

Conclusions

In this work, we presented a novel ^{13}C metabolic flux ratio method based on parallel labeling for studying isoprenoid biosynthesis along the MEP and MVA pathway. The theoretical design we developed enabled the analysis of the metabolic flux ratio between the glycolytic and isoprenoid pathways by exclusive measurement of the secreted reporter isoprenoid, amorphaadiene. The network was solved by using four equations, and it can in principle be applied to study the synthesis of any other isoprenoid. We used this method for studying the metabolism during amorphaadiene biosynthesis in the versatile bacterium *R. sphaeroides*. We could show that the ED pathway is the dominant glycolytic pathway, and that co-expression of the MEP and MVA pathways have a mutual stimulating effect. Yet, how the split ratio is controlled is unclear. All in all, this work shows the potential of tailoring ^{13}C metabolic flux analysis experiments by using parallel labeling. It also provides novel insights into the metabolism of isoprenoids and will help to improve their production in *R. sphaeroides* and in any other biotechnologically relevant species.

Acknowledgements

We thank Isobionics BV (The Netherlands) for providing the *R. sphaeroides* strain used in this work. Moreover, we thank A. De Maria for designing and implementing the Δpgi mutant, and D. van Gelder for helping in obtaining the Δeda mutant. Any request for the strain and its derivatives should be directed to Isobionics BV.

Funding

This project was financially supported by The Netherlands Ministry of Economic Affairs and a public-private NWO-Green Foundation for sustainable production and supply chains in agriculture and horticulture (870.15.130, 2015/05279/ALW).

Supplementary information

Table S1. Strains and plasmids used in this study.

Strains	Description	Reference
Rs265	Derivative of <i>R. sphaeroides</i> ATCC 35053	(134)
Rs265-MVA	Rs265 with genomic integration of the mevalonate (MVA) operon	(201)
Rs265-MVA- Δdxr	Rs265-MVA with deletion in the <i>dxr</i> gene	(201)
Rs265 Δpgi	Rs265 with deletion in the <i>pgi</i> gene	This study
Rs265 Δgdh	Rs265 with deletion in the <i>gdh</i> gene	This study
Rs265 Δeda	Rs265 with deletion in the <i>eda</i> gene	This study
Plasmids	Description	Reference
pBBR- <i>ads</i>	pBBR1MCS-2 + <i>crtE</i> promoter and <i>ads</i> (amorphadiene synthase)	(134)
pBBR-MVA- <i>ads</i>	pBBR1MCS-2 + <i>PcrtE-ads</i> + MVA enzymes	(91)
pSGC	Broad host range plasmid (KanR) containing the <i>cas9h</i> under the control of the constitutive Plac promoter and the non-targeting sgRNA under the control of the BBa_J95023 promoter and the BBa_J95029 terminator	(174)
pBBR-Cas9- <i>pgi</i> (sp1)	pSGC derivative plasmids for <i>pgi</i> removal by homologous recombination and Cas9 counter-selection	This study
pBBR-Cas9- <i>gdh</i> (sp1-sp3)	pSGC derivative plasmids for <i>gdh</i> removal by homologous recombination and Cas9 counter-selection	This study
pBBR-Cas9- <i>eda</i> (sp1-sp3)	pSGC derivative plasmids for <i>eda</i> removal by homologous recombination and Cas9 counter-selection	This study
pBBR-Cas9- <i>zwf</i> (sp1-sp6)	pSGC derivative plasmids for <i>zwf</i> removal by homologous recombination and Cas9 counter-selection	This study

Table S2. Targeting spacers used in this study.

Spacers	Sequence (5'-3')	PAM
<i>pgi_sp1</i>	GCGACGGTCTGAGCCTCTAC	CGG
<i>pgi_sp2</i>	CCGCTTGCCCGCCTCCGGAA	CGG
<i>pgi_sp3</i>	GCGCGACGAGGAATTCGCAG	GGG
<i>eda_sp1</i>	CGACGCGATCCGCATCATGG	CGG
<i>eda_sp2</i>	GTGGGGCAGAAAGTCACCTG	GGG
<i>eda_sp3</i>	TCATGGCGGAAGTCGAAGGT	GGG
<i>gdh_sp1</i>	CTCCTGTGGAAGTGGGACAG	CGG
<i>gdh_sp2</i>	CACCTTCAACTGGGGCTCCG	TGG
<i>gdh_sp3</i>	TGGCACTCGACGTGGCGACG	GGG
<i>zwf_sp1</i>	ACGGTTTCTCGACCACGATG	CGG
<i>zwf_sp2</i>	GGAGAGCTACGTCGATCACG	CGG
<i>zwf_sp3</i>	ACGCCCTTCTACCTGCGTAC	CGG
<i>zwf_sp4</i>	GCGATGATGCGGCTGTCGGG	CGG
<i>zwf_sp5</i>	CCGCGTCGTCCATCTCCGAG	CGG
<i>zwf_sp6</i>	GCGCGGCCCGCACCTGCGCG	CGG

Table S3. Primers used in this study.

Name	Sequence	Description
P301	CCATGTCGGCAGAATGCTTAATG	Conserved primer for pBBR_Cas9 assembly for every target gene. To be combined con gRNA_REV primers
P302	CATTAAGCATTCTGCCGACATGG	Conserved primer for pBBR_Cas9 assembly for every target gene. To be combined with P303
P303	GCCTGAATGGCGAATGGAAATTGTAA	Conserved primer for pBBR_Cas9 assembly for every target gene. To be combined with P302

Name	Sequence	Description
P304	GTGCGGGCCTCTTCGCTATTA	Conserved primer for pBBR_Cas9 assembly for every target gene. To be combined con gRNA_FWD primers
P245	TTACAATTTCCATTCGCCATTGAGCCTC AAGGTGATGATCAAGGAGC	For assembly of homology arm 1 in pBBR_Cas9_Δ <i>pgi</i> . To be combined with P246
P246	GAAAGCGGAAGGATCCCTCACATTGCA AGAATGCCTGTAATCC	For assembly of homology arm 1 in pBBR_Cas9_Δ <i>pgi</i> . To be combined with P245
P247	TGAGGGATCCTTCCGCTTTC	For assembly of homology arm 2 in pBBR_Cas9_Δ <i>pgi</i> . To be combined with P248
P248	TAATAGCGAAGAGGCCCGCACGAGCGG ATGTCGAGGAACAG	For assembly of homology arm 2 in pBBR_Cas9_Δ <i>pgi</i> . To be combined with P247
P267	GCGCGACGAGGAATTCGAGGTTTTAGA GCTAGAAATAGCAAGTTAAAATAAGGCTAGTC	gRNA_REV primer for sp3 variant of pBBR_Cas9_Δ <i>pgi</i>
P268	CTGCGAATTCCTCGTCGCGCAACCAGCG ATCCCGTCCG	gRNA_FWD primer for sp3 variant of pBBR_Cas9_Δ <i>pgi</i>
P281	GCGAGAACGTGCTCGTGATC	For checking <i>pgi</i> deletion via colony PCR. To be combined with P284
P282	CATACGGCCTCGCTCTTTCC	For genotyping of <i>pgi</i> deletion. To be combined with P283
P283	GTCACCGCGTTCTCTGATC	For genotyping of <i>pgi</i> deletion. To be combined with P282
P284	CGATATGGCCCGTCTCGTAG	For checking <i>pgi</i> deletion via colony PCR. To be combined with P281

Name	Sequence	Description
P338	CGACGCGATCCGCATCATGGGTTTTAGA GCTAGAAATAGCAAGTTAAAATAAGGCTAGTC	gRNA_REV primer for sp1 variant of pBBR_Cas9_Δeda
P339	CCATGATGCGGATCGCGTCGAACCAGCG ATCCCGTCCG	gRNA_FWD primer for sp1 variant of pBBR_Cas9_Δeda
P340	GTGGGGCAGAAAGTCACCTGGTTTATAGAGC TAGAAATAGCAAGTTAAAATAAGGCTAGTC	gRNA_REV primer for sp2 variant of pBBR_Cas9_Δeda
P341	CAGGTGACTTTCTGCCCCACAACCAGCGAT CCCGTCCG	gRNA_FWD primer for sp2 variant of pBBR_Cas9_Δeda
P342	TCATGGCGGAAGTCGAAGGTGTTTATAGAGC TAGAAATAGCAAGTTAAAATAAGGCTAGTC	gRNA_REV primer for sp3 variant of pBBR_Cas9_Δeda
P369	GTGATGGCTTCCATGTCGG	For Cas9 plasmids sequencing and for confirming Cas9 plasmid loss after confirming genes deletion
P370	GTGTTCTCGACGGGG	For Cas9 plasmids sequencing
P371	GTTAACACCGAGATTACCAAAG	For Cas9 plasmids sequencing
P372	GCCCGTTCTCGAGTTCG	For Cas9 plasmids sequencing
P373	GGAGGATATCCAGAAGGCTC	For Cas9 plasmids sequencing
P374	CGCAGTCGGCCTATTGG	For Cas9 plasmids sequencing
P375	GAATCGATCCTCCCAAGAG	For Cas9 plasmids sequencing
P376	ACCAATAACTGCCTTAAAAAA	For Cas9 plasmids sequencing
P377	CGCCCTATAGTGAGTCG	For Cas9 plasmids sequencing
P378	TTCCTCTTGCGGGTTTTTTTG	For Cas9 plasmids sequencing

Table S4. Amorphadiene mass distribution vector of the Rs265 Δ *pgi* + pBBR-*ads* strain.

1-¹³C					
m/z	A	B	C	Average	st.dev.
M	0.825958	0.823162	0.822308	0.823809	0.001559
M+1	0.157018	0.158787	0.159751	0.158519	0.001132
M+2	0.017024	0.018052	0.017941	0.017672	0.000461
4-¹³C					
m/z	A	B	C	Average	st.dev.
M	0.003223	0.003214	0.0031	0.003179	5.59E-05
M+1	0.012304	0.013161	0.010899	0.012121	0.000932
M+2	0.096101	0.09812	0.094703	0.096308	0.001402
M+3	0.769072	0.768672	0.774825	0.770856	0.002811
M+4	0.108677	0.107354	0.107543	0.107858	0.000584
M+5	0.010623	0.00948	0.00893	0.009678	0.000705

Table S5. Amorphadiene mass distribution vector of Rs265-MVA- Δ *dxr* + pBBR-*ads* strain.

1-¹³C					
m/z	A	B	C	Average	st.dev.
M	0.792912	0.788304	0.779658	0.786958	0.005494
M+1	0.190726	0.188634	0.182555	0.187305	0.003466
M+2	0.016362	0.018059	0.021206	0.018542	0.002007
M+3	0	0.005003	0.016581	0.007195	0.006944
4-¹³C					
m/z	A	B	C	Average	st.dev.
M	0.812493	0.809512	0.817906	0.813303	0.003475
M+1	0.187507	0.190488	0.182094	0.186697	0.003475
M+2	0	0	0	0	0
M+3	0	0	0	0	0
M+4	0	0	0	0	0
M+5	0	0	0	0	0

Table S6. Amorphadiene mass distribution vector of Rs265 + pBBR-*ads* strain.

1-¹³C				
m/z	A	B	Average	st.dev.
M	0.784698	0.793639	0.789168	0.004471
M+1	0.106436	0.190544	0.14849	0.042054
M+2	0	0.015817	0.007909	0.007909
M+3	0.108867	0	0.054433	0.054433
4-¹³C				
m/z	A	B	Average	st.dev.
M	0	0.048492	0.024246	0.024246
M+1	0	0.014266	0.007133	0.007133
M+2	0.072745	0.041353	0.057049	0.015696
M+3	0.694143	0.658865	0.676504	0.017639
M+4	0.201743	0.196628	0.199186	0.002557
M+5	0.03137	0.040396	0.035883	0.004513

Table S7. Amorphadiene mass distribution vector of Rs265 + pBBR-MVA-*ads* strain.

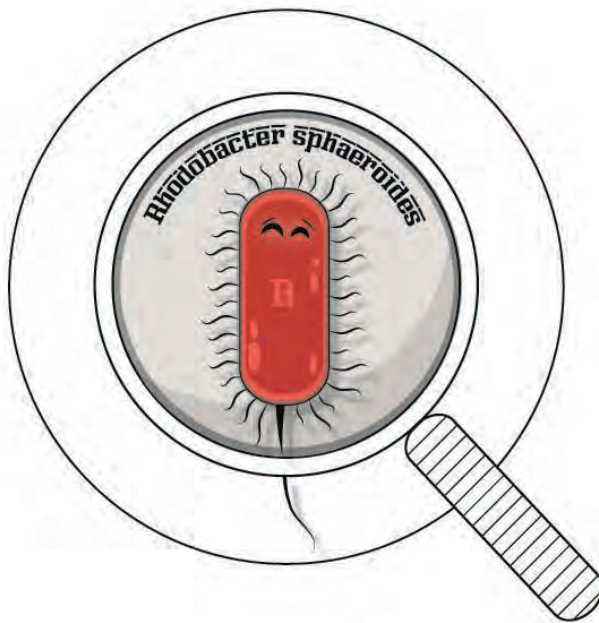
1-¹³C				
m/z	A	B	Average	st.dev.
M	0.7457	0.749209	0.747455	0.001754
M+1	0.218549	0.215237	0.216893	0.001656
M+2	0.033577	0.033473	0.033525	5.22E-05
M+3	0.002173	0.00208	0.002127	4.65E-05
4-¹³C				
m/z	A	B	Average	st.dev.
M	0.36932	0.375452	0.372386	0.003066
M+1	0.375006	0.387394	0.3812	0.006194
M+2	0.187309	0.174417	0.180863	0.006446
M+3	0.060386	0.056323	0.058354	0.002032
M+4	0.00798	0.006414	0.007197	0.000783
M+5	0	0	0	0

Table S8. Amorphadiene mass distribution vector of Rs265-MVA + pBBR-*ads* strain.

1-^{13}C					
m/z	A	B	C	Average	st.dev.
M	0.758999	0.759275	0.754311	0.757528	0.002278
M+1	0.210561	0.206883	0.213292	0.210246	0.002626
M+2	0.027799	0.030115	0.029311	0.029075	0.00096
M+3	0.002641	0.003726	0.003086	0.003151	0.000446
4-^{13}C					
m/z	A	B	C	Average	st.dev.
M	0.428866	0.358571	0.372843	0.38676	0.030338
M+1	0.356874	0.372396	0.379905	0.369725	0.00959
M+2	0.148498	0.162168	0.18127	0.163979	0.01344
M+3	0.065763	0.106865	0.065982	0.079536	0.019324
M+4	0	0	0	0	0
M+5	0	0	0	0	0

Table S9. Amorphadiene mass distribution vector of Rs265 + pBBR-MVA-*ads* strain after fosmidomycin cultivation (in mM).

1-^{13}C			
m/z	0 mM	1 mM	2 mM
M	0.754147	0.780194	0.783031
M+1	0.213423	0.192373	0.18991
M+2	0.027994	0.024953	0.022352
M+3	0.004436	0.00248	0.004706
4-^{13}C			
m/z	0 mM	1 mM	2 mM
M	0.350108	0.442089	0.463502
M+1	0.372592	0.355542	0.374543
M+2	0.195695	0.148085	0.149917
M+3	0.066697	0.042469	0.000882
M+4	0.013581	0.010615	0.009438
M+5	0.001327	0.0012	0.001718



Chapter 6

Growth-uncoupled isoprenoid synthesis in *Rhodobacter sphaeroides*

This chapter has been published as: Orsi, E.*, Mougialos, I.*, Post, W., Beekwilder, J., Dompè, M., Eggink, G., van der Oost, J., Kengen, S. W., & Weusthuis, R. A. (2020). Growth-uncoupled isoprenoid biosynthesis in *Rhodobacter sphaeroides*. *Biotechnology for Biofuels*, 13: 123.

*contributed equally

Abstract

Background: Microbial cell factories are usually engineered and employed for cultivations that combine product synthesis with growth. Such a strategy inevitably invests part of the substrate pool towards the generation of biomass and cellular maintenance. Hence, engineering strains for the formation of a specific product under non-growth conditions would allow to reach higher product yields. In this respect, isoprenoid biosynthesis represents an extensively studied example of growth-coupled synthesis with rather unexplored potential for growth-independent production. *Rhodobacter sphaeroides* is a model bacterium for isoprenoid biosynthesis, either via the native 2-methyl-D-erythritol 4-phosphate (MEP) pathway or the heterologous mevalonate (MVA) pathway, and for poly- β -hydroxybutyrate (PHB) biosynthesis.

Results: This study investigates the use of this bacterium for growth-independent production of isoprenoids, with amorphadiene as reporter molecule. For this purpose, we employed the recently developed Cas9-based genome editing tool for *R. sphaeroides* to rapidly construct single and double deletion mutant strains of the MEP and PHB pathways, and we subsequently transformed the strains with the amorphadiene producing plasmid. Furthermore, we employed ^{13}C -metabolic flux ratio analysis to monitor the changes in the isoprenoid metabolic fluxes under different cultivation conditions. We demonstrated that active flux via both isoprenoid pathways while inactivating PHB synthesis maximizes growth-coupled isoprenoid synthesis. On the other hand, the strain that showed the highest growth-independent isoprenoid yield and productivity, combined the plasmid-based heterologous expression of the orthogonal MVA pathway with the inactivation of the native MEP and PHB production pathways.

Conclusions: Apart from proposing a microbial cell factory for growth-independent isoprenoid synthesis, this work provides novel insights about the interaction of MEP and MVA pathways under different growth-conditions.

Keywords

Rhodobacter sphaeroides, isoprenoid biosynthesis, PHB, MEP, MVA growth-independent production.

Introduction

Isoprenoids (also known as terpenoids) have great industrial value as ingredients of pharmaceuticals, perfumes, food flavourings and most recently biofuels (5, 8, 46, 51, 107, 172). They are formed by the condensation of the five-carbon monomers isopentenyl pyrophosphate (IPP) and its isomer dimethylallyl pyrophosphate (DMAPP). The two naturally existing IPP/DMAPP production pathways in nature are the 2-C-methylerythritol 4-phosphate (MEP) pathway and the mevalonate (MVA) pathway (209). While the former branches in the central metabolism from glyceraldehyde 3-phosphate and pyruvate, the latter uses acetoacetyl-CoA (AA-CoA) as precursor (**Fig. 1**). These two pathways are, with few exceptions, phylogenetically distinct: the MEP pathway is present in prokaryotes, while the MVA pathway is found in archaea and eukaryotes (43). Plants express both metabolic routes, with the MEP pathway compartmentalized in the chloroplasts and the MVA pathway expressed in the cytosol (44). Since the first implementation of a heterologous MVA pathway in *Escherichia coli* (42), the number of studies focusing on the synthesis of isoprenoids via microbial cell factories has increased a lot. Efforts for improving bioproduction have been focusing either on engineering of the endogenous MEP pathway (167, 210, 211), or by co-expressing the heterologous MVA counterpart (42, 212, 213). Moreover, to limit the effect of unfavorable regulatory control of the endogenous pathway, substitution by an orthogonal isoprenoid pathway has been reported (201).

In microorganisms, isoprenoids are often membrane-bound molecules - like carotenoids, ubiquinones, chlorophylls and sterols – which are indispensable for growth (214, 215). Therefore, during a batch cultivation, their volumetric concentration is expected to increase as consequence of microbial growth inside the reactor. Such type of metabolism for isoprenoid biosynthesis is defined as

growth-coupled. For strain improvement purposes, growth-coupled production has been largely employed. In such a scenario, the product of interest becomes a mandatory by-product of growth, and therefore microbial growth becomes the driving force of production (216). This production-growth association has already been exploited for enhancing isoprenoid biosynthesis by laboratory evolution (217).

Nevertheless, growth-coupled production contains an inherent trade-off between substrate use for i) biomass production and maintenance, and ii) product formation (218). Thus, if biomass formation is prevented, in principle more substrate is available for product synthesis.

Microbial metabolism has been engineered to produce non-native isoprenoid molecules as pharmaceuticals, perfumes, food flavourings and biofuels (5, 8, 46, 51, 107, 172). These compounds are not required for growth, and often excreted. Coupling of product formation to microbial growth is therefore not a necessity, and growth-uncoupled production would be an advantageous option.

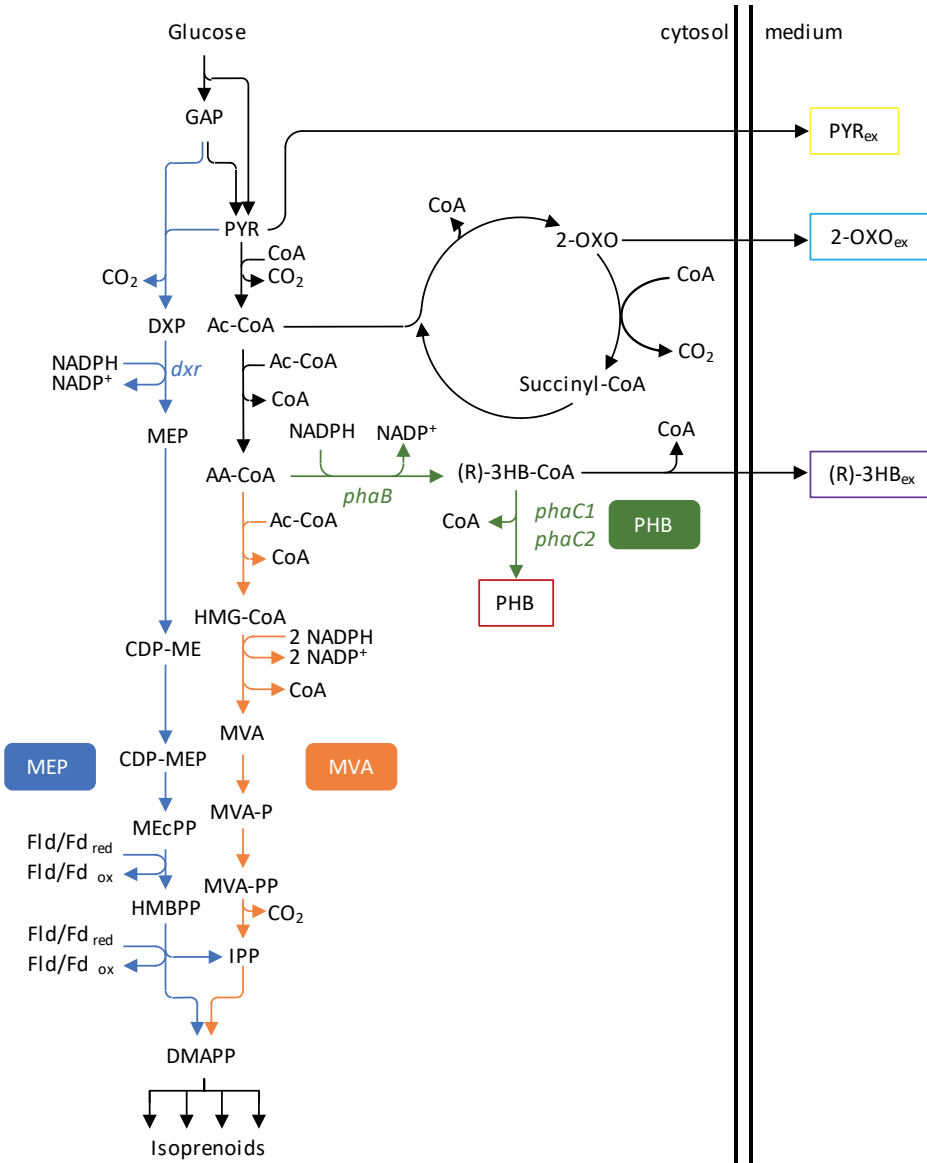


Figure 1. Network investigated in this work. The metabolic map shows the steps involved in the biochemical conversion of glucose to isoprenoids. Isoprenoid biosynthesis can occur via the two orthogonal 2-C-methyl-D-erythritol 4-phosphate (MEP, blue arrows) and mevalonate (MVA, orange arrows) pathways. For the MEP pathway, the 1-deoxy-D-xylulose 5-phosphate reductoisomerase (*dxr*) gene is shown. This gene is targeted for inactivating the endogenous isoprenoid pathway. Both modules branch from the central metabolism and converge to isopentenyl-diphosphate (IPP) and dimethylallyl-

diphosphate (DMAPP), which are the precursors of all isoprenoids. Moreover, the biosynthetic pathway of the storage compound PHB is included (box with red outline). This consists of two enzymatic reactions encoded by the genes *phaB* and *phaC1* and *phaC2* (both in green). The network includes also the schematic representation of the Krebs cycle, which includes conversion of 2-oxoglutarate (2-OXO) to succinyl-CoA. Eventually, accumulation of PYR or 2-OXO can result in their secretion in the medium (boxes with yellow and light-blue outline, respectively). Additionally, conversion of (R)-3hydroxybutyryl-CoA ((R)-3HB-CoA) to (R)-3HB can result in the secretion of the latter compound (box with purple outline). Other abbreviations: reduced flavodoxin (Fld), ferredoxin (Fd) red: reduced, ox: oxidized. GAP (glyceraldehyde-3-phosphate), PYR (pyruvate), CDP-ME (4-(cytidine 5'-diphospho)-2-C-methyl-D-erythritol), CDP-MEP (2-phospho-4-(cytidine 5'-diphospho)-2-C-methyl-D-erythritol), MEcPP (2-C-methyl-D-erythritol 2,4-cyclodiphosphate), Ac-CoA (acetyl-CoA), AA-CoA (acetoacetyl-CoA), HMG-CoA (S)-3-hydroxy-3-methylglutaryl-CoA, MVA-P ((R)-5-phosphomevalonate), MVA-PP ((R)-5-diphosphomevalonate).

Apart from C, H and O, isoprenoids do not contain other biomass-specific elements like P, S or N. Therefore, under P, S or N limited incubation conditions, glucose can in principle be converted into isoprenoid but not into microbial biomass. Improved isoprenoid/biomass ratios have already been obtained by using nutrient-limited culturing conditions (60, 82, 123, 219). Nonetheless, isoprenoid synthesis, as primary metabolite, is often strictly regulated to occur only under growing conditions, and this demotivated further studies on decoupling isoprenoid production from microbial growth as a production strategy.

In a recent study, the concept of redesigning biosynthetic networks based on orthogonality principles was introduced (220). This idea entails that a non-native metabolic route that minimizes the interaction with the endogenous biomass-producing pathways can be exploited for bioproduction. Intrinsic independence exists between the two isoprenoid pathways MEP and MVA. Therefore, regulatory control affecting the MEP pathway should not affect the MVA pathway, and *vice versa*. Moreover, in a recent study, functional replacement of the native MEP with the heterologous MVA pathway was described in the bacterium *Rhodobacter sphaeroides* (201), a microbial platform organism that is

gaining interest for isoprenoid biosynthesis. This organism is able to synthesize intracellular membranes which can accommodate isoprenoids such as carotenoids and bacteriochlorophylls. Moreover, it is also a natural producer of coenzyme Q₁₀. Apart from these native isoprenoid molecules, heterologous production of lycopene (90) and sesquiterpenes (91) has also been reported in this species.

Growth and isoprenoid synthesis in *R. sphaeroides* has been studied using defined medium, where the introduction of the heterologous MVA pathway revealed potential for growth-independent isoprenoid biosynthesis (134). Under these conditions, the storage compound poly- β -hydroxybutyrate (PHB) was also accumulated (134). Additionally, a mutual stimulating effect between the MEP and MVA pathways has been observed (187).

In this study, we investigate the behavior of the two isoprenoid pathways for amorphadiene production in *R. sphaeroides* during different growth modes, as well as their interaction with the pathway for the carbon- and energy reserve material poly- β -hydroxybutyrate, PHB. By means of ¹³C metabolic flux ratio analysis, we assess the effect of genetic modifications (i.e. for elimination of PHB accumulation) and environmental changes (nitrogen limitation) on isoprenoid pathways capacities. Ultimately, we demonstrate that exclusive use of the orthogonal MVA pathway in combination with elimination of PHB synthesis is a promising strategy for attaining growth-independent production of isoprenoids.

Materials and methods

Strains and standard cultivation conditions

The strains and plasmids used in this study are listed in **Table 1** and **Table 2**, respectively. The Rs265_Δ*phaC1*Δ*phaC2* strain was kindly donated by Isobionics BV. Preculturing of *R. sphaeroides* was performed in 250-mL Erlenmeyer flasks

containing 25 mL of modified Sistrom's minimal medium (SMM). As previously described (187), the medium contained glucose (3.0 g/L) as carbon source, and NH_4Cl (1.0 g/L) as nitrogen source. Moreover, the SMM contained (per liter): 3.48 g KH_2PO_4 , 0.5 g/L NH_4Cl , 0.1 g glutamic acid, 0.04 g L-aspartic acid, 0.5 g NaCl, 0.02 g nitrilotriacetic acid, 0.3 g $\text{MgSO}_4 \cdot 7\text{H}_2\text{O}$, 0.0334 g $\text{CaCl}_2 \cdot 2\text{H}_2\text{O}$, 0.002 g $\text{FeSO}_4 \cdot 7\text{H}_2\text{O}$, and 0.0002 g $(\text{NH}_4)_6\text{Mo}_7\text{O}_{24}$. Trace elements were added (0.01% v/v) from a stock solution containing: 17.65 g/L disodium EDTA, 109.5 g/L $\text{ZnSO}_4 \cdot 7\text{H}_2\text{O}$, 50 g/L $\text{FeSO}_4 \cdot 7\text{H}_2\text{O}$, 15.4 g/L $\text{MnSO}_4 \cdot 7\text{H}_2\text{O}$, 3.92 g/L $\text{CuSO}_4 \cdot 5\text{H}_2\text{O}$, 2.48 g/L $\text{Co}(\text{NO}_3)_2 \cdot 6\text{H}_2\text{O}$, and 0.0114 g/L H_3BO_3 . Vitamins were added (0.01% v/v) from a stock containing: 10 g/L nicotinic acid, 5 g/L thiamine HCl, and 0.1 g/L biotin.

Table 1. Strains used in this study.

Strain	Description	Source of reference
<i>E. coli</i>		
S17-1	Host strain for conjugation, <i>thi pro recA hsdR [RP4-2Tc::Mu-Km::Tn7] Tp^r Sm^r</i>	Laboratory stock
<i>R. sphaeroides</i>		
Rs265	wild-type	Derivative of ATCC 35035, Isobionics BV
Rs265_Δ <i>phaC1</i> Δ <i>phaC2</i>	Rs265 with deletion of <i>phaC1</i> and <i>phaC2</i> for PHB biosynthesis	Isobionics BV
Rs265_Δ <i>phaB</i>	Rs265 with deletion of <i>phaB</i> for PHB biosynthesis	(174)
Rs265-MVA_Δ <i>dxr</i>	Rs265 with chromosomally integrated MVA pathway operon and deletion of the endogenous MEP pathway (<i>dxr</i>)	(201)
Rs265-MVA_Δ <i>dxr</i> Δ <i>phaB</i>	Rs265 with chromosomally integrated MVA pathway operon and deletion of the endogenous MEP pathway (<i>dxr</i>) and PHB biosynthetic pathway (<i>phaB</i>)	This study

Table 2. Plasmids used in this study.

Plasmid	Description	Source of reference
pBBR- <i>ads</i>	pBBR1MCS-2 + <i>crtE</i> promoter and <i>ads</i> (amorphaadiene synthase)	(134)
pBBR-MVA- <i>ads</i>	pBBR1MCS-2 + <i>crtE</i> promoter controlling MVA enzymes and <i>ads</i>	(91)
pBBR_Cas9_Δ <i>phaB</i> _HR	pBBR1MCS-2 + codon harmonized cas9 sequence, sgRNA targeting <i>phaB</i> and 1kb homologous-recombination flanks for recombination with <i>phaB</i>	(174)

Generation of double-KO strain via CRISPR-Cas9 counter-selection

Deletion of *phaB* was performed as previously described (174), using the pBBR_Cas9_Δ*phaB*_HR plasmid. Such plasmid was transferred from *E. coli* S17 cells to Rs265-MVA_Δ*dxr* via diparental conjugation, resulting in the double mutant strain Rs265-MVA_Δ*dxr*Δ*phaB*. By employing the pBBR_Cas9_Δ*phaB*_HR plasmid, *phaB* could be removed by homologous-recombination, and Cas9-based counter-selection of cells with intact genomic copies of *phaB*.

Diparental conjugation of *R. sphaeroides*

Diparental conjugation for transferring amorphaadiene producing plasmids was performed as previously described (187) using RÄ medium. Such medium contained, per liter: 3 g malic acid, 0.2 g MgSO₄·7H₂O, 1.2 g (NH₄)₂SO₄, 0.07 g CaCl₂·2H₂O, 1.5 mL of microelements stock solution, 2 mL of vitamin stock solution and 5 mL of phosphate buffer. In case of RÄ agar medium, 15 g/L agar was added. The microelements solution contained: 0.5 g/L Fe(II)-Citrate, 0.02 g/L MnCl₂·4H₂O, 0.005 g/L ZnCl₂, 0.0025 g/L KBr, 0.0025 g/L KI, 0.0023 g/L CuSO₄·5H₂O, 0.041 g/L Na₂MoO₄, 0.005 g/L CoCl₂·6H₂O, 0.0005 g/L SnCl₂·2H₂O, 0.0006 g/L BaCl₂·2H₂O, 0.031 g/L AlCl₃, 0.41 g/L H₃BO₃, 0.02 g/L EDTA. The vitamin

solution contained: 0.2 g/L nicotinic acid, 0.4 g/L thiamine HCl, 0.008 g/L biotin, 0.2 g/L nicotinamide. The phosphate buffer contained 0.6 g/L KH_2PO_4 and 0.9 g/L K_2HPO_4 .

Cultivation in nitrogen excess and nitrogen limited conditions

After overnight preculturing on SMM, *R. sphaeroides* cultures were transferred to fresh SMM with a starting OD_{600} of 0.1, and incubated at 30 °C with 250 rpm. Cultivations were performed for biological triplicates in 250-mL Erlenmeyer flasks, each filled with 45 mL of SMM medium and 5-mL of filter-sterilized dodecane. SMM composition differed between nitrogen excess condition and nitrogen limited conditions only in the initial NH_4Cl concentration: 1.0 g/L and 0.25 g/L, respectively. Initial glucose concentration remained 3.0 g/L in both cases. Amorphadiene titers were measured after glucose depletion. This occurred after 24 h (for nitrogen excess condition) or after 48 h (for nitrogen limited condition). At the same time, the content of the flasks was harvested by centrifugation and further processed for analytical measurements.

^{13}C -metabolic flux ratio analysis of isoprenoid biosynthesis

Isoprenoid flux ratios analyses were performed as previously described (187) in 10-mL Erlenmeyer flasks containing 1.8 mL of labeled SMM medium and 0.2-mL of filter-sterilized dodecane. $[1-^{13}\text{C}]$ - and $[4-^{13}\text{C}]$ -glucose tracers had an initial concentration of 3.0 g/L. For nitrogen excess and limited conditions, the initial NH_4Cl concentration used was the same as for the cultivations in 250-mL flasks: 1.0 and 0.25 g/L, respectively. Samples for GC-MS measurement were taken at glucose depletion. MEP and MVA pathways capacities were obtained by multiplying the flux ratios determined via GC-MS with the amorphadiene titers measured via GC-FID for the 250-mL cultivations.

Cultivation under resting cell conditions

For resting cell cultivations, exponentially growing cells on SMM with nitrogen excess conditions were incubated until mid-exponential phase. Then, cells were pelleted by centrifugation at 4255 g for 10 min at room temperature. Subsequently, pellets were washed twice with sterile physiologic solution (NaCl 9 g/L) and centrifuged at 4255 g for 5 min. Washed pellets were inoculated with a starting OD₆₀₀ of 1.0 on 'nitrogen free SMM' containing 5.0 g/L glucose and 0.0 g/L NH₄Cl. Initial biomass concentration was determined at the moment of the inoculum with a sample of 5-mL for TOC-L analysis. Then, incubation proceeded at 30 °C with 250 rpm. Samples for OD₆₀₀, pH and amorphadiene measurements were taken at a regular interval until the pH dropped below 5.5. Determination of productivity and yields were performed for samples taken within the first 24 h.

Analytics

Cell density was monitored by measuring the optical density at 600nm (OD₆₀₀). Amorphadiene concentration was measured via GC-FID as previously described (134). Glucose, PHB and organic acid concentrations were determined via (U)HPLC as previously described (134). For pyruvate and crotonic acid (resulting from PHB hydrolysis) identification, DAD detector was used, while for glucose, 2-oxoglutarate and 3-hydroxybutyrate determination, the RID detector was used. Determination of biomass concentration via TOC-L was performed by measuring the nitrogen content of the pellet, which was then used to calculate the active biomass concentration using the elemental composition of *R. sphaeroides* of CH_{1.99}O_{0.5}N_{0.19} (134). Identification of unknown compounds in the spent medium was obtained via ¹H-nuclear magnetic resonance spectroscopy (¹H-NMR) measurements performed in D₂O on a Bruker Avance III 400 MHz NMR spectrometer.

Results

Prevention of PHB formation and its effect on amorphadiene biosynthesis

Culturing *R. sphaeroides* under nitrogen-limited conditions could theoretically result in growth-independent isoprenoid synthesis via the native MEP and the heterologous MVA pathways. However, upon consumption of the limited available nitrogen, *R. sphaeroides* stores excess carbon intracellularly as PHB, a nitrogen-free carbon and energy storage compound (134). Aiming to increase isoprenoid production, we reasoned that deletion of one of the PHB synthesis genes would block PHB production under nitrogen-limited conditions and could therefore increase the flux through the MVA pathway. Deletion of the *phaC1* and *phaC2* genes, that code for the PHB polymerase, is the established approach for eliminating PHB biosynthesis in *R. sphaeroides* (126, 137, 138, 221). Nonetheless, this does not prevent activity of the NADPH-dependent acetoacetyl-CoA reductase PhaB, which could result in the undesired accumulation of 3-hydroxybutyryl-CoA or excretion of 3-hydroxybutyrate (**Fig. 1**). In a recent study, we demonstrated that deletion of the *phaB* gene prevents PHB biosynthesis (174). Here, we confirmed that the deletion of either the *phaB* gene (Rs265_Δ*phaB* strain) or the combined deletion of the *phaC1* and *phaC2* genes (Rs265_Δ*phaC1*Δ*phaC2* strain) prevents PHB formation both under nitrogen excess and nitrogen-limited conditions (**Fig. 2a**). As observed before (134), the wild type (Rs265) strain produced substantial amounts of PHB, especially under nitrogen-limiting conditions.

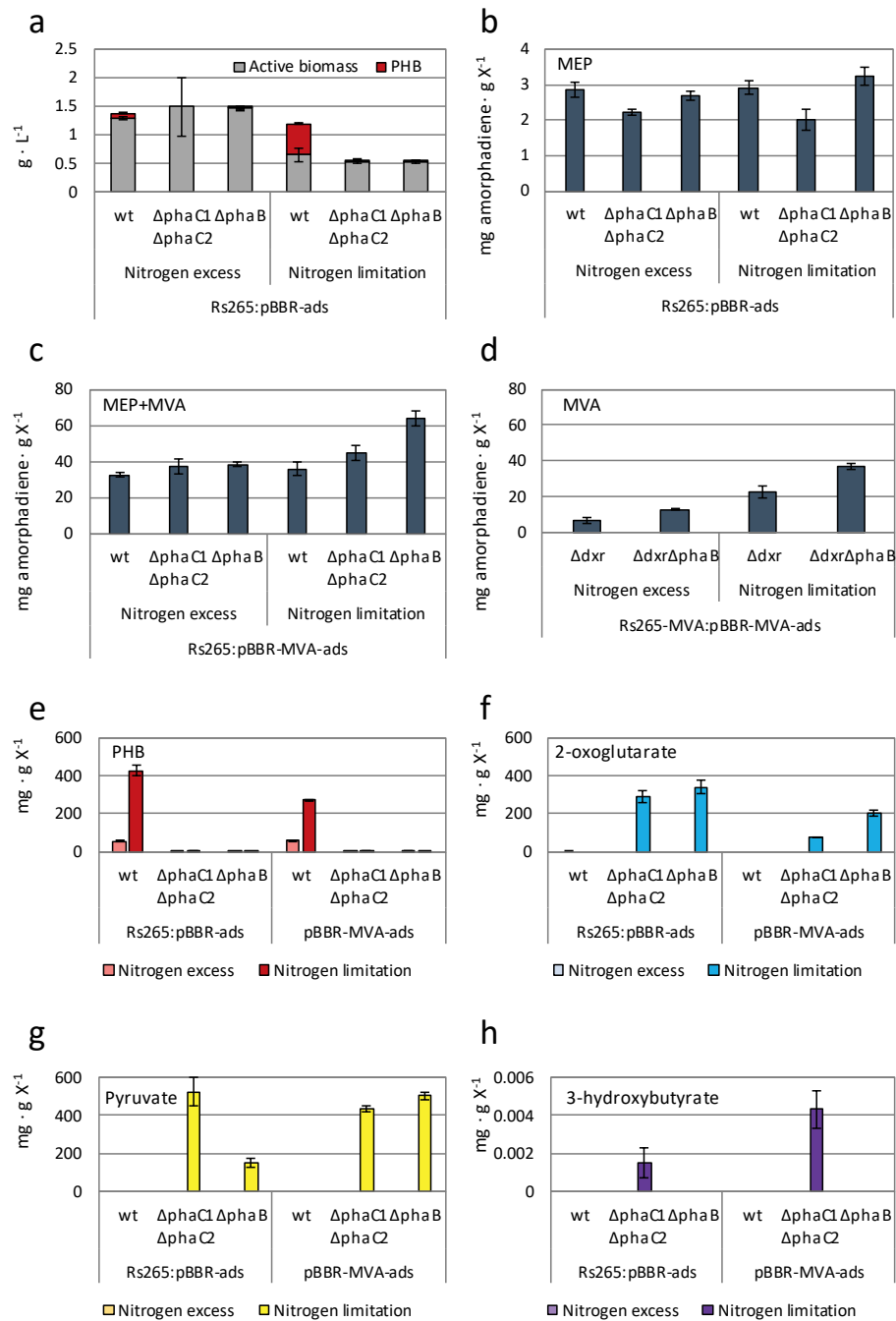


Figure 2. Prevention of PHB pathway and effect on amorphaadiene yield on biomass. a) effect of initial medium C/N ratio on active biomass and PHB concentrations. b-d) mg amorphaadiene · g of biomass⁻¹ for wt, $\Delta phaC1\Delta phaC2$ and $\Delta phaB$ background in strains relying on b) only MEP pathway, c) MEP and MVA pathway, d) only MVA pathway. e-f) mg · g of biomass⁻¹ calculated for e) PHB, f) 2-oxoglutarate, g) pyruvate and h) 3-hydroxybutyrate during nitrogen excess and nitrogen limited conditions.

The pBBR-*ads* plasmid harboring the heterologous amorphaadiene synthase gene was transferred to the various *R. sphaeroides* strains by conjugation. The resulting strains were cultured under both nitrogen excess and nitrogen-limited conditions. At glucose depletion, we determined the amorphaadiene concentration in the spent medium (**Table S1**), the active biomass concentration reached (**Table S2**) and, based on these two measurements, we calculated the amount of amorphaadiene produced per biomass (**Table S3**). We observed that, for the Rs265_Δ*phaB*:pBBR-*ads* and Rs265_Δ*phaC1ΔphaC2*:pBBR-*ads* strains that use only the endogenous MEP pathway (MEP-only strains), elimination of PHB synthesis does not result in higher amorphaadiene/biomass ratios compared to the Rs265 wt strain (**Fig. 2b**, **Table S3**). In fact, these ratios remained unaffected when moving from nitrogen excess to nitrogen-limited conditions (**Table S3**) with a value of 2.9 ± 0.2 mg · g of biomass⁻¹. Interestingly, the Rs265_Δ*phaC1ΔphaC2*:pBBR-*ads* strain showed an even lower amorphaadiene/biomass ratio compared to the Rs265:pBBR-*ads* and the Rs265_Δ*phaB*:pBBR-*ads* strains (**Table S3**). In summary, when only the endogenous MEP pathway was active, isoprenoid biosynthesis appeared to be strictly growth-coupled. Moreover, the MEP flux was insensitive or negatively affected by the impaired PHB synthesis.

We subsequently transformed the available Rs265, Rs265_Δ*phaC1ΔphaC2* and Rs265_Δ*phaB* strains with the orthogonal MVA pathway, cloned on the pBBR-MVA-*ads* plasmid. The amorphaadiene/biomass ratio increased 10- to 20-fold for

all the strains tested (**Fig. 2c, Table S3**). The highest increase was observed for the $\Delta phaB$ strain (Rs265_ $\Delta phaB$:pBBR-MVA-*ads*), reaching a ratio of 63.7 ± 4.0 mg · g of biomass⁻¹ (**Fig. 2b, Table S3**). This value was significantly higher than the ratio reached by the strain with a functional PHB synthesis (Rs265:pBBR-MVA-*ads*), which was 35.9 ± 3.6 mg · g of biomass⁻¹ (**Fig. 2b, Table S3**).

Increase of the MVA pathway flux, as consequence of the *phaB* deletion, was also confirmed for the Rs265-MVA_ Δdxr strain, for which the MEP pathway is inactivated via the deletion of the 1-deoxy-D-xylulose 5-phosphate reductoisomerase gene(*dxr*), after genomic integration of the MVA pathway (**Fig. 1**). This strain relies exclusively on the non-native isoprenoid route (MVA-only) (201). Also here, a substantial increase in the amorphadiene/biomass ratio was observed during both nitrogen excess and nitrogen-limited conditions (**Fig. 2d, Table S3**). The highest value observed was for the Rs265-MVA_ $\Delta dxr\Delta phaB$:pBBR-MVA-*ads* strain, with 36.9 ± 1.6 mg · g of biomass⁻¹ during nitrogen limitation.

In summary, although both the $\Delta phaC1\Delta phaC2$ and $\Delta phaB$ knockouts were equally effective in reducing PHB synthesis, the $\Delta phaB$ knock-out strain produced more amorphadiene, both volumetrically and per biomass unit (**Tables S1, S3**).

Organic acids secretion as consequence of PHB deletion

We reasoned that comparing the secretion profiles between $\Delta phaB$ and $\Delta phaC1\Delta phaC2$ could provide additional insights on the beneficial effect of $\Delta phaB$ on isoprenoid synthesis. Therefore, we quantified by HPLC analysis the organic acids in the spent medium of Rs265, Rs265_ $\Delta phaC1\Delta phaC2$ and Rs265_ $\Delta phaB$ harboring either pBBR-*ads* or pBBR-MVA-*ads* plasmids (**Fig. 2e-h**).

For both $\Delta phaB$ and $\Delta phaC1\Delta phaC2$ strains, 2-oxoglutarate (80 to 340 mg · g of biomass⁻¹, **Fig. 2f**) and pyruvate (150 to 500 mg · g of biomass⁻¹, **Fig. 2g**) were the main by-products. Both compounds require coenzyme A (CoA) for proceeding further in the metabolism via oxidative decarboxylation (**Fig. 1**). Excretion of these compounds suggests that free CoA is limiting when PHB biosynthesis is prevented.

The $\Delta phaC1\Delta phaC2$ strains secreted an additional unknown compound, which was identified as 3-hydroxybutyrate (3HB) by NMR (**Fig. S2**). The spent medium for the Rs265_ $\Delta phaC1\Delta phaC2$:pBBR-*ads* strain showed a value of 0.002 ± 0.001 mg 3HB · g of biomass⁻¹ (**Fig. 2h**). In contrast, a value of 0.004 ± 0.001 mg 3HB · g of biomass⁻¹ was observed for the Rs265_ $\Delta phaC1\Delta phaC2$:pBBR-MVA-*ads* strain, which expressed the heterologous MVA pathway (**Fig. 2h**). Therefore, under nitrogen limitation and upon expression of the MVA pathway, the amount of 3HB secreted increased significantly compared to when only the MEP pathway was active.

¹³C metabolic flux ratio analysis of isoprenoid biosynthesis under different growth conditions

The Rs265_ $\Delta phaB$:pBBR-MVA-*ads* strain, that overexpresses the MVA pathway and still has an active MEP pathway, showed the highest amorphadiene/biomass ratio under nitrogen-limited conditions (**Fig. 2c**). Additionally, we observed that, independent from the cultivation conditions and the presence of an active PHB synthesis pathway, the dual-pathway (co-expressing MEP and MVA pathways) strains largely outperformed the single-pathway strains (**Fig. 2b-d, Table S3**). We therefore decided to further investigate the separate and combined contribution of the isoprenoid pathways to the amorphadiene production by ¹³C flux ratio analysis.

MEP and MVA pathways are known to exert a reciprocal stimulation (187, 205). To better understand their mode of interaction under the conditions tested, we determined their contribution via ^{13}C metabolic flux ratio analysis of the Rs265:pBBR-MVA-*ads* and Rs265_ Δ *phaB*:pBBR-MVA-*ads* strains. We therefore compared the resulting amorphaadiene/biomass ratios for each pathway with the ones determined for i) the Rs265:pBBR-*ads* and Rs265_ Δ *phaB*:pBBR-*ads* (MEP-only) strains, and ii) the Rs265-MVA_ Δ *dxr*:pBBR-MVA-*ads* and Rs265-MVA_ Δ *dxrphaB*:pBBR-MVA-*ads* (MVA-only) strains. Previously, this ^{13}C -method provided important insights on the flux ratios upon co-expression of the MEP and MVA pathways (187). Under nitrogen excess condition, we observed that the dual-pathway strains with active MEP and MVA pathways showed a higher amorphaadiene/biomass ratio for each isoprenoid route compared to when these were active individually (**Fig. 3a**). We therefore confirmed that, during nitrogen excess conditions, co-expression of the two isoprenoid pathways resulted in enhancement of their capacities in the Rs265 and Rs265_ Δ *phaB* strains harboring the pBBR-MVA-*ads* plasmid (**Fig. 3a**). Moreover, the capacity of the MVA pathway in the Rs265_ Δ *phaB* and Rs265-MVA_ Δ *dxrphaB* strains was even further enhanced by the *phaB* deletion, as made obvious by comparison to strains that still contain the *phaB* gene (**Fig. 3a**). In contrast, the flux through the native MEP pathway remained unaffected by the *phaB* deletion. Thus, under nitrogen excess conditions, deletion of the *phaB* gene results in an increase of the isoprenoid flux exclusively via the MVA pathway (**Table 3**).

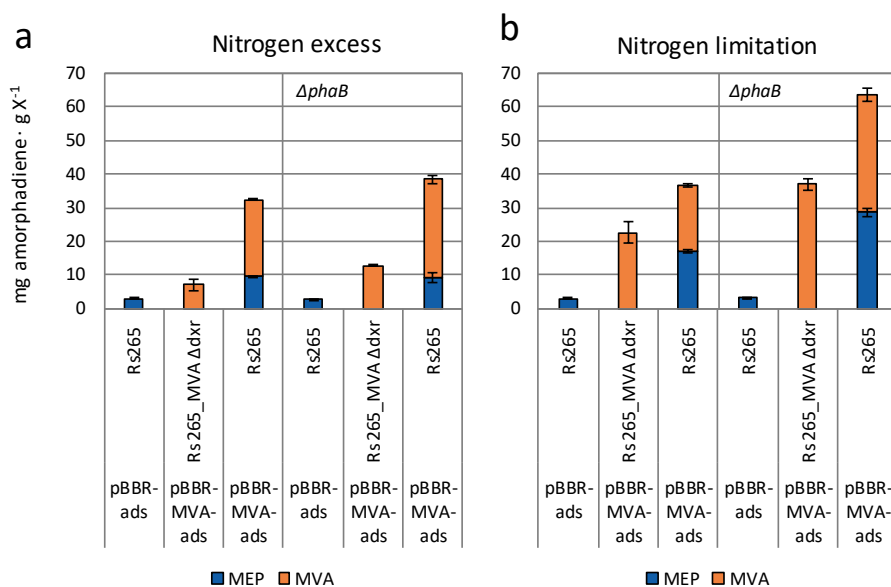


Figure 3. ¹³C metabolic flux ratio analysis of *R. sphaeroides* with different initial C/N ratios in the medium. The values are obtained from parallel labeling cultivation experiment. The isoprenoid flux ratios obtained were multiplied for the yield on biomass obtained for some of the strains of Figure 2. a) Nitrogen excess condition: enough nitrogen is provided to support cell division until depletion of glucose. b) Nitrogen limited condition: nitrogen will be depleted from the medium before glucose, and cell division is expected to stop and allow PHB accumulation.

Table 3. Isoprenoid flux ratio calculated for the Rs265 and Rs265_ΔphaB strains harboring the pBBR-MVA-ads plasmid after growth on different initial nitrogen concentrations.

Genomic background	Isoprenoid flux ratios				Pathway capacities (mg amorphaadiene · g biomass ⁻¹)			
	Nitrogen excess		Nitrogen limitation		Nitrogen excess		Nitrogen limitation	
	MEP	MVA	MEP	MVA	MEP	MVA	MEP	MVA
Rs265	0.29 ± 0.01	0.71 ± 0.01	0.46 ± 0.01	0.54 ± 0.1	9.4 ± 0.3	23.0 ± 0.3	16.9 ± 0.4	19.9 ± 0.5
Rs265_ΔphaB	0.24 ± 0.03	0.76 ± 0.03	0.45 ± 0.02	0.55 ± 0.03	9.2 ± 1.3	29.3 ± 1.3	28.7 ± 1.3	35.0 ± 1.9

We further studied the isoprenoid flux ratio under nitrogen-limited conditions (**Fig. 3b**, **Table 3**). The Rs265:pBBR-*ads* and Rs265_Δ*phaB*:pBBR-*ads* strains, which rely exclusively on the MEP pathway for isoprenoid production did not show any increase in the amorphaadiene/biomass ratio when compared to nitrogen excess conditions (**Fig. 3b**). In contrast, the amorphaadiene/biomass ratio for the strains that express only the MVA pathway was increased 3-fold when compared to this value obtained under nitrogen excess conditions (Rs265-MVA_Δ*dxr* and Rs265-MVA_Δ*dxr*Δ*phaB* strains harboring pBBR-MVA-*ads* plasmid, **Fig. 3**). Interestingly, for the strains that express both pathways (Rs265:pBBR-MVA-*ads* and Rs265_Δ*phaB*:pBBR-MVA-*ads* strains, **Fig. 3b**), there was only a minor increase of the MVA pathway capacity in the Rs265_Δ*phaB* strain when compared to nitrogen excess conditions (**Table 3**). On the other hand, the MEP pathway capacity increased by 80% for the Rs265 strain (from 9.4 ± 0.3 to 16.9 ± 0.4 mg amorphaadiene · g of biomass⁻¹) and by 300% for the Rs265_Δ*phaB* strain (from 9.2 ± 1.3 to 28.7 ± 1.3 mg amorphaadiene · g of biomass⁻¹). Thus, for the dual-pathway strain, the increase of the amorphaadiene/biomass ratio under nitrogen-limited conditions is attributed to the endogenous MEP pathway (**Table 3**).

Amorphaadiene biosynthesis during resting cells conditions

Under nitrogen-limited conditions a short exponential growth phase occurred, and therefore a short growth-associated amorphaadiene production phase could not be avoided. This resulted in non-linear growth and production kinetics, making it difficult to assess yields (mg amorphaadiene · glucose⁻¹) and productivities (mg amorphaadiene · L⁻¹ · h⁻¹). In order to focus exclusively on growth-uncoupled production, and to obtain linear kinetics, we decided to assess amorphaadiene production during resting cell conditions in nitrogen-free

medium. This cultivation setup simulates the production phase of a two-stage fermentation setup where growth and production are separated.

Since deletion of *phaB* and expression of the MVA pathway increased production during nitrogen limitation, we reasoned to assess the amorphaadiene production levels in the presence of also an active MEP pathway. Therefore, we further cultivated the strains Rs265, Rs265_ Δ *phaB*, Rs265-MVA_ Δ *dxr* and Rs265-MVA_ Δ *dxr* Δ *phaB* under resting cells condition. All these strains contained the pBBR-MVA-*ads* plasmid (**Fig. 4a**).

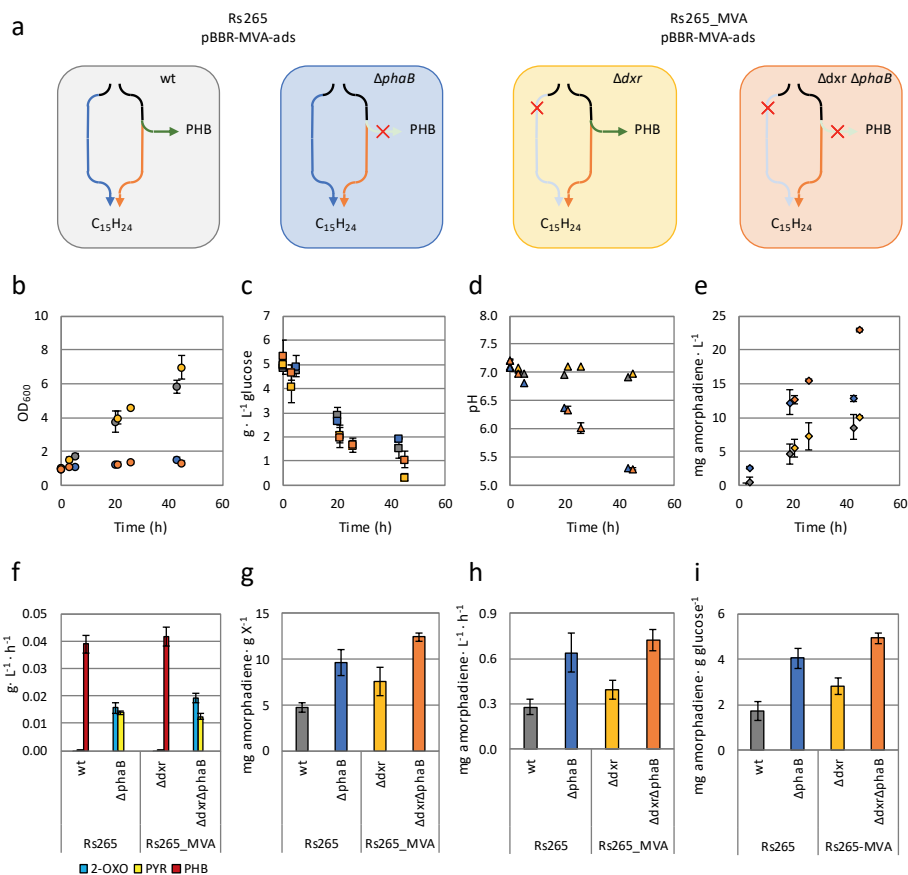


Figure 4. Growth-independent amorphadiene production. a) schematic overview of the strain tested. In blue is shown the endogenous MEP pathway, while in orange the orthogonal MVA pathway. In green the PHB biosynthetic pathway is depicted. Red cross represent genes deletion in either *dxr* (MEP pathway) or in *phaB* (PHB pathway). $C_{15}H_{24}$ is the brute formula of the reporter molecule amorphadiene. Monitoring of b) OD_{600} , c) glucose concentration, d) pH, e) amorphadiene concentration. f) volumetric productivities of PHB and organic acids (Pyr: pyruvate; 2-Oxo: 2-oxoglutarate). Determination of g) amorphadiene/biomass ratios, h) amorphadiene volumetric productivity and i) amorphadiene yield on glucose.

A linear increase in OD_{600} was observed for the strains with a functional PHB biosynthetic pathway (Rs265 and Rs265-MVA_Δ*dxr*, **Fig. 4b**). This trend is known to be associated with the accumulation of this storage compound (134), and it is associated with cell expansion rather than cell division. Accordingly, the

corresponding $\Delta phaB$ strains (Rs265_ $\Delta phaB$ and Rs265-MVA_ $\Delta dxr\Delta phaB$) did not show any increase in OD₆₀₀. Glucose consumption (**Fig. 4c**, **Fig. S1**), pH and amorphadiene concentrations (**Fig. 4d, e**) were followed over time. A decrease in the pH of the Rs265_ $\Delta phaB$ and Rs265-MVA_ $\Delta dxr\Delta phaB$ strains was observed (**Fig. 4d**), which can be explained by the secretion of organic acids upon prevention of PHB accumulation, mainly of pyruvate and 2-oxoglutarate (**Fig. 4f**).

Amorphadiene samples were collected over time from all the cultures (**Fig. 4e**), and yields and productivities were calculated for the first 24 h (**Fig. 4g-i**). The corresponding values for the Rs265 strain were the lowest among the tested strains. Deletion of *phaB* (Rs265_ $\Delta phaB$) resulted in a 2-fold increase of the amorphadiene/biomass ratio (**Fig. 4g**), the volumetric productivity (**Fig. 4h**) and the yield on glucose (**Fig. 4i**) compared to the Rs265 strain. Also, inactivation of the endogenous MEP pathway in the Rs265-MVA_ Δdxr strain resulted in an increase of those values compared to Rs265 strain (**Fig. 4h, i**). Hence, inactivation of either the PHB production pathway or the endogenous MEP pathway stimulates growth-independent production. Combined inactivation of the MEP and PHB production pathways (Rs265-MVA_ $\Delta dxr\Delta phaB$ strain) allowed to reach the highest amorphadiene/biomass ratio, volumetric amorphadiene productivity (**Fig. 4h**) and yield on glucose (**Fig. 4i**). All these values were 2.5-fold higher in the Rs265-MVA_ $\Delta dxr\Delta phaB$ strain, compared to the Rs265 control strain. Hence, deletion of the endogenous MEP and PHB biosynthetic pathways resulted in the best metabolic setup for exploiting non-growing conditions for amorphadiene production.

Discussion

Strain optimization for improved bioproduction often relies on strategies that couple production to microbial growth (216, 222). Nevertheless, an emerging

approach for metabolic engineering strategies is the one of dissociating production and growth (220). Following this view, in this work we engineered the isoprenoid and the PHB biosynthetic pathways in *R. sphaeroides*. Therefore, we could demonstrate that isoprenoid biosynthesis, a typically growth-coupled type of metabolism in microorganisms, can be uncoupled from biomass production by means of rational metabolic engineering.

A previous work indicated that isoprenoid synthesis is strictly growth-coupled via the endogenous MEP pathway (134). We applied nitrogen-limited conditions to a strain relying only on this isoprenoid pathway, but this did not result in increased amorphaadiene/biomass ratio (**Fig. 2b**). We reasoned that targeting the storage compound (PHB) synthesis could increase the flux via the MEP pathway during this condition. Nevertheless, inactivation of the PHB synthetic pathway did not result in any improvement (**Fig. 2b**), thereby indicating that the endogenous MEP pathway is inhibited during non-growing conditions.

Introduction of a heterologous MVA pathway was described to allow isoprenoid synthesis also during non-growing conditions (134). Here, we confirmed that nitrogen limited conditions increased the amorphaadiene/biomass ratio in a strain relying exclusively on the MVA pathway (**Fig. 2d**). Moreover, inactivation of PHB synthesis by targeting *phaB* increased amorphaadiene production when the MVA pathway was present (**Fig. 2c, d**). In order to calculate titers, rates and yields (TRY) of growth-independent amorphaadiene synthesis, we performed cultivation under resting cells condition (**Fig. 4**). The experimental data confirmed that exclusive isoprenoid flux via the MVA pathway combined with inactivation of PHB synthesis result in maximal TRY values (**Fig. 4e, g-i**).

^{13}C metabolic flux ratio analysis was performed to understand the interaction between the two isoprenoid pathways during nitrogen limitation. The analysis indicated that in the dual-pathway strain the endogenous MEP pathway capacity is substantially enhanced during nitrogen limitation (**Fig. 3b**). Therefore, presence of the MVA pathway helps in deregulating the endogenous MEP pathway during nitrogen limitation.

Despite the increase in flux, only a small part of the carbon that originally went to PHB production could be redirected to amorphaadiene. Organic acids – especially pyruvate and 2-oxoglutarate – were excreted instead. The accumulation of these two organic acids indicates that their downstream reactions, catalysed by the pyruvate dehydrogenase and 2-oxoglutarate dehydrogenase complexes respectively, were inhibited by the inability to produce PHB. These reactions require input of free CoA (**Fig. 1**), the co-enzyme released by the conversion of AA-CoA into PHB. We therefore speculate that knocking out either *phaB* or *phaC1* and *phaC2* decreased the availability of free CoA, that the capacity of the mevalonate pathway was insufficient to remedy this, and that this low CoA availability resulted in the accumulation of both pyruvate and 2-oxoglutarate. Possibly, secretion of 3HB after deletion of *phaC1* and *phaC2* allowed to release free CoA from the intermediate 3HB-CoA.

PHB synthesis results in (223): i) carbon storage, ii) regeneration of NADP^+ and iii) regeneration of free CoA for cellular homeostasis. Knocking out the ability to produce PHB should therefore increase the availability of precursors (AA-CoA) and NADPH for the MVA pathway. The relatively small increase in flux through the MVA pathway indicated that this pathway benefited from the increased amounts of AA-CoA and NADPH, but its capacity is limiting isoprenoid production. One of the rate-determining enzymes of the heterologous pathway

is HMG-CoA reductase, already described as crucial enzyme for enhancing isoprenoid flux (213, 224). We hypothesize that improving the catalytic efficiency of this enzyme might allow the MVA pathway to benefit from the higher availability of NADPH and AA-CoA. Such an improvement could allow to increase carbon flux towards isoprenoids, while reducing by-products secretion. Therefore, rational engineering strategies can build upon the findings of this work for further improving growth-independent isoprenoid biosynthesis in *R. sphaeroides*.

Conclusions

In this work, we assessed the contribution of the MEP and MVA pathway to amorphaadiene biosynthesis under different cultivation conditions. We confirmed that application of the heterologous MVA pathway holds potential for growth-independent production. In a dual-pathway strain, enhancement of the endogenous MEP pathway capacity was confirmed during nitrogen-limited conditions via ^{13}C metabolic flux ratio analysis.

Nevertheless, isoprenoid synthesis during resting cells condition was limited by the presence of an active endogenous MEP pathway. On the other hand, exclusive isoprenoid flux via the MVA pathway increased amorphaadiene synthesis under this condition. Additionally, prevention of PHB synthesis via *phaB* resulted in the highest TRY values for growth-independent amorphaadiene production.

Ultimately, this work proposed a metabolic engineering design for increasing growth-independent isoprenoid biosynthesis in *R. sphaeroides*, while providing novel insights about the interaction occurring between the two isoprenoid pathways.

Acknowledgements

The authors thank Isobionics BV for providing the *Rhodobacter sphaeroides* Rs265 strain used in this study. Any request for the strain and its derivatives should be directed to Isobionics BV. Moreover, we thank Rosyida Arifah for technical assistance in generating the Rs265-MVA_Δ*dxr*Δ*phaB* strain, and Frank E. Fluitman for providing the Rs265_Δ*phaC1*Δ*phaC2* strain.

Authors' contributions

EO, IM, SWMK, GE, JvO and RAW designed the work. IM, EO, WP JB and MD conducted, analyzed, and interpreted the experiments. EO and IM drafted and wrote the manuscript. All authors read and approved the final manuscript.

Funding

This project was financially supported by The Netherlands Ministry of Economic Affairs, via a public–private NWO-Green Foundation for sustainable production and supply chains in agriculture and horticulture (870.15.130,2015/05279/ALW). This project has received funding from the European Research Council (ERC) under the European Union's Horizon 2020 research and innovation programme, grant agreement No. 834279.

Supplementary information

Table S1. End-point amorphadiene titers determined in shake flasks experiments.

Plasmid	Cultivation condition	Genomic background	Amorphadiene (mg/L)	Standard deviation (mg/L)
pBBR- <i>ads</i>	Nitrogen excess	<i>wt</i>	4.4	0.3
		$\Delta phaC1 \Delta phaC2$	3.3	0.1
		$\Delta phaB$	4.7	0.2
	Nitrogen limited	<i>wt</i>	2.4	0.2
		$\Delta phaC1 \Delta phaC2$	1.4	0.2
		$\Delta phaB$	2.2	0.2
pBBR-MVA- <i>ads</i>	Nitrogen excess	<i>wt</i>	41.8	1.8
		$\Delta phaC1 \Delta phaC2$	39.3	4.4
		$\Delta phaB$	56.4	2.1
	Nitrogen limited	<i>wt</i>	23.6	2.3
		$\Delta phaC1 \Delta phaC2$	24.1	2.1
		$\Delta phaB$	34.4	2.2
pBBR-MVA- <i>ads</i>	Nitrogen excess	Δdxr	15.6	3.9
		$\Delta dxr \Delta phaB$	28.0	1.0
	Nitrogen limited	Δdxr	13.5	1.9
		$\Delta dxr \Delta phaB$	19.5	0.8

Table S2. End-point biomass concentrations determined in shake flasks experiments.

Plasmid	Cultivation condition	Genomic background	Biomass (g/L)	Standard deviation (g/L)
pBBR- <i>ads</i>	Nitrogen excess	<i>wt</i>	1.533	0.062
		$\Delta phaC1$	1.491	0.000
		$\Delta phaC2$	1.724	0.110
		$\Delta phaB$	0.805	0.122
	Nitrogen limited	<i>wt</i>	0.693	0.034
		$\Delta phaC1$	0.693	0.112
		$\Delta phaC2$	1.289	0.019
		$\Delta phaB$	1.060	0.856
	Nitrogen excess	<i>wt</i>	1.466	0.036
		$\Delta phaB$	0.656	0.115
pBBR-MVA- <i>ads</i>	Nitrogen limited	$\Delta phaC1$	0.539	0.260
		$\Delta phaC2$	0.539	0.022
		$\Delta phaB$	2.229	0.144
		Δdxr	2.187	0.080
	Nitrogen excess	$\Delta dxr\Delta phaB$	0.597	0.142
		<i>wt</i>	0.528	0.161
		Δdxr		
		$\Delta dxr\Delta phaB$		

Table S3. End-point yield of amorphadiene on biomass calculated for shake flasks experiments.

Plasmid	Cultivation condition	Genomic background	Amorphadiene on biomass (mg/g)	Standard deviation (mg/g)
pBBR- <i>ads</i>	Nitrogen excess	<i>wt</i>	2.9	0.2
		$\Delta phaC1$	2.2	0.1
		$\Delta phaC2$	2.7	0.1
	Nitrogen limited	<i>wt</i>	2.9	0.2
		$\Delta phaC1$	2.0	0.3
		$\Delta phaC2$	3.2	0.2
pBBR-MVA- <i>ads</i>	Nitrogen excess	<i>wt</i>	32.4	1.4
		$\Delta phaC1$	37.1	4.2
		$\Delta phaC2$	38.5	1.5
	Nitrogen limited	<i>wt</i>	35.9	3.6
		$\Delta phaC1$	44.8	3.9
		$\Delta phaC2$	63.7	4.0
pBBR-MVA- <i>ads</i>	Nitrogen excess	Δdxr	7.0	1.7
		$\Delta dxr\Delta phaB$	12.8	0.5
	Nitrogen limited	Δdxr	22.6	3.1
		$\Delta dxr\Delta phaB$	36.9	1.6

Table S4. Yield of amorphadiene on biomass calculated during resting cells condition in nitrogen free medium.

Plasmid	Cultivation condition	Genomic background	Amorphadiene on biomass (mg/g)	Standard deviation (mg/g)
pBBR-MVA- <i>ads</i>	Resting cell	<i>wt</i>	4.7	0.5
		$\Delta phaB$	9.6	1.4
		Δdxr	7.6	1.6
		$\Delta dxr\Delta phaB$	12.4	0.5

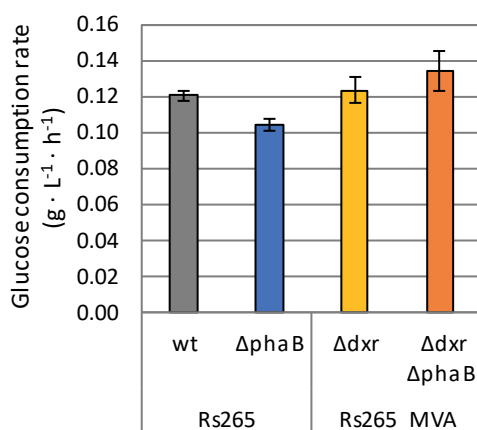


Figure S1. Glucose consumption rates during resting cells conditions. All strains harbored the pBBR-MVA-*ads* plasmid. Colors refer to different strains tested: grey (wild-type), blue ($\Delta phaB$), yellow (Δdxr), red ($\Delta dxr \Delta phaB$).

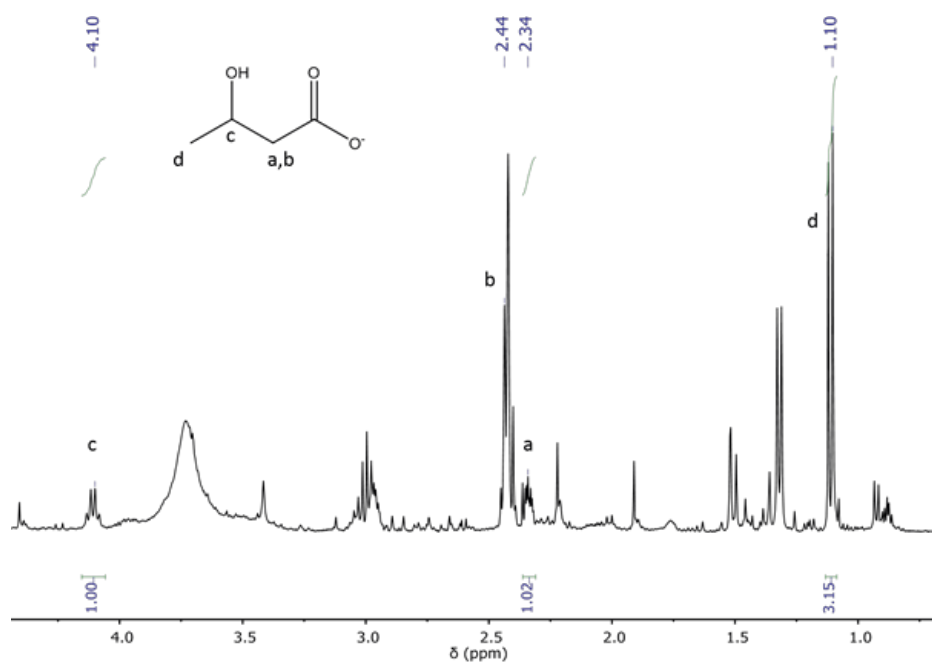


Fig. S2. NMR analysis of the spent medium for 3HB determination. The presence of the two hydrogen a,b close to the carboxylic groups was detected at 2.34 and 2.44 (both multiplets). The hydrogen c close to the hydroxyl group has been identified at 4.10

(multiplet). The three hydrogen belonging to the methyl group have been identified at 1.10 (doublet). The ratio among the hydrogen a:c:d is 1:1:3 as expected from the structure of the molecule. The hydrogen b at 2.44 is overlapping with the signal from other groups so it cannot be used for quantification. The results are in line with literature data.

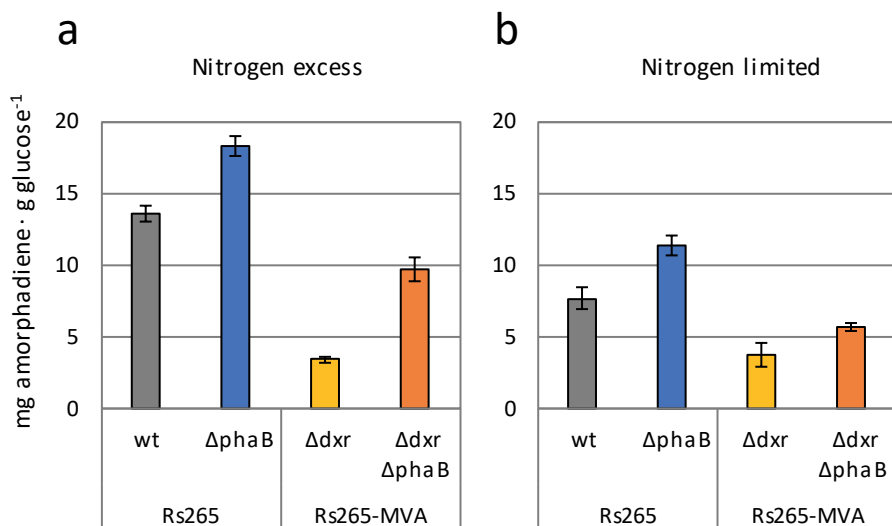
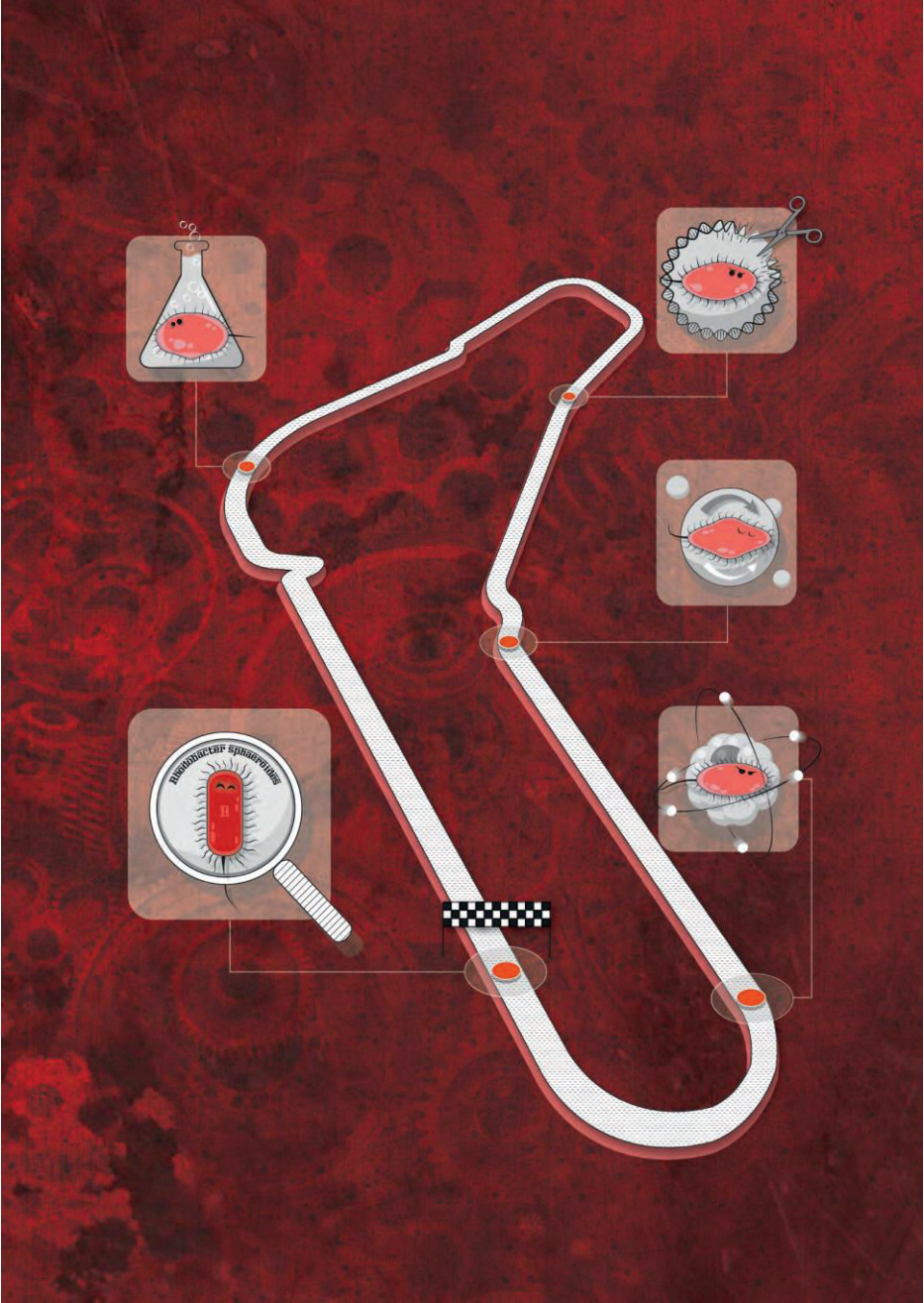


Figure S3. Amorphadiene yields on glucose calculated for shake flasks cultivation conditions under a) nitrogen excess and b) nitrogen limitation.



Chapter 7

General discussion

This chapter has been adapted from the submitted manuscript: Orsi, E., Beekwilder, J., Eggink, G., Kengen, S. W. & Weusthuis, R. A. (2020). The transition of *Rhodobacter sphaeroides* into a microbial cell factory.

Consolidation of *Rhodobacter sphaeroides* as microbial cell factory for isoprenoid biosynthesis

From its foundation, the field of metabolic engineering (22) has self-disciplined itself for structuring the approach used for strain optimization (33). As explained in **chapter 1**, this is currently based on the paradigm of ‘Design-Build-Test-Learn’ (DBTL) cycles. This model consists of iterative sequential phases which concur to the final aim of improving a microbial cell factory (**Fig. 1**). Such a pipeline involves four interdependent modules, starting with a ‘design’ phase for rationally planning the modifications to implement. Then, a ‘build’ phase follows where the outputs from the ‘design’ phase are translated into modification of the DNA of the organism of interest. Subsequently, in the ‘test’ phase the modifications carried out in the ‘build’ phase are assessed in terms of cellular physiology and metabolism using integrative approaches. Finally, in the ‘learning’ phase the information collected is thoroughly analysed and used as input for decision making for the ‘design’ phase of a novel cycle (28). Altogether, the outcome of the DBTL workflow should be a strain with an improved titer, rate and yield (TRY) for the product of interest (28). Additionally, an ideal microbial cell factory supports a streamlined flux towards universal precursors for the synthesis of a wide range of products (58, 59).

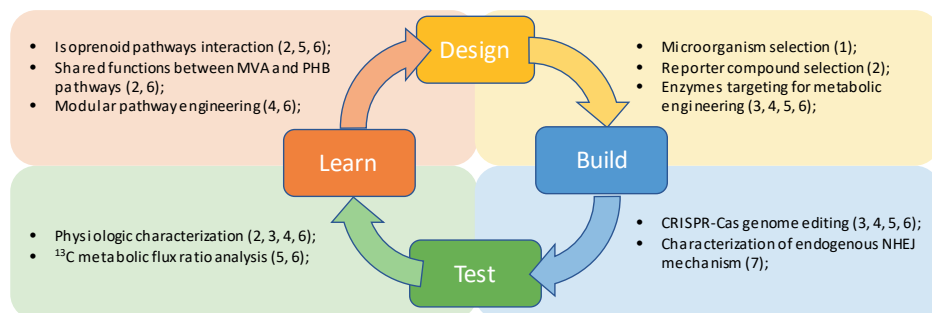


Figure 1. Schematic overview of the Design-Build-Test-Learn (DBTL) cycle developed in this thesis. The four iterative stages of the DBTL cycle are indicated by their capital letters and the associated colored rectangles. Each one contains a set of approaches or technologies employed for the accomplishment of the respective phase. The number between brackets refers to the chapter where each approach/technology was developed.

In this thesis, DBTL cycles were performed, resulting in improved *Rhodobacter sphaeroides* performances for isoprenoid biosynthesis. All these achievements were instructive for corroborating such bacterium as cell factory for isoprenoid production. Moreover, and scientifically more intriguing, the knowledge generated via this pipeline allowed to better understand the mechanisms of isoprenoid synthesis, while improving the tools for engineering and studying this bacterium.

We decided to follow the structure of the aforementioned DBTL cycle for discussing the improvements attained in this thesis (**Fig. 1**). For each phase, the corresponding findings or improvements are reasoned. Finally, developing from the insights discussed, future directions are suggested for further investigation.

Design

This phase has the purpose of predicting and identifying the targets for manipulation and analysis. Several design objectives were identified, and strategies were proposed in the various chapters of this thesis.

Choice of the microbial platform and the reporter isoprenoid molecule

The first design step consisted in the choice of the candidate platform organism. As explained in **chapter 1**, *R. sphaeroides* presented important innate traits associated with isoprenoid metabolism. These were the native synthesis of commercially relevant isoprenoid molecules like coenzyme Q₁₀ and carotenoids. Another important feature was its morphologic adaptation during the synthesis of these compounds, resulting in the formation of intracytoplasmic membranes (ICM) which increased the surface for the aggregation of isoprenoid molecules. Moreover, this species already presented some of the characteristics required by a microbial cell factory (16, 17). In fact, sequenced genomes already existed for this species (225–228), as well as metabolic models (100, 101) and mutant collections (229). Furthermore, a limited toolbox was already available for genome editing (87–89). To the selection of the microorganism, the choice of the reporter compound followed (33). In **chapter 2**, selection of amorphadiene as reporter isoprenoid is described. This sesquiterpene was chosen due to its lower molecular weight and higher volatility compared to endogenous membrane-bound compounds, whose determination and quantification is usually laborious. Following on this reasoning, the amorphadiene synthase gene was cloned in *R. sphaeroides*, and amorphadiene was used as reporter hereafter.

Enzymes targeted for metabolic flux inactivations and redirections

To the choice of the microorganism and reporter molecule, targeting of enzymes for pathway characterizations or flux redirections followed. In **chapter 3**, the genes *phaB* and *phbB* were proposed as targets for the inactivation of poly- β -hydroxybutyrate (PHB) biosynthesis. This allowed to identify some of the genes involved in the synthesis of this storage polymer. In fact, the first step of the metabolic route could putatively use either a NAD- or NADP-dependent *acetoacetyl-CoA reductase* for the conversion of acetoacetyl-CoA (AA-CoA) to

hydroxybutyryl-CoA (3HB-CoA). Hitherto, the only enzyme surely associated with the synthesis of this storage compound was PHB polymerase, encoded by *phaC* (126). However, a recent study described the involvement of eight different genes for PHB synthesis in *R. sphaeroides* (68).

In **chapter 4** the rational design of a *R. sphaeroides* strain exclusively employing the heterologous mevalonate (MVA) pathway was presented. In this strain, the integration of the MVA pathway was followed by the deletion of the gene *dxr* for endogenous MEP pathway inactivation. Therefore, this streamlined flux via the MVA pathway was combined with inactivation of PHB synthesis for maximizing growth-independent isoprenoid synthesis in **chapter 6**.

Other genes were targeted for pathway inactivation for validating the ^{13}C cultivation method described in **chapter 5**. In this case, each endogenous glycolytic pathway in *R. sphaeroides* was targeted by at least one gene. The targets of such investigation were *pgi*, *eda*, *zwf* and *gdh*.

Also, the effect of increasing the copy number of the heterologous MVA pathway enzymes was proposed, and this consisted in design of strains with such increased flux in **chapters 4, 5 and 6**.

Build

Within the 'build' phase, the genome of the *chassis* is edited accordingly to the modifications designed in the former phase. A successful 'build' phase allows to generate mutants rapidly and efficiently. Current DNA delivery system in *R. sphaeroides* relies upon diparental conjugation via an *Escherichia coli* donor. This system is chosen because of its efficiency, which guarantees a high-rate of *R. sphaeroides* colony forming units obtained on the conjugation plate. The vectors that can be transferred to this bacterium are quite limited. These include some

replicative plasmids, like pBBR1MCS2 (88) or pIND4 (86), or non-replicative ones (87). So far, chromosomal modifications in *R. sphaeroides* have been mediated by suicide plasmids, where double-recombination events are obtained via two distinguished selection steps (87). Such an approach was considered slow and inefficient. Hence, we decided to improve the available toolbox for genome editing in *R. sphaeroides* aiming to reduce the selection steps while increasing mutation efficiencies.

Efficient genome editing via Cas9-mediated counterselection

In **chapter 3**, a Cas9-based tool was developed, which resulted in increased efficiency for gene insertions and deletions. As mentioned above, previous genome editing strategies in *R. sphaeroides* were based on the use of two rounds of cross-over events, which can result in frequent wild-type revertants (87). On the other hand, the Cas9-tool developed allowed the double-crossover events to occur within the same selection step, and counter-selection on wild-type revertants was guaranteed by the endonuclease activity of Cas9 (154). It is reasoned that the development of such a highly-efficient tool can accelerate the molecular research within this species, as already demonstrated for other microbial cell factories (36, 37, 230–233). Accordingly, this tool was applied in all the following **chapters 4, 5 and 6** for rapidly generating knock-outs. For almost all genes targeted, the mutation rates obtained were high, generally allowing multiple mutant detections by screening up to 20 colonies on the conjugation plates. Conversely, for gene insertions the success rate was sensibly lower, although still at ‘easy-to-screen rates’, with 15% insertions reported in **chapter 3**. A critical aspect was tackled by designing multiple targeting plasmids each containing a different gRNA. Such an approach allowed to prevent spacer-dependent ineffective mutations, which commonly occurs (163). As alternative to the low insertion efficiencies, transposon insertion via Tn5 system was

presented in **chapter 4**, which allowed to introduce DNA templates of 8 kb within the genome of *R. sphaeroides*.

Towards rapid genome editing: characterizing the endogenous non-homologous end joining (NHEJ) repair mechanism

Rapid genome editing can accelerate the development of microbial cell factories. Therefore, such acceleration is desirable for consolidating *R. sphaeroides*' role as platform microorganism. This can be strengthened by further expanding the available genome editing toolbox. The Cas9-toolkit developed in **chapter 3** relies exclusively on the pBBR1MCS2 replicative backbone (88), therefore all the information for i) the *cas9* gene, ii) the targeting gRNA and iii) the flanking templates for homologous-recombination (HR) should be harbored in this vector. Although efficient, such setup allows a single mutation per conjugation round. Moreover, it requires cloning of multiple DNA fragments that can result in challenging cloning strategies. Reducing such complexity would simplify the cloning procedure.

A possible solution for reducing cloning complexity could be relying upon alternative strategies to HR that would not require any recombination template in the pBBR1MCS2 vector. Eukaryotes are known to employ an additional repair system to HR, which is template independent, called non-homologous end joining (NHEJ) (234). This mechanism has been exploited for double-stranded breaks (DSB) repair mechanisms in several species including filamentous fungi, where it is the dominant pathway for DSB repair (38). Sometimes, this has also been combined to multiplex genome editing (38, 235). Therefore, implementation of a NHEJ-based Cas9-toolkit in *R. sphaeroides* could potentially open possibilities for multiplexing in this species.

In prokaryotes, homologs of the eukaryotic NHEJ proteins have been identified (236). These are encoded by the genes *ku* and *ligD*, which are typically adjacent within a genome (237, 238). This mechanism is rare in bacteria, and it has seldom been exploited for genome editing purposes in this domain (163, 239, 240). Nevertheless, homologues of *ku* and *ligD* have been identified in the α -proteobacteria class (236), to which *R. sphaeroides* belongs. This motivated us to investigate the role of these proteins in this species.

Surprisingly, the genome of *R. sphaeroides* encompasses a NHEJ system consisting of 1 *ligD* and 2 *ku* homologs. The latter are located next to each other within the 1st chromosome of *R. sphaeroides*, in opposing directions with their stop codons being in proximity, while the *ligD* is located within the same chromosome but approximately 1 Mb upstream of the 2 *ku* homologs. Additionally, phylogenetic analysis of the *R. sphaeroides* NHEJ proteins sequences not only shows that they only cluster together with other α -proteobacteria NHEJ proteins but also that the 2 *ku* homologs are phylogenetically distant (**Fig. 2a**). The latter is also apparent from the great sequence dissimilarity of the 2 *ku* homologs (no apparent similarity on nucleotide level when aligned with BLASTn), which suggests that they cannot be the result of a duplication event.

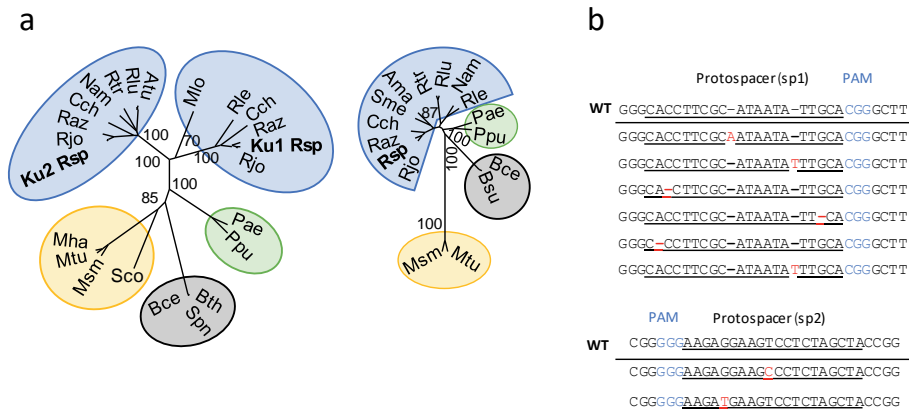


Figure 2. Characterization of the endogenous NHEJ system in *R. sphaeroides*. a) Phylogenetic comparison of Ku (left) and LigD (right) orthologues. Colours in the background are used to cluster taxa from the same phylogenetic class: Alphaproteobacteria (blue), Gammaproteobacteria (green), Bacilli (grey) and Actinobacteria (yellow). The evolutionary history was inferred using the Neighbor-Joining method (241). The percentage of replicate trees in which the associated taxa clustered together in the bootstrap test (1000 replicates) are shown next to the most important nodes. Evolutionary analyses were conducted in MEGA7 (242). Abbreviations: Rsp - *Rhodobacter sphaeroides*, Rjo - *Rhodobacter jorhii*, Raz - *Rhodobacter azotoformans*, Cch - *Cereibacter changlensis*, Sme - *Sinorhizobium meliloti*, Ama - *Aurantimonas manganooxydans*, Rtr - *Rhizobium tropici*, Rlu - *Rhizobium lusitanum*, Nam - *Nitrospirillum amazonense*, Rle - *Rhizobium leguminosarum*, Pae - *Pseudomonas aeruginosa*, Ppu - *Pseudomonas putida*, Bce - *Bacillus cereus*, Bsu - *Bacillus subtilis*, Mtu - *Mycobacterium tuberculosis*, Msm - *Mycobacterium smegmatis*, Mha - *Mycobacterium haemophilum*, Sco - *Streptomyces coelicolor*, Bth - *Bacillus thuringiensis*, Spn - *Streptococcus pneumoniae*, Mlo - *Mesorhizobium loti*, Atu - *Agrobacterium tumefaciens*. NCBI accession numbers of the proteins used for generating the phylogenetic tree are listed in **Table S1**. (b) Examples of insertions or deletions (indel, red) in the protospacer loci detected by the spacers sp1 and sp2 (underlined) in the *upp* gene. The protospacer adjacent motifs (PAM) are shown in light blue.

The existence of NHEJ genes within the genome of *R. sphaeroides* motivated to further study the genomic content of the colonies that escaped the spCas9 targeting of the *upp* gene (**chapter 3**). The *upp* targeting vectors pBBR_Cas9_sp1

and pBBR_Cas9_sp2 vectors showed the highest targeting efficiency in our previous experiment and were selected for further conjugation experiments. Surviving colonies were randomly selected and streaked on R_A_5-FU agar plates and only 7% of them were able to grow on the selection plates (data not shown). We genotyped all the colonies that survived spCas9 targeting and 5-FU selection, through colony PCR and sequencing. The results showed that all the 5-FU resistant colonies included mutations within the corresponding protospacer regions (**Fig. 2b**). We additionally genotyped all the colonies that survived spCas9 targeting but not 5-FU selection, through colony PCR and sequencing. The results showed that all the non 5-FU resistant colonies did not encompass mutations within the *upp* gene and promoter regions. We further cultured and isolated plasmid from 25% of the non-mutant escape colonies; surprisingly the sequencing results showed intact *spCas9* and sgRNA sequences for all of the examined plasmids, suggesting that still a small number of *R. sphaeroides* cells can survive spCas9 targeting. As bacteria often have more than a single copy of their chromosome, these survivors can result from the RecA-dependent HR repair of the formed DSB, with the use of an intact chromosomal copy of the targeted gene as template (163).

The obtained results suggest that the *R. sphaeroides* native NHEJ mechanism is active, repairing spCas9-induced DSBs through error prone correction. Alternatively, the spCas9 targeting mechanism acts as a selection tool in favor of cells containing random-naturally occurring mutations within the targeted protospacer regions. The second option though is considered unlikely, given the low natural rate of spontaneous Δupp mutants formation under 5-FU pressure as well as the relatively high rate of Δupp mutants formed upon spCas9 targeting, with mutations within the targeted protospacer regions.

Here, we demonstrated that the native NHEJ system of *R. sphaeroides* can repair spCas9-induced breaks at ‘easy-to-screen’ rates. This tool is based on a low complexity cloning approach, allowing for the simultaneous and cost-efficient construction of multiple spCas9-based targeting constructs at once. Hence, the development of an efficient Cas9-NHEJ tool in *R. sphaeroides* would allow rapid construction of an extensive library of knock-out strains for improving the current DBTL cycle (28). Potentially, the efficiency of the here developed tool could be further improved by the deletion of the *recA* gene from the *R. sphaeroides* genome. This approach was previously reported to enhance the spCas9 targeting efficiency in *E. coli*, regardless the employed spacer, and to eliminate non-mutated surviving colonies rescued by unedited genome templates via RecA-dependent HR (163).

Test

In this stage of the pipeline, the efficacy of the ‘design’ and ‘build’ steps is determined. This consists in both the verification of the DNA modifications (*e.g.* gene deletions or insertions) and the physiological characterization of the engineered strains (28). In order to facilitate the latter condition, we developed a cultivation system using a defined medium (**chapter 2**). Moreover, for studying metabolic pathways interaction, we developed in **chapter 5** a parallel labeling experiment based on two different ^{13}C glucose tracers. In the following two paragraphs, additional insights of these two approaches are discussed.

Physiological characterization on a defined medium

Hitherto, chemoheterotrophic cultivation of *R. sphaeroides* had always been performed using rich media. Therefore, undefined nutrient sources like yeast extract, corn steep liquor and molasses were available as substrates (79, 81, 82). Presence of such chemically undefined compounds encumbers interpretation of

substrate contributions to product synthesis. Conversely, in **chapter 2** the implementation of a defined medium allowed to understand the physiological response of *R. sphaeroides* to substrate variations. Thereby, such a medium was employed for cultivations in microtiter plates, flasks and bioreactors. It was observed that nitrogen was depleting prior to glucose from the medium. Nitrogen depletion is known to be one of the causes for inhibiting biomass formation while increasing isoprenoid synthesis in *E. coli* (123, 243). Therefore, it was possible to assess the effect of different initial carbon-to-nitrogen ratios in the medium and their effect on isoprenoids and byproducts formation. These different ratios were employed for confirming the elimination of PHB synthesis in **chapter 3**. Moreover, they were used for assessing the contribution of the two isoprenoid pathways to amorphadiene synthesis in different growth conditions in **chapter 6**. Eventually, use of such defined medium allowed to employ ^{13}C labeled substrates for accurately measuring pathways contributions in **chapters 4, 5 and 6**. Altogether, employment of such medium allowed to characterize the *R. sphaeroides* strains generated, while pinpointing the bottlenecks for further improvements.

^{13}C metabolic flux ratio analysis

Parallel labeling experiments on defined medium using $[1-^{13}\text{C}]$ - and $[4-^{13}\text{C}]\text{glucose}$ as tracers for flux ratio analysis were described in **chapter 5**. Such an experimental setup allowed to determine the carbon partitioning within glycolysis and isoprenoid metabolisms. Except for a single example where LC-MS was applied for the measurement of intracellular metabolites (205), no method was available for investigating microbial isoprenoid metabolism via ^{13}C cultivation. Therefore, we designed a method capable of determining ^{13}C atom incorporation within the universal precursors IPP and DMAPP. Accordingly, since

all isoprenoids are derived from these precursors, in principle this method can be employed for studying the synthesis of any isoprenoid molecule.

A crucial aspect for the validation of this technique was the employment of *R. sphaeroides* mutants presenting a single glycolytic or isoprenoid pathway active. Cultivation of these strains with labeled substrates resulted in no degree of freedom, thereby confirming the exclusive flux via the expected pathway.

Eventually, in **chapter 6** this method was implemented to assess the effect of nitrogen limitation on the isoprenoid split ratio, revealing important insights about the interaction of MEP and MVA pathways.

Learn

It has been reasoned that DBTL cycles can help in understanding the metabolism of a microbial *chassis* (28). In this final phase of the pipeline, experimental evidence collected from the ‘test’ phase is combined with the available literature data, formalizing the learning phase. Therefore, the knowledge gathered can be used as input for the next round of ‘design’, while also improving the understanding of the platform’s metabolism. Below, the most relevant insights collected through this project are discussed.

Novel insights on MEP and MVA pathways interaction

The first pioneering work expressing a MVA pathway in *E. coli* (42) demonstrated the importance of cloning a heterologous MVA pathway for increasing isoprenoid production. Subsequently, a plethora of efforts were taken focusing on the optimization of this pathway (55). Such an exclusive attention on the MVA pathway often failed in investigating the effect of these manipulations on the endogenous MEP pathway. For example, in **chapter 2** we demonstrated that the activity of the MEP pathway is strictly growth-coupled. Additional expression of

the MVA pathway allowed to increase substantially amorphaadiene synthesis during this condition. One would reason that such flux increase is consequence of exclusive flux via the MVA pathway. Nevertheless, it is important noting that a cross-talk between these two metabolic routes has been already known in plants (44, 244, 245). Moreover, a synergistic effect between these pathways was recently reported in *E. coli* (205), determining a paradigm shift on how isoprenoid pathways interact within microbial hosts. Consequently, we argued that a better understanding on MEP and MVA pathways interaction in *R. sphaeroides* was needed.

The method for flux ratio analysis developed in **chapter 5** was crucial for understanding such interaction. It was observed that, during exponential growth, the isoprenoid flux ratio remained fixed, independently from the copy numbers of MVA enzymes. The endogenous MEP pathway flux was increased when the MVA pathway was harbored on a plasmid. We reasoned that this increase in flux could be consequence of the presence of the enzyme isopentenyl-pyrophosphate isomerase -Idi-, which is included among the plasmid-borne MVA enzymes, and which is known to increase MEP pathway flux (208, 246). Therefore, we disrupted the first enzyme of the plasmid-borne MVA pathway (**Fig. 3a**) and measured final amorphaadiene titers (**Fig. 3b**). The outcome suggested that presence of MVA pathway enzymes (but not their active flux) is sufficient for increasing the MEP pathway flux in *R. sphaeroides*. Nevertheless, a more thorough analysis for confirming the positive effect of *idi* expression on MEP pathway capacity would require the cloning of this single gene on a plasmid and subsequent measurement of amorphaadiene titers.

Conversely, in **chapter 6**, cultivation under resting cell conditions showed a limitation in the overall isoprenoid flux via the dual-pathway strain. Therefore,

inactivation of the MEP pathway and exclusive flux via the MVA pathway allowed to significantly increase volumetric yields and amorphaadiene specific titers. All in all, these pieces of data indicate that, while exponential growth activates the MEP pathway and improves the isoprenoid flux, during resting cell conditions the endogenous regulation acting on this pathway limited overall isoprenoid flux.

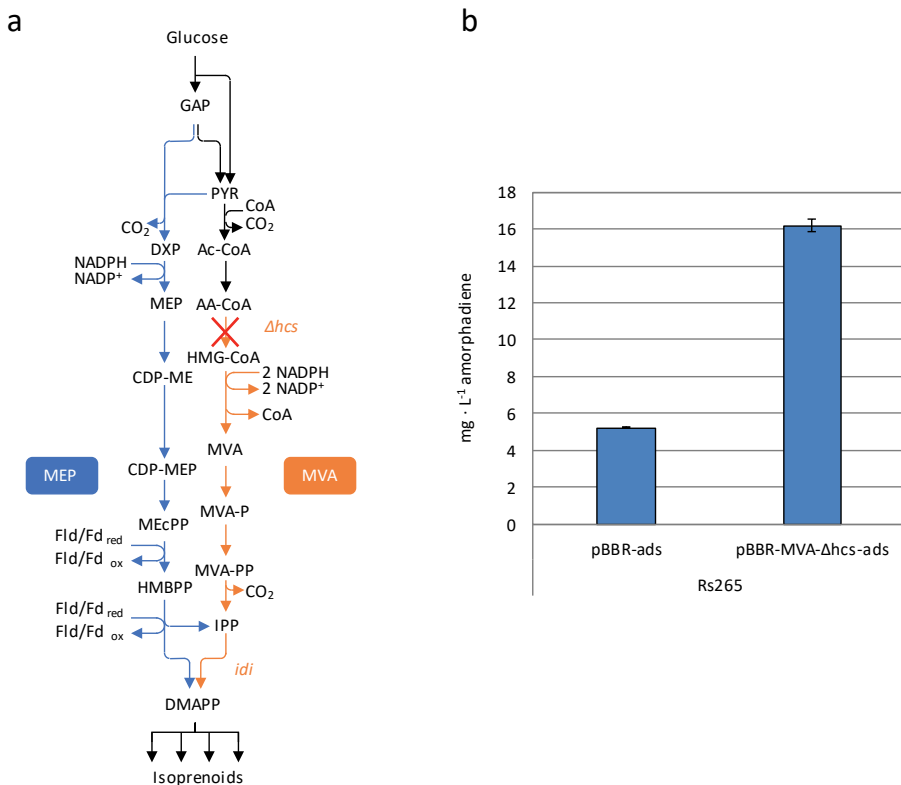


Figure 3. Effect of MVA pathway disruption on MEP pathway capacity. a) overview of the two isoprenoid pathways. The plasmid-borne MVA pathway was inactivated by disruption of the first gene of the pathway (*hcs*); also the *idi* gene is highlighted. b) Final amorphaadiene titers comparison between a strain harboring only the MEP pathway (Rs265:pBBR-*ads*) and another strain additionally harboring the disrupted MVA pathway (Rs265:pBBR-MVA-*Δhcs*-*ads*).

MVA pathway can (partially) fulfill the metabolic functions of NADPH oxidation and free-CoA release associated to PHB synthesis

PHB is the main storage compound accumulating in *R. sphaeroides* when nitrogen depletes from the medium (164), and its synthesis serves for carbon and energy conservation. The PHB flux is supported by high intracellular acetyl-CoA/CoA and NADPH/NADP⁺ ratios (247, 248), which increase when biomass formation is prevented, *e.g.* upon nutrient depletion. As shown in **chapter 2**, the start of PHB synthesis coincides with a halt of isoprenoid production via the MEP pathway. Nevertheless, introduction of the heterologous MVA pathway allowed to maintain an active, although reduced, amorphadiene productivity during PHB formation (**chapter 2**). In fact, the MVA pathway shares the precursor acetoacetyl-CoA (AA-CoA) with the PHB pathway. Moreover, this pathway's flux benefits from high intracellular concentrations of acetyl-CoA (Ac-CoA) and NADPH (54, 249, 250). We therefore hypothesized that the metabolic traits of i) NADPH oxidation and ii) free-CoA release that are exerted by the PHB pathway in a wild-type *R. sphaeroides* could be substituted by the MVA pathway. As described in **chapter 6**, we assessed the effect of inactivating PHB pathway synthesis in respect to isoprenoid synthesis. Deletion of *phaB* (which encodes the first enzyme of the pathway) forced the MVA pathway to fulfil the two aforementioned traits, and its expression resulted indeed in higher amorphadiene titers. Moreover, the deletion of *phaB* in a strain harboring the MVA pathway cultivated under resting cells conditions, led to a substantial increase in amorphadiene yields and productivities (specific and volumetric) compared to when PHB synthesis was still active. Therefore, prevention of PHB synthesis reduced competition between the two metabolic routes at the advantage of the MVA pathway. Nevertheless, the final titers of amorphadiene obtained were still considerably lower than the amount of PHB that was

prevented from being formed. Moreover, increased secretion of pyruvate and 2-oxoglutarate indicated that the current MVA pathway capacity is still too low to completely redirect all the intracellular AA-CoA pool towards amorphaadiene. Therefore, focus on engineering the rate limiting steps of the MVA pathway, *e.g.* HMG-CoA reductase (213, 250, 251), is highly recommended for further enhancing isoprenoid production via this metabolic route.

Modular pathway engineering allows to replace isoprenoid biosynthetic routes while reducing endogenous regulation

As described in **chapter 4**, intersection between synthetic biology and metabolic engineering resulted in the paradigm of modular pathways engineering (26, 166, 252). Thereafter, pathway modules have been edited for increasing bioproduction of several molecules, including isoprenoids (48, 167, 212, 253–255). Moreover, exclusive exploitation of non-native modules allowed to reduce endogenous control over biochemical routes (256, 257). As proof of principle, we assessed if this approach could be applied also to isoprenoid metabolism.

The successful replacement of the endogenous MEP with the heterologous MVA pathway was described in **chapter 4**. To our knowledge, this is also the first proof that an essential pathway can be replaced. The implanted MVA module has previously been described as ‘orthogonal’ to the MEP pathway because of the different intermediates which are generated (52, 258, 259). Such metabolites are in principle decoupled from the host’s metabolic network. This renders the pathway less sensitive (but still not completely independent) from the endogenous regulation of the microorganism (260). More precisely, the MEP pathway is known to be regulated both transcriptionally and post-transcriptionally, while a heterologous MVA pathway expressed in *R. sphaeroides* is affected mainly by post-transcriptional regulation. In fact,

transcription of MEP and carotenoid genes is initiated by low oxygen tension (131, 261) and, as demonstrated in **chapter 2 and 6**, endogenous MEP pathway activation occurs during exponential growth conditions. Oxygen is also responsible of the oxidation of the [4Fe-4S] clusters of the MEP enzymes IspG and IspH, which results in enzyme denaturation (186). Ultimately, the pyrophosphorylated products of the MEP pathway (*e.g.* IPP and DMAPP) are known to be responsible for feedback inhibition of several MEP enzymes (262). One example is Dxs, known to exert significant control over the pathway (246). Because the MVA pathway is also inhibited by the same pyrophosphorylated compounds (263–265), product-mediated feedback inhibition is the only post-translational regulatory mechanism expected to be shared between the MEP and MVA pathways (262–264, 266). Therefore, due to the reduced control imposed by the host on the MVA pathway, its exclusive exploitation holds promise for further improvement of isoprenoid synthesis (52).

As described in **chapter 6**, a scientifically intriguing condition for testing the advantage of MVA pathway replacement over the endogenous MEP pathway is growth-independent isoprenoid synthesis. In fact, growth-coupled synthesis has the disadvantage of investing an important fraction of the substrate, redox and energy carriers towards biomass formation and maintenance (218, 220). On the other hand, growth-independent production holds potential from a process perspective, because in principle it allocates all these metabolites for product formation (267). **Chapter 2** showed that, under non-growing conditions, the MEP pathway was inactive. Deletion of the MEP pathway described in **chapter 6** increased amorphaadiene synthesis under non-growing conditions. Hence, growth-independent isoprenoid synthesis benefited from the exclusive exploitation of the autonomous and non-native MVA pathway. Additionally, inactivation of PHB synthesis forced this pathway to fulfil alone the NADPH

oxidation and free-CoA release, resulting in the maximum yields and productivities obtained.

From a more general perspective, the work of **chapters 4 and 6** proved that it is in principle possible to minimize the interaction between host's regulatory system and the implemented production pathway. To further decouple the endogenous *R. sphaeroides* regulation from the heterologous MVA pathway, orthogonality principles could be exploited (220, 258). In fact, although the carbon flux between MEP and MVA pathways is independent, they still share similar metabolic currencies, i.e. NADPH and ATP (258). Therefore, complete orthogonality could be realized by engineering the substrate catabolic pathway and the implemented heterologous pathway for using new-to-nature reducing equivalents (268–270) which act independently from the rest of the metabolism.

Future perspectives: a new DBTL cycle for further improving *R. sphaeroides* as isoprenoid cell factory

This thesis allowed to improve DBTL cycles for consolidating *R. sphaeroides* as microbial cell factory. Moreover, the insights gathered via this iterative approach allowed to deepen the understanding of its metabolism. Imagining to continue with a novel DBTL cycle, few proposals for further investigations are provided.

Engineering the MEP pathway for increasing the endogenous isoprenoid flux

A strategy for further improving growth-coupled isoprenoid synthesis could be to employ a plasmid-borne MVA pathway while increasing the flux via the endogenous MEP pathway. In this metabolic route, in fact, overexpression of rate-limiting enzymes already proved to increase the isoprenoid flux, including in *R. sphaeroides* (93, 95). Moreover a library of promoters and RBSs is already available for this species (89). Such a *R. sphaeroides* strain with high flux via both

isoprenoid pathways would resemble the *E. coli* strain where the synergistic enhancement of MEP and MVA pathways capacities was first described (205). There, the cause for the mutual increase of both isoprenoid pathways fluxes was suggested in terms of complementation for cofactor regenerations between the two pathways (205). In fact, although both routes require reducing equivalents, the flux from glucose to isoprene via the EMP and MEP pathways necessitates investment of 2 NADPH molecules, while the balance via the EMP and MVA pathways results in a net formation of 4 NADPH. It was therefore reported (205) that, for reaching the maximum theoretical yield of isoprene, the isoprenoid flux ratio should be 0.46:0.54 (MEP:MVA), thereby more balanced than the one of 0.29:0.71 (MEP:MVA) reported in **chapter 5**.

Increasing the flux via the MEP pathway is therefore desirable for exploiting isoprenoid pathways synergy for redox equivalents. Moreover, in this scenario oxygen supply could be reduced resulting in several advantages: i) reduction of the negative regulation over the MEP pathway (63, 271) ii) decreased use of oxygen as electron acceptor for maintaining the NADPH/NADP⁺ balanced (272), iii) lower CO₂ formation as consequence of respiration (272), and iv) reduced operational costs for maintaining oxygen transfer and temperature under control (272). It is important noting that transcriptional regulation of photosynthetic genes (including the ones of the MEP pathway) is controlled by oxygen tension via - at least - three known mechanisms (73), some of which act as transcriptional factors involved in expression of many light and/or redox regulatory circuits (63, 271). Therefore, direct intervention for removing endogenous regulation on the MEP pathway can be challenging, while overexpression of the endogenous MEP genes is recommended for increasing its flux.

Enhancing the catalytic efficiency of the MVA pathway

As reported in **chapter 6**, deletion of PHB biosynthetic pathway via $\Delta phaB$ allowed a marginal increase of isoprenoid yields via the MVA pathway. Accordingly, secretion of pyruvate and 2-oxoglutarate was interpreted as a consequence of limitation in isoprenoid flux, caused by an increased pool size of Ac-CoA, AA-CoA and HMG-CoA. To confirm the increase of these intracellular pools in $\Delta phaB$, metabolome analysis could be performed. Of all these intermediates, Ac-CoA is expected to be the most concentrated intermediate (estimated $\Delta_r G^\circ$ of 26.1 ± 1.7 kJ/mol for: $2 \text{ Ac-CoA}_{\text{aq}} \rightleftharpoons \text{AA-CoA}_{\text{aq}} + \text{CoA}_{\text{aq}}$). Therefore, another way to show that the capacity of the MVA pathway is limited could be expression of an acetyltransferase (*e.g.* an ethanol acetyltransferase). Such an enzyme might catalyze the release of the CoA moiety resulting in the production of ethyl acetate, whose secretion could function as reporter.

Increase in MVA pathway capacity could be obtained via a rational approach targeting the rate-limiting enzymes. This can occur either by increasing their copy numbers or by improving their rate of catalysis (K_{cat}) (273). Currently, plasmid-borne expression of the MVA pathway is the most efficient system for isoprenoid synthesis via this metabolic route (**chapter 5**). Nevertheless, such a system is composed by a vector with medium copy-number (85), harboring a constitutively expressed operon. Most likely, such expression system allocates an important fraction of the proteome to the isoprenoid pathways, resulting in diminishing the proteome available for other processes (273). Therefore, since the cellular proteome is finite (273), increasing further the expression of MVA enzymes is discouraged because it would result in enhancement of the proteome burden.

On the other hand, improvement of the K_{cat} of rate-limiting enzymes is encouraged. Since the growth-independent production condition proposed in **chapter 6** determines high intracellular Ac-CoA/CoA and NADPH/NADP⁺ ratios, these would be expected to drive the reaction catalyzed by the enzyme *HMG-CoA reductase*, where NADP⁺ and free CoA are generated via the reaction: $\text{HMG-CoA} + 2\text{H}^+ + 2\text{NADPH} \rightleftharpoons \text{mevalonate} + \text{CoA} + 2\text{NADP}^+$. Therefore, increasing this reaction rate would be desirable for augmenting the MVA pathway flux, while reducing secretion of byproducts like pyruvate and 2-oxoglutarate. Several reports already described this enzyme as rate-limiting in the MVA pathway (55), and extensive screening for optimal homologs and overexpression strategies have already been proposed (250, 251). Alternatively, a library of mutants for directed evolution of HMG-CoA reductase is encouraged, as implemented for carotenoids-related genes in *Saccharomyces cerevisiae* (274).

Increasing the intracellular NADPH/NADP⁺ ratio

Once the capacity of the MVA pathway has been enhanced, improved coupling of cofactors regeneration to isoprenoid synthesis can be explored for further connecting substrate catabolism to product synthesis. This can be obtained by increasing the NADPH generated via glucose catabolism, *e.g.* by redirecting all the glycolytic flux (determined in **chapter 5**) towards the ED pathway (275). Moreover, increased NADPH generation during glycolysis can be obtained by changing the cofactor dependency in the lower glycolysis. In fact, by substituting the native NAD-dependent with a NADP-dependent glyceraldehyde dehydrogenase it is possible to further increase the intracellular NADPH pool, to which isoprenoid synthesis can be associated (276). An alternative strategy could be overexpressing the malic enzyme. This approach would result in an increased carbon flux in the gluconeogenic direction, determining i) increased pyruvate pool for the MVA pathway and ii) generation of NADPH, as already described for

lipid synthesis in *Yarrowia lipolytica* (277). Moreover, overexpression of the soluble transhydrogenase UdhA was reported to be effective for increasing isoprenoid synthesis in *E. coli* and *Y. lipolytica* (254, 277). Nevertheless, the latter strategy should be carefully considered, because both species employ the EMP pathway, which generates a surplus of NADH, while *R. sphaeroides* mainly uses the ED pathway, which generates NADPH (**chapter 5**).

Engineering glucose uptake rate and metabolic switches for two-stage fermentations strategy

Eventually, upon increased isoprenoid flux it would be possible to explore alternative process conditions. As explained in **chapter 6**, two-stage fermentations would allow to exploit a production phase where microbial growth is prevented, therefore allowing more substrate to be available for isoprenoid synthesis. Nevertheless, it has to be noted that two-stage fermentations are not automatically better than one-stage fermentations (218). Therefore, a thorough design of the candidate strain for two-stages fermentation should be performed. The major bottleneck during non-growing conditions is the substrate uptake rate, which is notoriously lower than during exponential growth (218, 243, 278). An elegant strategy for increasing glucose uptake rate during nitrogen starvation was implemented in *E. coli*, and consisted in the overexpression of the PtsI, an enzyme of the glucose uptake system (279). A complementary approach for improving productivities during non-growing conditions can be the employment of metabolic switches for reducing competitive pathways using CRISPR interference, CRISPRi (36, 280). In fact, by applying this technique it was already possible to perform growth-phase dependent metabolic switches in *E. coli* (281). Such an approach could be employed for silencing the expression of MEP enzymes when moving from growth to production phase. Thereby, mutual enhancement of the two

isoprenoid pathways could be exploited during the growth phase. Then, it would be followed by a silencing of the endogenous MEP pathway during the production phase, allowing exclusive flux via the less regulated MVA pathway. In the latter condition, in fact, it was demonstrated that the isoprenoid flux during resting cells condition was maximal.

Improving scalability: from plasmid-borne expression towards chromosomal integration of heterologous genes

Because current plasmid availability is limited in *R. sphaeroides*, alternatives to plasmid-based expression systems should be considered. Moreover, upscaling of engineered strains harboring replicative plasmids is discouraged. In fact, a selective pressure needs to be provided constantly in the process, which can be cumbersome under large-scale cultivations. Besides, as mentioned above, plasmid-borne enzymes expression may result in a burden due to proteome constraints (273). Through this thesis we presented two possible strategies for chromosomal integrations, which could be further employed. The Cas9-tool developed in **chapter 3** resulted in efficient gene integrations. Moreover, Tn5-insertion reported in **chapter 4** can be used for chromosomal integration of large-sized operons. For tuning the expression of the integrated genes, testing of libraries of promoters and ribosome-binding-sites (89) is recommended.

Final outlook: is *R. sphaeroides* the ideal platform for isoprenoid synthesis?

In this thesis, we investigated and engineered the metabolism of *R. sphaeroides* for improving its isoprenoid production. Following the structure of DBTL cycles, we developed novel tools for engineering and studying this bacterium, like a Cas9-based genome editing tool and a ^{13}C method for flux ratios analysis. Eventually, we generated strains capable of improved isoprenoid synthesis. The

increased flux towards IPP and DMAPP can be streamlined for the production of several isoprenoid molecules (59), thereby strengthening the position of *R. sphaeroides* as microbial cell factory for isoprenoid production.

As previously discussed, the reasons justifying the choice of this microorganism as production platform were: i) the innate synthesis of some commercially relevant isoprenoids (i.e. carotenoids and CoQ₁₀), ii) its morphological adaptation with the formation of an intracellular membrane (ICM) for increasing the surface available for allocating isoprenoid molecules and iii) the endogenous regulation which increased isoprenoid synthesis at low oxygen tensions. Moreover, this microorganism has been engineered for synthesis of heterologous isoprenoids like lycopene, farnesol and aromatic sesquiterpenes, with the latter being produced for commercialization (8). It is worth noting that isoprenoids for the aroma market are also being synthesized via traditional cell factories like *E. coli* and *S. cerevisiae* (8).

These workhorses demonstrated very promising performances in terms of TRY values for isoprenoid synthesis (50, 249). Consequently, these organisms are being investigated also for applications in the commodity chemicals and biofuel sectors (52, 53, 172). In this perspective, further improvement of *R. sphaeroides* as microbial cell factory could bridge the gap with traditional microbial platforms, thereby allowing to explore its application also for bio-based production of commodity chemicals and biofuels.

Nonetheless, it must be noted that *R. sphaeroides* is a highly versatile and metabolically complex bacterium (62). Therefore, it can thrive on various carbon sources and under different growth conditions, allowing to investigate isoprenoid metabolism and its regulation under many circumstances. Moreover,

addition of the novel tools generated within this thesis offers unprecedented opportunities for metabolic engineering of isoprenoid biosynthesis in *R. sphaeroides*, also under cultivation conditions other than chemoheterotrophy. Consequently, we envision a promising future for this bacterium as platform for investigating isoprenoid production, both from fundamental and applied perspectives.

Supplementary information

Table S1. List of bacteria and NCBI accession numbers of the proteins used for generating Ku and LigD phylogenetic trees.

LigD	
Species	Accession #
<i>Rhodobacter sphaeroides</i>	Sequenced genome (Isobionics)
<i>Rhodobacter azotoformans</i>	WP_101340727.1
<i>Cereibacter changlensis</i>	WP_107663713.1
<i>Sinorhizobium meliloti</i>	WP_088200687.1
<i>Aurantimonas manganoxydans</i>	WP_009208938.1
<i>Mycobacterium tuberculosis</i>	ALB18079.1
<i>Pseudomonas putida</i>	ADR60141.1
<i>Mycolicibacterium smegmatis</i>	AFP41860.1
<i>Rhizobium leguminosarum</i>	AUW40742.1
<i>Pseudomonas aeruginosa</i>	BAR68071.1
<i>Nitrospirillum amazonense</i>	ASG25270.1
<i>Rhodobacter johrii</i>	RAZ83231.1
<i>Rhizobium lusitanum</i>	SCB45385.1
<i>Mycobacterium tuberculosis</i>	AJF02293.1
<i>Bacillus cereus</i>	AUZ26128.1
<i>Rhizobium tropici</i>	RAX41073.1
<i>Bacillus subtilis</i>	AQZ90234.1
Ku	
Species	Accession #
<i>Rhodobacter sphaeroides</i> Ku1	Sequenced genome (Isobionics)
<i>Rhodobacter sphaeroides</i> Ku2	Sequenced genome (Isobionics)
<i>Rhodobacter azotoformans</i>	WP_101341724
<i>Cereibacter changlensis</i>	PTE23121
<i>Cereibacter changlensis</i>	WP_107662491
<i>Rhizobium leguminosarum</i>	WP_047555545
<i>Rhizobium leguminosarum</i>	WP_028734704.1
<i>Pseudomonas putida</i>	KZO53158.1
<i>Mycobacterium tuberculosis</i>	KXN95658.1
<i>Rhodobacter johrii</i>	WP_108223209.1
<i>Rhodobacter azotoformans</i>	WP_101340822.1

<i>Rhizobium lusitanum</i>	WP_092574817.1
<i>Nitrospirillum amazonense</i>	WP_004274142.1
<i>Agrobacterium tumefaciens</i>	WP_025591969.1
<i>Mycobacterium haemophilum</i>	WP_047314295.1
<i>Cereibacter changlensis</i>	WP_107662492.1
<i>Rhizobium tropici</i>	RAX38214.1
<i>Bacillus thuringiensis</i>	AKR33785.1
<i>Bacillus cereus</i>	PGV94828.1

Ku

Species	Accession #
<i>Rhodobacter johrii</i>	WP_069332344.1
<i>Streptococcus pneumoniae</i>	CRF99327.1
<i>Mesorhizobium loti</i>	OBQ66756.1
<i>Pseudomonas aeruginosa</i>	BAR68056.1
<i>Mycobacterium smegmatis</i>	YP_889815.1

Summary

A crucial aspect for innovation in industrial biotechnology is the development of microbial cell factories that can perform optimally within a bioprocess. Recently, technological improvement in -omics (genomics, transcriptomics, proteomics, metabolomics and fluxomics) techniques and genome editing technologies allowed to advance non-model organisms as platforms for bioproduction. Usually, these novel microbial cell factories are proposed due to their innate phenotypes which are beneficial for the processes considered. In **chapter 1**, *Rhodobacter sphaeroides* is introduced as promising cell factory for the production of terpenes (also known as isoprenoids), a relevant class of molecules for the bioeconomy. This bacterium is a native producer of important isoprenoid-derived molecules, such as coenzyme Q₁₀ and carotenoids. Moreover, the whole morphology of *R. sphaeroides* changes when it synthesizes isoprenoids, with the development of intracytoplasmic membrane (ICM) for maximizing the surface for the aggregation of isoprenoid molecules. These aspects make *R. sphaeroides* an interesting potential platform. Few studies were already reported for improving isoprenoid production in this species. Nevertheless, a thoroughly understanding of its physiological behavior during isoprenoid biosynthesis was missing. Such knowledge is necessary for further studying and improving the cell factory.

In **chapter 2** the physiology of isoprenoid biosynthesis in *R. sphaeroides* is studied via cultivation on a defined medium. Such a cultivation setup allowed to assess the bacterium response to variations in nutrients availabilities. For such type of study, the volatile sesquiterpene amorpho-4,11-diene was chosen as reporter molecule. After an initial screening of carbon sources for dark heterotrophic cultivation, glucose was chosen as substrate for further experimenting. Isoprenoid biosynthesis revealed to be strictly growth-coupled in

a strain relying exclusively on the endogenous 2-methyl D-erythritol 4-phosphate (MEP) pathway. When a heterologous mevalonate (MVA) pathway was additionally expressed on a plasmid, amorphaadiene biosynthesis increased up to eight-fold. Moreover, presence of the MVA pathway resulted in isoprenoid production also during non-growing conditions imposed by nitrogen limitation. Under this condition, the storage polymer poly- β -hydroxybutyrate (PHB) accumulated up to 60% of the dry-weight, as the major by-product of the process. Eventually, the effect of oxygen tension was also investigated, revealing its important regulatory effect on the activity of the endogenous MEP pathway.

In order to make *R. sphaeroides* a platform organism, an efficient genome editing toolkit needs to be established for this species. **Chapter 3** describes the implementation of a highly-efficient Cas9 genome editing tool for *R. sphaeroides*. In this setup, plasmid-based homologous recombination was combined with Cas9-based targeting for counter-selection. Hence, gene deletions, insertions and single nucleotide substitutions were obtained and revealed to accelerate genetic modifications compared to traditional suicide plasmid-based strategies. Additionally, this study further applied the Cas9 tool to elucidate the pathway leading to the synthesis of PHB in the bacterium. In fact, by deleting the *phaB* gene encoding an NADPH-dependent acetoacetyl-CoA reductase, synthesis of the storage compound was prevented. It is thereby demonstrated that this enzyme is the only responsible of the first step of PHB biosynthesis, and its inactivation is sufficient to prevent PHB accumulation in *R. sphaeroides*.

The ideal cell factory should have a minimal dependence of pathway fluxes from its endogenous regulation. A strategy for reducing such a constrain is to replace a native and strictly-regulated pathway with an independent and autonomous one. **Chapter 4** describes the functional replacement of isoprenoid pathway in *R.*

sphaeroides. More precisely, the endogenous MEP pathway was inactivated by Cas9-mediated deletion of *dxr* (encoding the second enzyme of the pathway) and isoprenoid flux was exclusively supported by a chromosomally integrated heterologous MVA pathway. Inactivation of the native pathway was possible only after integration of the orthogonal pathway, thereby confirming the essentiality of isoprenoid synthesis for cellular metabolism. Cultivation with ^{13}C -labeled glucose confirmed isoprenoid pathway substitution. Flux via the integrated MVA pathway supported growth at comparable levels to the control strain, but resulted in lower titers of the reporter isoprenoids. Nevertheless, upon including additional plasmid-borne copies of the MVA enzymes, differences in relative isoprenoid titers between the engineered strain and the wild-type control were erased. Additionally, it was demonstrated that the former strain relying exclusively on the integrated and plasmid-borne MVA enzymes obtained substantially higher yields of amorphadiene compared to the parental strain still maintaining the MEP pathway active. Apart from describing the design and implementation of a metabolic bypass for isoprenoid biosynthesis in *R. sphaeroides*, this study resulted in the generation of a strain subjected to lower endogenous regulation during amorphadiene biosynthesis.

Interest in understanding MEP and MVA pathway interactions resulted in **chapter 5**, where a tool for studying pathway contributions to isoprenoid biosynthesis was developed. In this study, a setup for parallel ^{13}C -labeling cultivation was designed to determine the metabolic flux ratios during glycolysis and isoprenoid biosynthesis in *R. sphaeroides*. Such method was implemented for integrating ^{13}C atoms within the universal isoprenoid building-blocks isopentenyl-pyrophosphate (IPP) and dimethylallyl-pyrophosphate (DMAPP). Determination of pathway contributions to IPP and DMAPP biosynthesis was

determined by exclusive measurement of the secreted reporter amorphaadiene. It was proven that by parallel cultivation with 100% [1-¹³C]- or [4-¹³C]-glucose, glycolysis via the Entner-Doudoroff (ED) or the Embden-Meyerhof-Parnas (EMP) pathways could be determined, as well as the isoprenoid flux via the MEP or MVA pathways. For validation purposes, strains with 100% flux via one of the target pathways were generated. Among those, Cas9-based deletion of *pgi* inactivated the EMP pathway, Δeda the ED pathway, and Δdxr the MEP pathway (the latter generated in **chapter 4** upon previous integration of the MVA pathway). Parallel ¹³C cultivations in these strains resulted in no degree of freedom, thereby confirming the reliability of the experimental design. The method was therefore applied to study the metabolic flux ratio in glycolysis, confirming a predominance of the ED pathway over the EMP pathway. Moreover, it indicated that the MEP and MVA pathways have a reciprocal stimulating effect which results in increase of both pathways capacities. The reason for this reciprocal stimulation is not clear yet.

Chapter 6 focused on understanding the interaction between isoprenoid and PHB biosynthetic pathways in *R. sphaeroides*. The reasoning behind this study was to assess if isoprenoid production, natively growth-coupled in this bacterium, could be efficiently obtained during growth-independent conditions. Eventually, comprehension of these aspects allowed to improve amorphaadiene biosynthesis during non-growing conditions. **Chapter 2** reported growth-independent amorphaadiene synthesis when the MVA pathway was present, although resulting in PHB accumulation. Therefore, the effect of inactivating PHB was assessed in respect to amorphaadiene production. Deletion of *phaB* (described in **chapter 3**) resulted in substantial increase of amorphaadiene titers when the MVA pathway was also present. In fact, both the PHB and the MVA pathways show the metabolic traits of NADPH oxidation and intracellular free-

CoA release. Metabolic flux ratio analysis developed in **chapter 5** was applied, confirming the increased MVA pathway capacity upon deletion of *phaB*. Interestingly, it was also demonstrated that presence of the MVA pathway enhanced MEP pathway capacity during nitrogen-limited cultivation, revealing that the isoprenoid flux ratio is affected by the environmental factors like nutrients availability. When moving to resting cells conditions, $\Delta phaB$ resulted in improved growth-independent amorphadiene production. Eventually, the maximum yields and productivities under this condition were obtained when combining $\Delta phaB$ with MEP pathway inactivation. Such strain streamlined all isoprenoid flux via the less regulated MVA pathway, which could further benefit from the lack of PHB accumulation. Interestingly, amorphadiene specific titers in the strains relying exclusively on the MVA pathway did not change when comparing exponential growth to resting cells condition. On the other hand, additional presence of an active MEP pathway largely affected these values, with a beneficial effect during growth-coupled production. These results suggest that, although growth-coupled synthesis via both MEP and MVA pathways is still the most efficient condition for isoprenoid production, growth-independent biosynthesis can be obtained (and further improved) via exclusive exploitation of the deregulated MVA pathway.

Chapter 7 is the general discussion of this thesis, which combines and further evaluates the main findings of the different chapters. Attention is given to the consolidation of *R. sphaeroides* as microbial cell factory obtained via a Design-Build-Test-Learn cycle. Moreover, an endogenous non-homologous end joining mechanism for DNA repair is described, which could accelerate the genome editing in this species. Then, a speculation of the possible interaction of MEP and MVA pathways is provided, followed by an interpretation on the advantage of

exploiting the MVA pathway in relation to endogenous PHB accumulation. Eventually, advantages on modular pathway engineering for exclusive employment of the MVA pathway for growth-independent isoprenoid synthesis are reported. As conclusions, future perspective for investigation and improvement of critical factors are proposed.

References

1. A. Aguilar, T. Twardowski, R. Wohlgemuth, Bioeconomy for sustainable development. *Biotechnol. J.* **14**, 1800638 (2019).
2. M. M. Bugge, T. Hansen, A. Klitkou, What is the bioeconomy? A review of the literature. *Sustain.* **8** (2016), doi:10.3390/su8070691.
3. R. Carlson, Laying the foundations for a bio-economy. *Syst. Synth. Biol.* **1**, 109–117 (2007).
4. M. S. G. Lopes, Engineering biological systems toward a sustainable bioeconomy. *J. Ind. Microbiol. Biotechnol.* **42**, 813–838 (2015).
5. S. Y. Park, D. Yang, S. H. Ha, S. Y. Lee, Metabolic engineering of microorganisms for the production of natural compounds. *Adv. Biosyst.* **2** (2018), pp. 1–41.
6. S. Y. Lee, D. Mattanovich, A. Villaverde, Systems metabolic engineering, industrial biotechnology and microbial cell factories. *Microb. Cell Fact.* (2012), pp. 11–13.
7. C. J. Paddon, P. J. Westfall, D. J. Pitera, K. Benjamin, K. Fisher, D. McPhee, M. D. Leavell, A. Tai, A. Main, D. Eng, D. R. Polichuk, K. H. Teoh, D. W. Reed, T. Treynor, J. Lenihan, M. Fleck, S. Bajad, G. Dang, D. Dengrove, D. Diola, G. Dorin, K. W. Ellens, S. Fickes, J. Galazzo, S. P. Gaucher, T. Geistlinger, R. Henry, M. Hepp, T. Horning, T. Iqbal, H. Jiang, L. Kizer, B. Lieu, D. Melis, N. Moss, R. Regentin, S. Secrest, H. Tsuruta, R. Vazquez, L. F. Westblade, L. Xu, M. Yu, Y. Zhang, L. Zhao, J. Lievense, P. S. Cavello, J. D. Keasling, K. K. Reiling, N. S. Renninger, J. D. Newman, High-level semi-synthetic production of the potent antimalarial artemisinin. *Nature*. **496**, 528–32 (2013).
8. F. M. Schempp, L. Drummond, M. Buchhaupt, J. Schrader, Microbial cell factories for the production of terpenoid flavor and fragrance compounds. *J. Agric. Food Chem.* (2017), doi:10.1021/acs.jafc.7b00473.
9. S. F. Yuan, H. S. Alper, Metabolic engineering of microbial cell factories for production of nutraceuticals. *Microb. Cell Fact.*, 1–11 (2019).
10. H. Yim, R. Haselbeck, W. Niu, C. Pujol-Baxley, A. Burgard, J. Boldt, J. Khandurina, J. D. Trawick, R. E. Osterhout, R. Stephen, J. Estadilla, S. Teisan, H. B. Schreyer, S. Andrae, T. H. Yang, S. Y. Lee, M. J. Burk, S. Van Dien, Metabolic engineering of *Escherichia coli* for direct production of 1,4-butanediol. *Nat. Chem. Biol.* **7**, 445–452 (2011).
11. J. C. Liao, L. Mi, S. Pontrelli, S. Luo, Fuelling the future: microbial engineering for the production of sustainable biofuels. *Nat. Rev. Microbiol.* (2016), doi:10.1038/nrmicro.2016.32.
12. P. P. Peralta-Yahya, F. Zhang, S. B. Del Cardayre, J. D. Keasling, Microbial engineering for the production of advanced biofuels. *Nature*. **488**, 320–328 (2012).
13. X. Chen, L. Zhou, K. Tian, A. Kumar, S. Singh, B. A. Prior, Z. Wang, Metabolic engineering of *Escherichia coli*: a sustainable industrial platform for bio-based chemical production. *Biotechnol. Adv.* (2013), , doi:10.1016/j.biotechadv.2013.02.009.
14. K. K. Hong, J. Nielsen, Metabolic engineering of *Saccharomyces cerevisiae*: a key cell factory platform for future biorefineries. *Cell. Mol. Life Sci.* **69**, 2671–2690 (2012).

15. B. L. Adams, The next generation of synthetic biology chassis: moving synthetic biology from the laboratory to the field. *ACS Synth. Biol.* **5**, 1328–1330 (2016).
16. P. Calero, P. I. Nikel, Chasing bacterial *chassis* for metabolic engineering: a perspective review from classical to non-traditional microorganisms. *Microb. Biotechnol.* **12** (2019), pp. 98–124.
17. H. Liu, A. M. Deutschbauer, Rapidly moving new bacteria to model-organism status. *Curr. Opin. Biotechnol.* **51**, 116–122 (2018).
18. M. Gustavsson, S. Y. Lee, Prospects of microbial cell factories developed through systems metabolic engineering. *Microb. Biotechnol.* **9**, 610–617 (2016).
19. S. Y. Lee, H. U. Kim, Systems strategies for developing industrial microbial strains. *Nat. Biotechnol.* **33**, 1061–1072 (2015).
20. T. Moses, P. Mehrshahi, A. G. Smith, A. Goossens, Synthetic biology approaches for the production of plant metabolites in unicellular organisms. *J. Exp. Bot.* **68**, 4057–4074 (2017).
21. J. E. Bailey, Toward a Science of Metabolic Engineering. *Science* (80-.). **252**, 1668–1675 (1991).
22. G. Stephanopoulos, Metabolic fluxes and metabolic engineering. *Metab. Eng.* **1**, 1–11 (1999).
23. J. Nielsen, It is all about metabolic fluxes. *J. Bacteriol.* **185**, 7031–7035 (2003).
24. J. Nielsen, M. Fussenegger, J. Keasling, S. Y. Lee, J. C. Liao, K. Prather, B. Palsson, Engineering synergy in biotechnology. *Nat. Chem. Biol.* **10**, 319–322 (2014).
25. J. D. Keasling, Synthetic biology and the development of tools for metabolic engineering. *Metab. Eng.* **14**, 189–195 (2012).
26. G. Stephanopoulos, Synthetic biology and metabolic engineering. *ACS Synth. Biol.* **1**, 514–525 (2012).
27. J. Nielsen, Systems biology of metabolism. *Annu. Rev. Biochem.* **11**, 1–31 (2017).
28. J. Nielsen, J. D. Keasling, Engineering cellular metabolism. *Cell.* **164**, 1185–1197 (2016).
29. Y. Liu, J. Nielsen, Recent trends in metabolic engineering of microbial chemical factories. *Curr. Opin. Biotechnol.* **60** (2019), pp. 188–197.
30. C. J. Petzold, L. J. G. Chan, M. Nhan, P. D. Adams, Analytics for metabolic engineering. *Front. Bioeng. Biotechnol.* **3**, 1–11 (2015).
31. R. Chao, S. Mishra, T. Si, H. Zhao, Engineering biological systems using automated biofoundries. *Metab. Eng.* **42**, 98–108 (2017).
32. S. C. C. Shih, C. Moraes, Next generation tools to accelerate the synthetic biology process. *Integr. Biol. (United Kingdom)*. **8**, 585–588 (2016).
33. K. Campbell, J. Xia, J. Nielsen, The impact of systems biology on bioprocessing. *Trends Biotechnol.* **35**, 1156–1168 (2017).
34. G. B. Kim, W. J. Kim, H. U. Kim, S. Y. Lee, Machine learning applications in systems metabolic engineering. *Curr. Opin. Biotechnol.* **64**, 1–9 (2020).
35. C. J. Vavricka, T. Hasunuma, A. Kondo, Dynamic metabolomics for engineering biology: accelerating learning cycles for bioproduction. *Trends Biotechnol.* **38**, 68–82 (2020).
36. I. Mougiakos, E. F. Bosma, J. Ganguly, J. Van Der Oost, R. Van Kranenburg, R. Kranenburg, Hijacking CRISPR-Cas for high-throughput bacterial metabolic

- engineering: advances and prospects. *Curr. Opin. Biotechnol.* **50**, 146–157 (2018).
37. T. Jakočiūnas, M. K. Jensen, J. D. Keasling, CRISPR/Cas9 advances engineering of microbial cell factories. *Metab. Eng.* **34**, 44–59 (2015).
38. Y. Tong, T. Weber, S. Y. Lee, CRISPR/Cas-based genome engineering in natural product discovery. *Nat. Prod. Rep.* **36**, 1262–1280 (2019).
39. N. Hillson, M. Caddick, Y. Cai, J. A. Carrasco, M. W. Chang, N. C. Curach, D. J. Bell, R. Le Feuvre, D. C. Friedman, X. Fu, N. D. Gold, M. J. Herrgård, M. B. Holowko, J. R. Johnson, R. A. Johnson, J. D. Keasling, R. I. Kitney, A. Kondo, C. Liu, V. J. J. Martin, F. Menolascina, C. Ogino, N. J. Patron, M. Pavan, C. L. Poh, I. S. Pretorius, S. J. Rosser, N. S. Scrutton, M. Storch, H. Tekotte, E. Travník, C. E. Vickers, W. S. Yew, Y. Yuan, H. Zhao, P. S. Freemont, Building a global alliance of biofoundries. *Nat. Commun.* **10**, 1038–1041 (2019).
40. C. J. Paddon, J. D. Keasling, Semi-synthetic artemisinin: a model for the use of synthetic biology in pharmaceutical development. *Nat. Rev. Microbiol.* **12**, 355–367 (2014).
41. N. J. White, Qinghaosu (artemisinin): the price of success. *Science (80-.).* **320**, 330–334 (2008).
42. V. J. J. Martin, D. J. Pitera, S. T. Withers, J. D. Newman, J. D. Keasling, Engineering a mevalonate pathway in *Escherichia coli* for production of terpenoids. *Nat. Biotechnol.* **21**, 796–802 (2003).
43. J. Lombard, D. Moreira, Origins and early evolution of the mevalonate pathway of isoprenoid biosynthesis in the three domains of life. *Mol. Biol. Evol.* **28**, 87–99 (2011).
44. E. Vranová, D. Coman, W. Gruissem, Network analysis of the MVA and MEP pathways for isoprenoid synthesis. *Annu. Rev. Plant Biol.* **64**, 665–700 (2013).
45. J. Grünler, J. Ericsson, G. Dallner, Branch-point reactions in the biosynthesis of cholesterol, dolichol, ubiquinone and prenylated proteins. *Biochim. Biophys. Acta (BBA)/Lipids Lipid Metab.* **1212**, 259–277 (1994).
46. P. K. Ajikumar, K. Tyo, S. Carlsen, O. Mucha, T. H. Phon, G. Stephanopoulos, Terpenoids: opportunities for biosynthesis of natural product drugs using engineered microorganisms. *Mol. Pharm.* **5**, 167–190 (2008).
47. M. C. Y. Chang, J. D. Keasling, Production of isoprenoid pharmaceuticals by engineered microbes, 1–9 (2006).
48. C. Li, C. A. Swofford, A. J. Sinskey, Modular engineering for microbial production of carotenoids. *Metab. Eng. Commun.* **10**, e00118 (2020).
49. S. Q. E. Lee, T. S. Tan, M. Kawamukai, E. S. Chen, Cellular factories for coenzyme Q₁₀ production. *Microb. Cell Fact.* **16** (2017), pp. 1–16.
50. L. Ye, X. Lv, H. Yu, Engineering microbes for isoprene production. *Metab. Eng.* **38**, 125–138 (2016).
51. R. Mewalal, D. K. Rai, D. Kainer, F. Chen, C. Kulheim, G. F. Peter, G. A. Tuskan, Plant-derived terpenes: a feedstock for specialty biofuels. *Trends Biotechnol.* **35**, 227–240 (2016).
52. F. Zhang, S. Rodriguez, J. D. Keasling, Metabolic engineering of microbial pathways for advanced biofuels production. *Curr. Opin. Biotechnol.* **22**, 775–783

- (2011).
53. P. P. Peralta-Yahya, F. Zhang, D. S. B. Cardayre, J. D. Keasling, Microbial engineering for the production of advanced biofuels. *Nature*. **488**, 320–328 (2012).
 54. M. Li, F. Hou, T. Wu, X. Jiang, F. Li, H. Liu, M. Xian, H. Zhang, Recent advances of metabolic engineering strategies in natural isoprenoid production using cell factories. *Nat. Prod. Rep.* (2020), doi:10.1039/c9np00016j.
 55. P. Liao, A. Hemmerlin, T. J. Bach, M. L. Chye, The potential of the mevalonate pathway for enhanced isoprenoid production. *Biotechnol. Adv.* **34** (2016), , doi:10.1016/j.biotechadv.2016.03.005.
 56. S. Tippmann, Y. Chen, V. Siewers, J. Nielsen, From flavors and pharmaceuticals to advanced biofuels: production of isoprenoids in *Saccharomyces cerevisiae*. *Biotechnol. J.*, 1435–1444 (2013).
 57. C. M. Immethun, A. G. H. Connor, A. Balassy, T. S. Moon, Microbial production of isoprenoids enabled by synthetic biology. *Front. Microbiol.* **4**, 1–8 (2013).
 58. Q. Wang, S. Quan, H. Xiao, Towards efficient terpenoid biosynthesis: manipulating IPP and DMAPP supply. *Bioresour. Bioprocess.* **6** (2019), pp. 1–13.
 59. J. Nielsen, Yeast cell factories on the horizon. *Science (80-.).* **349**, 1050–1051 (2015).
 60. H. Tsuruta, C. J. Paddon, D. Eng, J. R. Lenihan, T. Horning, L. C. Anthony, R. Regentin, J. D. Keasling, N. S. Renninger, J. D. Newman, High-level production of amorpho-4, 11-diene, a precursor of the antimalarial agent artemisinin, in *Escherichia coli*. *PLoS One*. **4**, e4489 (2009).
 61. P. J. Westfall, D. J. Pitera, J. R. Lenihan, D. Eng, F. X. Woolard, R. Regentin, T. Horning, H. Tsuruta, D. J. Melis, A. Owens, S. Fickes, D. Diola, K. R. Benjamin, J. D. Keasling, M. D. Leavell, D. J. McPhee, N. S. Renninger, J. D. Newman, C. J. Paddon, Production of amorphadiene in yeast, and its conversion to dihydroartemisinic acid, precursor to the antimalarial agent artemisinin. *Proc. Natl. Acad. Sci. U. S. A.* **109**, E111–8 (2012).
 62. C. Mackenzie, J. M. Eraso, M. Choudhary, J. H. Roh, X. Zeng, P. Bruscella, A. Puskás, S. Kaplan, Postgenomic adventures with *Rhodobacter sphaeroides*. *Annu. Rev. Microbiol.* **61**, 283–307 (2007).
 63. S. Elsen, M. Jaubert, D. Pignol, E. Giraud, PpsR: a multifaceted regulator of photosynthesis gene expression in purple bacteria. *Mol. Microbiol.* **57**, 17–26 (2005).
 64. S. Masuda, C. E. Bauer, AppA is a blue light photoreceptor that antirepresses photosynthesis gene expression in *Rhodobacter sphaeroides*. *Cell*. **110**, 613–623 (2002).
 65. A. Puskas, E. P. Greenberg, S. Kaplan, A. L. Schaefer, A quorum-sensing system in the free-living photosynthetic bacterium *Rhodobacter sphaeroides*. *J. Bacteriol.* **179**, 7530–7537 (1997).
 66. S. L. Porter, G. H. Wadhams, J. P. Armitage, *Rhodobacter sphaeroides*: complexity in chemotactic signalling. *Trends Microbiol.* **16**, 251–260 (2008).
 67. H. Koku, I. Eroğlu, U. Gündüz, M. Yücel, Aspects of the metabolism of hydrogen production by *Rhodobacter sphaeroides*. *Int. J. Hydrogen Energy*. **27**, 1315–1329

- (2002).
68. J. Kobayashi, A. Kondo, Disruption of poly (3-hydroxyalkanoate) depolymerase gene and overexpression of three poly (3-hydroxybutyrate) biosynthetic genes improve poly (3-hydroxybutyrate) production from nitrogen rich medium by *Rhodobacter sphaeroides*. *Microb. Cell Fact.* **18**, 1–13 (2019).
 69. H. P. Lang, C. N. Hunter, The relationship between carotenoid biosynthesis and the assembly of the light-harvesting LH2 complex in *Rhodobacter sphaeroides*. *Biochem. J.* **298** (Pt 1, 197–205 (1994).
 70. M. T. Madigan, G. Howard, Growth of the photosynthetic bacterium *Rhodospseudomonas capsulata* chemoautotrophically in darkness with H₂ as the energy source. *J. Bacteriol.* **137**, 524–530 (1979).
 71. S. Romagnoli, F. R. Tabita, in *The Purple Phototrophic Bacteria* (2009; http://link.springer.com/10.1007/978-1-4020-8815-5_28), pp. 563–576.
 72. S. Kaplan, J. Eraso, J. H. Roh, Interacting regulatory networks in the facultative photosynthetic bacterium, *Rhodobacter sphaeroides* 2.4.1. *Biochem. Soc. Trans.* **33**, 51–5 (2005).
 73. J. H. Zeilstra-Ryalls, S. Kaplan, Oxygen intervention in the regulation of gene expression: the photosynthetic bacterial paradigm. *Cell. Mol. Life Sci.* **61**, 417–436 (2004).
 74. S. Imam, D. R. Noguera, T. J. Donohue, Global analysis of photosynthesis transcriptional regulatory networks. *PLoS Genet.* **10** (2014), doi:10.1371/journal.pgen.1004837.
 75. R. Pandey, J. P. Armitage, G. H. Wadhams, Use of transcriptomic data for extending a model of the AppA/PpsR system in *Rhodobacter sphaeroides*. *BMC Syst. Biol.* **11**, 1–13 (2017).
 76. R. A. Niederman, Membrane development in purple photosynthetic bacteria in response to alterations in light intensity and oxygen tension. *Photosynth. Res.* **116**, 333–348 (2013).
 77. H. S. Zahiri, K. A. Noghabi, Y. C. Shin, Biochemical characterization of the decaprenyl diphosphate synthase of *Rhodobacter sphaeroides* for coenzyme Q₁₀ production. *Appl. Microbiol. Biotechnol.* **73**, 796–806 (2006).
 78. H.-W. Yen, C.-H. Chiu, The influences of aerobic-dark and anaerobic-light cultivation on CoQ₁₀ production by *Rhodobacter sphaeroides* in the submerged fermenter. *Enzyme Microb. Technol.* **41**, 600–604 (2007).
 79. H. W. Yen, T. Y. Shih, Coenzyme Q₁₀ production by *Rhodobacter sphaeroides* in stirred tank and in airlift bioreactor. *Bioprocess Biosyst. Eng.* **32**, 711–716 (2009).
 80. H. W. Yen, C. Y. Feng, J. L. Kang, Cultivation of *Rhodobacter sphaeroides* in the stirred bioreactor with different feeding strategies for CoQ₁₀ production. *Appl. Biochem. Biotechnol.* **160**, 1441–1449 (2010).
 81. N. B. Kien, I. S. Kong, M. G. Lee, J. K. Kim, Coenzyme Q₁₀ production in a 150-L reactor by a mutant strain of *Rhodobacter sphaeroides*. *J. Ind. Microbiol. Biotechnol.* **37**, 521–529 (2010).
 82. L. Zhang, L. Liu, K. F. Wang, L. Xu, L. Zhou, W. Wang, C. Li, Z. Xu, T. Shi, H. Chen, Y. Li, H. Xu, X. L. Yang, Z. Zhu, B. Chen, D. Li, G. Zhan, S. L. Zhang, L. X. Zhang, G. Y. Tan, Phosphate limitation increases coenzyme Q₁₀ production in industrial

- Rhodobacter sphaeroides* HY01. *Synth. Syst. Biotechnol.* **4**, 212–219 (2019).
83. S. E. Nybo, N. E. Khan, B. M. Woolston, W. R. Curtis, Metabolic engineering in chemolithoautotrophic hosts for the production of fuels and chemicals. *Metab. Eng.* **30**, 105–120 (2015).
84. O. P. Serdyuk, L. D. Smolygina, E. M. Chekunova, E. P. Sannikova, G. N. Shirshikova, A. N. Khusnutdinova, N. V. Yartseva, Direct transition of pGA482:Ipt plasmid bearing the cytokinin biosynthesis gene into the cells of phototrophic purple bacteria *Rhodobacter sphaeroides* and *Rhodopseudomonas palustris* by electroporation. *Dokl. Biochem. Biophys.* **451**, 194–197 (2013).
85. M. Inui, K. Nakata, J. H. Roh, A. A. Vertès, H. Yukawa, Isolation and molecular characterization of pMG160, a mobilizable cryptic plasmid from *Rhodobacter blasticus*. *Appl. Environ. Microbiol.* **69**, 725–733 (2003).
86. D. Jun, R. G. Saer, J. D. Madden, J. T. Beatty, Use of new strains of *Rhodobacter sphaeroides* and a modified simple culture medium to increase yield and facilitate purification of the reaction centre. *Photosynth. Res.* **120**, 197–205 (2014).
87. P. R. Jaschke, R. G. Saer, S. Noll, J. T. Beatty, in *Methods in Enzymology* (2011), vol. 497, pp. 519–538.
88. I. B. Tikh, M. Held, C. Schmidt-Dannert, BioBrick™ compatible vector system for protein expression in *Rhodobacter sphaeroides*. *Appl. Microbiol. Biotechnol.* **98**, 3111–9 (2014).
89. J. Huo, thesis, Utah State University (2011).
90. A. Su, S. Chi, Y. Li, S. Tan, S. Qiang, Z. Chen, Y. Meng, Metabolic redesign of *Rhodobacter sphaeroides* for lycopene production. *J. Agric. Food Chem.* **66**, 5879–5885 (2018).
91. J. Beekwilder, A. van Houwelingen, K. Cankar, A. D. J. van Dijk, R. M. de Jong, G. Stoop, H. Bouwmeester, J. Achkar, T. Sonke, D. Bosch, Valencene synthase from the heartwood of Nootka cypress (*Callitropsis nootkatensis*) for biotechnological production of valencene. *Plant Biotechnol. J.* **12**, 174–182 (2014).
92. X. Chen, X. Jiang, M. Xu, M. Zhang, R. Huang, J. Huang, F. Qi, Co-production of farnesol and coenzyme Q10 from metabolically engineered *Rhodobacter sphaeroides*. *Microb. Cell Fact.* **18**, 1–12 (2019).
93. W. Lu, L. Ye, H. Xu, W. Xie, J. Gu, H. Yu, Enhanced production of coenzyme Q₁₀ by self-regulating the engineered MEP pathway in *Rhodobacter sphaeroides*. *Biotechnol. Bioeng.* **111**, 761–769 (2014).
94. W. Lu, Y. Shi, S. He, Y. Fei, K. Yu, H. Yu, Enhanced production of CoQ₁₀ by constitutive overexpression of 3-demethyl ubiquinone-9 3-methyltransferase under tac promoter in *Rhodobacter sphaeroides*. *Biochem. Eng. J.* **72**, 42–47 (2013).
95. W. Lu, L. Ye, X. Lv, W. Xie, J. Gu, Z. Chen, Y. Zhu, A. Li, H. Yu, Identification and elimination of metabolic bottlenecks in the quinone modification pathway for enhanced coenzyme Q10 production in *Rhodobacter sphaeroides*. *Metab. Eng.* **29**, 208–216 (2015).
96. Y. Zhu, L. Ye, Z. Chen, W. Hu, Y. Shi, J. Chen, C. Wang, Y. Li, W. Li, H. Yu, Synergic

- regulation of redox potential and oxygen uptake to enhance production of coenzyme Q₁₀ in *Rhodobacter sphaeroides*. *Enzyme Microb. Technol.* **101**, 36–43 (2017).
97. Y. Zhu, W. Lu, L. Ye, Z. Chen, W. Hu, C. Wang, J. Chen, H. Yu, Enhanced synthesis of coenzyme Q10 by reducing the competitive production of carotenoids in *Rhodobacter sphaeroides*. *Biochem. Eng. J.* **125**, 50–55 (2017).
98. M. Xu, H. Wu, P. Shen, X. Jiang, X. Chen, J. Lin, J. Huang, F. Qi, Enhancement of NADPH availability for coproduction of coenzyme Q₁₀ and farnesol from *Rhodobacter sphaeroides*. *J. Ind. Microbiol. Biotechnol.* (2020), doi:10.1007/s10295-020-02261-z.
99. J. Zhang, D. Gao, J. Cai, H. Liu, Z. Qi, Improving coenzyme Q10 yield of *Rhodobacter sphaeroides* via modifying redox respiration chain. *Biochem. Eng. J.* **135**, 98–104 (2018).
100. S. Imam, S. Yilmaz, U. Sohmen, A. S. Gorzalski, J. L. Reed, D. R. Noguera, T. J. Donohue, iRsp1095: a genome-scale reconstruction of the *Rhodobacter sphaeroides* metabolic network. *BMC Syst. Biol.* **5**, 116 (2011).
101. S. Imam, D. R. Noguera, T. J. Donohue, Global insights into energetic and metabolic networks in *Rhodobacter sphaeroides*. *BMC Syst. Biol.* **7**, 89 (2013).
102. R. F. Tabita, *The biochemistry and metabolic regulation of carbon metabolism and CO₂ fixation in purple bacteria* (Springer, Dordrecht, 1995; http://dx.doi.org/10.1007/0-306-47954-0_41).
103. J. P. O’Gara, J. M. Eraso, S. Kaplan, A redox-responsive pathway for aerobic regulation of photosynthesis gene expression in *Rhodobacter sphaeroides* 2.4.1. *J. Bacteriol.* **180**, 4044–4050 (1998).
104. O. V. Moskvina, L. Gomelsky, M. Gomelsky, Transcriptome analysis of the *Rhodobacter sphaeroides* PpsR regulon: PpsR as a master regulator of photosystem development. *J. Bacteriol.* **187**, 2148–2156 (2005).
105. J. Gershenzon, N. Dudareva, The function of terpene natural products in the natural world. *Nat. Chem. Biol.* **3**, 408–414 (2007).
106. S. T. Withers, J. D. Keasling, Biosynthesis and engineering of isoprenoid small molecules. *Appl. Microbiol. Biotechnol.* **73**, 980–990 (2007).
107. J. Kirby, J. D. Keasling, Biosynthesis of plant isoprenoids: perspectives for microbial engineering. *Annu. Rev. Plant Biol.* **60**, 335–355 (2009).
108. M. H. Alvès, H. Sfeir, J. F. Tranchant, E. Gombart, G. Sagorin, S. Caillol, L. Billon, M. Save, Terpene and dextran renewable resources for the synthesis of amphiphilic biopolymers. *Biomacromolecules*. **15**, 242–251 (2014).
109. J. L. Fortman, S. Chhabra, A. Mukhopadhyay, H. Chou, T. S. Lee, E. Steen, J. D. Keasling, Biofuel alternatives to ethanol: pumping the microbial well. *Trends Biotechnol.* **26**, 375–381 (2008).
110. A. Banerjee, Y. Wu, R. Banerjee, Y. Li, H. Yan, T. D. Sharkey, Feedback inhibition of deoxy-D-xylulose-5-phosphate synthase regulates the methylerythritol 4-phosphate pathway. *J. Biol. Chem.* **288**, 16926–16936 (2013).
111. N. E. Khan, S. E. Nybo, J. Chappell, W. R. Curtis, Triterpene hydrocarbon production engineered into a metabolically versatile host- *Rhodobacter capsulatus*. *Biotechnol. Bioeng.* **112**, 1523–1532 (2015).

112. Y. Zhu, L. Ye, Z. Chen, W. Hu, Y. Shi, J. Chen, C. Wang, Y. Li, W. Li, H. Yu, Synergic regulation of redox potential and oxygen uptake to enhance production of coenzyme Q10 in *Rhodobacter sphaeroides*. *Enzyme Microb. Technol.* **101**, 36–43 (2017).
113. M. Hümbelin, A. Thomas, J. Lin, J. Li, J. Jore, A. Berry, Genetics of isoprenoid biosynthesis in *Paracoccus zeaxanthinifaciens*. *Gene*. **297**, 129–139 (2002).
114. M. Hümbelin, J. Beekwilder, J. G. T. Kierkels, *Rhodobacter* for preparing terpenoids (2015), p. Patent no. WO2014014339A3.
115. W. R. Sistrom, A Requirement for sodium in the growth of *Rhodopseudomonas spheroides*. *J. Gen. Microbiol.* **22**, 778–785 (1960).
116. R. Simon, U. Priefer, A. Pühler, A broad host range mobilization system for in vivo genetic engineering: transposon mutagenesis in Gram negative bacteria. *Nat. Biotechnol.* **1**, 784–791 (1983).
117. M. E. Kovach, P. H. Elzer, D. S. Hill, G. T. Robertson, M. A. Farris, R. M. Roop, K. M. Peterson, Four new derivatives of the broad host range cloning vector pBBR1MCS, carrying different antibiotic resistance cassettes. *Gene*. **166**, 175–176 (1995).
118. R. Carpine, F. Raganati, G. Olivieri, K. J. Hellingwerf, A. Pollio, P. Salatino, A. Marzocchella, Poly- β -hydroxybutyrate (PHB) production by *Synechocystis* PCC6803 from CO₂: Model development. *Algal Res.* **29**, 49–60 (2018).
119. M. Waligórska, K. Seifert, K. Górecki, M. Moritz, M. Łaniecki, Kinetic model of hydrogen generation by *Rhodobacter sphaeroides* in the presence of NH₄⁺ ions. *J. Appl. Microbiol.* **107**, 1308–1318 (2009).
120. A. Gupta, G. Rao, A study of oxygen transfer in shake flasks using a non-invasive oxygen sensor. *Biotechnol. Bioeng.* **84**, 351–358 (2003).
121. R. Dixon, D. Kahn, Genetic regulation of biological nitrogen fixation. *Nat. Rev. Microbiol.* **2**, 621–631 (2004).
122. E. Hustede, A. Steinbüchel, H. G. Schlegel, Relationship between the photoproduction of hydrogen and the accumulation of PHB in non-sulphur purple bacteria. *Appl. Microbiol. Biotechnol.* **39**, 87–93 (1993).
123. S. Li, C. B. Jendresen, A. T. Nielsen, Increasing production yield of tyrosine and mevalonate through inhibition of biomass formation. *Process Biochem.* **51**, 1992–2000 (2016).
124. W. de Koning, R. A. Weusthuis, W. Harder, L. Dijkhuizen, Methanol-dependent production of dihydroxyacetone and glycerol by mutants of the methylotrophic yeast *Hansenula polymorpha* blocked in dihydroxyacetone kinase and glycerol kinase. *Appl. Microbiol. Biotechnol.* **32**, 693–698 (1990).
125. Y. Tao, D. Liu, X. Yan, Z. Zhou, J. K. Lee, C. Yang, Network identification and flux quantification of glucose metabolism in *Rhodobacter sphaeroides* under photoheterotrophic H₂-producing conditions. *J. Bacteriol.* **194**, 274–283 (2012).
126. M.-H. Ryu, N. C. Hull, M. Gomelsky, Metabolic engineering of *Rhodobacter sphaeroides* for improved hydrogen production. *Int. J. Hydrogen Energy*. **39**, 6384–6390 (2014).
127. S. H. Hong, S. J. Park, S. Y. Moon, J. P. Park, S. Y. Lee, In silico prediction and validation of the importance of the Entner-Doudoroff pathway in poly(3-

- hydroxybutyrate) production by metabolically engineered *Escherichia coli*. *Biotechnol. Bioeng.* **83**, 854–863 (2003).
128. T. Fuhrer, E. Fischer, U. Sauer, Experimental identification and quantification of glucose metabolism in seven bacterial species. *J. Bacteriol.* **187**, 1581–1590 (2005).
129. J. C. Choi, H. D. Shin, Y. H. Lee, Modulation of 3-hydroxyvalerate molar fraction in poly(3-hydroxybutyrate-3-hydroxyvalerate) using *Ralstonia eutropha* transformant co-amplifying *phbC* and NADPH generation-related *zwf* genes. *Enzyme Microb. Technol.* **32**, 178–185 (2003).
130. C. E. Bauer, A. Setterdahl, J. Wu, B. R. Robinson, in *The Purple Phototrophic Bacteria* (2009; http://link.springer.com/10.1007/978-1-4020-8815-5_35), pp. 707–725.
131. C. T. Pappas, J. Sram, O. V. Moskvina, P. S. Ivanov, R. C. Mackenzie, M. Choudhary, M. L. Land, F. W. Larimer, S. Kaplan, M. Gomelsky, Construction and validation of the *Rhodobacter sphaeroides* 2.4.1 DNA microarray: transcriptome flexibility at diverse growth modes. *J. Bacteriol.* **186**, 4748–58 (2004).
132. D. Zannoni, B. Schoepp-Cothenet, J. Hosler, in *The Purple Phototrophic Bacteria* (Springer, 2009), pp. 537–561.
133. M. Kim, D. Kim, J. Cha, J. K. Lee, Effect of carbon and nitrogen sources on photo-fermentative H₂ production associated with nitrogenase, uptake hydrogenase activity, and PHB accumulation in *Rhodobacter sphaeroides* KD131. *Bioresour. Technol.* **116**, 179–183 (2012).
134. E. Orsi, P. L. Folch, V. T. Monje-López, B. M. Fernhout, A. Turcato, S. W. M. Kengen, G. Eggink, R. A. Weusthuis, Characterization of heterotrophic growth and sesquiterpene production by *Rhodobacter sphaeroides* on a defined medium. *J. Ind. Microbiol. Biotechnol.* **46**, 1179–1190 (2019).
135. J. P. Porter, S. L. Wadhams, G. H. Armitage, In vivo and in vitro analysis of the *Rhodobacter sphaeroides* chemotaxis signaling complexes. *Methods Enzymol.* **423**, 392–413 (2007).
136. S. Qiang, A. P. Su, Y. Li, Z. Chen, C. Y. Hu, Y. H. Meng, Elevated β -Carotene synthesis by the engineered *Rhodobacter sphaeroides* with enhanced CrtY expression. *J. Agric. Food Chem.* **67**, 9560–9568 (2019).
137. T. Shimizu, H. Teramoto, M. Inui, Introduction of glyoxylate bypass increases hydrogen gas yield from acetate and L-glutamate in *Rhodobacter sphaeroides*. *Appl. Environ. Microbiol.* **85**, 1–17 (2019).
138. I. H. Lee, J. Park, D. Kho, M. S. Kim, J. Lee, Reductive effect of H₂ uptake and poly- β -hydroxybutyrate formation on nitrogenase-mediated H₂ accumulation of *Rhodobacter sphaeroides* according to light intensity. *Appl. Microbiol. Biotechnol.* **60**, 147–153 (2002).
139. I. Mougiakos, E. F. Bosma, K. Weenink, E. M. Vossen, K. Goijvaerts, J. Van Der Oost, R. van Kranenburg, Efficient genome editing of a facultative thermophile using the mesophilic spCas9. *ACS Synth. Biol.* **6**, 849–861 (2017).
140. I. Mougiakos, P. Mohanraju, E. F. Bosma, V. Vrouwe, M. Finger Bou, M. I. S. Naduthodi, A. Gussak, R. B. L. Brinkman, R. Van Kranenburg, J. Van Der Oost, Characterizing a thermostable Cas9 for bacterial genome editing and silencing.

- Nat. Commun.* **8** (2017), doi:10.1038/s41467-017-01591-4.
141. M. Jinek, K. Chylinski, I. Fonfara, M. Hauer, J. A. Doudna, E. Charpentier, A programmable dual-RNA-guided DNA endonuclease in adaptive bacterial immunity. *Science* (80-.). **337**, 816–822 (2012).
 142. P. D. Hsu, E. S. Lander, F. Zhang, Development and applications of CRISPR-Cas9 for genome engineering. *Cell*. **157**, 1262–1278 (2014).
 143. K. Selle, R. Barrangou, Harnessing CRISPR-Cas systems for bacterial genome editing. *Trends Microbiol.* **23**, 225–232 (2015).
 144. J. A. Doudna, E. Charpentier, The new frontier of genome engineering with CRISPR-Cas9. *Science* (80-.). **346** (2014), doi:10.1126/science.1258096.
 145. U. Gophna, T. Allers, A. Marchfelder, Finally, archaea get their CRISPR-Cas toolbox. *Trends Microbiol.* **25**, 430–432 (2017).
 146. A. E. Stachler, A. Marchfelder, Gene repression in haloarchaea using the CRISPR (Clustered regularly interspaced short palindromic repeats)-Cas I-B system. *J. Biol. Chem.* **291**, 15226–15242 (2016).
 147. R. T. Leenay, C. L. Beisel, Deciphering, Communicating, and Engineering the CRISPR PAM. *J. Mol. Biol.* **429**, 177–191 (2017).
 148. T. Arazoe, A. Kondo, K. Nishida, Targeted nucleotide editing technologies for microbial metabolic engineering. *Biotechnol. J.* **1700596**, 1–12 (2018).
 149. D. Bikard, W. Jiang, P. Samai, A. Hochschild, F. Zhang, L. A. Marraffini, Programmable repression and activation of bacterial gene expression using an engineered CRISPR-Cas system. *Nucleic Acids Res.* **41**, 7429–7437 (2013).
 150. C. Dong, J. Fontana, A. Patel, J. M. Carothers, J. G. Zalatan, Synthetic CRISPR-Cas gene activators for transcriptional reprogramming in bacteria. *Nat. Commun.* **9** (2018), doi:10.1038/s41467-018-04901-6.
 151. K. Zheng, Y. Wang, N. Li, F.-F. Jiang, C.-X. Wu, F. Liu, H.-C. Chen, Z.-F. Liu, Highly efficient base editing in bacteria using a Cas9-cytidine deaminase fusion. *Commun. Biol.* **1**, 32 (2018).
 152. S. Banno, K. Nishida, T. Arazoe, H. Mitsunobu, A. Kondo, Deaminase-mediated multiplex genome editing in *Escherichia coli*. *Nat. Microbiol.* **3**, 423–429 (2018).
 153. N. M. Gaudelli, A. C. Komor, H. A. Rees, M. S. Packer, A. H. Badran, D. I. Bryson, D. R. Liu, Programmable base editing of A T to G C in genomic DNA without DNA cleavage. *Nature*. **551**, 464–471 (2017).
 154. I. Mougiakos, E. F. Bosma, W. M. de Vos, R. van Kranenburg, J. van der Oost, Next generation prokaryotic engineering: the CRISPR-Cas toolkit. *Trends Biotechnol.* **34**, 575–587 (2016).
 155. N. J. Claassens, M. F. Siliakus, S. K. Spaans, S. C. A. Creutzburg, B. Nijse, P. J. Schaap, T. E. F. Quax, J. Van Der Oost, Improving heterologous membrane protein production in *Escherichia coli* by combining transcriptional tuning and codon usage algorithms. *PLoS One*. **12** (2017), doi:10.1371/journal.pone.0184355.
 156. H. Li, C. R. Shen, C. H. Huang, L. Y. Sung, M. Y. Wu, Y. C. Hu, CRISPR-Cas9 for the genome engineering of cyanobacteria and succinate production. *Metab. Eng.* **38**, 293–302 (2016).
 157. K. E. Wendt, J. Ungerer, R. E. Cobb, H. Zhao, H. B. Pakrasi, CRISPR/Cas9 mediated

- targeted mutagenesis of the fast growing cyanobacterium *Synechococcus elongatus* UTEX 2973. *Microb. Cell Fact.* **15**, 1–8 (2016).
158. Y. Jiang, F. Qian, J. Yang, Y. Liu, F. Dong, C. Xu, B. Sun, B. Chen, X. Xu, Y. Li, R. Wang, S. Yang, CRISPR-Cpf1 assisted genome editing of *Corynebacterium glutamicum*. *Nat. Commun.* **8**, 1–11 (2017).
159. S. S. Cohen, J. G. Flaks, H. D. Barner, M. R. Loeb, J. Lichtenstein, The mode of action of 5-fluorouracil and its derivatives. *Proc. Natl. Acad. Sci.* **44**, 1004–1012 (1958).
160. V. Singh, M. Brecik, R. Mukherjee, J. C. Evans, Z. Svetlíková, J. Blaško, S. Surade, J. Blackburn, D. F. Warner, K. Mikušová, V. Mizrahi, The complex mechanism of antimycobacterial action of 5-fluorouracil. *Chem. Biol.* **22**, 63–75 (2015).
161. K. Selle, T. R. Klaenhammer, R. Barrangou, CRISPR-based screening of genomic island excision events in bacteria. *Proc. Natl. Acad. Sci. U. S. A.* **112**, 8076–8081 (2015).
162. R. B. Vercoe, J. T. Chang, R. L. Dy, C. Taylor, T. Gristwood, J. S. Clulow, C. Richter, R. Przybilski, A. R. Pitman, P. C. Fineran, Cytotoxic chromosomal targeting by CRISPR/Cas systems can reshape bacterial genomes and expel or remodel pathogenicity islands. *PLoS Genet.* **9** (2013), doi:10.1371/journal.pgen.1003454.
163. L. Cui, D. Bikard, Consequences of Cas9 cleavage in the chromosome of *Escherichia coli*. *Nucleic Acids Res.* **44**, 4243–4251 (2016).
164. H. Brandl, R. A. Gross, R. W. Lenz, R. Lloyd, R. C. Fuller, The accumulation of poly(3-hydroxyalkanoates) in *Rhodobacter sphaeroides*. *Arch. Microbiol.* **155**, 337–340 (1991).
165. S. A. Benner, A. M. Sismour, Synthetic biology. *Nat. Rev. Genet.* **6**, 533–543 (2005).
166. C. Kendig, T. T. Eckdahl, Reengineering metaphysics: modularity, parthood, and evolvability in metabolic engineering. *Philos. Theory, Pract. Biol.* **9**, 1–21 (2017).
167. P. K. Ajikumar, W. H. Xiao, K. E. J. Tyo, Y. Wang, F. Simeon, E. Leonard, O. Mucha, T. H. Phon, B. Pfeifer, G. Stephanopoulos, Isoprenoid pathway optimization for Taxol precursor overproduction in *Escherichia coli*. *Science (80-.)*. **330**, 70–74 (2010).
168. K. Zhou, K. Qiao, S. Edgar, G. Stephanopoulos, Distributing a metabolic pathway among a microbial consortium enhances production of natural products. *Nat. Biotechnol.* **33**, 377–383 (2015).
169. W. Jiang, J. B. Qiao, G. J. Bentley, D. Liu, F. Zhang, Modular pathway engineering for the microbial production of branched-chain fatty alcohols. *Biotechnol. Biofuels.* **10**, 1–15 (2017).
170. J. Wu, P. Liu, Y. Fan, H. Bao, G. Du, J. Zhou, J. Chen, Multivariate modular metabolic engineering of *Escherichia coli* to produce resveratrol from L-tyrosine. *J. Biotechnol.* **167**, 404–411 (2013).
171. W. Bonacci, P. K. Teng, B. Afonso, H. Niederholtmeyer, P. Grob, P. A. Silver, D. F. Savage, Modularity of a carbon-fixing protein organelle. *Proc. Natl. Acad. Sci.* **109**, 478–483 (2012).
172. F. X. Niu, Q. Lu, Y. F. Bu, J. Z. Liu, Metabolic engineering for the microbial production of isoprenoids: carotenoids and isoprenoid-based biofuels. *Synth.*

- Syst. Biotechnol.* **2**, 167–175 (2017).
173. A. Zurbruggen, H. Kirst, A. Melis, Isoprene production via the mevalonic acid pathway in *Escherichia coli* (Bacteria). *Bioenergy Res.* **5**, 814–828 (2012).
174. I. Mougiakos, E. Orsi, M. R. Ghiffari, A. De Maria, W. Post, B. Adiego-Perez, S. W. M. Kengen, R. A. Weusthuis, J. van der Oost, Efficient Cas9-based genome editing of *Rhodobacter sphaeroides* for metabolic engineering. *Microb. Cell Fact.* **18**, 1–13 (2019).
175. J. Beekwilder, I. M. van der Meer, A. Simic, J. Uitdewilligen, J. van Arkel, R. C. H. de Vos, H. Jonker, F. W. A. Verstappen, H. J. Bouwmeester, O. Sibbesen, I. Qvist, J. D. Mikkelsen, R. D. Hall, Metabolism of carotenoids and apocarotenoids during ripening of raspberry fruit. *Biofactors.* **34**, 57–66 (2008).
176. Z. Lin, X. Cui, C. Zhao, S. Yang, J. F. Imhoff, Pigments accumulation via light and oxygen in *Rhodobacter capsulatus* strain XJ-1 isolated from saline soil. *J. Basic Microbiol.* **54**, 828–834 (2014).
177. J. Kirby, M. Nishimoto, R. W. N. Chow, E. E. K. Baidoo, G. Wang, J. Martin, W. Schackwitz, R. Chan, J. L. Fortman, J. D. Keasling, Enhancing Terpene yield from sugars via novel routes to 1-deoxy-D-xylulose 5-phosphate. *Appl. Environ. Microbiol.* **81**, 130–138 (2015).
178. A. O. Chatzivasileiou, V. Ward, S. M. Edgar, G. Stephanopoulos, Two-step pathway for isoprenoid synthesis. *Proc. Natl. Acad. Sci.* **116**, 506–511 (2019).
179. K. J. Puan, H. Wang, T. Dai, T. Kuzuyama, C. T. Morita, *fldA* is an essential gene required in the 2-C-methyl-D-erythritol 4-phosphate pathway for isoprenoid biosynthesis. *FEBS Lett.* **579**, 3802–3806 (2005).
180. L. Loiseau, C. Gerez, M. Bekker, S. Ollagnier-De Choudens, B. Py, Y. Sanakis, J. T. De Mattos, M. Fontecave, F. Barras, ErpA, an iron-sulfur (Fe-S) protein of the A-type essential for respiratory metabolism in *Escherichia coli*. *Proc. Natl. Acad. Sci. U. S. A.* **104**, 13626–13631 (2007).
181. T. J. Erb, B. S. Evans, K. Cho, B. P. Warlick, J. Sriram, B. M. K. Wood, H. J. Imker, J. V. Sweedler, F. R. Tabita, J. A. Gerlt, A RubisCO-like protein links SAM metabolism with isoprenoid biosynthesis. *Nat. Chem. Biol.* **8**, 926–932 (2012).
182. A. Flamholz, E. Noor, A. Bar-Even, R. Milo, EQuilibrator - The biochemical thermodynamics calculator. *Nucleic Acids Res.* **40**, 770–775 (2012).
183. F. K. Bentley, A. Zurbruggen, A. Melis, Heterologous expression of the mevalonic acid pathway in cyanobacteria enhances endogenous carbon partitioning to isoprene. *Mol. Plant.* **7**, 71–86 (2014).
184. S. Carlsen, P. K. Ajikumar, L. R. Formenti, K. Zhou, T. H. Phon, M. L. Nielsen, A. E. Lantz, M. C. Kielland-Brandt, G. Stephanopoulos, Heterologous expression and characterization of bacterial 2-C-methyl-d-erythritol-4-phosphate pathway in *Saccharomyces cerevisiae*. *Appl. Microbiol. Biotechnol.* **97**, 5753–5769 (2013).
185. S. Partow, V. Siewers, L. Daviet, M. Schalk, J. Nielsen, Reconstruction and evaluation of the synthetic bacterial MEP pathway in *Saccharomyces cerevisiae*. *PLoS One.* **7**, 1–12 (2012).
186. J. Kirby, K. L. Dietzel, G. Wichmann, R. Chan, E. Antipov, N. Moss, E. E. K. Baidoo, P. Jackson, S. P. Gaucher, S. Gottlieb, J. LaBarge, T. Mahatdejkul, K. M. Hawkins, S. Muley, J. D. Newman, P. Liu, J. D. Keasling, L. Zhao, Engineering a functional 1-

- deoxy-D-xylulose 5-phosphate (DXP) pathway in *Saccharomyces cerevisiae*. *Metab. Eng.* **38**, 494–503 (2016).
187. E. Orsi, J. Beekwilder, S. Peek, G. Eggink, S. W. M. Kengen, R. A. Weusthuis, Metabolic flux ratio analysis by parallel ^{13}C labeling of isoprenoid biosynthesis in *Rhodobacter sphaeroides*. *Metab. Eng.* **57**, 228–238 (2020).
188. C. C. Liu, M. C. Jewett, J. W. Chin, C. A. Voigt, Toward an orthogonal central dogma. *Nat. Chem. Biol.* **14**, 103–106 (2018).
189. J. Wang, S. Niyompanich, Y.-S. Tai, J. Wang, W. Bai, P. Mahida, T. Gao, K. Zhang, *Appl. Environ. Microbiol.*, in press, doi:10.1128/AEM.02178-16.
190. S. Niefenführ, W. Wiechert, K. Nöh, How to measure metabolic fluxes: A taxonomic guide for ^{13}C fluxomics. *Curr. Opin. Biotechnol.* **34**, 82–90 (2015).
191. W. Wiechert, ^{13}C metabolic flux analysis. *Metab. Eng.* **3**, 195–206 (2001).
192. W. Guo, J. Sheng, X. Feng, ^{13}C -metabolic flux analysis: an accurate approach to demystify microbial metabolism for biochemical production. *Bioengineering*. **3**, 1–32 (2015).
193. E. Fischer, U. Sauer, Metabolic flux profiling of *Escherichia coli* mutants in central carbon metabolism using GC-MS. *Eur. J. Biochem.* **270**, 880–891 (2003).
194. H. Maaheimo, J. Fiaux, Z. P. Cakar, Central carbon metabolism of *Saccharomyces cerevisiae* explored by biosynthetic fractional ^{13}C labeling of common amino acids. *Eur. J. Biochem.*, 2464–2479 (2001).
195. Z. Dai, J. W. Locasale, Understanding metabolism with flux analysis: from theory to application. *Metab. Eng.* **43**, 94–102 (2017).
196. S. B. Crown, M. R. Antoniewicz, Parallel labeling experiments and metabolic flux analysis: past, present and future methodologies. *Metab. Eng.* **16**, 21–32 (2013).
197. J. E. Gonzalez, C. P. Long, M. R. Antoniewicz, Comprehensive analysis of glucose and xylose metabolism in *Escherichia coli* under aerobic and anaerobic conditions by ^{13}C metabolic flux analysis. *Metab. Eng.* **39**, 9–18 (2017).
198. A. Woo Suk, M. R. Antoniewicz, Parallel labeling experiments with [1,2- ^{13}C]glucose and [U- ^{13}C]glutamine provide new insights into CHO cell metabolism. *Metab. Eng.* **15**, 34–47 (2013).
199. R. W. Leighty, M. R. Antoniewicz, COMPLETE-MFA: complementary parallel labeling experiments technique for metabolic flux analysis. *Metab. Eng.* **20**, 49–55 (2013).
200. A. Nanchen, T. Fuhrer, U. Sauer, in *Metabolomics* (2007), vol. 358, pp. 177–197.
201. E. Orsi, J. Beekwilder, D. van Gelder, A. van Houwelingen, G. Eggink, S. W. M. Kengen, R. A. Weusthuis, Functional replacement of isoprenoid biosynthetic pathways in *Rhodobacter sphaeroides*. *Microb. Biotechnol.* (2020), doi:10.1111/1751-7915.13562.
202. T. Liu, L. Zhu, W. Wei, Z. Zhou, Function of glucose catabolic pathways in hydrogen production from glucose in *Rhodobacter sphaeroides* 6016. *Int. J. Hydrogen Energy*. **39**, 4215–4221 (2014).
203. J. D. Newman, J. Marshall, M. Chang, F. Nowroozi, E. Paradise, D. Pitera, K. L. Newman, J. D. Keasling, High-level production of amorpha-4,11-diene in a two-phase partitioning bioreactor of metabolically engineered *Escherichia coli*. *Biotechnol. Bioeng.* **95**, 684–691 (2006).

204. S. Sreevalli, M. Larhed, C. Björkelid, T. Bergfors, A. Karlén, T. A. Jones, M. Desroses, S. Sooriyaarachchi, S. L. Mowbray, S. Dharavath, S. Suresh, B. R. Srinivasa, A. M. Jansson, M. Lindh, R. Nikhil, M. Andaloussi, A. Więckowska, S. Yahiaoui, DXR inhibition by potent mono- and disubstituted fosmidomycin analogues. *J. Med. Chem.* **56**, 6190–6199 (2013).
205. C. Yang, X. Gao, Y. Jiang, B. Sun, F. Gao, S. Yang, Synergy between methylerythritol phosphate pathway and mevalonate pathway for isoprene production in *Escherichia coli*. *Metab. Eng.* **37**, 79–91 (2016).
206. N. Zamboni, S. M. Fendt, M. Rühl, U. Sauer, ¹³C-based metabolic flux analysis. *Nat. Protoc.* **4**, 878–892 (2009).
207. R. Conrad, H. G. Schlegel, Influence of aerobic and phototrophic growth conditions on the distribution of glucose and fructose carbon into the Entner-Doudoroff and Embden-Meyerhof pathways in *Rhodospseudomonas sphaeroides*. *J. Gen. Microbiol.* **101**, 277–290 (1977).
208. X. Lv, H. Xu, H. Yu, Significantly enhanced production of isoprene by ordered coexpression of genes *dxs*, *dxr*, and *idi* in *Escherichia coli*. *Appl. Microbiol. Biotechnol.* **97**, 2357–2365 (2013).
209. T. Kuzuyama, H. Seto, Two distinct pathways for essential metabolic precursors for isoprenoid biosynthesis. *Proc. Japan Acad. Ser. B.* **88**, 41–52 (2012).
210. L. Z. Yuan, P. E. Rouvière, R. A. LaRossa, W. Suh, Chromosomal promoter replacement of the isoprenoid pathway for enhancing carotenoid production in *E. coli*. *Metab. Eng.* **8**, 79–90 (2006).
211. Q. Li, F. Fan, X. Gao, C. Yang, C. Bi, J. Tang, T. Liu, X. Zhang, Balanced activation of IspG and IspH to eliminate MEP intermediate accumulation and improve isoprenoids production in *Escherichia coli*. *Metab. Eng.* **44**, 13–21 (2017).
212. J. R. Anthony, L. C. Anthony, F. Nowroozi, G. Kwon, J. D. Newman, J. D. Keasling, Optimization of the mevalonate-based isoprenoid biosynthetic pathway in *Escherichia coli* for production of the anti-malarial drug precursor amorpha-4, 11-diene. *Metab. Eng.* **11**, 13–19 (2009).
213. D. J. Pitera, C. J. Paddon, J. D. Newman, J. D. Keasling, Balancing a heterologous mevalonate pathway for improved isoprenoid production in *Escherichia coli*. *Metab. Eng.* **9**, 193–207 (2007).
214. E. L. Kannenberg, K. Poralla, Hopanoid biosynthesis and function in bacteria. *Naturwissenschaften.* **86**, 168–176 (1999).
215. J. K. Volkman, Sterols in microorganisms. *Appl. Microbiol. Biotechnol.* **60**, 495–506 (2003).
216. A. Von Kamp, S. Klamt, Growth-coupled overproduction is feasible for almost all metabolites in five major production organisms. *Nat. Commun.* **8**, 1–10 (2017).
217. L. H. Reyes, J. M. Gomez, K. C. Kao, Improving carotenoids production in yeast via adaptive laboratory evolution. *Metab. Eng.* **21**, 26–33 (2014).
218. S. Klamt, R. Mahadevan, O. Hädicke, When do two-stage processes outperform one-stage processes? *Biotechnol. J.* **13** (2018), doi:10.1002/biot.201700539.
219. C. Willrodt, A. Hoschek, B. Bühler, A. Schmid, M. K. Julsing, Decoupling production from growth by magnesium sulfate limitation boosts de novo limonene production. *Biotechnol. Bioeng.* **113**, 1305–1314 (2016).

220. A. V. Pandit, S. Srinivasan, R. Mahadevan, Redesigning metabolism based on orthogonality principles. *Nat. Commun.* **8**, 1–11 (2017).
221. M. Kim, J. Baek, J. K. Lee, Comparison of H₂ accumulation by *Rhodobacter sphaeroides* KD131 and its uptake hydrogenase and PHB synthase deficient mutant. **31**, 121–127 (2006).
222. R. Mans, J. M. G. Daran, J. T. Pronk, Under pressure: evolutionary engineering of yeast strains for improved performance in fuels and chemicals production. *Curr. Opin. Biotechnol.* **50**, 47–56 (2018).
223. T. A. Leaf, F. Srienc, Metabolic modeling of polyhydroxybutyrate biosynthesis. *Biotechnol. Bioeng.* **57**, 557–570 (1998).
224. Y. Sasaki, T. Eng, R. A. Herbert, J. Trinh, Y. Chen, A. Rodriguez, J. Gladden, B. A. Simmons, C. J. Petzold, A. Mukhopadhyay, Engineering *Corynebacterium glutamicum* to produce the biogasoline isopentenol from plant biomass hydrolysates. *Biotechnol. Biofuels.* **12**, 41 (2019).
225. A. Suwanto, S. Kaplan, Physical and genetic mapping of the *Rhodobacter sphaeroides* 2.4.1 genome: presence of two unique circular chromosomes. *Microbiology.* **171**, 5840–5849 (1989).
226. G. W. Naylor, H. a Addlesee, L. C. D. Gibson, C. N. Hunter, The photosynthesis gene cluster of *Rhodobacter sphaeroides*. *Photosynth. Res.* **62**, 121–139 (1999).
227. C. Mackenzie, M. Choudhary, F. W. Larimer, P. F. Predki, S. Stilwagen, J. P. Armitage, R. D. Barber, T. J. Donohue, J. P. Hosler, J. E. Newman, J. P. Shapleigh, R. E. Sockett, J. Zeilstra-Ryalls, S. Kaplan, The home stretch, a first analysis of the nearly completed genome of *Rhodobacter sphaeroides* 2.4.1. *Photosynth. Res.* **70** (2001), pp. 19–41.
228. S. L. Porter, D. A. Wilkinson, E. D. Byles, G. H. Wadhams, S. Taylor, N. J. Saunders, J. P. Armitage, Genome sequence of *Rhodobacter sphaeroides* strain WS8N. *J. Bacteriol.* **193**, 4027–4028 (2011).
229. H. P. Lang, R. J. Cogdell, S. Takaichi, Complete DNA sequence, specific Tn5 insertion map and gene assignment of the carotenoid biosynthesis pathway of *Rhodobacter sphaeroides*. **177**, 2064–2073 (1995).
230. P. D. Donohue, R. Barrangou, A. P. May, Advances in industrial biotechnology using CRISPR-Cas systems. *Trends Biotechnol.* **36**, 134–146 (2018).
231. M. I. S. Naduthodi, M. J. Barbosa, J. van der Oost, Progress of CRISPR-Cas based genome editing in photosynthetic microbes. *Biotechnol. J.* **1700591**, 1–9 (2018).
232. K. R. Choi, S. Y. Lee, CRISPR technologies for bacterial systems: current achievements and future directions. *Biotechnol. Adv.* **34**, 1180–1209 (2016).
233. P. Cai, J. Gao, Y. Zhou, CRISPR-mediated genome editing in non-conventional yeasts for biotechnological applications. *Microb. Cell Fact.* **18** (2019), pp. 1–12.
234. E. Sonoda, H. Hochegger, A. Saberi, Y. Taniguchi, S. Takeda, Differential usage of non-homologous end-joining and homologous recombination in double strand break repair. *DNA Repair (Amst.)* **5**, 1021–1029 (2006).
235. B. Adiego-Pérez, P. Randazzo, J. M. Daran, R. Verwaal, J. A. Roubos, P. Daran-Lapujade, J. Van Der Oost, Multiplex genome editing of microorganisms using CRISPR-Cas. *FEMS Microbiol. Lett.* **366**, 1–19 (2019).
236. R. Bowater, A. J. Doherty, Making ends meet: repairing breaks in bacterial DNA

- by non-homologous end-joining. *PLoS Genet.* **2**, 93–99 (2006).
237. L. Aravind, E. V. Koonin, Prokaryotic homologs of the eukaryotic DNA-end-binding protein Ku, novel domains in the Ku protein and prediction of a prokaryotic double-strand break repair system. *Genome Res.* **11**, 1365–1374 (2001).
 238. A. J. D. Y, S. P. Jackson, Identification of bacterial homologues of the Ku DNA repair proteins. *FEBS Lett.* **500**, 186–188 (2001).
 239. Y. Tong, P. Charusanti, L. Zhang, T. Weber, S. Y. Lee, CRISPR-Cas9 based engineering of actinomycetal genomes. *ACS Synth. Biol.* **4**, 1020–1029 (2015).
 240. T. Su, F. Liu, P. Gu, H. Jin, Y. Chang, Q. Wang, Q. Liang, Q. Qi, A CRISPR-Cas9 assisted non-homologous end-joining strategy for one-step engineering of bacterial genome. *Sci. Rep.* **6**, 1–11 (2016).
 241. N. Saitou, M. Nei, The neighbor-joining method: a new method for reconstructing phylogenetic trees. *Mol. Biol. Evol.* **4**, 406–425 (1987).
 242. S. Kumar, G. Stecher, K. Tamura, MEGA7: molecular evolutionary genetics analysis version 7.0 for bigger datasets. *Mol. Biol. Evol.* **33**, 1870–1874 (2016).
 243. A. Masuda, Y. Toya, H. Shimizu, Metabolic impact of nutrient starvation in mevalonate-producing *Escherichia coli*. *Bioresour. Technol.* **245**, 1634–1640 (2017).
 244. A. Hemmerlin, J. F. Hoeffler, O. Meyer, D. Tritsch, I. A. Kagan, C. Grosdemange-Billiard, M. Rohmer, T. J. Bach, Cross-talk between the cytosolic mevalonate and the plastidial methylerythritol phosphate pathways in tobacco bright yellow-2 cells. *J. Biol. Chem.* **278**, 26666–26676 (2003).
 245. O. Laule, A. Fürholz, H. S. Chang, T. Zhu, X. Wang, P. B. Heifetz, W. Grissem, B. M. Lange, Crosstalk between cytosolic and plastidial pathways of isoprenoid biosynthesis in *Arabidopsis thaliana*. *Proc. Natl. Acad. Sci. U. S. A.* **100**, 6866–6871 (2003).
 246. D. C. Volke, J. Rohwer, R. Fischer, S. Jennewein, Investigation of the methylerythritol 4 - phosphate pathway for microbial terpenoid production through metabolic control analysis. *Microb. Cell Fact.*, 1–15 (2019).
 247. S. Centeno-Leija, G. Huerta-Beristain, M. Giles-Gómez, F. Bolivar, G. Gosset, A. Martinez, Improving poly-3-hydroxybutyrate production in *Escherichia coli* by combining the increase in the NADPH pool and acetyl-CoA availability. *Antonie van Leeuwenhoek, Int. J. Gen. Mol. Microbiol.* **105**, 687–696 (2014).
 248. R. J. Van Wegen, S. Y. Lee, A. P. J. Middelberg, Metabolic and kinetic analysis of poly(3-Hydroxybutyrate) production by recombinant *Escherichia coli*. *Biotechnol. Bioeng.* **74**, 70–80 (2001).
 249. A. L. Meadows, K. M. Hawkins, Y. Tsegaye, E. Antipov, Y. Kim, L. Raetz, R. H. Dahl, A. Tai, T. Mahatdejkul-Meadows, L. Xu, L. Zhao, M. S. Dasika, A. Murarka, J. Lenihan, D. Eng, J. S. Leng, C.-L. Liu, J. W. Wenger, H. Jiang, L. Chao, P. Westfall, J. Lai, S. Ganesan, P. Jackson, R. Mans, D. Platt, C. D. Reeves, P. R. Saija, G. Wichmann, V. F. Holmes, K. Benjamin, P. W. Hill, T. S. Gardner, A. E. Tsong, Rewriting yeast central carbon metabolism for industrial isoprenoid production. *Nature.* **537**, 694–697 (2016).
 250. S. M. Ma, D. E. Garcia, A. M. Redding-Johanson, G. D. Friedland, R. Chan, T. S.

- Batth, J. R. Haliburton, D. Chivian, J. D. Keasling, C. J. Petzold, T. Soon Lee, S. R. Chhabra, Optimization of a heterologous mevalonate pathway through the use of variant HMG-CoA reductases. *Metab. Eng.* **13**, 588–597 (2011).
251. K. Paramasivan, S. Mutturi, Regeneration of NADPH coupled with HMG-CoA reductase activity increases squalene synthesis in *Saccharomyces cerevisiae*. *J. Agric. Food Chem.* **65**, 8162–8170 (2017).
252. V. G. Yadav, M. De Mey, C. Giaw Lim, P. Kumaran Ajikumar, G. Stephanopoulos, The future of metabolic engineering and synthetic biology: towards a systematic practice. *Metab. Eng.* **14**, 233–241 (2012).
253. J. Zhao, Q. Li, T. Sun, X. Zhu, H. Xu, J. Tang, X. Zhang, Y. Ma, Engineering central metabolic modules of *Escherichia coli* for improving β -carotene production. *Metab. Eng.* **17**, 42–50 (2013).
254. W. Xu, J. Yao, L. Liu, X. Ma, W. Li, X. Sun, Y. Wang, Improving squalene production by enhancing the NADPH/NADP⁺ ratio, modifying the isoprenoid-feeding module and blocking the menaquinone pathway in *Escherichia coli*. *Biotechnol. Biofuels.* **12**, 68 (2019).
255. N. J. Claassens, H. He, A. Bar-Even, Synthetic methanol and formate assimilation via modular engineering and selection strategies. *Curr. Issues Mol. Biol.*, 237–248 (2019).
256. N. G. A. Kuijpers, D. Solis-Escalante, M. A. H. Luttik, M. M. M. Bisschops, F. J. Boonekamp, M. van den Broek, J. T. Pronk, J.-M. Daran, P. Daran-Lapujade, Pathway swapping: toward modular engineering of essential cellular processes. *Proc. Natl. Acad. Sci.* **113**, 15060–15065 (2016).
257. A. Sánchez-Pascuala, L. Fernández-Cabezón, V. de Lorenzo, P. I. Nikel, Functional implementation of a linear glycolysis for sugar catabolism in *Pseudomonas putida*. *Metab. Eng.* **54**, 200–211 (2019).
258. J. Mampel, J. M. Buescher, G. Meurer, J. Eck, Coping with complexity in metabolic engineering. *Trends Biotechnol.* **31**, 52–60 (2013).
259. C. A. Testa, C. Lherbet, F. Pojer, J. P. Noel, C. D. Poulter, Cloning and expression of IspDF from *Mesorhizobium loti*. Characterization of a bifunctional protein that catalyzes non-consecutive steps in the methylerythritol phosphate pathway. *Biochim. Biophys. Acta - Proteins Proteomics.* **1764**, 85–96 (2006).
260. V. de Lorenzo, Beware of metaphors chasses and orthogonality in synthetic biology. *Bioeng. Bugs.* **2**, 1–5 (2011).
261. H. Arai, J. H. Roh, S. Kaplan, Transcriptome dynamics during the transition from anaerobic photosynthesis to aerobic respiration in *Rhodobacter sphaeroides* 2.4.1. *J. Bacteriol.* **190**, 286–99 (2008).
262. A. Banerjee, T. D. Sharkey, Methylerythritol 4-phosphate (MEP) pathway metabolic regulation. *Nat. Prod. Rep.* **31**, 1043–55 (2014).
263. Y. A. Primak, M. Du, M. C. Miller, D. H. Wells, A. T. Nielsen, W. Weyler, Z. Q. Beck, Characterization of a feedback-resistant mevalonate kinase from the archaeon *Methanosarcina mazei*. *Appl. Environ. Microbiol.* **77**, 7772–7778 (2011).
264. Z. Fu, N. E. Voynova, T. J. Herdendorf, H. M. Miziorko, J. J. P. Kim, Biochemical and structural basis for feedback inhibition of mevalonate kinase and isoprenoid metabolism. *Biochemistry.* **47**, 3715–3724 (2008).

265. S. Lund, R. Hall, G. J. Williams, An artificial pathway for isoprenoid biosynthesis decoupled from native hemiterpene metabolism. *ACS Synth. Biol.* **8**, 232–238 (2019).
266. G. K. Hinson DD, Chambliss KL, Toth MJ, Tanaka RD, Post-translational regulation of mevalonate kinase by intermediates of the cholesterol and nonsterol isoprene biosynthetic pathways. *J. Lipid Res.* **38**, 2216–2223 (1997).
267. J. M. Burg, C. B. Cooper, Z. Ye, B. R. Reed, E. A. Moreb, M. D. Lynch, Large-scale bioprocess competitiveness: the potential of dynamic metabolic control in two-stage fermentations. *Curr. Opin. Chem. Eng.* **14** (2016), pp. 121–136.
268. L. Wang, D. Ji, Y. Liu, Q. Wang, X. Wang, Y. J. Zhou, Y. Zhang, W. Liu, Z. K. Zhao, Synthetic cofactor-linked metabolic circuits for selective energy transfer. *ACS Catal.* **7**, 1977–1983 (2017).
269. W. B. Black, L. Zhang, W. S. Mak, S. Maxel, Y. Cui, E. King, B. Fong, A. Sanchez Martinez, J. B. Siegel, H. Li, Engineering a nicotinamide mononucleotide redox cofactor system for biocatalysis. *Nat. Chem. Biol.*, 87–94 (2019).
270. Y. Liu, Y. Feng, L. Wang, X. Guo, W. Liu, Q. Li, X. Wang, S. Xue, Z. K. Zhao, Structural insights into phosphite dehydrogenase variants favoring a non-natural redox cofactor. *ACS Catal.* **9**, 1883–1887 (2019).
271. L. Gomelsky, O. V. Moskvina, R. A. Stenzel, D. F. Jones, T. J. Donohue, M. Gomelsky, Hierarchical regulation of photosynthesis gene expression by the oxygen-responsive PrrBA and AppA-PpsR systems of *Rhodobacter sphaeroides*. *J. Bacteriol.* **190**, 8106–14 (2008).
272. R. A. Weusthuis, I. Lamot, J. van der Oost, J. P. M. Sanders, Microbial production of bulk chemicals: development of anaerobic processes. *Trends Biotechnol.* **29**, 153–8 (2011).
273. J. Nielsen, Cell factory engineering for improved production of natural products. *Nat. Prod. Rep.* **36**, 1233–1236 (2019).
274. W. Xie, X. Lv, L. Ye, P. Zhou, H. Yu, Construction of lycopene-overproducing *Saccharomyces cerevisiae* by combining directed evolution and metabolic engineering. *Metab. Eng.* **30**, 69–78 (2015).
275. C. Y. Ng, I. Farasat, C. D. Maranas, H. M. Salis, Rational design of a synthetic Entner-Doudoroff pathway for improved and controllable NADPH regeneration. *Metab. Eng.* **29**, 86–96 (2015).
276. I. Martínez, J. Zhu, H. Lin, G. N. Bennett, K. Y. San, Replacing *Escherichia coli* NAD-dependent glyceraldehyde 3-phosphate dehydrogenase (GAPDH) with a NADP-dependent enzyme from *Clostridium acetobutylicum* facilitates NADPH dependent pathways. *Metab. Eng.* **10**, 352–359 (2008).
277. K. Qiao, T. M. Wasylenko, K. Zhou, P. Xu, G. Stephanopoulos, Lipid production in *Yarrowia lipolytica* is maximized by engineering cytosolic redox metabolism. *Nat. Biotechnol.* **35**, 173–177 (2017).
278. V. Chubukov, U. Sauer, Environmental dependence of stationary-phase metabolism in *Bacillus subtilis* and *Escherichia coli*. *Appl. Environ. Microbiol.* **80**, 2901–2909 (2014).
279. V. Chubukov, J. J. Desmarais, G. Wang, L. J. G. Chan, E. E. K. Baidoo, C. J. Petzold, J. D. Keasling, A. Mukhopadhyay, Engineering glucose metabolism of *Escherichia*

- coli* under nitrogen starvation. *npj Syst. Biol. Appl.* **3**, 1–7 (2017).
280. Y. Zheng, T. Su, Q. Qi, Microbial CRISPRi and CRISPRa systems for metabolic engineering. *Biotechnol. Bioprocess Eng.* **24**, 579–591 (2019).
281. S. Li, C. B. Jendresen, A. Grünberger, C. Ronda, S. I. Jensen, S. Noack, A. T. Nielsen, Enhanced protein and biochemical production using CRISPRi-based growth switches. *Metab. Eng.* **38**, 274–284 (2016).

About the author

Enrico Orsi was born on November 18th 1991, in Bologna (Italy). He obtained his BSc degree in Biotechnology at University of Bologna. His BSc thesis was supported by an Erasmus Exchange scholarship with the Universitat de Barcelona (Spain), with an internship at the Institute for Research in Biomedicine under the supervision of dr. Ferran Azorín and dr. Olga Moreno-Moreno.



In 2013, Enrico started his MSc in Molecular and Cellular Biotechnology at Wageningen University. In September 2014, he started his MSc thesis at the Bioprocess Engineering (BPE) department under the supervision of dr. Kiira Vuoristo and prof. Ruud Weusthuis. Here, he investigated how to improve itaconic acid production in the bacterium *Escherichia coli*. Then, in Spring 2015 he performed a minor thesis at University of California San Diego (USA) in the laboratory of prof. Susan Golden. During this experience, he studied molecular mechanisms of circadian rhythms in the cyanobacterium *Synechococcus elongatus*.

In January 2016, Enrico started his PhD research at the BPE department under the supervision of prof. Ruud Weusthuis, dr. Servé Kengen and prof. Gerrit Eggink. During this project, he worked on characterizing and engineering the metabolism of the bacterium *Rhodobacter sphaeroides* for isoprenoid production. Most of his work is described in this thesis.

Currently, Enrico is employed as PostDoc researcher at the System and Synthetic Metabolism group of dr. Arren Bar-Even at the Max Planck Institute of Molecular Plant Physiology in Potsdam (Germany).

List of publications

Orsi, E., Folch, P. L., Monje-López, V. T., Fernhout B. M., Turcato, A., Kengen, S. W., Eggink, G. & Weusthuis, R. A. (2019). Characterization of heterotrophic growth and sesquiterpene production by *Rhodobacter sphaeroides* on a defined medium. *Journal of industrial microbiology & biotechnology*, 46(8), 1179-1190. DOI: 10.1007/s10295-019-02201-6.

Mougiakos, I.* , Orsi, E.*, Ghiffary, M. R., Post, W., de Maria, A., Adiego-Perez, B., Kengen, S. W. M., Weusthuis, R. A. & van der Oost, J. (2019). Efficient Cas9-based genome editing of *Rhodobacter sphaeroides* for metabolic engineering. *Microbial cell factories*, 18(1), 204. DOI:10.1186/s12934-019-1255-1.

Orsi, E., Beekwilder, J., Peek, S., Eggink, G., Kengen, S. W., & Weusthuis, R. A. (2020). Metabolic flux ratio analysis by parallel ¹³C labeling of isoprenoid biosynthesis in *Rhodobacter sphaeroides*. *Metabolic Engineering*, 57, 228-238. DOI: 10.1016/j.ymben.2019.12.004.

Orsi, E.*, Beekwilder, J.* , Peek, S., Eggink, G., Kengen, S. W., & Weusthuis, R. A. (2020). Functional replacement of isoprenoid biosynthetic pathways in *Rhodobacter sphaeroides*. *Microbial Biotechnology*, 13(4), 1082-1093. DOI: 10.1111/1751-7915.13562.

Orsi, E.*, Mougiakos, I.* , Post, W., Beekwilder, J., Dompè, M., Eggink, G., van der Oost, J., Kengen, S. W., & Weusthuis, R. A. (2020). Growth-uncoupled isoprenoid synthesis in *Rhodobacter sphaeroides*. *Biotechnology for Biofuels*, 13: 123. DOI: 10.1186/s13068-020-01765-1.

Orsi, E., Beekwilder, J., Eggink, G., Kengen, S. W., & Weusthuis, R. A. (2020). The transition of *Rhodobacter sphaeroides* into a microbial cell factory. *Biotechnology and Bioengineering*, submitted.

Other publications:

Vuoristo, K. S., Mars, A. E., van Loon, S., Orsi, E., Eggink, G., Sanders, J. P., & Weusthuis, R. A. (2015). Heterologous expression of *Mus musculus* immunoresponsive gene 1 (irg1) in *Escherichia coli* results in itaconate production. *Frontiers in microbiology*, 6, 849. DOI: 10.3389/fmicb.2015.00849.

Finger-Bou, M., Orsi, E., van der Oost, J., Staals, R. H. J. (2020). CRISPR with a happy ending: non-templated DNA repair for prokaryotic genome engineering. *Biotechnology journal*, 15, 1900404. DOI: 10.1002/biot.201900404.

Finger-Bou, M.*, Orsi, E.*, Mougiakos, I., Bastian, G., Morini, L., Pool, V., de Maria, A., Ghiffary, M. R., Kengen, S. W., Weusthuis, R. A., van Kranenburg, R., Claassens, N. J., Staals, R. J. H., van der Oost, J. Template-independent genetic engineering of *Rhodobacter sphaeroides*. Manuscript in preparation.

*contributed equally

Overview of completed training activities

Discipline specific activities

Courses

Metabolic Engineering & Systems Biology (Gothenburg, Sweden)	2017
Advanced Course Microbial Physiology and Fermentation Technology, BDSL (Delft, The Netherlands)	2018

Conferences

Microbial Biotechnology 2.0, KNVM (Delft, The Netherlands)	2015
NBC-16 'Next Level Biotechnology' (Wageningen, The Netherlands)	2016
Microbial Biotechnology 3.0, KNVM (Delft, The Netherlands)	2016
WUR Microbiology Centennial Symposium (Wageningen, The Netherlands)	2017
Industrial Synthetic Biology (Munich, Germany)	2018
Microbial Biotechnology 6.0, KNVM (Delft, The Netherlands)	2019

General courses

VLAG PhD week (Baarlo, The Netherlands)	2016
Chemometrics, VLAG (Wageningen, The Netherlands)	2016
Applied Statistics, VLAG (Wageningen, The Netherlands)	2016
Workshop PhD Carousel, WGS (Wageningen, The Netherlands)	2016
Orientation on Teaching for PhD Students, WGS (Wageningen, The Netherlands)	2016
Scientific Writing, WGS (Wageningen, The Netherlands)	2017
Project and Time Management, WGS (Wageningen, The Netherlands)	2017
Phylosophy and Ethics of Food Science and Technology	2017
Supervising BSc & MSc thesis students	2017
Career Perspectives, WGS (Wageningen, The Netherlands)	2019

Optional activities

Green Terpene progress meetings, BPE (Wageningen, The Netherlands)	2016-2019
BPE group meetings	2016-2019
Organising member PhD trip committee, BPE (Wageningen, The Netherlands)	2017-2018
PhD study tour to San Diego (San Diego, USA)	2018

Acknowledgements

With this final section, a 4-years journey comes to an end. I described the research within this booklet using a car-racing metaphor. Nevertheless, its development felt more like a marathon. Finalizing such a long distance run wouldn't have been possible without the help and support of many people I am grateful to.

I would like to start with my supervisors, whose support was crucial during these years. It helped me in developing not only as a scientist, but also as an adult. **Ruud**, during my MSc thesis you offered me to continue staying at BPE as PhD student. Retrospectively, I think accepting your proposal was the best decision I could have taken. We encountered several challenges during the project, and we always tackled them together. This strengthen our bond, which developed in a solid and friendly cooperation. Your love for Italy has always been explicit, and became tangible in our *basil&beetroot* beer for the BPE beer contest. This is just one among many examples of the connection I am grateful we have established. I always knew you were accessible for giving suggestions when I had doubts, while being sympathetic and supportive when I faced hard times. Thank you for that, because this is proof of your genuine interest in the wellbeing of your students.

Servé, we also met before the beginning of my PhD project, as you were my supervisor during my MSc internship. Through these years I learned to appreciate your kind and calm personality. It allowed to see the positive sides of the advancements we were obtaining, also in moments we felt bit stuck. At the same time, it helped in being realistic in our expectations when new ones were coming in. It was very nice talking about science and life with you on our trip to Geleen for the final meeting with Isobionics. There, I discovered your more personal side, and I could experience your passion for extremophiles and exotic

enzyme complexes. Thank you for the patience you put in revising my wordy manuscripts. Your inputs always gave a better spin to the storylines, making them concise and convincing.

Gerrit, thanks to you I understood the importance of maintaining a clear big picture of the project, while being busy in the daily activities of the lab. This helped in the formulation of the research questions for the final chapters of this thesis. Although you were not physically at BPE during the last months of the project, you always found time to provide useful inputs and comments to our manuscripts, which improved and broadened the scope of our work. I am happy we also established a personal connection through these years. It was nice also listening to your stories of your times as PhD students during borrels and bbqs.

Special thanks go to the R&D team of Isobionics. Our interaction resulted in a friendly and prolific collaboration. I enjoyed a lot our progress meetings, where I received important inputs for my growth as critical scientist. **Jules**, during our collaboration you transitioned from WUR to Isobionics. You participated in this project with a sociable and constructive attitude. I am very happy to have collaborated with you. Altogether, your inputs led to the implementation of the ^{13}C -method, which had to be created from scratch, and that I experienced as the biggest intellectual challenge of this project. Moreover, it also resulted in the nice work on the pathway replacement (chapter 4), which could be used in two other research chapters (5 and 6). **Georg** and **Matthew**, thanks for your support and responsiveness to my requests to revision papers for submission. I apologize for sometimes being a bit pushy with deadlines, and I am grateful for your patience and punctual help. **Wouter**, thank you for your insights on *Rhodobacter* physiology and fermentation procedures. **Elena**, thank you for your help in teaching the protocols for conjugation and genetic engineering of *Rhodobacter*.

Frank, also you helped in getting acquainted in working with the bug. Moreover, I enjoyed the nice discussions on the cloning and metabolic engineering aspects of the project.

There have been several co-authors for the chapters of this thesis which deserve a special mention. **Pauline**, you joined the project for few months in a moment in which chapter 2 needed a closure. You taught me to be methodic and structured in the experimental setup (including precultures!), and this resulted in an incredible decrease of the standard deviations in all the measurements from that point onwards. Thank you also for your help in the revision of the manuscript and the reading version of the thesis. And thank for taking me out of the lab when I was clearly in need of some alcohol. **Ioannis**, we had an explosive start in our collaboration, which gradually settled and became a profitable interaction resulting in two nice manuscripts. Without your prompt help, it wouldn't have been possible to develop the CRISPR-Cas9 system so quickly. Thank you for that. From our collaboration, I also learned the importance of having a nice story to present in a paper, and it is something I will definitely make a good use of. Good luck for your future academic career! **Marco**, besides being the best goal keeper I have played with, you are also a great scientist and friend. Thank for the help with the NMR, it was a very important addition to our story. **Dewi and Adèle**, thank you for your help in the experimental work in described in chapter 4.

During these years I also supervised many MSc and BSc students. It has been a privilege for me working with all of you, and being involved in your personal and professional development. I hope you enjoyed our interaction as much as I did. **Belén and Vicente**, we started working on the project at the same time, with the same experience (almost zero) and you immediately set the bar high. It was very

beneficial for me to work with you, as you started the research that lead to chapters 2 and 3. I had no doubt that you would have continued your path as scientist with a PhD project. **Mario**, you were the most ‘computational’ of all the students. I enjoyed the chance of being involved in your modelling project, and I appreciated your enthusiasm and team building initiatives, which resulted in a nice dinner organized at your place. Good luck in finishing your PhD! **Bas**, you have been an extremely efficient scientist. You provided very nice data, while maintaining a healthy work/life balance. I greatly admired this aspect of yours. Thank you also for setting up a protocol for the bioreactors, which was very useful in the months following your graduation. **Alice** and **Alessandro**, you brought some home feeling at work. You both had a good click, which maintained your interaction active and cheerful. I enjoyed our conversations on cultural differences between an Emiliano, Piemontese e Veneto. After your graduation, you both moved to the pharmaceutical industry, and I am sure you will have plenty of interesting career opportunities ahead. **Philipp**, you started your thesis with a much more important challenge ahead of you, which was the one of becoming a father. You managed to do well during your thesis while getting used to this new role of yours. This was impressive. You also had a nice humor, and made our interaction easy and relaxed. **Ghiffa**, you started working on this project with very little experience in molecular biology, and in few months you developed the final CRISPR-Cas9 toolkit. You worked very hard, and you obtained a well-deserved PhD project in a prestigious institute in South Korea. Well done! **Alberto**, you are the personification of what I think a genuine *regaz* from Bologna should be. Proactive, participative, helpful and *polleggiato* (and also king of ragù!). Our paths crossed several times, although shifted in time. I am happy we will keep on working together in Potsdam. Btw, thank for your helping me to settle there. **Siebe** and **Wilbert**, you were the first people

putting hands on the brand new CRISPR-toolkit for doing metabolic engineering. You had a quick start, managing to produce interesting mutants, which were used in chapters 3, 5 and 6. Thank you both for your hard work, and good luck in your future steps. **Rosy**, you joined as my last student in the moment I had to close all my research lines. I am sorry if you sometimes felt pressure on you. You showed deep understanding of the scientific literature, and you had good ideas for the experimental design. Unfortunately, we did not have time to implement that. I hope you will find what you really like and use your potential in the way you consider best for you!

I would also like to thank my colleagues for the support they gave me through these years. Thanks to the BPE staff. **Fred, Wendy, Snezana, Sebastiaan, Rick**. I knew I could always count on you for support, both practically, but also emotionally. **Dewi** and **Bregje**, we collaborated during challenging times of your lives. I learned a lot from our collaborations, and I will treasure these experiences. I wish you all the best for your future! I would also like to thank **René, Marina, Miranda, Rick, Rafa C., Marian, Antonietten, Hans, Maria, Corjan, Iago, Iulian, Marta, Dirk, Michel, Arjen, Giuseppe, Marcel, Sarah** and **Iris**, although we weren't directly involved in each other's work, you were ready to give practical suggestions and personal hints for developing myself further. Moreover, I enjoyed the nice times in borrels, dinners and social activities. The time in BPE has been fun also thanks to you!

Of course, this time would have been different without the support of nice and cheerful colleagues at the office. I would like to thank my officemates **Xiao, Richard, Pauline, Anna, August, Chunzhe**. You were always keen to keep a nice atmosphere in the office. Thank you for keeping an eye on me when I was working too much. With you I felt in a safe and warm place.

Of course, also the other colleagues and friends were very important for me during these years. **Christian, Edgar** and **Alex**, it was nice passing by your office for some late afternoon chats. Thank you for the nice inputs to my work, and also for the questionable talks and dirty jokes we had during drinking sessions. These were very healthy stress release therapies. **Camilo**, weon, you are definitely not the most talkative guy, but you were always accessible for a consult. Thanks for teaching me the tricks for making nice figures, the chess matches, and for running so much on the football field after my 'precise' passages. Thank you also for the 'plastic surgery' to my picture in this booklet. **Youri, pistolero**, it has been great having you around in BPE, and it is a pity we could not see each other that often after you left. Nevertheless, I am happy we kept in touch, and I am sure we will continue. **Aziz**, thanks for giving me the chance to know the real *sultano* during your last months in Wageningen. May the berfusion be with you! **Carl**, thanks for your company during swimming and the talks in the sauna. You gave me important tips for my development, and I really appreciate that. **Narcis** and **Jort**, our football stars. I enjoyed playing football with you guys, although I would have preferred a more suitable league for the team. I enjoyed a lot talking about history with you, as well as with **Jesse**, and I hope there will be visiting together Girona with Mr. *Impressive* as Cicerone. **Kylie**, it was nice talking about music and politics together. Your radical positions were always a good starting point for a thorough confrontation in front of a beer. **Calvin**, I will never stop thanking you for your help with matrices calculations. I would also like to thank **Catalina, Elisa, Renske, Rocca, Barbara, Ana, Gin, Pieter, Sabine, Robin, Jorijn, Jeroen, Giulia, Calvin, Sebastian, Lukas, Kylie, Agi, Josue, Joao, (ostia)-Rafa, Stephanie, Ilse, Gerard, Mitsue** for the nice times through these years.

Sometimes, I was also around MIB and SSB for some meetings and presentations. I would like to thank **John, Raymond, Maria S., Nico, Max, Belén, Ivette, Lorenzo, Joyshree, Thijs, Prarthna, Costas, Christos, Mihris, Wen, Mamou, Despoina, Eric and James**, it was very beneficial presenting at BacGen meetings, and it allowed me to get important inputs from the molecular aspects of the project. **Nico**, I am very happy to continue your work at Potsdam. I am sure we will keep in touch in the upcoming years. **Max**, same for you. I also enjoyed our chats on life and science in our free time. Thanks for inviting me to participate to your mini-review. **Lorenzo**, thanks for having me around for longer than expected. **Joyshree**, thanks for the fun chats, especially outside Helix.

I would like to thank the members of la *Casa del Popolo*. Many nice friends have passed around this house, which became the center of my nightlife activities. Starting from the *Sindaco* **Fabian**, we have been very close during these years of PhD. Countless are the times you welcomed me at your home. Countless are the adventures and laughs! For sure, the PhD would have been much less fun without you around. Your cocktails are definitely going to be missed. Also, thank you for the deep conversations we had. Because we were not always on the same line, they made me value our friendship. Looking forward for the chance of bringing you to the Balorda! To the *assessori* **Marco** (delega: sport), **Nicolò** (sfoglina) e **Riccardo** (cortesia), an applause to your great administration of BBQs, shishas, guitar sessions and board games. **Stefano**, thank you for all the nice wine we drunk together also with **Francesco C.** and **Elena**. Also, thank you for reminding me how beautiful Emilia-Romagna is. **Valentina**, thank you for your friendship and your emotional support in all these years. Thanks also to **Lavinia** - *persona cattiva (cit.)* -, **Francesca, Camilla, Erika, Giustina, Giulia, Pietro, Claudio, Maria Elena** for the nice moments spent together.

Elvira, Claudine, Joyshree and **Raisa**, you were coming to visit Patricia at home, but I always enjoyed your company and chilling around you. Thanks for cheering up my evenings as well!

Some friends from my previous chapters kept on being around in my life. From the MSc studies, I would like to thank **Daisuke, Yutaka** and **Nanami** for welcoming at their place and treating me as a king every time they can. **Oscar**, I enjoyed partying with you, especially for the celebrations like the last couple of 5th of May. I don't remember much though! **Ivan** and **Javier**, thanks for keeping this bond through the years. I am sure we will be in touch wherever we will end up. **Stefano**, we also maintained a close interaction through these years, and we could exchange our views about science and the life of a scientist. **Miguel, Andy, JoJo** and **Daniel**, thanks for keeping alive memories from the old times in Fire House during our meetings. We are all older now, but I think overall we aged well. **Guidoriccio, Janne, Lupo** and **Donna**, thanks for rodas de samba in Utrecht, and thanks also to **Santos** and **Lucia** for the dinners they organized at their place. **Carlo**, you are the most elegant football player I have played with. A real *virtuoso*, both in the pitch and outside. I am looking forward for some proper summer evenings in *Amarcord* style in our beautiful Romagna. I am very happy of our friendship, and very proud of having you as designer of the cover of this thesis! **Juliana** and **Durk**, I promise I will keep on playing board games to be ready when there will be a chance of a game night (with Italian background music, of course!). **Vanessa**, I have a lot of laughs in remembering our backpacking trip around Southern India as properly deserved trip to combine to **Adithi's** wedding. **Silvia** and **Anna**, thanks for making me feel clever and thanks for actively keeping our bond from Barcelona's time tight.

Nice memories are associated to my time in Utrecht. Thanks **Luisa** and **Yannis** for the nice atmosphere we had. Thanks also to **Sarah, Kiki, Stavros, Thodoris, Maria** and **Stratos** for the chill moments in St. Gotthard.

From my Italian times, I remained in touch with nice and important friends. Thanks to **Piri, Terry, Anvita, Caterina, Alessandra, Ludo(Vica), Cisty, Vektor, Arianna, Dave, Cesco** for maintaining the nice times of the *Merdoteca*, and the reunions we did around Europe. **Piri**, you proved to be a friend I can always count on, and I am very lucky to have you in my life. I hope through these years you realized how much I value our friendship. Thanks also to **Randaz, Bomberino, Paul, Lotner, Chacha, Sefo, Monto, Vivi, Civ** and **Silvi** for showing me that there are some aspects of life in Bologna that never change. Thanks also **Wayza** and **Bumba** for coming visiting me, **Federico** and **Sara** during Kingsday.

Grazie alla mia famiglia per aver cercato di capire su cosa io abbia lavorato in questi anni. Probabilmente, questo sforzo dovrà continuare ancora per un po'. **Laura C., Lorenzo, Fabio, Novella, Paola P., Pera, Laura G., Paola F., Alberto, zia Maria, Carla, James** mi ha fatto piacere intrattenervi sui ai miei usi e costumi in Olanda. Purtroppo, non ci saranno più bulbi di tulipani per Natale dall'anno prossimo. Rimedierò con qualcosa di cruccio. **Beaver** e **Milly**, grazie per le visite a Wageningen e le ospitate ad Amsterdam. **Michela** e **Francesco**, grazie per farmi sentire a casa ogni volta che passo da Berna. Spero veniate a trovarmi presto a Berlino, anche con **Giovanni** e **Rita**. E perché no, pure **Teresa, Maurizio, Alessio, Gibbi** e **Dorota. Mamma (T.)** e **Papà (B.)**, grazie per avermi insegnato l'importanza della resilienza (stringere il culo) e di intraprendere le sfide con un approccio positivo. Un grazie enorme per avermi supportato in tutte le mie scelte di vita. Se sono arrivato fin qua é anche perché la vostra fiducia non mi é mai mancata.

Patricia, você entrou na minha vida na ponta dos pés, e agora você é o pilar. Obrigado por compartilhar comigo a importância da liberdade e de ser você mesmo. Estou ansioso para começar um novo capítulo juntos!

Infine, un pensiero per la **zia Sara**, che sarebbe stata molto contenta di partecipare ad un altro traguardo dei suoi nipoti.

About thesis title and cover

Racing-red *chassis* is a metaphor borrowed from car-racing, and is used here to describe the development of a competitive microbial cell factory. Because *Rhodobacter sphaeroides* is a red microorganism, racing-red (*rosso corsa*) was chosen as colour for this *chassis*. The latter term is used both in Formula 1 and synthetic biology jargon, and describes the platform that is being engineered. Since study and improvement of *R. sphaeroides* has occurred via iterative cycles, the track of a Formula 1 circuit (Monza) is shown in the cover. Ideally, each lap of the circuit represents a design-build-test-learn (DBTL) cycle. The chapters contributing to the improvement of the DBTL stages are shown as checkpoints of the track, and eventually lead to an improved and better understood strain at the checkered flag.

The research described in this thesis was financially supported by The Netherlands Ministry of Economic Affairs, via a public-private NWO-Green Foundation for sustainable production and supply chains in agriculture and horticulture (870.15.130,2015/05279/ALW).

Cover design by Carlo Leonardi

Printed by Digiforce || ProefschriftMaken

